UNIVERSITY OF NEUCHÂTEL

CENTRE OF HYDROGEOLOGY

MODELLING GROUNDWATER SALINISATION IN IRRIGATED COASTAL AREAS: FROM SOLUTE RECYCLING CONCEPTS TO QUANTITATIVE RISK ASSESSMENT

PhD thesis presented to the faculty of Sciences at the University of Neuchâtel to satisfy the requirements of the degree of Doctor of Philosophy in Science

By

Ellen Milnes

Thesis Jury defence date: 17th June 2005

Public presentation Date: 30th September 2005

Prof. Pierre Perrochet, University of Neuchâtel

Dr. Philippe Renard, University of Neuchâtel

Prof. Olivier Besson, University of Neuchâtel

Prof. André Mermoud, Federal Institute of Technology, Lausanne

Prof. Rachid Ababou, National Institute of Polytechnics, Toulouse, France

Prof. Jesus Carrera, Technical University of Catalogna, Barcelona, Spain

IMPRIMATUR POUR LA THESE

Modelling groundwater salinisation in irrigated coastal areas : from solute recycling concepts to quantitative risk assessment

Ellen MILNES

UNIVERSITE DE NEUCHATEL

FACULTE DES SCIENCES

La Faculté des sciences de l'Université de Neuchâtel, sur le rapport des membres du jury

P. Perrochet (directeur de thèse),
O. Besson, P. Renard,
A. Mermoud (EPF Lausanne), J. Carrera (Barcelone E)
et R. Ababou (Toulouse F)

autorise l'impression de la présente thèse.

Neuchâtel, le 24 juin 2005

La doyenne:

Prof. M. Rahier

Acknowledgements

My greatfullness goes to everybody who has contributed to this work, in some way or the other. There are so many that I am afraid it will be difficult to list everybody separately.

I cannot thank Pierre Perrochet enough for having been given the privilege of undertaking this thesis. His ability to get me back onto the track when I was getting lost in dead ends and his patience in guiding me into the 'jungle of Laplace space' as well as his eagerness in developping ideas have been extremely encouraging. Getting on when big obstacles were encountered was very much facilitated by the fact that his door was always open. Also, for the great time we had in the field and expeditions I am very greatful.

Very special thanks go to Philippe Renard who has followed the evolution of this work all along with enthousiasm. His openness, support and conspicuous advice have been extremely beneficial and important throughout this work. His door, too, was always open to any discussion or questions which I appreciated enormously. Also, I want to thank him for the great time we have had in the field and on travels.With his great personal involvement, the thesis was tied into a European Project, SWIMED (Sustainable water management in coastal Mediterranean aquifers) which did not only finance an important part of the thesis but also led to interaction with other partners, working on related subjects.

I also want to thank all people working at Chyn for creating such a pleasant and amusing working environment, which makes it almost the 'second home'. In particular, I would like to thank Daniel Hunkeler, Heinz Surbeck and Pierre Schnegg for their involvment in this project, leading to numerous results and very fruitful discussions.

Without the close collaboration with the Cyprus Water Development Department, field work in Cyprus would not have been possible. Their interest and support and fruitful discussions were very much appreciated. Special thanks go to Dr. Andreas Christodoulides, whose personal involvement in helping us with anything we needed during the field campaigns in Cyprus will remain unforgettable.

Special thanks go to the managements of the Lanitis and Phasouri plantations, who authorised the implementation of the monitoring wells and who provided a lot of logistical support.

A very special thank goes to Fabien Cornaton for all the support and help he has given me throughout these years, with many discussions leading onto new tracks. Also, I want to thank him for all the long-distance trouble-shooting and debugging across the oceans and corrections he did for me in the last phase of the work.

My parents and family I want to thank so much for all the unforgettable support I got from them, particularly in the very last and difficult phase of the work. My father's patience in correcting my 'awkward' english and his pertinent comments and advice kept me going.

Finally, I am very greatful to the Professors R. Ababou, O. Besson, J. Carrera and A. Mermoud who accepted to be members of the jury.

Abstract

The main objective of this thesis is the quantitative investigation of groundwater salinisation induced by solute recycling from irrigation, and its implications for the overall salinisation in coastal settings. Since the modelling approaches proposed in literature to simulate seawater-intruded areas rarely account for the coupled and superimposed effects of solute recycling and seawater intrusion, simulation procedures have been developed, to evaluate the impact of salinisation induced by seawater intrusion and solute recycling.

The problem of solute recycling is identified and illustrated on an example from Cyprus, the Kiti aquifer, where field investigations suggested that the observed salinity distribution is not only related to seawater intrusion, but also to solute recycling. Two numerical simulation scenarios were carried out, with and without solute recycling. The simulation scenario with solute recycling led to a wide saline zone inland, which compared well with field observations and indicates that considerable errors may occur in a predictive solute mass budget if the recycling process is not accounted for in the calculation.

A mathematical description of the solute recycling process is first carried out for a 1-D advective system and then extended to arbitrary advective-dispersive systems by means of the transfer function theory. This yields a formulation for the transient solute mass flux at an irrigation well, which is obtained from the solute mass flux captured by the well from the boundaries and the recycling transfer function (RTF). The RTF is derived from the sum of the n-fold convolutions of the travel time probability density function between the irrigated surface and the extraction well. This allows definition of a distributed 'recycling source' in the general form of the advection-dispersion equation. The solute recycling process is thereby reduced to a simple flow and transport problem, allowing evaluation of the effect of solute recycling on spatial groundwater salinisation with any standard groundwater simulation code for average steady state hydraulic conditions. At late times, the 'recycling source' is a function of the capture zone probability and the lateral solute mass flux only and yields the salinisation potential, which describes the maximum salinity distribution that will be attained for the given hydraulic setting in response to solute recycling. The effect of transient hydraulic conditions on groundwater salinisation induced by solute recycling is solved numerically in a time-stepping procedure.

Then, a framework for a process-based salinisation risk assessment methodology is proposed in which seawater intrusion and solute recycling salinisation are evaluated separately. By decomposing the overall salinity into a seawater intrusion and solute recycling component, a salinisation risk index is defined as the potential of further salinisation with respect to either salinisation process. The risk index is obtained by comparing the respective 'present state' salinisation with the salinisation potential. The obtained risk index maps reveal areas prone to further salinity increase due to solute recycling and seawater, respectively.

In the last section, a 3-D finite element model, reflecting the main features of another aquifer in Cyprus, the Akrotiri aquifer, was used as a 'hypothetical' reality to illustrate the proposed salinisation risk assessment procedure. The results obtained from the simulations indicate zones running danger of further salinisation with respect to solute recycling and seawater intrusion, which correlate with the spatial distribution of the dominant salinity sources derived from field investigations. But they also revealed that data essential for calibration and cross-validation related to solute recycling is rarely monitored in coastal aquifers. This leads to a discussion on the qualitative estimation of key-factors, identified during the mathematical analysis of the solute recycling process, based on classical hydrogeological data. Such estimations can be a preliminary and inexpensive field approach to identify areas potentially endangered by solute recycling, indicating where the installation of monitoring networks would be advisable in order to obtain the data necessary for a quantitative salinisation risk assessment.

Glossary

Solute recycling: Solute recycling describes the process of solutes that have been extracted from irrigation wells, applied on irrigated surfaces and then transferred through the soil to the groundwater again.

Solute return flow from irrigation: Solute return flow from irrigation denotes the transfer of any solutes transferred through the unsaturated zone to the groundwater (e.g. agrochemical additives), not only the solutes that were previously extracted from the groundwater.

Irrigation return flow: Irrigation return flow denotes the amount of applied irrigation water which is returned to the groundwater by deep percolation.

Frequently used abreviations and symbols

List of abbreviations

ADE	Advection-dispersion equation
PDF	Probability density function
RTF	Recycling transfer function
RP	Solute recycling potential
SIP	Seawater intrusion potential

Mathematical symbols

r_r	return flow ratio [-]
q_{in}	lateral inflow [L^3T^{-1}]
q_{out}	regional discharge [L^3T^{-1}]
q_p	well extraction rate [L^3T^{-1}]
q_i	irrigation rate [L^3T^{-1}]
c_{in}	concentration at inflow boundary [ML^3]
c_{rf}	concentration of irrigation return flow [ML^3]
m_i	inflowing solute mass flux [M^{T-1}]
m_{rf}	solute mass flux in irrigation return flow [M^{T-1}]
m_{pr}	solute mass flux from solute recycling [M^{T-1}]
g^{γ}_t	travel time PDF between irrigation point/zone to irrigation well [T^{-1}]
g^{γ}_{in}	recycling transfer function [T^{-1}]
g_0	redistribution PDF, between irrigation plot and any point in the domain [T^{-1}]
J_p	solute mass flux extracted from irrigation well [MT^{-1}]
I	solute mass captured by the well from the boundaries [MT^{-1}]

TABLE OF CONTENTS

CHAPTER 1

INTRODUCTION

1.1 Background

World-wide, the threat of soil and groundwater salinisation induced by irrigation is increasing and becoming a major issue in hydrogeology, agronomy, and soil and irrigation sciences. The United Nations have declared the irrigation-induced salinisation problem to be a 'global environmental crisis' and state that two million hectares of land are lost each year due to mis-management and constrained irrigation schemes. One of the main problems irrigated agriculture faces today is the challenge of providing food to an ever-expanding population with increasingly poor water quality (Oster 1994). In semi-arid and arid regions, freshwater resources are scarce, particularly during the main crop season, and this often leads to over-exploitation of the groundwater resources beyond sustainable levels (Tanji 1990). The problem is even more serious in coastal areas, aggravated by the fact that the groundwater resources are also vulnerable to seawater intrusion. According to the UN Atlas of the oceans, half the world's population lives in coastal areas and the demand for water is a major challenge in groundwater management (Post 2005). The European Environmental Agency has estimated that in Europe alone at least 100 coastal aquifers are affected by seawater intrusion, particularly in the Mediterranean region.

The work which forms the basis for the present thesis was carried out against this global backcloth and attempts to make a contribution towards an increased understanding of the complex processes underlying groundwater salinisation in coastal irrigated areas. With focus on one particular salinisation process related to irrigation, solute recycling, the main conclusion is that not only seawater intrusion is a threat in coastal aquifers, but also, and in some places dominantly, solute recycling from irrigation. Solute recycling describes the process of solutes that have been extracted from irrigation wells, applied on irrigated surfaces and then transferred through the soil to the groundwater again. Solute recycling from irrigation has often been neglected in coastal areas and the thesis develops a framework for its integration into future optimisation and risk assessment studies.

1.2 Salinisation processes in coastal irrigated areas

In aquifers underlying coastal irrigated areas, many different salinisation processes can occur. In addition to the two main processes under study, seawater intrusion and solute recycling from irrigation, local conditions may lead to important effects from trapped ancient seawater, geogenic

salt deposits, mineral precipitation and dissolution, and agrochemical inputs (Custodio 1997, Vengosh & Rosenthal 1994). These salinisation processes depend very much upon the local conditions, whereas seawater intrusion and solute recycling from irrigation are intimately linked and depend to a lesser extend on the local settings.

Solutes which are extracted from irrigation wells and re-distributed on fields, will sooner or later be returned to the groundwater again by solute return flow from irrigation, if they do not leave the system by drains or surface run-off or other processes (e.g. chemical processes and plant uptake). This leads to solute recycling, since the same solute may return to an irrigation well several times, increasing salinisation. Seawater intrusion, being the second salinisation process under study, is strongly enhanced in overexploited coastal aquifers, where the groundwater table is lowered below the mean seawater level causing landward directed movement of seawater towards pumping wells.

Although seawater intrusion and solute recycling are completely different salinisation processes, they are both related to the exploitation of a coastal aquifer and therefore interconnected. The main difference between solute recycling and seawater intrusion (and other salinisation processes such as geogenic salt and agricultural additives) is that solute recycling does not actually add any solutes to the system but can lead to salinisation by re-distribution of solutes that have been imported into the system by other salinisation processes. Also, seawater intrusion is completely governed by the hydrodynamic setting, which partly results from the exploitation schemes, whereas solute recycling from irrigation additionally depends on the irrigation scheme, the vegetation and soil cover, and climatic factors. Proper identification of these two distinctly different salinisation processes can be of critical importance, since, as shown in this thesis, proposed remedial measures based on assuming that only one or the other of the processes is operative can virtually be opposed.

1.2.1 Solute return flow from irrigation, and solute recycling

In irrigated agriculture, most salinisation problems are caused by strong evapotranspiration of the applied irrigation water or by direct evaporation from shallow water tables, leading to salt accumulation in the root zones and reducing the yields, particularly in semi-arid and arid regions (e.g. Shainberg & Shalhevet 1984). For plant growth, flushing of solutes below the root zone, either to the groundwater or to drains, is crucial, and for economic reasons, minimising the fraction of deep percolation is important (van Schilfgaarde 1984). It is estimated, for example, that one hectare of irrigated crop land in the Ebro Valley yields 20 tons of salt per year (Aragüés et al. 1985) from solute return flow from irrigation. Again, in places where irrigation takes place with extracted groundwater, flushing of the solutes to the groundwater will lead to solute recycling.

Hence the flushed solutes will be transferred by solute return flow or solute recycling to the receiving water bodies, the groundwater or the surface water, causing contamination and leading to

deterioration of the water resources (e.g. Bouwer 1987). These very resources, however, are the basis of irrigated agriculture, leading to the vicious circle which has been observed in many areas over the past decades, and calling for sustainable solutions. As Beltrán (1999) has pointed out, optimal *soil* salinity control is not necessarily the optimal *groundwater* salinity control and different salinity effects induced by irrigation require management solutions exceeding the field and farm scale. The phenomenon of solute recycling from irrigation can result in continuously increasing groundwater salinisation, since the same solutes are continuously being extracted, redistributed on the irrigated surfaces, then concentrated by evapotranspiration and eventually flushed to the groundwater, as irrigation proceeds.

1.2.2 Seawater intrusion

In contrast to solute recycling from irrigation in coastal areas, seawater intrusion is a well known and well-documented phenomenon that affects coastal aquifers around the world. Seawater intrusion is defined by Freeze and Cherry (1979) as the migration of seawater into fresh water aquifers under the influence of groundwater development and exploitation. Seawater intrusion becomes a problem in coastal areas where fresh water aquifers are hydraulically connected with seawater. When large amounts of fresh groundwater are withdrawn, landward-directed hydraulic gradients cause flow of seawater towards the pumping wells. This phenomenenon has been intensively studied for over a century, starting with Badon Ghijben (1888) and Herzberg (1901), who described the interface geometry between the seawater and fresh groundwater by accounting for the difference in density between freshwater and seawater.

1.3 Irrigation management and groundwater management - the need for an integrated approach

Over-exploitation in coastal aquifers is to a high degree caused by irrigated agriculture and therefore it can be expected that both irrigation-induced as well as seawater intrusion-related salinisation occur in combination. The two main groundwater salinisation problems outlined above, solute return flow from irrigation and seawater intrusion, are major fields of research, but to a large extend in different disciplines. The former is a topic mainly treated by soil scientists and agronomists, with focus on soil and drainage water salinisation, while seawater intrusion is a major research topic in hydrogeology, focussing on salinity distributions and evolutions within the groundwater. The major aim of irrigation schemes is to avoid or minimise soil salinity, whereas the fate of the solutes as they percolate downward beneath the root zone is less important. In contrast, groundwater management solutions in coastal aquifers designed by hydrogeologists focus on the prevention of seawater intrusion, since this process is more directly related to groundwater dynamics. Hence, what we often observe in coastal aquifers is that the two management schemes

coexist, but not in a coordinated way. The first seeks to flush the accumulated solutes out of the root zone into the aquifer and the second seeks to protect the groundwater from seawater intrusion. The effect of solute return flow and solute recycling as a major process causing groundwater salinisation is therefore often left unattended by both management schemes, although, in a non-coastal context, this salinisation process would be addressed with priority.

A major issue is, therefore, to identify the different salinisation processes in coastal settings. This has mainly been done by means of hydrochemical investigations. As examples, Stigter et al. (1998), El Alcheb et al. (2001) and Kass et al. (2005) use hydrochemical approaches to identify different salinisation sources, and have thus identified solute return flow from irrigation in different coastal aquifers around the Mediterranean region. Cardona et al. (2004) investigated a coastal aquifer in Mexico where they identified three superimposed salinisation mechanisms. They found that solute return flow from irrigation was the most important factor, followed by the dissolution of geogenic salt deposits, and then, but only in the vicinity of the coast, by seawater intrusion. They observed that the groundwater management had been done in the belief that seawater intrusion was the main cause of groundwater quality degradadtion. The management scheme was based on the successive landward displacement of salt-affected wells, but these were rapidly affected by salinisation again, since solute return flow from irrigation, and not seawater intrusion, was the main salinisation mechanism. Hence, the design of adequate groundwater management schemes related to salinisation problems in coastal irrigated areas depends on the correct identification and understanding of the different involved processes.

1.4 The management dilemma - an illustration from Cyprus

Many of the ideas in the present thesis were developed during work on Cyprus, and the Akrotiri aquifer, west of Limassol, in southern Cyprus, is the subject of one of the chapters (Chapter 6). The Akrotiri aquifer is a good illustration of the groundwater management dilemma, outlined above. It underlies a coastal irrigated area and has been managed in the belief that seawater intrusion is the only salinisation porcess. In the FAO Information System on Water and Agriculture (www.fao.org/ag/agl/aglw/aquastat/countries/cyprus/), one can read that other processes, such as soil salinisation and water-logging, are not present in Cyprus, although it is noted that contamination of groundwater with fertilizers is of concern in certain areas, where agriculture is intensively practiced.

Groundwater degradation in the Akrotiri aquifer, being the largest coastal aquifer in Southern Cyprus, was becoming very alarming by the end of the 1980's and pushed the authorities to declare the aquifer a 'water conservation area' in the early 1990's. This implied an authority-controlled groundwater management scheme to prevent further seawater intrusion (thought to be the only salinisation mechanism), assigning extraction rates to each farmer according to the size of

the plots. Extractions beyond the fixed amount were/are fined and regularly controlled by means of installed water meters. The winter 2003/2004 was exceptionally wet, causing a significant rise of the groundwater table and measurable retreat of the seawater/freshwater front. However, several hectares of orange trees situated far from the seashore died within few weeks, as a consequence of water-logging followed by a very hot period, enhancing evapotraspiration and salt accumulation in the root zone (Fig. 1.1). Although the land owners had seen that evaporation from the shallow groundwater led to salt accumulation, causing the tree deaths, they were not immediately allowed by the authorities to extract any groundwater to lower the water table below the root zone, in order to save the trees. This example goes to illustrate the importance of the spatial identification of the vulnerability of a system towards different salinisation processes. It also shows that remedial measures can be opposed. Limiting extraction rates prevents or reduces seawater intrusion, whereas, in the case shown in Fig.1.1, increasing the extraction rate to lower the water table would have been the only immediate measure to save the trees from dying.

Fig. 1.1: Several hectares of orange trees died within few weeks due to water-logging and salt accumulation in the root zone after an exceptionally wet winter. The oranges around the trunks show that the trees died rapidly, since the groundwater table could not be lowered by surplus extraction due to the adopted groundwater management scheme.

1.5 Salinisation modelling approaches

We first became aware of the problem of solute recycling when studying and modelling another aquifer in southern Cyprus (the Kiti aquifer, see Chapter 2). This led to an attempt to test and

develop different salinisation modelling approaches, since simulation approaches linking seawater intrusion and solute recycling are rarely found in the literature.

Numerous seawater intrusion models have been developed in the past decades, taking into account the bouyancy effects produced by the density difference between seawater and fresh groundwater. Classical theoretical examples of seawater intrusion were modelled by Henry (1959), Frind (1982) and Huyakorn (1987), and since these pioneer works, three-dimensional density-dependent flow and transport models have been made for many real case studies (e.g. Essaid 1990, Xue et al. 1995, Larabi et al. 1997, Voss 1999, Oude Essink 2001). Such modelling is becoming increasingly important for management purposes. As an example, Cheng et al. (2000) present analytical solutions and structured messy genetic algorithms for pumping well optimisation with the aim of maximising the total pumping rate subject to the constraint of no seawater intrusion.

With respect to modelling approaches addressing the process of irrigation-induced salinity alone (i.e. not in areas threatened simultaneously by seawater intrusion), one of the earliest conceptual hydrosalinity models for predicting the salt load in irrigation return flows was developed by Tanji (1977). This model was later used to establish mass budgets for an irrigated area in Spain (Aragüés et al. 1985). Prendergast et al. (1994) developed an analytical expression describing the solute recycling process, with which the long-term salinity evolution at a well can be predicted and the sustainability of conjunctive water use for salinity control in irrigated areas was evaluated.

Modelling approaches in seawater-intruded coastal areas reported in literature rarely introduce the extracted *solute* mass back into the system, although in reality the extracted solutes from irrigation wells are distributed on the irrigated fields, and will therefore be recycled into the groundwater system, sooner or later. Solute recycling from irrigation may not always be of importance, but in areas where irrigation rates exceed infiltration rates, i.e. in semi-arid and arid regions, its impact can be expected to be considerable and needs to be evaluated.

1.6 Aim and structure of the present thesis

The main objective of this thesis is the quantitative investigation of solute recycling induced by irrigation, and its implications for the overall salinisation in coastal settings. Since the modelling approaches proposed in the literature to simulate seawater-intruded areas rarely account for the coupled and superimposed effects of solute recycling and seawater intrusion, appropriate simulation procedures have been developed. Based on a mathematical description of the solute recycling process, a direct simulation approach is developed which allows its simulation with any standard groundwater simulation package for average hydraulic steady state conditions. For transient state hydraulic conditions, the solute recycling process is solved numerically in a time-stepping procedure. Since distinction between the two superimposed salinisation processes is an important step in the design of adequate remedial measures and effective groundwater

management, a procedure is proposed with which the simulated salinisation derived from solute recycling can be decoupled from the effects of seawater intrusion. This allows identification of the spatial impact and the superposition of the two salinisation mechanisms. Based on the developed simulation procedures, a framework for a salinisation risk assessment is established, treating seawater intrusion and solute recycling from irrigation separately, which in future could be used as a dynamic tool and be linked to optimisation procedures. The application of the proposed salinisation risk assessment methodology to a real case study and comparison with independent data obtained from field investigations leads to a discussion of the data requirements for a successful elaboration of a quantitative salinisation risk assessment.

The structure of the thesis follows from this line of argument.

Chapter 2 shows how the solute recycling problem in coastal irrigated areas was identified during the elaboration of a seawater intrusion model for the Kiti aquifer in Southern Cyprus in 2001. The results of the field investigations and the simulation results clearly indicated that solute recycling from irrigation was an important salinisation mechanism, superimposed on the effects of seawater intrusion. The results of this case study, which instigated the investigation of the problem on a more general basis (in the present thesis), have been published in a recent paper (Milnes & Renard 2004).

In Chapter 3, a mathematical analysis is carried out to identify the parameters which govern the solute mass evolution at irrigation wells in response to solute recycling, with a view to defining a distributed solute source on irrigated surfaces. A formulation for the transient solute mass flux at a well is developed for arbitrary advective-dispersive systems by means of the transfer function theory (Jury 1982). This allows prediction of the well response and can thus be used to define a distributed ‘recycling source’ term in the general form of the advection-dispersion equation in arbitrary systems for average hydraulic steady state conditions.

In Chapter 4, the spatial groundwater salinisation induced by solute recycling is investigated by means of different simulation procedures. Direct simulation of solute recycling is proposed for steady state hydraulic conditions, whereas a numerical time-stepping procedure is adopted for transient hydraulic conditions.

The results of Chapters 3 and 4 are then, in Chapter 5, placed in a coastal context and a framework for a salinisation risk assessment methodology is proposed, in which seawater intrusion and solute recycling salinisation are evaluated separately.

In Chapter 6, the developed quantitative risk assessment methodology is applied to a real case study, the Aktoriri aquifer in Southern Cyprus, and the results are compared with the distribution of dominant salinisation processes as derived from hydrochemical fingerprints and field experiments. The real case application leads to a discussion of monitoring requirements related to

the solute recycling process in coastal areas. Based on the mathematical description of the solute recycling process in Chapter 3, key-factors are then identified with which to qualitatively estimate the spatial impact of the solute recycling process using classical field data. Such uncostly estimations can be used in a preliminary stage, for instance to implement monitoring networks, necessary to obtain data for the quantitative salinisation risk assessment.

In Chapter 7, the main conclusions are summarised, and limitations and future perspectives discussed.

CHAPTER 2

THE PROBLEM OF SALT RECYCLING AND SEAWATER INTRUSION IN COASTAL IRRIGATED PLAINS: AN EXAMPLE FROM THE KITI AQUIFER (SOUTHERN CYPRUS)

Ellen Milnes & Philippe Renard

Journal of Hydrology, **288**, 327-343, 2004

Modification with respect to the published version: The different notions used to describe 'solute recycling' were replaced accordingly for the purpose of consistency with the rest of the document (apart from in the title)

Abstract

In coastal aquifers which are exploited for agricultural purposes, salinisation by solute recycling from irrigation is superimposed on the effects of seawater intrusion. Water quality degradation of irrigation pumping wells caused by seawater intrusion further enhances salinisation by irrigation, as the extracted solute mass is recycled and is not withdrawn from the system.

The main objective of this study is the investigation and quantification of the impact of solute recycling from irrigation relative to seawater intrusion. A *solute mass budget* was established by expressing the recycled solute mass as fraction of the extracted solute mass from wells by means of a *solute mass return flow ratio* (r_r). The obtained expression for the relative contribution of solute recycling from irrigation is an exponential function of the return flow ratio r_r and normalised time $\bar{t}$ only (time versus system turnover time).

This expression was applied to an example, the Kiti aquifer (Southern Cyprus), where field observations suggest that solute recycling is a super-imposed salinisation mechanism. The contribution from solute recycling normalised with the solute mass flux entering from the sea after 20 years was found to be 1.5-8.5% in the extracted solute mass flux, depending on the estimation of the system turnover time.

Subsequently, a coupled finite element model, reflecting the main features of the Kiti aquifer was used as a possible 'synthetic reality', to test the relative impact of solute recycling on the spatial salinity distribution in a complex hydrogeological and geometrical setting. This was done by running two simulation scenarios: 1) recycling all the extracted solute back into the system and 2) leaving solute recycling aside and comparing the results of these two scenarios relative to eachother and to patterns observed in the field. The results showed, that by introducing solute recycling into the numerical model as coupled boundary condition does not only respect the overall solute mass balance but can have an important impact on the salinity distribution, leading to a significant spreading of the mixing zone, similar to what was observed in the field.

2.1 Introduction

In numerous coastal aquifers, particularly in semi-arid and arid regions, over-exploitation has led to groundwater quality degradation. As a consequence seawater intrusion has been intensively studied for several decades (see Bear et al. 1999 for a recent synthesis). The growing demand in groundwater resources is mostly linked to an intensification of agricultural activity, which is very

dependent on water from irrigation. In this work we focus on the effects of seawater intrusion combined with the super-imposed effects of groundwater quality degradation related to solute recycling from irrigation. The salinisation mechanisms governing seawater intrusion and solute mass recycling from irrigation are very different, but they are coupled by the fact that the water quality degradation observed in pumping wells, initially caused by seawater intrusion as a consequence of landward directed hydraulic gradients, is further enhanced by salinisation due to solute recycling from irrigation. Since the potential remedial measures are very different for seawater intrusion settings as opposed to irrigation return flow affected areas, it is important to distinguish between the two salinisation mechanisms and to understand how they are linked. Many geochemical techniques have been developed to identify different origins of salinity in coastal contexts, but they are often equivocal (e.g. Vengosh and Rosenthal 1994, Vengosh et al. 1999, 2002, Kolodny et al. 1999, El Alcheb et al. 2001, Kim et al. 2003).

The physics of seawater intrusion are rather well understood and numerical modelling approaches, using sophisticated software packages allowing density-dependent flow and transport simulations, are regularly used as tools to evaluate future salinity evolutions or for optimisation purposes (e.g. Essaid 1990, Xue et al. 1995, Gambolati et al. 1999, Voss 1999, Gordon et al. 2000, Oude Essink 2001, Paniconi et al. 2001). Unfortunately, in many cases the model applications are limited, on the one side, by the data availability, and on the other side, by the fact that, even under extremely controlled conditions, when all the physical properties of the medium are independently measured, the numerical models require a very fine discretisation to reproduce the results of physical experiments accurately (Johannsen et al. 2002). This shows rather clearly the limitations of what one could expect in a complex natural system when the geometry, the physical parameters, and the boundary conditions are not well defined.

Looking at the other side of the problem, groundwater quality degradation due to solute return flow and recycling from irrigation has received a lot of attention, particularly in the United States and Australia, in areas far from the sea. Authors such as Konikow and Person (1985), Bouwer (1987), Close (1987), Beke et al. (1993), and Prendergast et al. (1993) have focused on the establishment of solute mass budgets and on the quantification of the mechanisms of groundwater salinisation by the solute mass loading of the unsaturated soil due to irrigation practices and subsequent flushing and transfer to the groundwater body. Salinities up to 10 mS/cm can often be found in areas where miss-management and poor irrigation practices have led to groundwater deterioration.

The main objective of the present work is the investigation of the importance of solute recycling from irrigation relative to seawater intrusion based on an analysis of the behaviour of a *solute mass budget* as function of *solute recycling* from irrigation. A pertinent reason for evaluating the

contribution of solute recycling from irrigation, is if a long-term numerical flow and transport approach is envisaged. What we will call 'the classical numerical approach' used in seawater intrusion settings does not introduce solute recycling from irrigation as a coupled boundary condition, being a function of the extracted solute mass flux from the well boundary conditions. To give an example of a 'classical numerical approach', Sherif and Hamza (2001) discussed the possibility of mitigating seawater intrusion by pumping brackish water and using it for irrigating certain crops or developing green lands. In a 2D vertical model, the effect of pumping in the brackish mixing zone led to a reduction of the dispersion or mixing zone width. This is certainly true for the case where the pumped water is not used for irrigation but removed from the system (e.g. rejection back to the sea), but if it is supposed to be used for irrigation within the modelled system as suggested, it reflects a modelling approach, which does not comply with the true solute mass balance. Therefore, what we call the classical numerical approach yields 'best-case' results, since it removes all the extracted solutes from the system. The reason why solute recyclingfrom irrigation is not included in flow and transport models is that the physical process of solute redistribution from pumping wells onto the fields is a man-made process. Sometimes numerical approaches of seawater affected areas do include irrigation return flow from irrigation (e.g. Paniconi et al. 2001), but making the assumption that no solute recycling takes place. Others assign a fixed value to the contribution from solute return flow from irrigation, in which case the assigned value is not a function of the solutes extracted from well boundary conditions (e.g. Voss 1999).

The paper is subdivided into three main sections. In the first part, we develop a simplified transient solute mass budget, based on long-term average (steady-state) flow conditions. In the second section, an example from a coastal area in Cyprus, the Kiti aquifer, is presented. A field assessment of the salinisation combined with interpretation of historical data suggested that solute recycling is a superimposed important salinisation mechanism in the area, where agricultural activity is intensive. The impact of solute recycling is then assessed by the analytical expression established in the first section. In the third part, a coupled finite element flow and transport model is used for the purpose of testing the impact of solute recycling on the spatial salinity distribution in a complicated hydrodynamic and geometrical context.

2.2 Solute mass budget

In over-exploited coastal aquifers, most of the extracted water used for irrigation leaves the system by means of evapo-transpiration. The solutes remain and are concentrated within the unsaturated zone before they are leached and transported to the groundwater again when the soil is flushed by percolation of precipitation. The only possible losses of solutes in coastal aquifers are to the sea

and export of extracted water (e.g. water supply), being the two main system outlets. However, export of extracted groundwater is done for water with low solute contents and is therefore not an important salt sink, and in over-exploited aquifers the sea is more of a recharge area than a discharge area and is thus a source of salinisation, not a sink. Hence, the more a coastal aquifer is salinised, the less salt is exported and therefore, over-exploited coastal aquifers can be considered as solute traps.

In this section, our aim is to consider the over-exploited aquifer as a closed system and to evaluate the contribution of solute recycling to the overall salinisation (solute mass) of the system.

We make the assumption that the aquifer of interest is exploited in a regime of equilibrium with respect to flow. In other words, if only the fluxes of water are considered, the aquifer has reached steady state in which the reserves are not varying and pumping is fully compensated by the inflow from recharge and from seawater intrusion. Such a hypothesis can only be supported, if the chosen steady-state condition is based on long-term averages, and if the variations of the reservoir storage over the chosen long-term period can be neglected.

In the following, the aquifer is not discretised and therefore an average concentration $C(t)$ representing the 'perfect system mixture' of the entire aquifer will be considered. Even though we are aware of the fact, that operating with an average concentration does not provide any result in itself concerning the spatial solute distribution, it has been found very useful in isolating the contribution of solute recycling from irrigation from the salinisation effect due to seawater intrusion.

Assuming perfect mixing, the solute mass conservation can be written as the balance between the in-flowing and the out-flowing components:

$$\frac{\partial(\phi VC)}{\partial t} = \sum q_{\text{in}} c_{\text{in}} - \sum q_{\text{out}} C + S \qquad (2.1)$$

where C [ML^{-3}] represents the mean concentration of the system, ϕ [-] the porosity, V [L^3] the volume of the aquifer, $q_{\text{in/out}}$ [L^3T^{-1}] the fluid mass fluxes, c_{in} the respective inflowing concentrations [ML^{-3}] and S [MT^{-1}] the sources and sinks. The specific components of Eq. (2.1) in a coastal environment are defined and illustrated in Fig. 2.1.

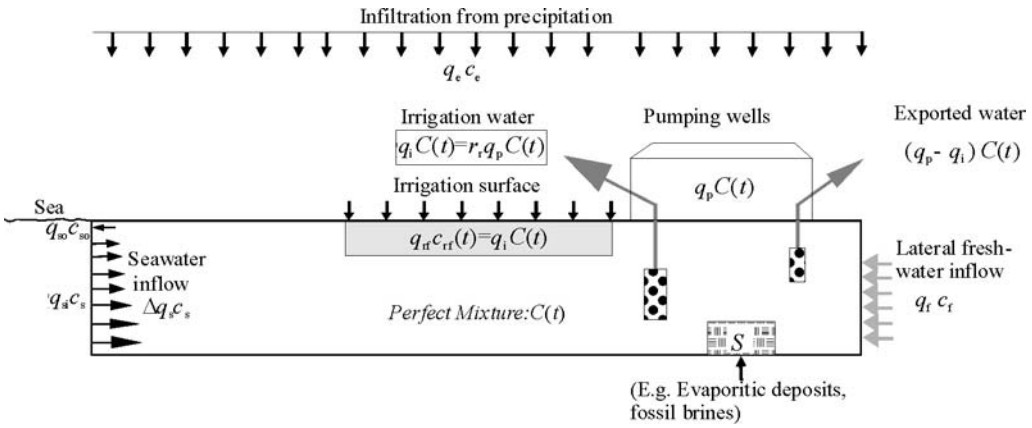

Fig. 2.1: Schematic illustration of flow components and their respective concentrations. For average (steady state) flow conditions, the sum of the in and out going flow rates equal zero. Both the sea and freshwater concentrations are considered as time-invariant.

We then define a solute mass return flow ratio r_r [-] as the ratio of the solute mass flux entering the system by solute recycling versus the extracted solute mass flux from wells:

$$r_r = \frac{q_{rf} c_{rf}(t)}{q_p C(t)} \tag{2.2}$$

with q_{rf} representing the vertical flux of water which percolates down to the groundwater below irrigated surfaces, c_{rf} (t) the corresponding concentration, q_p the extraction rate, and $C(t)$ the concentration of the extracted fluid. For r_r=0, all the extracted solute mass is exported from the system, and for r_r=1, the entire extracted solute mass is recycled.

Since $c_{rf}(t)$ in Eq. (2.2) is usually unknown, another equivalent definition is required to determine r_r. Defining q_i as the amount of the extracted fluid flux q_p which is not exported out of the system, thus representing the part used for irrigation (with $C(t)$ being its concentration), another expression can be found for r_r. Since the solute mass flux $q_i C(t)$ applied for irrigation is equal to the solute mass flux which will be recycled into the aquifer system, replacing $q_{rf} c_{rf}(t)$ in (2) by $q_i C(t)$ yields,

$$r_r = \frac{q_i}{q_p} \tag{2.3}$$

The return flow ratio is thus defined as the proportion of extracted fluid flux used for irrigation (containing the solute mass which will be recycled to the system) relative to the total extracted

fluid flux. This quantity can usually be estimated fairly well in irrigated aquifers, thus allowing determination of r_r.

According to the definition of r_r, we can express the solute mass flux derived from solute recycling $m_{rf}(t)$ by means of the extracted solute mass flux as follows:

$$m_{rf}(t) = q_i C(t) = r_r q_p C(t) \tag{2.4}$$

The other terms in Eq. (2.1) are characterised by time-invariant known concentrations (Fig. 2.1). Along the coastline, and due to the fact that we are considering an over-exploited aquifer, we assume that the balance of the fluxes $\Delta q_s = (q_{si} - q_{so})$ is always positive and that $q_{si} >> q_{so}$, with q_{si} being the seawater flux entering the system along the shoreline and q_{so} the fluid flux leaving the system along the shoreline. Therefore, the concentration of Δq_s is close to seawater concentration and will be approximated in the following by seawater concentration c_s, which will lead to a slight underestimation of the entering solute mass flux. The lateral freshwater inflow q_f has a mean freshwater concentration c_f and finally, the effective vertical infiltration q_e is given the concentration of rainwater c_e. All the above-mentioned constant components can be used to define the total constant incoming solute mass flux (m_i) as follows:

$$m_i = \Delta q_s c_s + q_f c_f + q_e c_e \tag{2.5}$$

Making use of Eqs. (2.4) and (2.5) the in-flowing and out-flowing components in Eq. (2.1) can be written as follows,

In: $$\sum q_{in} c_{in}(t) = m_i + m_{rf}(t) = m_i + r_r q_p C(t) \tag{2.6}$$

Out: $$\sum q_{out} C(t) = q_p C(t) \tag{2.7}$$

For reasons of simplicity the source term in Eq. (2.1) will be left aside, although it can be added at any time.

Combining Eqs. (2.6) and (2.7) allows us to reformulate Eq. (2.1) as follows,

$$\frac{\partial C}{\partial t} = \frac{1}{\phi V}\left[m_i + (r_r - 1) q_p C(t) \right] \tag{2.8}$$

for which the solution of the differential Eq. (2.8) with initial condition $C(0)=0$ is:

$r_r < 1$ $$C(t) = \frac{m_i}{q_p(1-r_r)}\left[1 - e^{-\frac{q_p(1-r_r)t}{\phi V}}\right] \quad (2.9)$$

$r_r = 1$ $$C(t) = \frac{m_i}{\phi V}t \quad (2.10)$$

For a return flow ratio r_r=1 the concentration will increase linearly with time.

Still making the hypothesis that the well extractions are the only exiting fluxes, the system turnover time t_0 being the ratio of the porous volume to steady flow rate reads:

$$t_0 = \frac{\phi V}{q_p} \quad (2.11)$$

Introducing t_0 into Eq. (2.9) and defining the ratio t/t_0 as $\bar{t}$ leads to the following expressions for the mean system concentration after reformulation,

$r_r < 1$ $$C(\bar{t}, r_r) = \frac{m_i}{q_p(1-r_r)}\left[1 - e^{-\bar{t}(1-r_r)}\right] \quad (2.12)$$

$r_r = 0$ $$C(\bar{t}) = \frac{m_i}{q_p}\left[1 - e^{-\bar{t}}\right] \quad (2.13)$$

For values of r_r < 1 the concentration of Eq. (2.12) will tend towards an asymptotic steady state concentration at infinity which equals the ratio between the constant incoming solute flux m_i and the exported fluid flux $q_p(1-r_r)$:

$$C(\infty) = \frac{m_i}{q_p(1-r_r)} \quad (2.14)$$

Eq. (2.13) describes the mean system concentration evolution for the case that no recycling takes place. When comparing it to Eq. (2.12) one can see that $C(\bar{t}, r_r)$ will always be higher in the case of existing recycling than for the case $C(\bar{t}, r_r = 0)$.

We define $m_{pr}(\bar{t}, r_r)$ as the solute mass flux extracted from pumping wells originating from solute recycling from irrigation. To estimate it, we simply make the difference between the total solute mass flux $C(\bar{t}, r_r)q_p$ and the solute mass flux if no recycling takes place $C(\bar{t}, r_r=0)q_p$. The contribution of solute recycling can then be expressed as follows:

$$m_{pr}(\bar{t}, r_r) = C(\bar{t}, r_r)q_p - C(\bar{t}, r_r = 0)q_p \tag{2.15}$$

Using Eqs. (2.12) and (2.13) and normalising $m_{pr}(\bar{t}, r_r)$ with m_i, the following expression can be written for the relative contribution of solute recycling $\bar{m}_{pr}(\bar{t}, r_r)$ to the overall extracted solute mass flux, being a function of the normalised time $\bar{t}$ and the return flow ratio r_r only:

$$\bar{m}_{pr}(\bar{t}, r_r) = \frac{m_{pr}(\bar{t}, r_r)}{m_i} = \frac{1}{(1-r_r)}\left[1 - e^{-\bar{t}(1-r_r)}\right] - \left[1 - e^{-\bar{t}}\right] \tag{2.16}$$

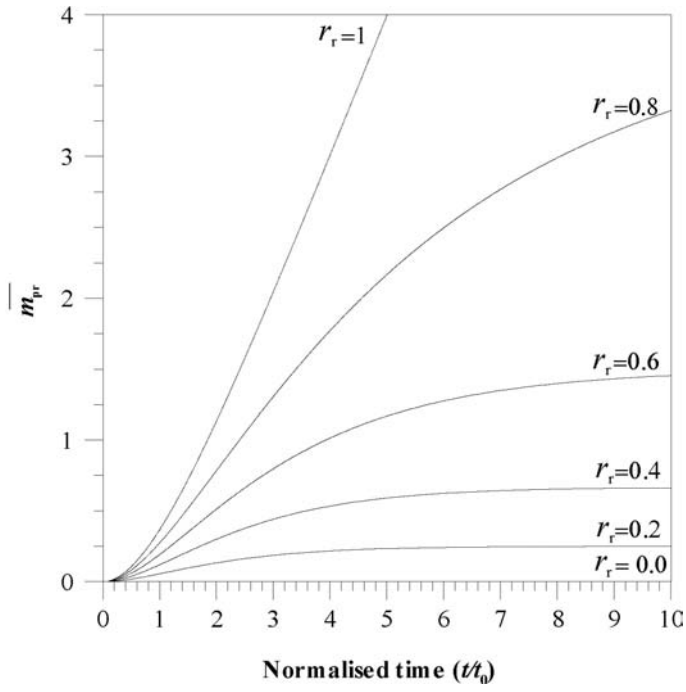

Fig. 2.2: Graphical representation of Eq. (2.16) with the dimensionless time $\bar{t}$ (t/t_0) as *x*-axis versus the relative contribution of solute recycling from irrigation $\bar{m}_{pr}(\bar{t}, r_r)$. This dimensionless graphic is valid for any system for which the formulated assumptions are valid.

Fig. 2.2 is the graphical representation of Eq. (2.16) for a range of different return flow ratios. If the turnover time t_0 is known, the relative contribution of solute recycling $\bar{m}_{pr}(t)$ can easily be deduced for any characteristic time t of interest (e.g. simulation time-span, exploitation time-span) and return flow ratio r_r. It reveals, that the relative contribution of solute recycling $\bar{m}_{pr}(\bar{t}, r_r)$ increases with increasing r_r and increasing $\bar{t}$. In other words, for one and the same extraction rate and return flow ratio, but for different reservoir sizes, the smaller reservoir with a shorter turnover time will be more affected by solute recycling from irrigation, since $\bar{t}$ is bigger. On the other hand, for the same size reservoir and extraction rate, an increasing return flow ratio r_r will increase the impact of solute recycling from irrigation.

The relative impact of solute recycling is thus completely conditioned by the ratio of the characteristic time t relative to the mean system turnover time t_0, and by the return flow ratio r_r.

2.3 An example from Southern Cyprus: the Kiti aquifer

At this point we would like to present a case study carried out in Southern Cyprus, which initially triggered the investigation of the importance of solute recycling from irrigation as a potential super-imposed coupled mechanism to salinisation of coastal aquifers. The assessment of the spatial and temporal behaviour of the salinity distribution within the aquifer revealed that the smaller the saturated thickness and the more intensive agricultural activity was, the wider was the mixing zone. This observation was not directly interpretable within the usual seawater intrusion paradigm and led to this quantitative investigation of the importance of solute recycling from irrigation. In this section we present an overview of the field observations and then apply the solute mass balance approach elaborated in section 2.2 to evaluate the potential impact of solute recycling for the Kiti aquifer.

2.3.1 Hydrogeological context

The Kiti aquifer is situated in the east of Southern Cyprus, south of Larnaca (Fig. 2.3), an area with a semi-arid climate, forming a plain with elevations reaching up to 20 masl in the north and with a surface area of approximately 30 km^2.

In the Kiti aquifer, as in numerous coastal aquifers, over-exploitation has led to groundwater quality degradation during the past decades. Locally, over-exploitation temporarily diminished the hydraulic head by as much as 12 m below sea-level in the early 80s, leading to pronounced landward directed gradients, and thus to an acceleration of seawater intrusion.

Groundwater abstraction, mainly for irrigation, was an average of 3×10^6 m^3/year up to 1981, but was subsequently reduced to 1.8×10^6 m^3/year by the mid 90s and to $1.3\text{-}1.5\times10^6$ m^3/year in recent years. The water table recovered somewhat in the 90s but is still below sea level during the main pumping season.

The shoreline forms the southern and, partially, the eastern boundary of the aquifer, while two salt lakes are situated in the northeast. The aquifer system is layered, consisting of an upper, unconfined, alluvial aquifer separated from a lower, confined carbonate aquifer by Pliocene marls (Fig. 2.4), a similar hydrogeological setting as presented by Frind (1982). The inland aquifer limit was defined as the area within which the alluvial aquifer is saturated. The position of the bedrock was deduced from borelog records and geophysical data. The saturated thickness of the unconsolidated alluvial aquifer ranges from 3-10 m in the east to a maximum of 50 m in the west, where a Miocene paleo-erosional surface of the Thremithos River has formed a gully-shaped channel in the bedrock. Fig. 2.4 shows an idealized N-S geological cross-section through the Kiti aquifer system, with indicated zones of potential drainage from the carbonate aquifer towards the alluvial aquifer and also the areas where the alluvial aquifer is saturated. The Miocene NS-directed paleo-channel of the Tremithos River can be clearly seen in the bedrock topography.

Annual recharge by infiltration of precipitation and subsurface inflow was estimated to be an average of 1.8 to 2.5×10^6 m^3/year for the 1980s (Schmidt et al. 1988).

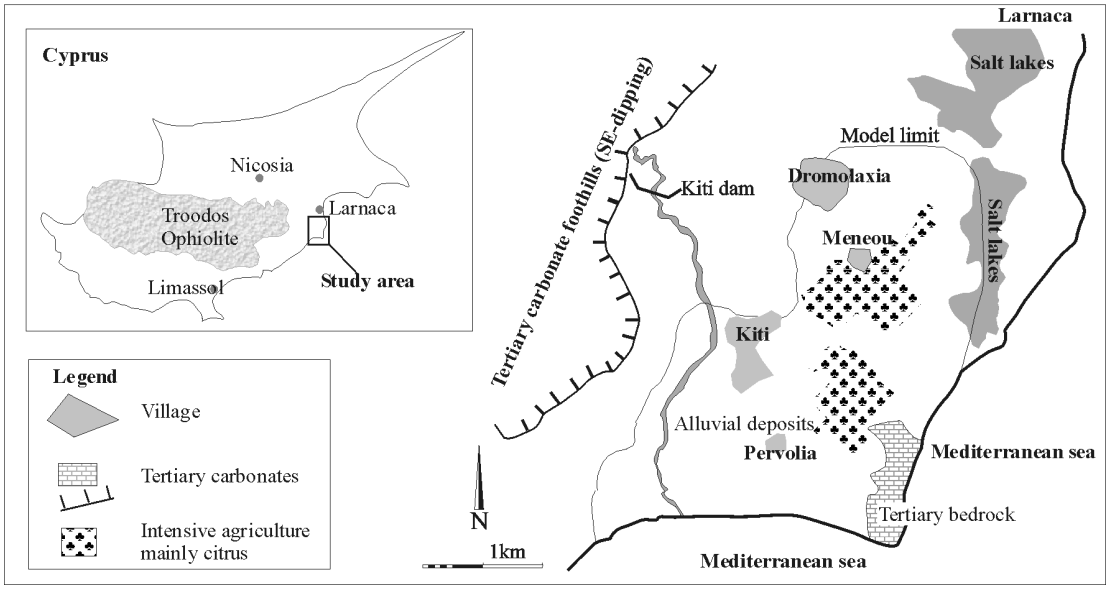

Fig. 2.3: Main physiographic features of the Kiti area, Southern Cyprus, showing the limit of the Kiti aquifer with respect to the sea, the main villages, the most important agricultural areas, the salt lakes and the outcropping bedrock (carbonates).

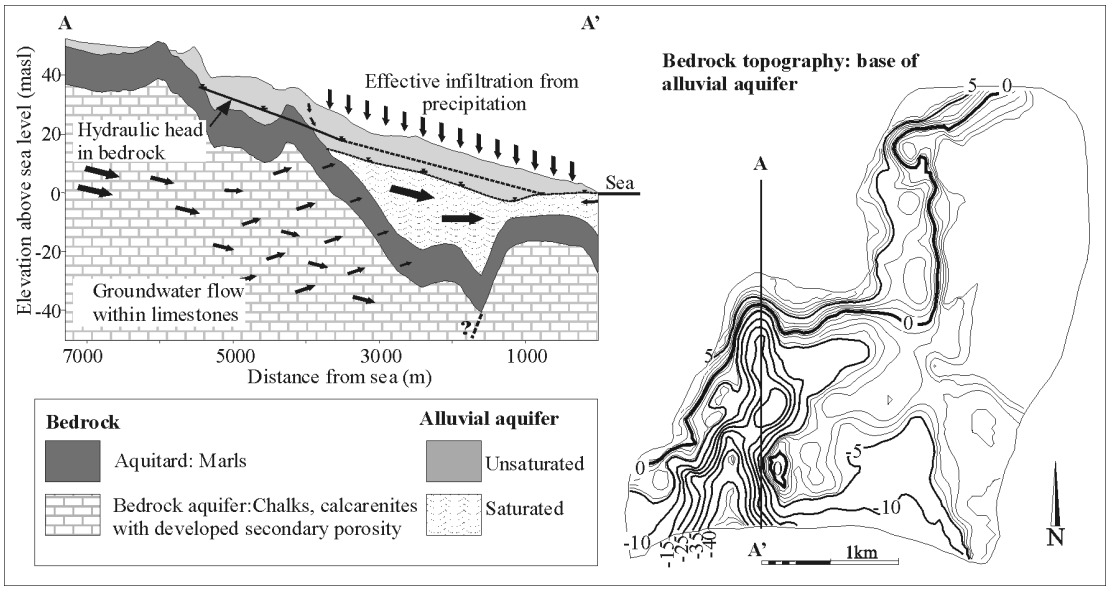

Fig. 2.4: Simplified geological N-S-cross-section through the Kiti aquifer system visualising the conceptual model based on geologic and hydrodynamic data. The bedrock topography or base of the alluvial aquifer is shown, revealing the prominent Miocene NS-oriented paleo-channel in the west.

2.3.2 *Assessment of salinisation*

To characterise the seawater intrusion in the Kiti aquifer, historical chloride data were compared to the established time-equivalent piezometric maps. The most pronounced hydraulic depressions were found to be situated in the west, in the area of the paleo-channel, whereas the most prominent salinity anomalies were generally observed in the central zone. Fig. 2.5 shows the distribution of the electrical conductivity as derived from 76 measurements taken at depths of app. 3-5 m below the water table in open wells within the alluvial aquifer. In the area of the Tremithos paleo-channel, the seawater intrusion has advanced far inland and the salinity iso-contours indicate a relatively narrow transition zone between the seawater and the freshwater. In the central area, where the saturated alluvial aquifer thickness is only a few meters and agriculture is intensive, a large tongue-like anomaly reaches 3 kilometres inland. In this area, a high salinity anomaly (exceeding 10 mS/cm) is laterally disconnected from the seawater front. Most of the central area is characterised by electrical conductivities between 2-6 mS/cm and the transition is blurred. The salinity distribution appears patchy with locally high variations. Note that pumping wells used for irrigation in the entire area are not abandoned until the electrical conductivities exceed 5-8 mS/cm. Agricultural redistribution of the solute mass on fields goes hand in hand with the addition of nutrients (mostly nitrates) and pesticides. Sampling for chemical analysis (major ions) was done in 20 wells in the area. The results revealed a prominent impact of agriculture in all the samples taken within the central plain, with nitrate concentrations reaching up to 360 ppm. A positive correlation

between chloride and nitrate concentration can be seen on Fig. 2.5, a feature that cannot be explained by pure mixing of the two end-members (seawater-freshwater). Evaporation of irrigation water leads to a mass loading within the unsaturated zone which is subsequently flushed and leached during heavy rainfall events (Stigter et al. 1998, Sites and Kraft 2000, Pearce and Schumann 2001).

These indications support the hypothesis that solute mass recycling from irrigation is a vertical salinisation mechanism superimposed on to the lateral seawater intrusion process, even though other salinity sources cannot be completely excluded. However, the existence of geogenic salt sources, typically being Messinian deposits in the Mediterranean area (Hsü 1973), have most probably been eroded in the Kiti area, since they are not found in any of the borelog records and they do not crop out in the catchment of the Kiti aquifer. A geochemical survey in the region carried out by Ploethner et al. (1986) does not clearly reveal any characteristic water facies related to evaporitic deposits but mentions the possible existence of fossil brines.

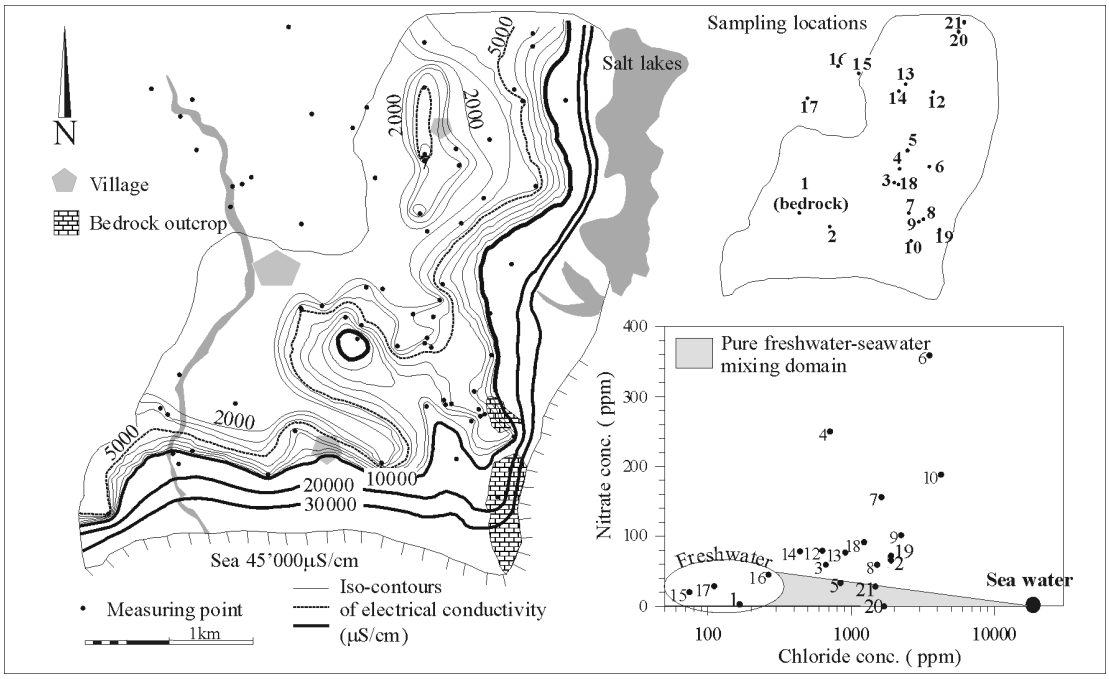

Fig. 2.5: Electrical conductivity distribution as derived from 78 measurements (black dots) in the alluvial aquifer (May 2001). NO_3 versus chloride concentrations are shown with chloride concentrations on a logarithmic scale. The nitrate concentrations are positively correlated in the central plain with the chloride concentrations. The area of pure seawater-freshwater mixing is indicated, and can be seen to exclude most of the samples.

2.3.3 Evaluation of solute recycling component in the Kiti aquifer

According to Eq. (2.16), we can estimate the potential impact of solute recycling from irrigation for the Kiti aquifer. The mean system turnover time t_0 and the return flow ratio r_r had to be estimated first. In the Kiti aquifer, an average of 90% of the average extracted water q_p has been and is used for irrigation purposes, only a few water supply wells are situated further inland (10%). Assuming that the irrigation techniques are sufficiently optimised that run-off can be neglected, we can estimate the return flow ratio to be r_r= 0.9. The saturated aquifer volume (V) for the entire aquifer-aquitard system was found to be app. 8 10^8 m^3, as derived from the constructed 3D body, with a porosity (ϕ) in the range of 8-20%, being an estimated average value for the combination of the overlying silt-clay-rich sandy, gravely deposits and the underlying marls and limestones (Höltin, 1996). The mean system porosity is the most sensitive parameter, since it significantly influences the system turnover time t_0, and therefore it is better to define a porosity range rather than fixing a single value. The average extraction rate q_p for the past 20 years has been app. $1.5\times10^6 m^3$/year, leading to a mean system turnover time of 42-100 years. Introducing these values into Eq. (2.16) for t_0=42 years and t_0=100 years and a return flow ratio r_r=0.9 provides a bandwidth for the relative temporal impact of solute recycling (Fig. 2.6). The sensitivity of this approach with respect to the estimation of the mean turnover time can be seen. Doubling the reservoir (by doubling the porosity) reduces the relative impact of solute recycling exponentially with time. For the time-span we are interested in simulating in the following (20 years), the relative impact of solute recycling can be seen to lie between 1.5-8.5% of the entering solute mass flux. This can be very significant in terms of absolute concentrations, depending on the absolute value of m_i.

If, on the other hand, we are interested in evaluating whether the observed salinity distribution in the field is partly related to solute recycling we can consider a 50 year-span, which corresponds to the time that the aquifer has been heavily exploited. For this time-length, the contribution from solute recycling from irrigation lies between 8-42%, if the average extraction rate used in the solute mass budget is representative for the past 50 years. In the Kiti aquifer, however, the average extraction rate for the past 50 years is higher than for the past 20 years, which suggests an even more pronounced impact of recycling from irrigation than what was determined above. According to this evaluation, the salinity distribution observed in the Kiti aquifer is likely to be related to both seawater intrusion and solute recycling from irrigation.

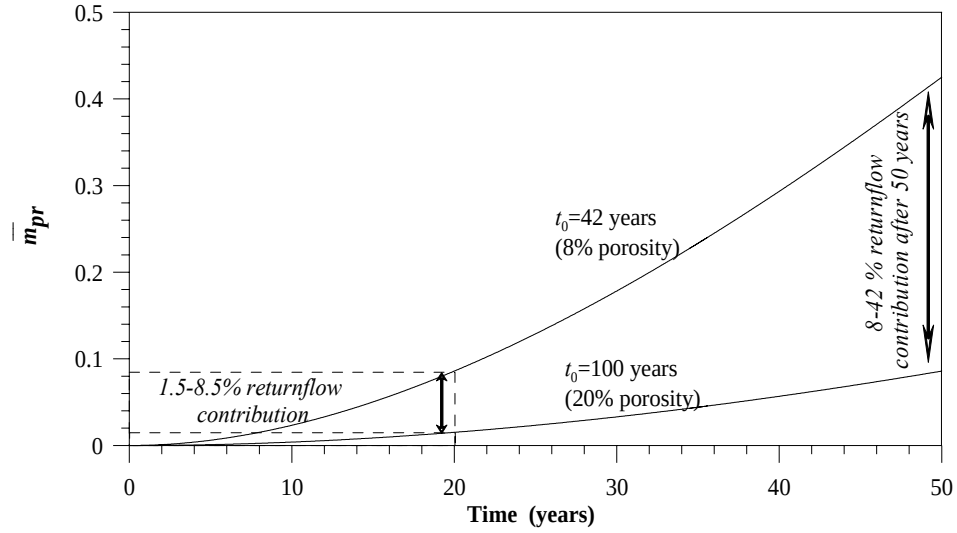

Fig. 2.6: Evaluation of relative solute recycling contribution $\bar{m}_{pr}$ in the Kiti aquifer based on the average extraction rates of the past 20 years for a range of estimated average system porosity (8%-20%). After 20 years the relative contribution can be seen lie between 1.5-8.5% of the solute mass flux entering from the sea. Projection to 50 years (corresponding to historical exploitation time-span) indicates, that 8-42% of extracted solute mass flux is potentially derived from recycled solute mass, depending on the estimated mean porosity.

2.4 Density dependent flow and transport simulations

Based on the field investigations and historical data as well as former work carried out in the area (Jackovides et al. 1982, Schmidt et al. 1988), a coupled finite element flow and transport model was established, reflecting the conceptual model of the Kiti aquifer (Fig. 2.4). The finite element code FEFLOW (Diersch 1998) was used to build the three-dimensional model of the Kiti aquifer.

In the following, a description of the model and its boundary conditions will be given. Even though the parameter distribution is a result of a calibration procedure, it is very likely that the model suffers from non-uniqueness. We therefore used the model as a possible 'synthetic reality' to carry out transient flow and transport simulations for a 20-year period using the identical model for two different scenarios: (1) including solute recycling from irrigation by re-introducing the extracted solute mass flux on the respective square kilometers, r_r=1; and (2) without solute recycling, r_r=0, being the classical numerical approach. This was done with the aim of testing the relative effect of the two extreme solute return flow ratios on the spatial salinity distribution in a complicated hydrodynamic and geometrical context. Introducing solute recycling from irrigation into a numerical model implies definition of a coupled mass boundary condition (solute recycling

on irrigated plots) which depends on the time-variable cumulated solute mass flux extracted from the system by the wells, which complicates the simulation procedure.

The results from the transport simulations are then qualitatively compared to the field observations and suggest that solute recycling from irrigation is likely to be the reason for the important spreading of the mixing zone in the central area, where agricultural activity is intensive and the saturated thickness of the aquifer is small.

2.4.1 Boundary conditions and parameters

2.4.1.1 Flow boundary conditions and parameters

Along the northern limit, a lateral flux boundary condition was imposed within the bedrock aquifer, corresponding to the recharge from infiltration of precipitation on upstream outcropping carbonates. Depth-dependent equivalent fresh-water head boundary conditions were imposed along the sea shore. The eastern boundary leads through salt lakes to the north. On the surface of the salt lakes, an out-going flux boundary condition was assigned, mimicking intensive evaporation. The mean effective infiltration was estimated on a monthly basis with the Thorntwaite method, and the annual mean value is comparable to an earlier estimation of effective infiltration in the Kiti area, carried out by Schmidt et al. (1988). The pumping wells were implemented within the alluvial aquifer (shallow wells) as extraction nodes. All other limits were defined as no flow boundaries (Fig. 2.7).

Average values for effective infiltration, lateral water inflow, extraction rates and observed water tables for the time-span 1994-1997 were used to calibrate the hydraulic conductivity distribution. A steady-state analysis could be carried out since the trend of the water-table showed that the storage of the system did not change significantly during this time-period. Manual adjustment of the average heads of 30 observation points according to geological criteria was followed by inverse modelling, using the Pest algorithm. Seventeen different hydraulic conductivies were adjusted. Comparing this to only 30 observation points makes it clear, that the obtained parameter distribution is likely to be non-unique, but does reflect a possible reality. Transient calibration was then carried out with the *K*-values as derived from the steady-state calibration to obtain the storage coefficients. For this purpose the averaged values of the same time-period 1994-1997 were decomposed into monthly values, leading to time-dependent functions for the precipitation, extraction rates and subsurface inflow.

The reliability of the model cannot be evaluated, since no sensitivity study was carried out. Indeed, and once again, we were interested in using the numerical model as a possible ‘synthetic reality’,

reflecting the conceptual model of the Kiti aquifer with a hydrodynamic and geometrical complexity typical of real aquifers.

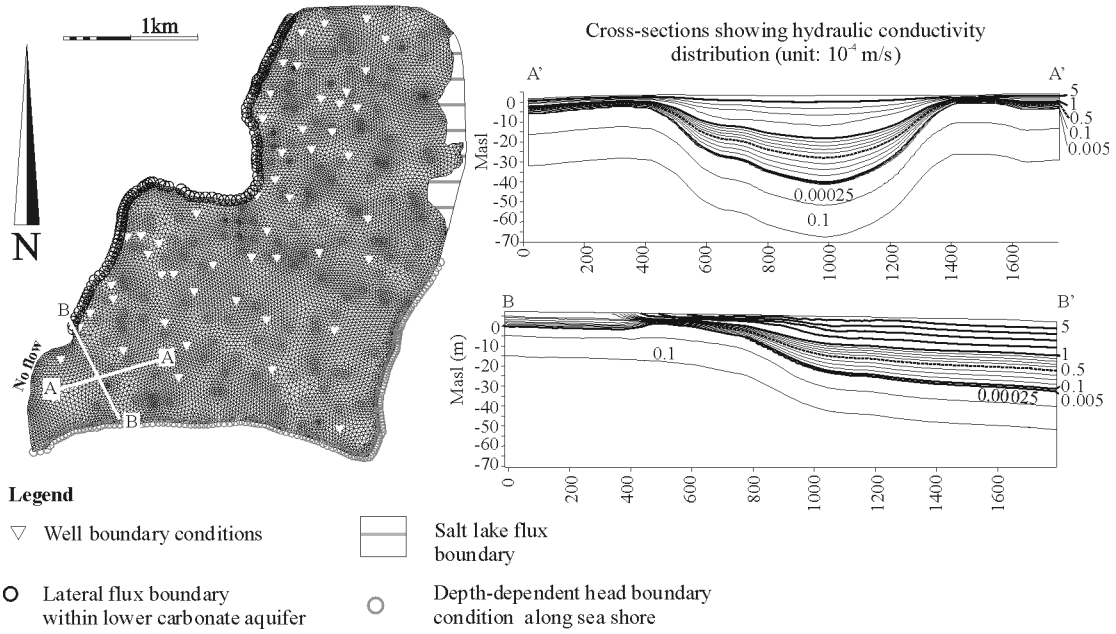

Fig. 2.7: Plan view of boundary conditions and finite element mesh (vertically discretised into 6 layers). The two cross-sections illustrate the parameter distribution as obtained from inverse modelling.

2.4.1.2 Transport boundary conditions and parameters

Relative chloride concentrations were imposed along the shoreline (concentration C_{max}=1) and the relative northern boundary concentration was kept at C_{min}=0. The coefficient of longitudinal dispersivity (α_L) was fixed to the same order of magnitude as the cell sizes (35 m) due to the lacking knowledge of the physical value of α_L, whereas the transversal dispersion (α_T) was defined as 10% of the longitudinal dispersion.

The porosity distribution used for all simulations was attributed according to the three main geological units: porosity 10% for the alluvial heterogeneous deposits, 5% for the aquitard and 3% for the carbonates. This porosity distribution leads to a volume average of 8% for the entire aquifer, which is believed to be a rather low estimate and therefore it was used as lower boundary of the porosity range tested in the evaluation of the solute recycling in section 2.3.3.

The initial concentration distribution for the two scenarios was identical and was obtained as a result of a 20 year density dependent transport simulation run using the average hydraulic situation between 1985-2001 to create a shape of the seawater intrusion which was qualitatively comparable to what was observed in the early 80s.

The only difference between the two simulation scenarios lies in a coupled areal solute mass boundary condition, introduced only for the scenario with solute recycling. The solute recycling from irrigation was calculated from the cumulated extracted solute mass flux from the wells at the end of each year for each square kilometre, and subsequently re-introduced as source term in the first layer of the respective square kilometres. The graph on the bottom left of Fig. 2.8 shows the mass of solute extracted annually from the wells (dashed line) and the annually re-introduced solute mass (solid line). The delay of one year can be seen. Leaching and solute mass recycling is believed to take place when percolation down to the groundwater after heavy rainfall takes place. A re-introduction period of 10 days was defined with a constant mass input signal. This is not based on a well defined /observed physical process, but on the assumption that the accumulated solute mass within the unsaturated zone can only be flushed when percolation takes place. However, it is not known whether the delay is longer than a year, or not. The aim was to provide long-term mass-conservation and not to simulate the physical processes taking place within the unsaturated zone.

2.4.2 Results from transient transport simulations for two scenarios (with and without solute recycling)

As already emphasised, neither the flow nor transport parameters were validated, and therefore the results of the two scenarios have to be compared relative to each other in the first place. Comparison with the real situation can only be done qualitatively, since the model reflects a conceptual hydrogeological model only.

Fig. 2.8 shows the results of the transport simulations with and without solute recycling from irrigation. The spreading of the low concentration iso-contours can be observed in the simulations with solute recycling, whereas the transition zone remains narrow in the simulations without solute recycling. Between the two simulation results the relative mass distribution as observed in the field is shown for the years 1990 and 2001 for visual comparison. It shows that, even though the absolute values simulated with the scenario with solute mrecycling are too low, the distribution and particularly the spreading of the iso-contours in the lower concentration range are in better accordance with reality than results from the scenario without solute recycling. In cross-section BB', one can see that the introduced mass, which is visible in the top layers after the 10 days input period, disappears at the end of the year due to dilution, whereas the opposite effect is seen in cross-sections AA'. Cross-section AA' having a thickness of only approximately 20 % of cross-section BB' does not allow as much dilution of the recycled solute mass. This shows, that differences in aquifer characteristics, such as saturated thickness, will influence the degree of salinisation.

Fig. 2.9a shows the comparison between the simulated concentrations of the two scenarios. The points on the correlation line represent the observation wells situated within the active seawater intrusion zone. The observation wells located far away of the correlation line are the observation points situated in the central area. For several of these points the simulated relative concentrations are lower than 10^{-4} for the scenario with r_r=0, whereas for the scenario with solute recycling (r_r =1) the relative concentrations are found to lie between 10^{-3}-10^{-1}. This shows the impact of solute mass recycling on the spatial salinity distribution, as it is the only process, which is different between the two scenarios. Fig. 2.9b and 2.9c show the comparison between the observed and simulated relative concentrations at the end of the 20-year period for the two scenarios. As mentioned before, the comparison between the observed and simulated relative concentrations is qualitative. The graphs in Fig. 2.9b and 2.9c allow the identification of the observation wells in the central area relative to the ones situated in the seawater domain. For the scenario without solute recycling (Fig. 2.9b), all the observation wells placed inland are situated very far from the correlation line, whereas some of the observation wells are in good agreement with the measured concentrations, reflecting the observation points which are located within the effective seawater intrusion domain. For the scenario with solute recycling (Fig. 2.9c), a better correlation of the low relative concentrations is obtained (note that we are dealing with a logarithmic scale). Compared to Fig. 2.9b, the shifted values correspond to the observation wells situated in the central area of the aquifer which are not directly affected by the seawater intrusion. There, salinisation is likely to be dominated by solute recycling from irrigation.

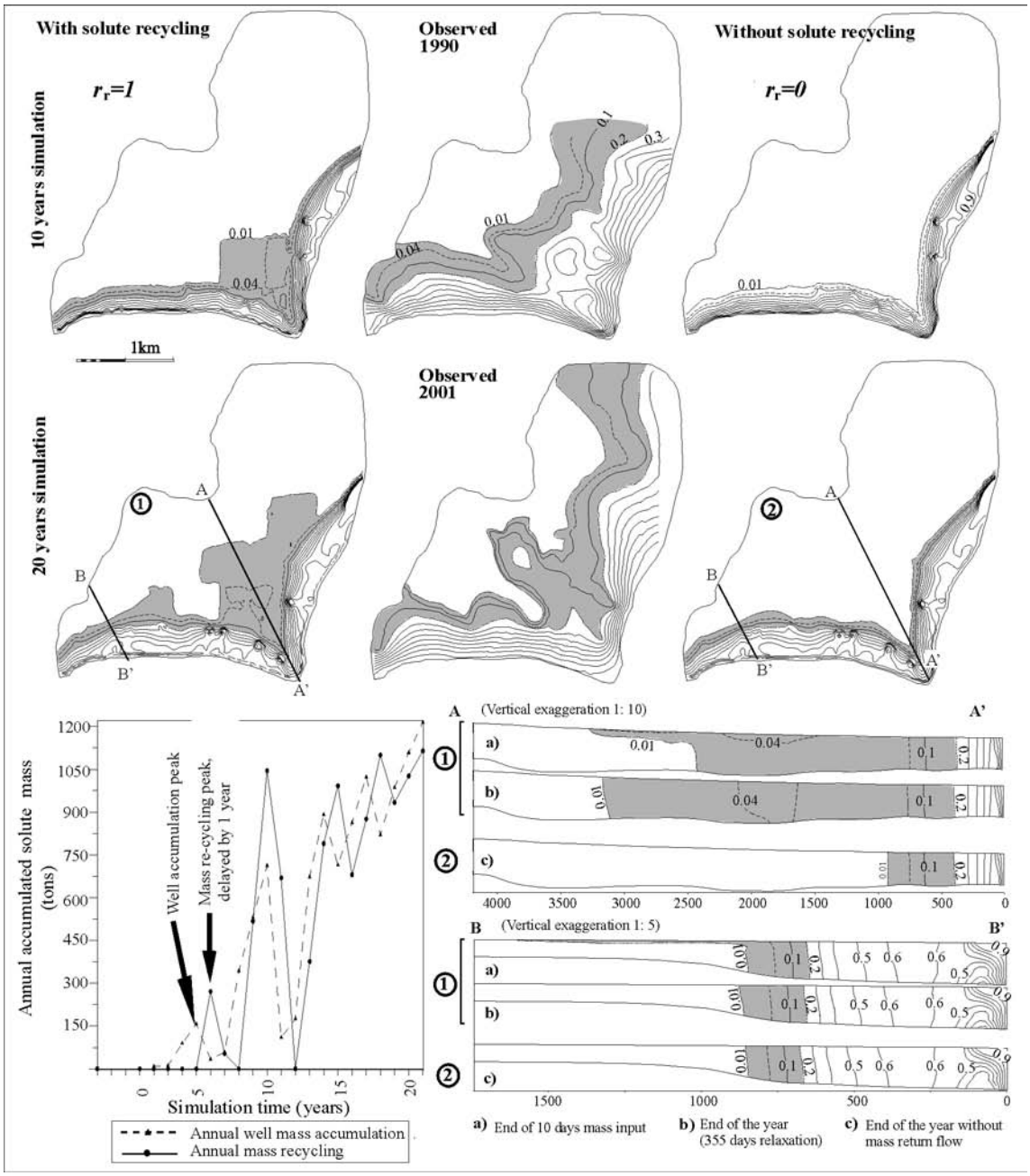

Fig. 2.8: Results of the numerical simulations, showing the relative mass distribution after 10 and 20 years respectively for the two scenarios with (left) and without (right) solute recycling. In the central column, observed relative salinities are shown for 1990 and 2001 as qualitative comparison. The gray areas indicate the zones with relative concentrations between 0.01-0.2. The cross-sections show the mass distribution for the simulation scenario with solute recycling: (1a) mass distribution just after the 10 days of solute recycling, and (1b) after another 355 days of simulation without solute recycling and for the simulation scenario without solute recycling (2c) at the end of the 20 year simulation period. The graph shows the well solute mass accumulation, which was calculated at the end of each year and re-introduced into the model in the following year.

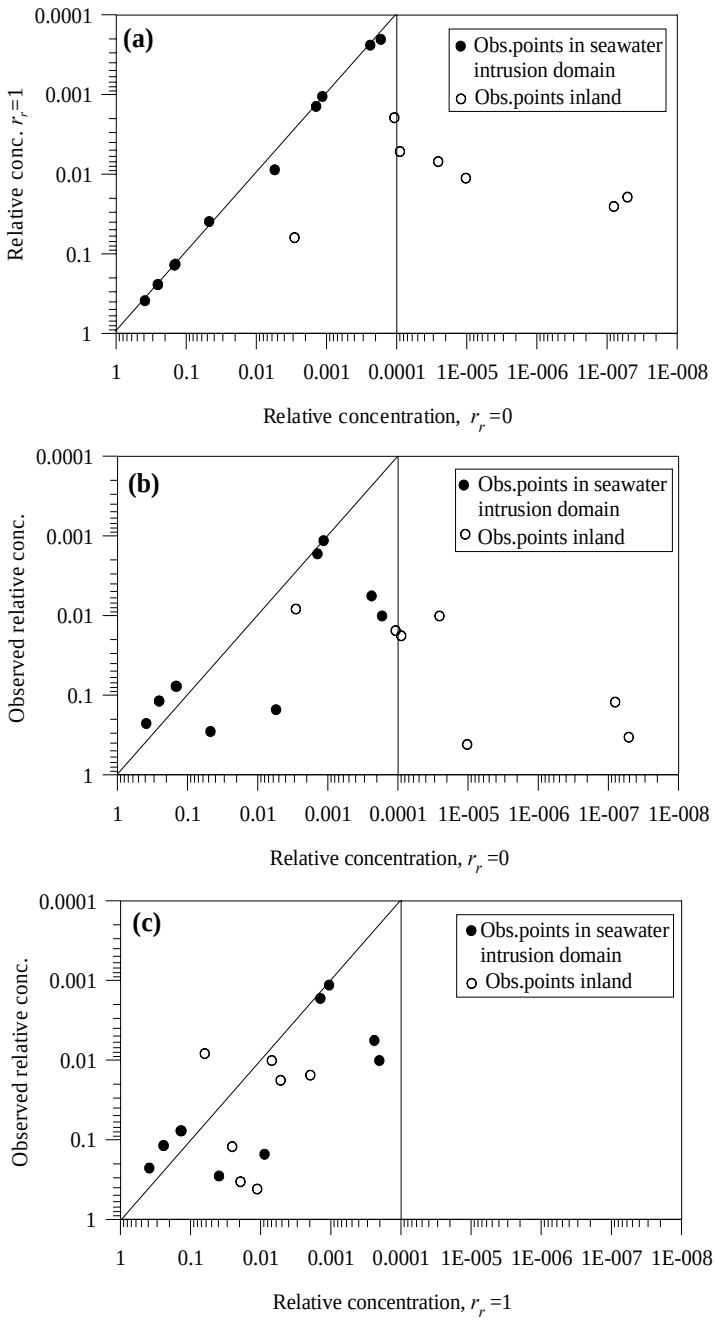

Fig. 2.9: Correlation between measured and simulated relative salinities as obtained at the end of the 20-year simulation periods with and without solute recycling from irrigation: (a) compares the results of the two simulated scenarios. The observation points located on the correlation line (black dots) are located within the active seawater intrusion domain, whereas the observation points inland (white dots) are characterised by relative concentrations below 10^{-4} for the scenario r_r=0; (b) shows results from scenario without solute recycling (r_r=0) compared to relative observed salinities, revealing a prominent scatter; (c) shows the comparison of the scenario with solute recycling (r_r=1) with relative observed salinities and reveals that the simulated concentrations for the observation points inland (white dots) are within the zone of 'measureable' salinities. Thus, introducing solute recycling into the model widens the mixing zone.

2.5 Discussion

For the Kiti aquifer the evaluation of the relative impact of solute recycling from irrigation by means of the simplified solute mass balance approach led to an estimation of 1.5-8.5% of the extracted solute mass originating from recycling after a time-span of 20 years. These numbers are interesting because they seem to be small on the considered time-scale and one could be tempted to interpret them as reflecting a minor phenomenon. However, this amount seems to be sufficient to lead to groundwater degradation below a large part of the surface in the central area, where the aquifer thickness is small (Fig. 2.8), and can therefore have a high impact on agriculture. Furthermore, in the long-term, recycling will considerably accelerate the deterioration of groundwater quality of the aquifer. The only brake to the acceleration is that the wells are eventually abandoned when a certain threshold concentration is attained. This fact was neither considered in the solute budget nor in the transient transport simulations.

The results from the three dimensional density dependent flow and transport model indicated that solute recycling can explain the large spreading of the transition zone between fresh and seawater within an aquifer, depending on where solute recycling takes place. The main interest of this modelling approach lies in revealing the impact of the aquifer geometry, extraction and solute re-distribution pattern on the spatial salinity distribution, when solute recycling from irrigation is included in the simulations.

Using the simplified mass balance calculations in a pre-processing stage of numerical modelling can be a useful supplementary tool. The simplified solute mass balance approach is a quick and simple way of estimating whether solute recycling can be neglected with the mere knowledge of the return flow ratio r_r and the mean system turnover time t_0. However, it does not give any indications on the impact of solute recycling on the spatial salinity distribution and can therefore by no means substitute transport simulations.

Many assumptions were made within the mass balance calculations, as for instance the definition and use of a mean system concentration for the solute mass budget approach, which is the opposite characteristic of real coastal aquifers. However, by assuming that the extracted fluid has a mean system concentration, the potential danger can be formulated. Whether this hypothesis is reasonable or not can be evaluated by estimating whether the average extracted solute concentration is representative of the mean system concentration. This would be the case if extraction wells with similar discharge rates are homogeneously distributed over the whole aquifer. However, as an example, if extraction wells are situated far inland within the pure freshwater domain and the impact of solute recycling is evaluated for a time span shorter than the time it takes for the wells to become affected by seawater intrusion, then the impact will be over-

estimated. Another drawback is that the physics and chemistry of the solute recycling were not considered, and neither were the processes taking place within the unsaturated zone (adsorption, precipitation, dissolution, etc.). We simply assured that the solute mass balance was respected.

Possible other salinisation sources, such as salinisation from water-rock interactions within the bedrock formations and leaching into the base of the unconfined aquifer, were neglected but can be added at any time. As the purpose of this study was to investigate the possible impact of solute recycling from irrigation, no other salinity sources were incorporated.

Keeping the limitations of our models in mind, we would still like to emphasize the potential importance of solute recycling in coastal aquifers, as it is very likely to be a wide-spread phenomenon in many over-exploited irrigated coastal plains, not only in the Mediterranean area. Furthermore, it seems that up to now, most of the published groundwater flow and transport models in coastal aquifers have neglected solute recycling and might therefore have provided too optimistic forecasts. In view of sustainable groundwater exploitation in semi-arid coastal aquifers, the possible impact of solute recycling should be evaluated as an additional salinisation mechanism, directly coupled to seawater intrusion.

2.6 Conclusion

To investigate and quantify the impact of solute recycling from irrigation relative to seawater intrusion in over-exploited coastal aquifers, a simplified solute mass budget approach was established, allowing decomposition of the overall salinity extracted from wells into a contribution from the sea and a contribution from solute recycling. The transient solution for the relative contribution from solute recycling yielded a negative exponential function of the normalised time $\bar{t}$ (time t normalised with the system turnover time t_0) and the return flow ratio r_r, valid for any system, for which the specified hypotheses can be made.

Using the established simplified solute mass balance approach, the relative impact of solute recycling was evaluated for an example from Cyprus, the Kiti aquifer. Field observations and analysis of historical data suggested that the effect of solute recycling from irrigation is superimposed on the salinisation mechanism of seawater intrusion. The solute mass budget approach suggested that after 20 years 1.5-8.5% of the total extracted solute mass flux originates from solute recycling, for an estimated average system porosity range of 8-20%.

Numerical transport simulations were then carried out for a 20-year period, for two solute return flow ratios (r_r=0: classical numerical approach, and r_r=1: complete solute recycling from irrigation), to investigate the impact of solute recycling on the spatial salinity distribution using a

finite element model, which reflected the main hydrodynamic characteristics of the Kiti aquifer. The results were compared relative to each other and showed that the spatial salinity distributions obtained with r_r= 1 led to a spreading of the mixing zone in the central area, similar to what has been observed in the field, whereas the simulation without solute recycling revealed a very narrow transition zone at the end of the 20-year simulation period.

The interest of the simplified solute mass balance approach lies in the decomposition of the extracted solute mass flux into a component related to solute recycling and another component connected to seawater intrusion. It can be used if the return flow ratio r_r, the mean system turnover time t_0 and a characteristic time t can be estimated. This approach is thus a useful tool in a pre-processing stage of time-consuming numerical transport simulations to evaluate if solute recycling can be neglected or if it should be incorporated in the simulation procedure.

The advantage of transient transport simulations, on the other hand, lies in the capacity to reflect the impact of extraction/recharge and recycling patterns and aquifer geometry (e.g. aquifer thickness influencing dilution of recycled solute) etc., on the spatial salinity distribution but can only do this reliably, if the sources of groundwater contamination have been well defined. Hence, if solute recycling is important, then the salinity distribution cannot be simulated with a classical numerical approach (r_r=0). A future objective is therefore to implement solute recycling in a numerical tool as coupled boundary condition and to link it to the physical processes taking place within the unsaturated zone.

As soon as a clear spatial distinction can be made between seawater intrusion and solute recycling, the salinisation risk potential towards the coupled salinisation mechanisms can be defined, and with it, the different potential remedial measures.

CHAPTER 3

SOLUTE RECYCLING: PROCESS IDENTIFICATION AND MATHEMATICAL ANALYSIS

Partially submitted to Advances in Water Resources

Abstract

A mathematical analysis is carried out to identify the parameters which govern the solute mass evolution at irrigation wells in response to solute recycling, in view of defining a distributed solute source on irrigated surfaces. An analytical solution of the 1-D advective transport equation is developed, by defining a distributed 'recycling source', corresponding to the solute extracted from the well. The behaviour of the well response to spatial variations of solute recycling is investigated and two parameters are identified with which the late time concentration slope at the well can be described: 1) the travel time between the recycling point and the extraction well, and 2) the lateral solute mass flux captured by the well from the boundaries. Then, a formulation for the transient extracted solute mass flux is developed for arbitrary advective-dispersive systems by means of the transfer function theory (Jury 1982). A recycling transfer function (RTF) $g_{in}(\gamma,t)$ is expressed as the sum of the n-fold self-convolutions of the travel time probability density function between the recycling point and the extraction well. Convolution of the RTF with the solute mass captured from the boundaries yields the exact transient well solute response to solute recycling in arbitrary advective-dispersive systems. Hence, the well solute mass response can be predicted and can be used to define a distributed 'recycling source' term in the general form of the advection dispersion equation in arbitrary systems for average hydraulic steady state conditions. At late times, the solute mass flux extracted from wells is a function of the capture zone probability and the lateral solute mass flux only.

3.1 Introduction

In the previous chapter, the problem of solute recycling was explored on a field example and a simple solute mass budget was established for perfectly mixed systems. This allowed distinction between the solute mass flux at wells derived from solute recycling as opposed to seawater intrusion. The transient transport simulations showed, however, that the spatial salinity distribution will very much depend on the position of the extraction wells and the irrigation plots.

In this chapter, we will focus on the identification of the solute recycling process by describing it mathematically. For that purpose we will not consider any seawater front but merely focus on lateral boundaries, which can either be fresh groundwater boundaries or seawater boundaries. Hence, the approach to solute recycling presented here is applicable to any setting, in which irrigation takes place with water extracted from the underlying aquifer.

In irrigation sciences, the problem of solute recycling to tile drains has been investigated in many field experiments and also described mathematically for several decades. Prediction of the future

concentration evolution in drainage water is of particular interest in areas, where reuse is considered as a management option, which leads to solute recycling (e.g. Jury 1975a,b, Kelleners et al. 2000). Prendergast et al. (1993) established an analytical solution to estimate the long term concentration behaviour at a well in response to solute recycling from irrigation. In another context, a recycling process was coupled with reactive transport and applied to evaluate the efficiency of remediating recirculation wells (Cirpka & Kitanidis 2000).

In this chapter, the main focus will be placed on the well concentration evolution in response to spatial differences of irrigation. The spatial salinisation evolution in a system caused by solute recycling can only be understood if the well response has been described, and the spatial parameters which govern the salinisation process are identified.

In the first section, a general description of the solute recycling process is presented which leads to the formulation of the 1-D advective solute transport equation with a distributed recycling source. The transient concentration evolutions are investigated and the parameters governing solute recycling salinisation are isolated. The effect of the unsaturated zone on the salinisation process is also evaluated. In the second section, the mathematical description of the solute recycling process is extended to arbitrary advective-dispersive systems by means of the transfer function theory (Jury 1982, Jury et al. 1986).

3.2 General description of the solute recycling process

The main difficulty in describing the solute recycling process is that the water and solute cycles are partly disconnected (Fig. 3.1). If the solute mass flux applied with the irrigation water does not leave a system by means of drains or surface runoff, it is sooner or later returned to the groundwater below the irrigation surfaces by deep percolation, while the applied irrigation water will partly leave the system by evapotranspiration. This only holds if processes which eliminate solutes from the system are neglected (e.g. mineral precipitation, plant uptake).

Fig. 3.1 schematises a 1-D open system in hydraulic steady state with one extraction well, a lateral inflow boundary and a regional discharge area. The irrigation plot covers the entire surface between the inlet ($x = 0$) and the extraction well ($x = L$), on which all the extracted solute mass flux from the extraction well is distributed with the applied irrigation water. In such a system, if all the extracted water is used for irrigation, the difference between the water and the solute cycles are caused by evaporative losses, leaving solutes behind (i.e. evapotranspiration reduces the applied irrigation water, and concentrates the extracted solute mass, leading to a salinity increase in the deep percolation).

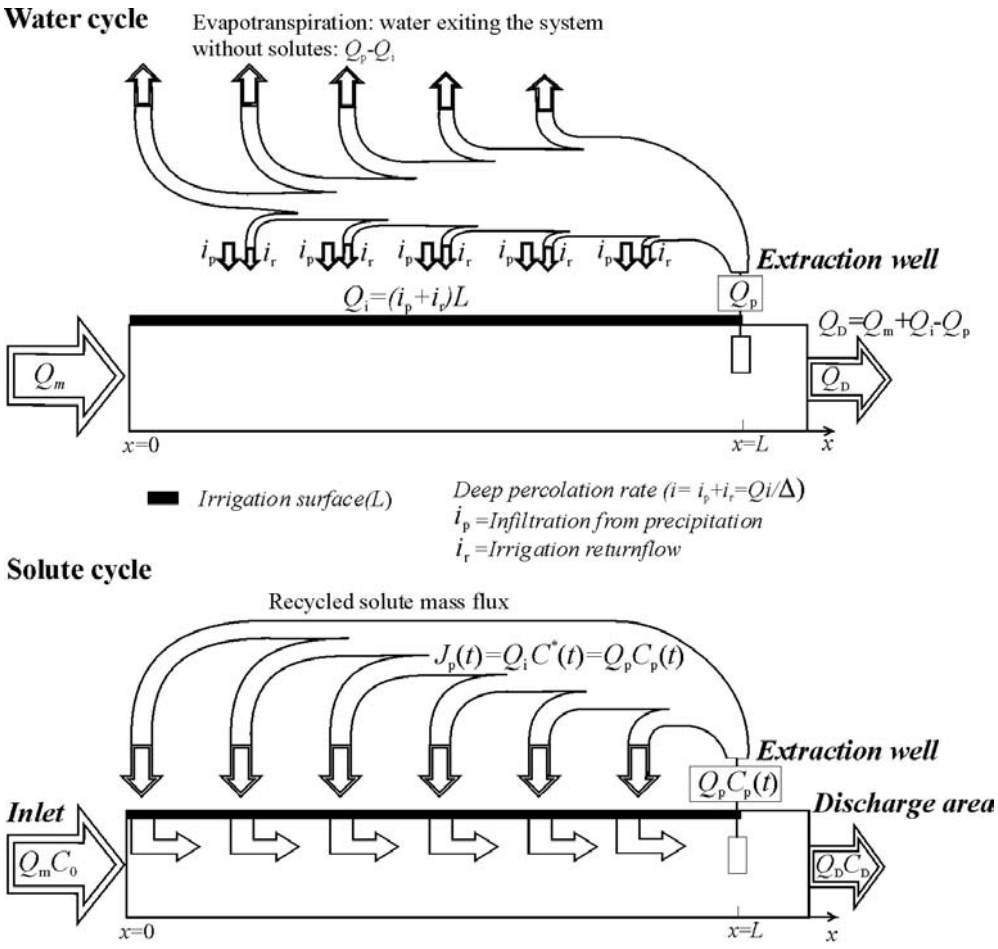

Fig. 3.1: Schematised irrigated system with one inlet boundary, an extraction well which is used for irrigating the entire surface, and a regional discharge area. The differences in the water and solute cycles, induced by evapotranspiration are shown.

In Fig. 3.1, Q_m [L^2T^{-1}] is the lateral inflow with a concentration $C_0 > 0$ [ML^{-3}], while Q_p [L^3T^{-1}] stands for the well extraction rate with $C_p(t)$ being the concentration of the extracted water, which will be called well concentration in the following. Q_D [L^2T^{-1}] denotes the regional discharge rate with a concentration $C_D(t)$ [ML^{-3}]. C^* is the concentration of the areal infiltration rate Q_i [L^3T^{-1}], consisting of the irrigation return flow (i_rL) plus the effective infiltration from precipitation (i_pL). The irrigation surface is denoted L[L].

In a system like that shown in Fig. 3.1, the extracted solute mass flux $J_p(t) = Q_pC_p(t)$ is transferred to the groundwater by the deep percolation Q_i. The ratio of the total infiltration rate Q_i and the extraction rate Q_p (in this case = net irrigation rate) corresponds to the leaching fraction LF (e.g. Oster 1984). This ratio will determine, whether the recycled solutes will lead to an increase in groundwater salinity. If the infiltration rate is smaller than the extraction rate, the system concentration will increase, since the water deficit will be constantly compensated by lateral

inflow. In closed systems, with no regional discharge area, the solutes entering the system will be trapped. If the infiltration rate equals or exceeds the extraction rate, the concentration will not increase, since no solutes are conveyed into the system. Hence, the main prerequisite for groundwater salinisation by solute recycling from irrigation is that extraction rates exceed infiltration rates. Such conditions are typically found in arid and semi-arid regions, where pan evaporation and irrigation requirements are high and deep percolation is small.

3.3 Advective solute-transport equation with 'recycling source'

In this section, the process of solute recycling is described mathematically by coupling the extracted solute mass flux $J_p(t)$ to a distributed solute source on the domain. If we consider the aquifer configuration shown in Fig. 3.1, we can formulate the 1-D advective transport equation with a solute source, which will subsequently be coupled to the extracted solute mass flux as follows:

$$e\phi\frac{\partial C}{\partial t} = -\frac{\partial}{\partial x}(eqC) + iC^* \quad ; \quad \frac{\partial(eq)}{\partial x} = i_r + i_p = i \tag{3.1}$$

In Eq. (3.1), the thickness of the domain is e [L], ϕ [-] is the porosity or mobile water content, C [ML^{-3}] the concentration, x [L] the spatial coordinate, q [LT^{-1}] the specific discharge, i [LT^{-1}] the source strength corresponding to the net infiltration rate consisting of percolated irrigation water (i_r in Fig. 3.1) and infiltration from precipitation (i_p in Fig. 3.1) and C^* the infiltration concentration, which is directly governed by the solute extraction at the well when solute recycling takes place. In the following, other solute sources will not be considered, although they can be added at any time.

When considering a closed system, we assume that no discharge other than by the extraction well takes place (no regional discharge). The lateral flow rate Q_m, the total infiltration rate Q_i, the well extraction rate Q_p and the regional discharge Q_D shown in Fig. 3.1 can then be defined as follows:

$$Q_m = eq_0 \quad ; \quad Q_i = iL \quad ; \quad Q_p = Q_m + Q_i \quad ; \quad Q_D = 0 \tag{3.2}$$

where q_0 [LT^{-1}] is the flow rate at the spatial coordinate $x = 0$. The well is located at $x = L$. If solute recycling takes place homogeneously over the entire domain (L), and chemical reactions taking place in the unsaturated zone are neglected, the solute source iC^* in Eq. (3.1) can be expressed by means of the extracted solute mass flux as follows:

$$iC^* = \frac{C_p Q_p}{L} = \frac{J_p(t)}{L} \tag{3.3}$$

Eq.(3.3) suggests instantaneous solute recycling between the extraction well and the recycling point although a delay τ can be added at any time, such that $iC^*(t)=J_p(t-\tau)$.

However, solute recycling might only take place over a given interval ($x_1 \le x \le x_2$), in which case Eq. (3.3) has to be modified as follows:

$$iC^* = \frac{C_p Q_p \left[\mathrm{H}(x-x_1) - \mathrm{H}(x-x_2) \right]}{(x_2 - x_1)} \tag{3.4}$$

The Heaviside function H(x) is used to delimit and uniformly re-introduce the extracted solute mass flux from the well on the recycling zone between x_1 and x_2. Eq. (3.3) is a special case of Eq. (3.4), for $x_1 = 0$ and $x_2 = L$.

Inserting Eq. (3.4) into Eq. (3.1), making use of Eq. (3.2) and then developing the first RHS term in Eq. (3.1), and multiplying with $\frac{L}{Q_p}$ yields:

$$\frac{Le\phi}{Q_p}\frac{\partial C}{\partial t} = -\frac{L}{Q_p}(Q_m + ix)\frac{\partial C}{\partial x} - \frac{Q_i C}{Q_p} + \frac{C_p L[\mathrm{H}(x-x_1) - \mathrm{H}(x-x_2)]}{(x_2 - x_1)} \tag{3.5}$$

The following dimensionless variables are defined:

$$\alpha = \frac{Q_i}{Q_p} \quad ; \qquad \beta = \frac{x}{L} \quad ; \qquad C' = \frac{C}{C_0} \tag{3.6}$$

where C_0 >0 is the concentration at the lateral inflow boundary.

Inserting the dimensionless variables α and C' as defined in Eq. (3.6) into Eq. (3.5) yields:

$$\frac{Le\phi}{Q_p}\frac{\partial C'}{\partial t} = -(L(1-\alpha) + \alpha x)\frac{\partial C'}{\partial x} - \alpha C' + \frac{C'_p L[\mathrm{H}(x-x_1) - \mathrm{H}(x-x_2)]}{(x_2 - x_1)} \tag{3.7}$$

Additionally, we define the dimensionless or relative time t' [-] counted in pore volumes:

$$t' = \frac{t}{\bar{t}} = \frac{Q_p t}{Le\phi} \tag{3.8}$$

where t [T] is the time and $\bar{t}$ [T] the mean system turnover time. For reasons of simplicity, we denote from now on C' as C and t' as t. After introducing the mean system turnover time $\bar{t} = Le\phi/Q_p$ and the space increment $dx = Ld\beta$ [L], Eq. (3.7) can be written as follows:

$$\frac{\partial C}{\partial t} = -(1-\alpha+\alpha\beta)\frac{\partial C}{\partial \beta} - \alpha C + \frac{C_{\mathrm{p}}[\mathrm{H}(\beta-\beta_1)-\mathrm{H}(\beta-\beta_2)]}{(\beta_2-\beta_1)} \tag{3.9}$$

Applying a Laplace transform to Eq. (3.9), where r is the dimensionless Laplace variable ($r = p\bar{t}$), and p [T^{-1}] the Laplace variable, yields the following general expression which includes the process of solute recycling:

$$r\hat{C} - C(\beta,0) = -(1-\alpha+\alpha\beta)\frac{\partial \hat{C}}{\partial \beta} - \alpha\hat{C} + \frac{\hat{C}_{\mathrm{p}}[\mathrm{H}(\beta-\beta_1)-\mathrm{H}(\beta-\beta_2)]}{(\beta_2-\beta_1)} \tag{3.10}$$

where the angular over-scores or 'hat' signs ($\hat{C}, \hat{C}_{\mathrm{p}}$) describe the Laplace transformed functions and is the notation that will be adopted throughout this work. The assumption we make in Eq. (3.10) is that all the extracted water Q_{p} applied on the irrigation zone between β_1 and β_2 evaporates and that deep percolation takes place with infiltration from precipitation only. The expression is based on homogeneous infiltration over the entire domain. To maintain this homogeneous infiltration over the entire domain when irrigation takes place on a certain zone only, the assumption is made that infiltration from irrigation return flow is zero on the irrigation surface (i_{r} in Fig. 3.1). Solute recycling will then take place with infiltration from precipitation (i_{p} in Fig. 3.1), which is homogeneous over the domain. This assumption can be justified with the fact, that in intensely irrigated agriculture, deep percolation is often minimised to such an extent that $i_{\mathrm{r}} << i_{\mathrm{p}}$.

3.3.1 Concentration evolution at any point for homogeneous recycling on entire domain

For the special case that $\beta_1 = 0$ and $\beta_2 = 1$, recycling takes place homogeneously on the entire domain and Eq. (3.10) simplifies to:

$$r\hat{C} = -(1-\alpha+\alpha\beta)\frac{\partial \hat{C}}{\partial \beta} - \alpha\hat{C} + \hat{C}_{\mathrm{p}} \tag{3.11}$$

with the boundary and initial conditions:

$$\hat{C}(0) = \frac{1}{r} \quad ; \qquad \hat{C}(1) = \hat{C}_{\mathrm{p}} \quad ; \qquad C(\beta,0) = 0 \tag{3.12}$$

The constant lateral concentration $C(0) = 1$ in the time domain becomes $(1/r)$ in Laplace space. Eq. (3.11) is first solved for $\hat{C}(1) = \hat{C}_{\mathrm{p}}$ with the boundary and initial conditions Eq. (3.12). The

expression is then re-introduced into Eq. (3.11), substituting $\hat{C}_p$ before solving the equation for $\hat{C}(\beta)$.

The solution is then:

$$\hat{C}(\beta) = \frac{-(1-\alpha)^{(\frac{r}{\alpha})}\left[(1-\alpha+\alpha\beta)^{-(\frac{r}{\alpha})}(r+\alpha-1)-\alpha(1-\beta)+1)\right]}{r(1-\alpha+\alpha\beta)\left[1-\frac{r}{1-\alpha}-(1-\alpha)^{(\frac{r}{\alpha})}\right]} \tag{3.13}$$

Fig. 3.2 shows the time-domain solution of Eq. (3.13) for different spatial coordinates and a value of α = 0.05 obtained by numerical inversion compared with the result of a finite element simulation using a time-stepping procedure to simulate solute recycling with minimum dispersivity, corresponding to the mesh size. The numerical inversion of the Laplace transformed function $\hat{C}(\beta)$ was performed by the algorithm of Crump (1976). At early times, there are several concentration bends, which render the solution complicated. However, for late times the solution tends towards a line with a constant slope. Although solute recycling is homogeneous over the entire domain, the concentration distribution within the domain is not. The concentration increases towards the extraction well (β=1), since the fraction derived from irrigation return flow within the flowrate increases, containing the recycled solutes. For the same reason, if no solute recycling takes place, the concentration decreases towards the extraction well, due to the increasing dilution effect of infiltration.

To obtain the concentration slope $m(\beta)$ at late times, Eq. (3.13) is multiplied by r^2 as described in Box 3.1 and the limit value for r = 0 is sought, according to (B 3.1.3). In a closed system, the concentration slope $m(\beta)$ is a characteristic space-dependent variable that can be used to describe the spatial salinity evolution in response to solute recycling:

$$m(\beta, t=\infty) = \frac{\alpha^2\beta}{(1-\alpha+\alpha\beta)(\frac{\alpha}{1-\alpha}+\ln(1-\alpha))} \tag{3.14}$$

Eq. (3.14) shows that α, in this case corresponding to the leaching fraction, is the only parameter determining the long-term behaviour of the spatial concentration evolution in closed systems, apart from the spatial coordinate (β).

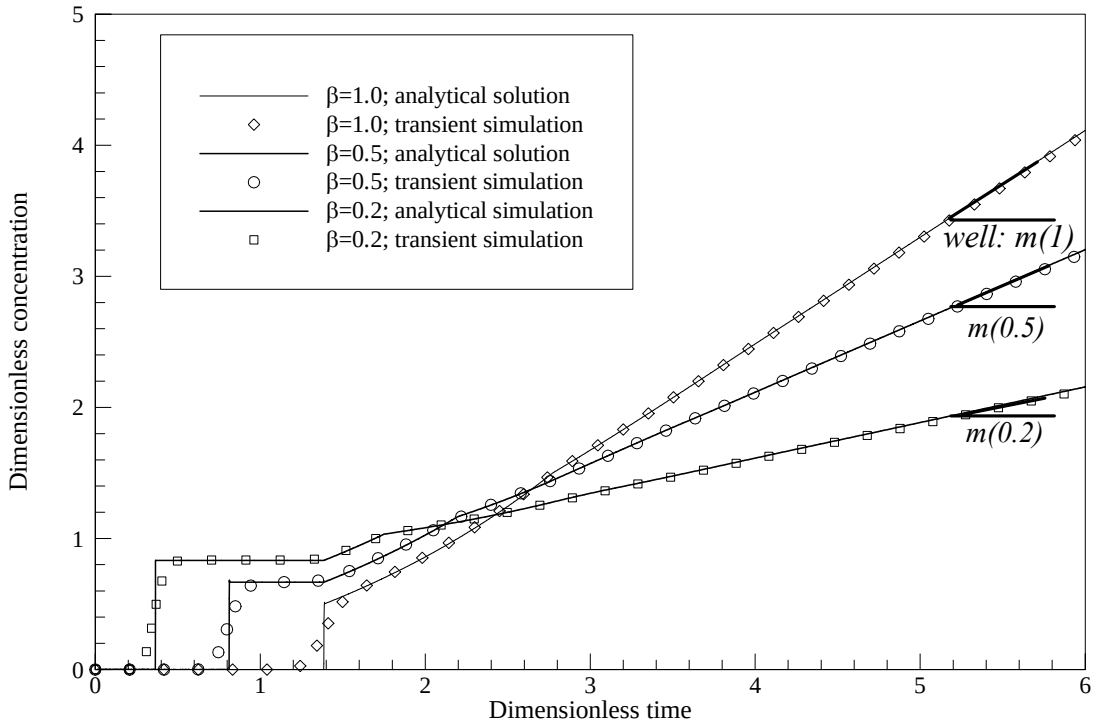

Fig. 3.2: Dimensionless concentration evolution for three spatial coordinates (β=0.2, 0.5, 1.0) for a value of α = 0.05 along the 1-D domain described in Fig. 3.1, after numerical inversion of Eq. (3.13), compared with results from a finite element simulation with minimal dispersivity corresponding to mesh size, using a time-stepping procedure (cf. Appendix 1). The late time concentration slopes $m(\beta)$ are indicated.

The limit value of Eq. (3.14) for $\alpha \to 0$ is the following:

$$\lim_{\alpha \to 0} m(\beta) = 2\beta \tag{3.15}$$

Eq. (3.15) shows that the slope tends towards 2β for recycling of 'pure' solute mass (Q_i tending towards zero), implying that velocity is constant throughout the 1-D domain. Since all the recycled solute mass is distributed on the entire domain, the mean travel time to the well of all the recycled solutes will equal the travel time between β = 0.5 and the well at β = 1. Hence, the longterm slope observed at the well for solute recycling over the entire domain is equivalent to solute recycling at β = 0.5, which leads to a concentration slope $m(\beta = 1)$ = 2, as reflected by Eq. (3.15). The smaller the volume within which the solutes are recycled, the bigger the concentration slope will be.

Box 3.1: Derivation of late-time slopes in Laplace space

As can be seen in Fig. 3.2, Eq. (3.13) yields a function $C(\beta, t)$ in the time-domain with a constant slope $m(\beta)$ for late times ($t \to \infty$). This slope $m(\beta)$ can be derived for any Laplace transformed solution $\hat{C}$ as follows:

$$m(\beta,\infty) = \frac{\partial C(t=\infty)}{\partial t} = \int_0^\infty \frac{\partial^2 C}{\partial t^2} dt + \frac{\partial C}{\partial t}(t=0) = \lim_{r\to 0} \int_0^\infty e^{-rt} \frac{\partial^2 C}{\partial t^2} dt + \frac{\partial C}{\partial t}(t=0) = \lim_{r\to 0}\left[r\int_0^\infty e^{-rt} \frac{\partial C}{\partial t} dt \right] \quad \text{(B 3.1.1)}$$

Making use of the definition of the Laplace transform:

$$\int_0^\infty e^{-rt} \frac{\partial C}{\partial t} dt = r\hat{C} - C(0) \quad \text{(B 3.1.2)}$$

(B 3.1.1) can be written as:

$$m(\beta,\infty) = \lim_{r\to 0}(r^2\hat{C} - rC(0)) = \lim_{r\to 0}(r^2\hat{C}) \quad \text{(B 3.1.3)}$$

To obtain the slope $m(\beta)$ in Eq. (3.14), Eq. (3.13) was multiplied by r^2 according to (B 3.1.3) prior to seeking the limit value for $r = 0$.

Similarly, we can evaluate the concentration at late times $C(t=\infty)$ as follows:

$$C(t=\infty) = \int_0^\infty \frac{\partial C}{\partial t} dt + C(t=0) = \lim_{r\to 0}\left[\int_0^\infty e^{-rt} \frac{\partial C}{dt} dt + C(t=0) \right] \quad \text{(B 3.1.4)}$$

Using the definition of the Laplace transform given in (B 3.1.2) yields:

$$C(t=\infty) = \lim_{r\to 0}(r\hat{C}) \quad \text{(B 3.1.5)}$$

3.3.2 Concentration evolution at a well with solute recycling through the unsaturated zone

In the previous section, we considered solute recycling to be instantaneous between the extraction well and the saturated zone below the irrigation surface. Even if we neglect mineral precipitation, dissolution and plant uptake, processes taking place in the unsaturated zone may be important in the short-term and medium-term groundwater salinisation (e.g. van Genuchten & Dalton 1980, Oster 1990). If transfer of solutes between the root zone and the groundwater is slow, net soil salinity will increase, while groundwater salinisation will be slowed down. On the other hand, fast transfer of solutes will more rapidly affect the groundwater, since solutes are not stored. In the

following, we assume that solutes within the applied irrigation water are not affected by processes, such as degradation, plant uptake or mineral precipitation and dissolution.

For many applications, the irrigated area of interest is large compared to the depth through which solutes are transferred to the groundwater. Under such conditions, the traverse mixing time will be much longer than the time for solutes moving through the unsaturated zone, and consequently, transfer through the soil column can be approximated by purely vertical movement. Hence, one way of taking the unsaturated zone into account is to represent its effect with a transfer function, acting as a filter, inhibiting lateral mixing (Jury 1982).

We are interested in identifying the role of the soil as buffer on the transient salinity evolution at an extraction well and not in exactly simulating conservative solute transfer through the unsaturated zone. For this purpose, we make the assumption that the recycled solute mass flux is redistributed onto an irrigation surface and transferred to the saturated zone by means of a transfer function $F_{\text{soil}}(t)$ without any solute losses. This implies that $\int_0^\infty F_{\text{soil}}(t)dt = 1$. For the considered 1-D system, in which solute reycling takes place homogeneously on the entire domain, Eq. (3.11) can be modified as follows, accounting for the transfer through the unsaturated zone by means of the transfer function $F_{\text{soil}}(t)$ as follows:

$$r\hat{C} = -(1-\alpha+\alpha\beta)\frac{\partial C}{\partial \beta} - \alpha\hat{C} + \hat{C}_{\text{p}}\hat{F}_{\text{soil}} \tag{3.16}$$

where $\hat{F}_{\text{soil}}$ is the Laplace transformed transfer function through the 'soil buffer'. The last RHS term corresponds to the distributed 'recycling source', which reflects the concentration signal resulting from the convolution integral of the well concentration response $\hat{C}_{\text{p}}$ with the soil transfer function $\hat{F}_{\text{soil}}$. In Laplace space, a convolution integral reduces to a simple product of the Laplace transformed functions. As an example, the following simple step-function $F_{\text{soil}}(x,t)$ with length (t_2-t_1) = Δt and first arrival time t_1 was used as transfer function through the unsaturated zone:

$$F_{\text{soil}}(t) = \frac{1}{\Delta t}\left[\text{H}(t-t_1) - \text{H}(t-t_2)\right] \tag{3.17}$$

where $t_2 = t_1+\Delta t$, Eq. (3.17) can be written in Laplace space as follows:

$$\hat{F}_{\text{soil}}(r) = \frac{1 - e^{-r\Delta t}}{p\Delta t e^{rt_1}} \tag{3.18}$$

Introducing Eq. (3.18) into Eq. (3.16), solving it for the boundary conditions in Eq. (3.12) in the same way as Eq. (3.11) was solved, and inverting the result, leads to different concentration evolutions at the same spatial coordinate, depending on the parameters Δt and t_1.

Fig. 3.3 shows the time-domain solution of Eq. (3.16) for the case of no soil filter (full line with circles, corresponding to Eq. 3.11) as compared to two cases with soil filters (Eq. 3.16 with Eq. 3.18) for different first arrival times t_1 but with the same signal length Δt. The well concentration response $C_p(t)$ to the presence of a soil transfer function with the later arrival time t_1=1 leads to a small slope, since the mean travel time through the soil column is longer than for the case of t_1=0.5 (t_1=1 means that transit through the soil column equals the mean turnover time in the groundwater system). Hence, the presence of a 'soil buffer' will slow down the process of solute recycling, although concentrations in such a closed system will eventually all tend towards infinity.

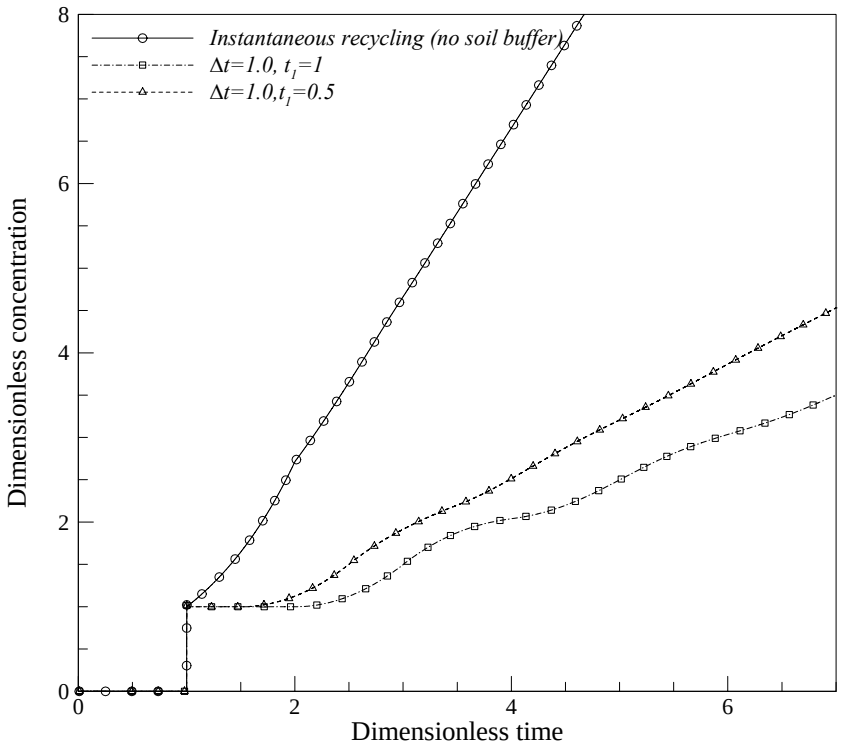

Fig. 3.3: Concentration slopes at well obtained from the inverted result of the 1-D solution of Eq. (3.16) with and without soil 'buffer'. Full line with circles: instantaneous solute recycling; Dashed line with triangles: Δt=1.0, t_1=0.5 in Eq. (3.18); Dashed-dotted line with squares: Δt=1, t_1=1.0 in Eq. (3.18).

3.3.3 Late-time concentration evolution at a well for recycling at a single point

When β_1 tends towards β_2 in Eq. (3.10), so that $\beta_1 = \beta_2 = \beta_i$, solute recycling takes place on a single point β_i only. Solving it for the boundary conditions in Eq. (3.12) and looking for the late time slopes according to Box 3.1, leads to a formulation for the concentration slope $m(\beta)$ at late times for recycling at any point β_i within the domain:

$$m(\beta, t=\infty) = -\frac{\alpha(1-\alpha)\,\mathrm{H}(\beta-\beta_i)}{(1-\alpha+\alpha\beta)\ln(1-\alpha+\alpha\beta_i)} \tag{3.19}$$

If Eq. (3.19) is solved for $\beta = 1$ and $\beta_i < 1$, we obtain the concentration slope m_p at the well:

$$m_p = -\frac{\alpha(1-\alpha)}{\ln(1-\alpha+\alpha\beta_i)} = \frac{1-\alpha}{t_{TR}} \tag{3.20}$$

Eq. (3.20) incorporates the expression of the travel time t_{TR} between the recycling point β_i and the extraction well ($\beta = 1$), which is obtained by spatial integration of the inverse of the pore velocity $v(\beta)$ between the injection point β_i and the well ($\beta = 1$):

$$t_{TR} = \int_{\beta_i}^{1} \frac{1}{v(\beta)}\,d\beta = \int_{\beta_i}^{1} \frac{1}{1-\alpha+\alpha\beta}\,d\beta = -\frac{\ln(1-\alpha+\alpha\beta_i)}{\alpha} \tag{3.21}$$

Hence, the well concentration slope m_p at late times (Eq. 3.20) can be obtained by multiplying the inverse of the travel time (Eq. 3.21) with (1-α). According to Eq. (3.2) and Eq. (3.6) the term (1-α) describes the ratio between the lateral flow rate and the extraction rate, reflecting the water deficit induced by evapotranspiration. If we assume that the lateral solute mass flux is proportional to the water flux, (1-α) is a measure for either the fraction of the extracted solute mass flux derived directly from the limits or for the fraction of the extracted water that will be evapotranspired, leading to concentration.

The well concentration slope m_p, as obtained from Eq. (3.20), can be subdivided into two components: (1) the inverse of the mean travel time between the recycling point and the well ($1/t_{TR}$), a space-dependent intrinsic parameter which will vary throughout the domain, and (2) the 'solute-importation' parameter (1-α), being space-independent, describing the rate of solute-importation from the limits, compensating evapotranspiration.

3.3.4 Transient well concentration evolution for recycling at a single point

Having isolated two components (α and t_{TR}) which will determine solute recycling, we can formulate the well response in an alternative way, without making use of the 1-D advective transport equation. First we will observe the well response to a unit-mass released at any point in the system to spatial variations of solute recycling. The released unit mass will arrive at the well after t_{TR} and then be immediately recycled. Thus, the well response will be a series of Dirac's delta 'functions' $\delta(t\text{-}nt_{TR})$, $n = 0,1,2,...,\infty$, appearing at a frequency of $1/t_{TR}$ (recycling frequency). This describes the behaviour of the first component, which was identified in Eq. (3.20). To obtain the concentration evolution at the well $C_p(t)$ in response to solute recycling, the series of Diracs' delta 'functions' $\delta(t\text{-}nt_{TR})$, $n = 0,1,2,...,\infty$, is convoluted with the solute flux arriving at the well from the boundary $(1\text{-}\alpha)$, which is the second component governing the concentration slope m_p in Eq. (3.20). This convolution integral yields the following series of superimposed step functions:

$$C_p(t) = (1-\alpha)\int_t \sum_{n=0}^{\infty} \delta(t - nt_{TR})dt = (1-\alpha)\sum_{n=0}^{\infty} H(t - nt_{TR}) \tag{3.22}$$

The observed concentration evolution at the well is an infinite sum of step-functions, one for each recycling cycle, each with an intensity of $(1\text{-}\alpha)$, but delayed by t_{TR} from the previous step-function (Fig. 3.4).

For the advective 1-D example, the concentration at the well at time nt_{TR} can be subdivided into n equal contributions. In a water sample taken at the well, there will be equally many solute particles that have finished their 0^{th} to n^{th} recycling cycles, respectively. Hence, the concentration or solute mass flux response at a well is the sum of the contributions of all recycling cycles that have already taken place. Since recycling takes place at a single point only, a solute that has been recycled twice from the same injection point has travelled twice as far as a solute that has been recycled only once. An n-fold identical travel distance equals an n-fold travel time and this is reflected in the step-function in Eq. (3.22). All sampled 'recycling ages' will be a multiple of the travel time between the injection and the extraction point. If we assume that solutes have an age zero when they enter the system by the lateral boundary, the mean solute age in the system will steadily increase, while the mean water age will remain at steady state.

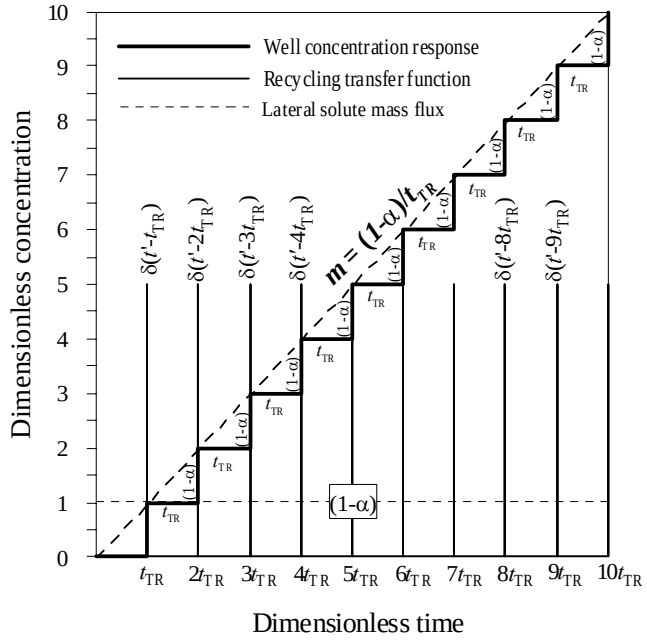

Fig. 3.4: Dimensionless concentration evolution at the well caused by recycling at a point β_i in the system. The step-function results from convolution of the series of Dirac's delta 'functions' $\delta(t\text{-}nt_{TR})$, $n = 0,1,2,\ldots,\infty$ (schematised in the graph with frequency $1/t_{TR}$) with the constant lateral solute inflow $(1\text{-}\alpha)$.

Fig. 3.4 shows the relative concentration response at the well according to Eq. (3.22), resulting from the convolution integral of the laterally inflowing solute mass flux $(1\text{-}\alpha)$ with the series of Diracs' delta 'functions' $\delta(t\text{-}nt_{TR})$, $n = 0,1,2,\ldots,\infty$. The long-term slope m_p at the well, as derived from Eq. (3.20), can be seen to approximate the concentration evolution at the well, composed of the ratio between $(1\text{-}\alpha)$ and t_{TR} respectively, whereas Eq. (3.22) yields the exact concentration evolution for this purely advective configuration.

This purely advective example infers that the exact concentration evolution can be obtained from the convolution of the well response to a narrow pulse with the lateral solute mass flux captured from the boundary. This principle forms the basis of the transfer function theory, which will be used in the following section to describe the solute recycling process in arbitrary advective-dispersive systems.

3.4 Formulation of the solute recycling process in advective-dispersive systems by means of the transfer function theory

In this section, we will investigate how the extracted solute mass flux, or the well concentration, in response to solute recycling can be described by means of the transfer function theory for advective-dispersive systems (Jury 1982, Jury et al. 1986). For the examples shown in section 3.3, we observed that the well salinity evolution in purely advective systems will vary as a function of the travel time between the recycling point and the well. In section 3.3.4, the transfer function approach was already inferred for a purely advective system, by deducing the exact concentration evolution at the well from the convolution integral of the recycling response to a narrow pulse with the lateral solute mass flux (Fig. 3.4).

In advective-dispersive systems, the travel times between two points are described by a transfer function, corresponding to the travel time probability density function (PDF) that reflects the distribution of solute travel times τ_{life} between an inlet and an observation point, conditional on τ_{in}, the time at which solutes entered the system (Jury & Roth 1990). The internal dynamics between an inlet and an observation point are characterised by the transfer function, corresponding to the travel time PDF $g_t^{\gamma}(t)$, defined as the response of the system to a narrow pulse input at inlet as follows (Jury & Roth 1990):

$$J_p(t) = Q_p C_p(t) = \int_0^t g_t^{\gamma}(\tau_{in})\delta(\boldsymbol{x}, t-\tau_{in}) m^* d\tau_{in} = m^* g_t^{\gamma}(t) \tag{3.23}$$

where $g_t^{\gamma}(t) = g_t(\boldsymbol{x}'|t, \boldsymbol{x}, \tau_{in})$ [T^{-1}] is the travel time PDF between the injection point at the Cartesian coordinates $\boldsymbol{x}$ and the extraction well $\boldsymbol{x}$', and m^* [M] is the mass released at $\boldsymbol{x}$. The flow path between $\boldsymbol{x}$ and $\boldsymbol{x}$' are symbolised by the index γ in $g_t^{\gamma}(t)$. The travel time PDF $g_t^{\gamma}(t)$ is the product of the well extraction rate Q_p [L^3T^{-1}] and the flux concentration $C_p(t)$ [ML^{-3}] at the well, corresponding to the well solute mass response $J_p(t)$ [MT^{-1}] to an instantaneous mass release at inlet $\boldsymbol{x}$. For a unit mass input of $m^* = 1$, the solute mass response $J_p(t)$ at the irrigation well equals the travel time PDF $g_t^{\gamma}(t)$, with its integral corresponding to the probability $P(\boldsymbol{x})$ of a solute injected at $\boldsymbol{x}$ being captured by the well at $\boldsymbol{x}'$ as follows (Jury & Roth 1990, Neupauer & Wilson 1999).

$$P(\boldsymbol{x}) = \int_0^{\infty} g_t^{\gamma}(t)dt \tag{3.24}$$

Transfer functions, as described by Eq. (3.23) are used to model output flux signals at an observation point (e.g. well) as a function of any given input flux released at a point ***x***. According to Jury and Roth (1990), the output flux signal $J_p(t)$ is obtained by the convolution integral of the input signal $I(\boldsymbol{x},t)$ with the transfer function $g_t^{\gamma}(t)$ as follows:

$$J_p(t) = Q_p C_p(t) = \int_0^t g_t^{\gamma}(\tau_{in}) I(\boldsymbol{x}, t-\tau_{in}) d\tau_{in} \tag{3.25}$$

The main assumption required for the transfer function model to work is the applicability of the principle of linear superposition, which presupposes steady-state hydraulic conditions and only linearly reactive solute transport.

To apply the transfer function theory to describe solute recycling, we have to account for the reintroduction of the extracted solute mass flux $J_p(t)$ into the system on the irrigation point ***x***. The well response $J_p(t)$ can be obtained by means of Eq. (3.25), under the condition that a transfer function is found, which describes the transformation that a mass signal captured by the well will suffer when solute recycling takes place.

In the following, we formulate a recycling transfer function (RTF) by means of the travel time PDF $g_t^{\gamma}(t)$ between the recycling point ***x*** and the well. Then, we will substitute the travel time PDF $g_t^{\gamma}(t)$ in Eq. (3.25) by the RTF to obtain the well response $J_p(t)$, resulting from solute importation from the boundaries and solute recycling.

3.4.1 The recycling transfer function (RTF)

According to Eq. (3.23) the transfer function $g_t^{\gamma}(t)$ between a point ***x*** and an extraction well ***x'*** is obtained from the mass-normalised well response to a narrow pulse input at ***x***. This travel time PDF $g_t^{\gamma}(t)$ may either represent the travel time PDF in the saturated zone only, or reflect the transfer function resulting from the transit through the unsaturated and saturated zones.

When solute recycling takes place, the first well response to a narrow input signal at the recycling point ***x*** corresponds to the travel time PDF $g_t^{\gamma}(t)$. This output signal will be reintroduced into the system on the recycling point ***x***, thus representing the continuation of the mass input signal, which will again be convoluted with the travel time PDF $g_t^{\gamma}(t)$. This process leads to self-convolution of the travel time PDF $g_t^{\gamma}(t)$, since the mass input signal at ***x*** corresponds to the well response, resulting from convolution with the travel time PDF $g_t^{\gamma}(t)$. The mass-normalised transient well

response to solute recycling resulting from an initial instantaneous mass release at ***x*** will be denoted the *recycling transfer function* $g_{\mathrm{in}}^{\gamma}(t)$. The *recycling transfer function* (RTF) transforms an input signal that is captured in the recycling circuit into the resulting well response and can be obtained step-by-step, by describing each recycling cycle separately.

The RTF can be separated into *n* recycling cycle PDFs, resulting from the self-convolution of the travel time PDF $g_{\mathrm{t}}^{\gamma}(t)$. A solute that has been recycled twice, has transited the flow path between ***x*** and ***x'*** twice (to be symbolised by the index 2γ). The travel time PDF corresponding to the response at the well of all solutes that have transited the flow path between ***x*** and ***x***' twice describes the second recycling cycle PDF $g_{\mathrm{t}}^{2\gamma}(t)$ and is obtained by self-convolution of the travel time PDF $g_{\mathrm{t}}^{\gamma}(t)$ as follows:

$$g_{\mathrm{t}}^{2\gamma}(t) = \int_0^t g_{\mathrm{t}}^{\gamma}(t-u)\, g_{\mathrm{t}}^{\gamma}(u)\, du = g_{\mathrm{t}}^{\gamma}(t) * g_{\mathrm{t}}^{\gamma}(t) \tag{3.26}$$

The relationship in Eq.(6) is true for any multiple transit of the flow path between ***x'*** and ***x*** and can therefore be used to express any recycling cycle PDF $g_{\mathrm{t}}^{n\gamma}(t)$ by means of the travel time PDF $g_{\mathrm{t}}^{\gamma}(t)$ between the recycling point ***x*** and the well ***x***'. The respective recycling cycle PDFs $g_{\mathrm{t}}^{n\gamma}(t)$ can either be expressed in the time domain or in Laplace space, where a convolution integral reduces to a simple product, as follows:

<u>*Recycling cycle PDFs*</u> (3.27)

	Time domain	*Laplace space*
0th recycling cycle:	$g_{\mathrm{t}}^{0\gamma}(t) = \delta(t)$	$\hat{g}_{\mathrm{t}}^{0}(p) = 1$
1st recycling cycle:	$g_{\mathrm{t}}^{1\gamma}(t) = g_{\mathrm{t}}^{\gamma}(t)$	$\hat{g}_{\mathrm{t}}^{1\gamma}(p) = \hat{g}_{\mathrm{t}}^{\gamma}(p)^1$
2nd recycling cycle:	$g_{\mathrm{t}}^{2\gamma}(t) = g_{\mathrm{t}}^{\gamma}(t) * g_{\mathrm{t}}^{\gamma}(t)$	$\hat{g}_{\mathrm{t}}^{2\gamma}(p) = \hat{g}_{\mathrm{t}}^{\gamma}(p)^2$
nth recycling cycle:	$g_{\mathrm{t}}^{n\gamma}(t) = g_{\mathrm{t}}^{\gamma}(t) * g_{\mathrm{t}}^{\gamma}(t) * .. * g_{\mathrm{t}}^{\gamma}(t)$	$\hat{g}_{\mathrm{t}}^{n\gamma}(p) = \hat{g}_{\mathrm{t}}^{\gamma}(p)^n$

where p [T^{-1}] is the Laplace variable. The resulting output signal of any recycling cycle yields the input signal of the following recycling cycle, which is reflected in the series of self-convolutions.

The 0^{th} recycling cycle PDF $g_t^{0\gamma}(t)$ indicates instantaneous recycling between the well and the recycling point ***x*** at the moment of the unit mass release at $t = 0$. The recycling cycle PDF $g_t^{n\gamma}(t)$ at a time τ yields the travel time contribution to the RTF that has transited the flow path between ***x*** and ***x'*** n-times. Hence, the RTF $g_{in}^{\gamma}(t)$ can be written as sum of the contributions of all possible recycling cycles PDFs $g_t^{n\gamma}(t)$, $n = 0,1,2,\ldots,\infty$, as follows:

$$g_{in}^{\gamma}(t) = \sum_{n=0}^{\infty} g_t^{n\gamma}(t) = \delta(t) + g_t^{\gamma}(t) + g_t^{\gamma}(t) * g_t^{\gamma}(t) + \ldots + g_t^{\gamma}(t) * g_t^{\gamma}(t) * \ldots * g_t^{\gamma}(t) \quad (3.28)$$

Or, expressed in Laplace space:

$$\hat{g}_{in}^{\gamma}(p) = \sum_{n=0}^{\infty} \hat{g}_t^{\gamma}(p)^n = \frac{1}{1-\hat{g}_t^{\gamma}(p)}; \quad \left|\hat{g}_t^{\gamma}(p)\right| \le 1 \quad (3.29)$$

The RTF $g_{in}^{\gamma}(t)$ reflects a travel time distribution consisting of solutes that have been recycled different numbers of times. Hence, for a given solute life time τ_{life} represented in the RTF $g_{in}^{\gamma}(t)$, no difference is made in the number of times a solute has been recycled. As an example, a solute that has been recycled once has a given probability of arriving at the well after τ_{life}, while a solute that has been recycled twice will have suffered an additional convolution with the travel time PDF $g_t^{\gamma}(t)$ and thus have a higher probability of arriving after τ_{life}. In the RTF $g_{in}^{\gamma}(t)$, the probability of arriving after τ_{life}, will consist of the lumped probability of all possible recycling cycles of arriving after τ_{life}. The main difference between the travel time PDF $g_t^{\gamma}(t)$ and the RTF $g_{in}^{\gamma}(t)$ is that one and the same solute in the RTF will represent multiple solute lifetimes, whereas in the PDF $g_t^{\gamma}(t)$ every initially released solute will represent only one life time.

Fig. 3.5 shows the RTF $g_{in}^{\gamma}(t)$ and the recycling cycle PDFs $g_t^{n\gamma}(t)$ of several recycling cycles for a 1-D closed system. Closed systems are characterised by a travel time PDF $g_t^{\gamma}(t)$ with a capture probability $P(\boldsymbol{x}) = 1$, according to Eq. (3.24). The capture probability of the n-fold convolution of the travel time PDF $g_t^{\gamma}(t)$ will therefore remain unchanged and reflects, that solutes that are captured in the recycling circuit will be trapped. For a given solute arrival or life time τ, indicated on Fig. 3.5b, the contribution from the first and the second recycling cycle PDFs $g_t^{1\gamma}(t)$ and $g_t^{2\gamma}(t)$ tend towards zero, while the contributions from the third and fourth recycling cycles, $g_t^{3\gamma}(t)$ and $g_t^{4\gamma}(t)$, add up to the RTF $g_{in}^{\gamma}(t)$. In Fig. 3.5c, the surface P_3 represents the probability of a solute within the third recycling cycle of having an arrival time τ inferior to the arrival time of solutes

within the fourth recycling cycle: in other words, it is the probability of solutes in the third recycling cycle of not being 'overtaken' by solutes of a higher order cycle. P_4 represents the probability of a solute arrival time in the fourth recycling cycle being superior to all lower order recycling cycles. $P_{3/4}$ is the probability of solutes within either the third or the fourth recycling cycle of having the same arrival time: these are the solutes which are 'just about' to overtake or to be overtaken. The time $\tau_{3/4}$ corresponds to the solute life time, for which the contributions to the RTF of the two neighbouring PDFs are identical. The more a system is dispersive or the shorter the travel times are to the extraction well, the more likely it becomes that solutes which have already been recycled *n* times will 'overtake' solutes of a lesser recycling order. The 'overtaking' leads to a homogenisation and therefore to a smoothening of the response at late times, only possible in dispersive systems.

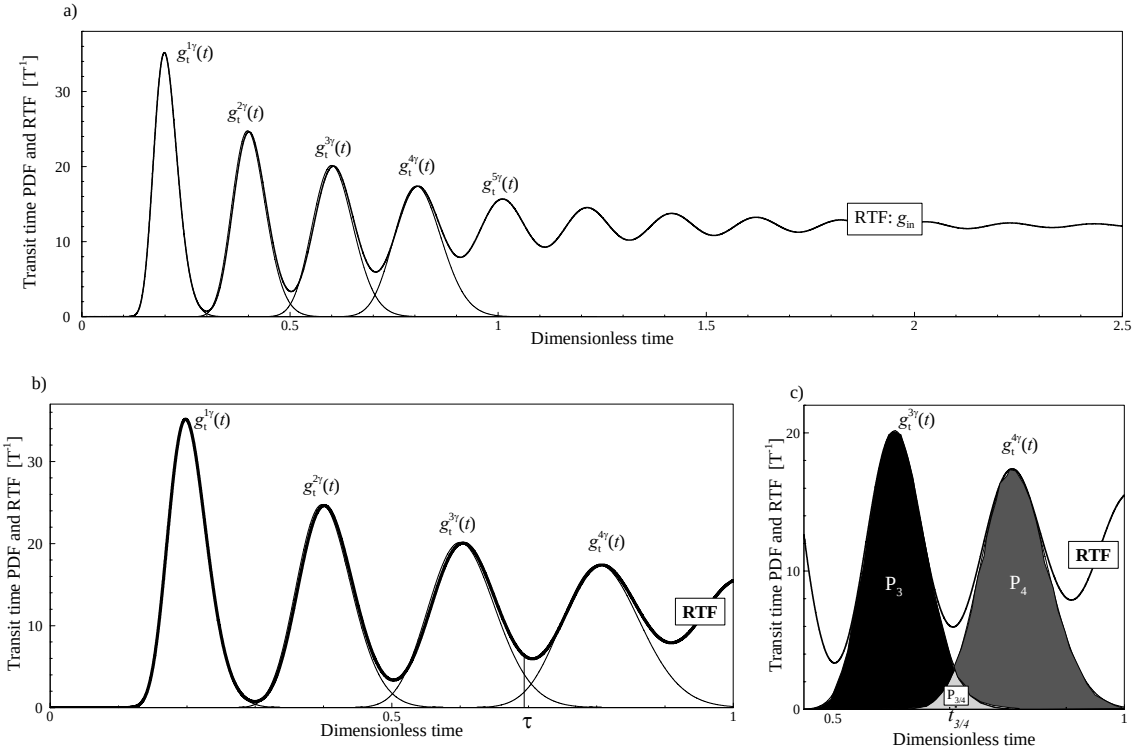

Fig. 3.5: Graphical representation of the advective dispersive solute recycling process in a closed system, showing the superposition of the recycling cycle PDFs, corresponding to the solute mass flux contributions of different recycling cycles as well as the recycling transfer function RTF $g^{\gamma}{}_{tn}(t)$**.** a) Showing the RTF as well as four recycling cyle PDFs $g^{\gamma}{}_{t}(t)$. b) Close-up of the four recycling cyle PDFs $g^{\gamma}{}_{t}(t)$, γ =1, 2, 3, 4, with indicated life time $\boldsymbol{\tau}$ to which mainly $g^{3\gamma}{}_{t}(t)$ and $g^{4\gamma}{}_{t}(t)$ contribute. c) Close-up of $g^{3\gamma}{}_{t}(t)$ and $g^{4\gamma}{}_{t}(t)$ with indicated surfaces corresponding to recycling probabilities.

Fig. 3.6 shows the RTFs $g_{in}^{\gamma}(t)$ (full lines) for solute recycling at two relative spatial coordinates (β = 0.6 and β = 0.8) in a 1-D closed (Fig. 3.6a) and open system (Fig. 3.6b), with a lateral inflowing boundary located at β = 0 with $C(\beta = 0,t) = 1$, and an irrigation well at β = 1. In closed systems, the value of the RTF at late times can be shown to be the inverse of the 1st moment (see Box 3.2, Eq. B.3.2.4). For a constant lateral solute mass flux I in Eq. (3.25) the RTF $g_{in}^{\gamma}(t)$ scaled by I is the first time-derivative of the solute mass flux at the well (Fig. 3.6a). Hence, the late-time value of the RTF and the lateral solute mass flux define the late-time slope of the concentration evolution at the well which is equivalent to advective late-time concentration slope as defined in Eq. (3.20). However, the RTF scaled by I yields the well concentration slope along the entire time-axis, not only at late times.

In open systems, the RTF $g_{in}^{\gamma}(t)$ at late times will drop to zero (Fig. 3.6b), since the n-fold convolution (for $n = \infty$) of a PDF $g_{t}^{\gamma}(t)$ with an integral inferior to one will tend towards zero (i.e. $P(\boldsymbol{x}) < 1$). In this 1-D example, the capture probability was reduced by recycling only a fraction of the extracted solute mass flux. In this way, solutes which enter the recycling circuit could also exit the circuit. Hence, in open systems, a steady state solute mass flux will be attained, which reflects the equilibrium between solutes entering the recycling circuit and solutes exiting. As soon as equilibrium is reached, the mean recycling time t_{rec} can be obtained by calculating the first moment of the RTF $g_{in}^{\gamma}(t)$, as described in Box. 3.2 (Eq. B.3.2.7) and yields:

$$t_{rec} = \frac{t_{TR}}{1 - P(\boldsymbol{x})} \tag{3.30}$$

where t_{TR} is the mean travel time between the recycling point and the well and $P(\boldsymbol{x})$ the capture probability as defined in Eq. (3.24). The mean recycling time t_{rec} equals the mean travel time between the recycling point x and the well normalised by the probability of exiting the recycling circuit (1-$P(\boldsymbol{x})$). Therefore, the higher the probability of arriving at the well from point x is, the longer the mean recycling time and the larger the solute mass accumulation in the system will be. Fig. 3.6b shows two RTFs $g_{in}^{\gamma}(t)$ with a capture probability of $P(\boldsymbol{x})$ = 0.5 between the recycling point x and the well with the indicated mean recycling time corresponding to $2t_{TR}$, according to Eq. (3.30).

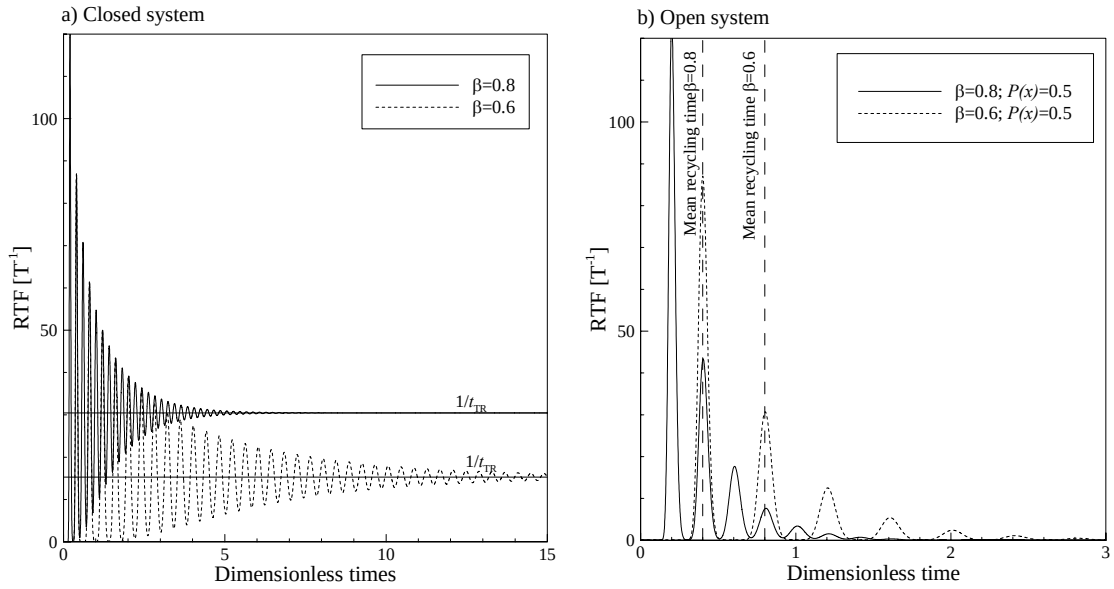

Fig. 3.6: RTFs $g^{\gamma}_{\text{in}}(t)$ at two different spatial coordinates (β = 0.6, 0.8) in a 1-D closed and open system. a) Closed system: the asymptotic value of the RTF corresponds to the inverse of the mean travel time between the recycling point and the well. b) Open system: two RTFs tending towards zero at late times ($P(\boldsymbol{x})$ = 0.5). The mean recycling transit times $t_{\text{rec}}=2t_{\text{TR}}$, according to Eq. (3.30) are indicated.

In this section, we have described the behaviour of solutes in recycling circuits by defining the recycling RTF $g^{\gamma}_{\text{in}}(t)$. In the same way as the travel time PDF $g^{\gamma}_{\text{t}}(t)$ defines the transformation of an input signal released at $\boldsymbol{x}$ by the time of arrival at an outlet, the RTF $g^{\gamma}_{\text{in}}(t)$ describes how a solute signal captured by the well will be transformed by the process of solute recycling. However, the RTF $g^{\gamma}_{\text{in}}(t)$ cannot be considered in terms of one PDF, but has to be regarded as a multitude of PDFs. Nevertheless, the RTF $g^{\gamma}_{\text{in}}(t)$ acts as transfer function and can therefore substitute the transfer function $g^{\gamma}_{\text{t}}(t)$ in Eq. (3.25) to obtain the solute mass flux response $J_{\text{p}}(t)$ at the well to solute recycling.

Box 3.2: Moment equations applied to the RTF

Closed systems: In Laplace space, the general definition of the n^{th} moment can be written as follows, with $\lim_{p\to 0}\hat{g}^{\gamma}_{\text{t}}(p)=1$ (i.e. $P(\boldsymbol{x})$=1):

$$\mu_n(\hat{g}^{\gamma}_{\text{t}}(p))=(-1)^n\lim_{p\to 0}\frac{\partial^n\hat{g}^{\gamma}_{\text{t}}(p)}{\partial p^n} \qquad \text{(B 3.2.1)}$$

At late times, the RTF $g^{\gamma}_{\text{in}}(t)$ tends towards a constant $g^{\gamma}_{\text{in}}(t=\infty)=m$ (Fig. 3.6). According to Eq. (B 3.1.5) the constant value at late times can be written as follows:

$$m = p\hat{m} = \lim_{p\to 0} p\hat{g}^{\gamma}_{\text{in}}(p) \tag{B 3.2.2}$$

Making use of Eq. (3.29) for the definition of $\hat{g}^{\gamma}_{\text{in}}(p)$, m can be expressed as follows:

$$m = \lim_{p\to 0} \frac{p}{1-\hat{g}^{\gamma}_{\text{t}}(p)} \tag{B 3.2.3}$$

which is undefined, since $\lim_{p\to 0}\hat{g}^{\gamma}_{\text{t}}(p)=1$. Applying the rule of l'Hospital to overcome this, yields:

$$m = \lim_{p\to 0} \frac{p}{1-\hat{g}^{\gamma}_{\text{t}}(p)} = \lim_{p\to 0} \frac{1}{-\frac{\partial(\hat{g}^{\gamma}_{\text{t}}(p))}{\partial p}} \tag{B 3.2.4}$$

Comparing (B 3.2.4) with the definition of the 1st moment given in (B 3.2.1) shows that the RTF at late times tends towards the inverse of the first moment, corresponding to the mean travel time between the recycling point ***x*** and the well:

$$m = \frac{1}{\mu_1(\hat{g}^{\gamma}_{\text{t}}(p))} \tag{B 3.2.5}$$

Open systems: In Laplace space, the general definition of the n^{th} moment can be written as follows, with $\lim_{p\to 0}\hat{g}^{\gamma}_{\text{t}}(p)<1$ (i.e. $P(\boldsymbol{x})$ < 1)**:**

$$\mu_n(\hat{g}^{\gamma}_{\text{t}}(p)) = \lim_{p\to 0}\left[\frac{(-1)^n}{\hat{g}^{\gamma}_{\text{t}}(p)}\frac{\partial^n \hat{g}^{\gamma}_{\text{t}}(p)}{\partial p^n}\right] \tag{B 3.2.6}$$

The RTF $\hat{g}^{\gamma}_{\text{in}}(p)$ in open systems tends towards zero at late times. To obtain the mean recycling time t_{rec}, we apply the first moment equation (B.3.2.6) to the RTF $\hat{g}^{\gamma}_{\text{in}}(p)$, making use of Eq. (3.29):

$$\mu_1(\hat{g}^{\gamma}_{\text{in}}(p)) = \lim_{p\to 0}\left[\frac{-1}{\hat{g}^{\gamma}_{\text{in}}(p)}\frac{\partial \hat{g}^{\gamma}_{\text{in}}(p)}{\partial p}\right] = \lim_{p\to 0}\left[\frac{-1}{1-\hat{g}^{\gamma}_{\text{t}}(p)}\frac{\partial \hat{g}^{\gamma}_{\text{t}}(p)}{\partial p}\right] =$$

$$= \frac{\mu_1(g^{\gamma}_{\text{t}}(t))}{1-P(x)} = \frac{t_{\text{TR}}}{1-P(x)} \tag{B 3.2.7}$$

(B 3.2.7) shows that the first moment of the RTF $\hat{g}^{\gamma}_{\text{in}}(p)$ equals the first moment of the PDF $\hat{g}^{\gamma}_{\text{t}}(p)$ divided by the probability of not being captured by the well (1 - $P(\boldsymbol{x})$, probability of exiting the recycling circuit).

3.4.2 The well solute mass response $J_p(t)$

To obtain the well solute mass response, the travel time PDF $g_t^{\gamma}(t)$ in Eq. (3.25) is replaced by the RTF $g_{in}^{\gamma}(t)$ and convoluted with the solute mass flux $I(t)$ that is captured by the well from the boundaries.

Making use of Eq. (3.29), in which the RTF $g_{in}^{\gamma}(t)$ is expressed by means of the travel time PDF $g_t^{n\gamma}(t)$, the convolution integral in Eq. (3.25) can be written in Laplace space as follows:

$$\hat{J}_p = \hat{I}\hat{g}_{in}^{\gamma}(p) = \hat{I}\sum_{n=0}^{\infty}\hat{g}_t^{\gamma}(p)^n = \hat{I}\frac{1}{1-\hat{g}_t^{\gamma}(p)} \tag{3.31}$$

Eq. (3.31) yields the solute mass response at a well $\hat{J}_p$ for arbitrary systems and time-dependent lateral solute mass flux $\hat{I}$, under the condition that the travel time PDF $g_t^{\gamma}(t)$ between the recycling point ***x*** and the extraction well ***x'*** is known. Eq. (3.31) is of particular interest for simulation purposes, since it allows us to define a distributed transient 'recycling source' term in the general form of the advection dispersion equation (ADE) for arbitrary systems. In this way, transient solute recycling simulations can be run without coupling the extracted solute mass flux from the wells to distributed solute sources on irrigation surfaces in a time-stepping procedure.

For a constant lateral solute mass flux $I(t)=I$ (in Laplace space written as $\hat{I} = I/p$), Eq. (3.31) can be reformulated as follows:

$$p\hat{J}_p = I\frac{1}{(1-\hat{g}_t^{\gamma}(p))} \quad , \qquad I = \int_{\Gamma^-} PC_0\mathbf{q}\cdot\mathbf{n} \tag{3.32a}$$

where integration over the inflowing limits Γ^- of the product of the solute mass flux ($C_0\mathbf{q}\cdot\mathbf{n}$) and the capture probability P yields the constant lateral solute mass flux I captured by the well from the boundaries. Eq. (3.32a) shows that the RTF $g_{in}^{\gamma}(t)$ scaled by the constant solute mass flux I equals the first time derivative of the solute mass evolution at the well. Eq. (3.32a) in the time domain yields:

$$\frac{\partial J_{\mathrm{p}}}{\partial t} = I g_{\mathrm{in}}^{\gamma}(t) \tag{3.32b}$$

Fig. 3.7 shows the flow rate normalised well solute mass responses (i.e. well concentrations, dashed lines with circles) and the corresponding RTFs $g_{\mathrm{in}}^{\gamma}(t)$ (full lines) for solute recycling at two relative spatial coordinates (β = 0.2 and β = 0.8) in a 1-D closed and open system, with a lateral inflow boundary located at β = 0 with $C(\beta = 0, t) = 1$, and one extraction well at β = 1. In the closed system (Fig. 3.7a and 3.7b), in which the solute mass remains in the recycling circuit, the RTFs attain a threshold value at late times (see Fig. 3.6), when the initially released mass is perfectly mixed within the recycling circuit. Being the first time derivative of the solute mass flux, the threshold value of the RTF $g_{\mathrm{in}}^{\gamma}(t)$ scaled by the lateral solute mass flux I corresponds to the solute mass slope at late times, reflecting a perfectly homogenised solute arrival frequency which equals the inverse of the mean travel time between the recycling point $\boldsymbol{x}$ and the well, as shown in (B.3.2.4).

In the case of open systems (Fig. 3.7c and 3.7d), in which a fraction of the solutes leave the circuit, the RTF will tend towards zero at late times. Therefore, the extracted solute mass flux $J_{\mathrm{p}}(t)$ and well concentration $C(t)$ will stabilise as soon as the solute mass loss from the recycling circuit equals the solute mass influx (Fig. 3.7c,d).

In Fig. 3.7a-d, the RTFs $g_{\mathrm{in}}^{\gamma}(t)$ were scaled by the lateral constant solute mass flux I, then integrated and normalised with the constant well extraction rate Q_{p} to obtain the transient well concentration response $C_{\mathrm{p}}(t)$ (dashed lines with circle symbols). The transient well concentration responses $C_{\mathrm{p}}(t)$ compare well with the results from numerical transient simulations run with solute recycling (bold lines). Hence, knowing the PDF $g_{\mathrm{t}}^{\gamma}(t)$ and the solute mass flux I at the well is sufficient to simulate the transient well solute mass flux $J_{\mathrm{p}}(t)$, using the relationship established in Eq. (3.32).

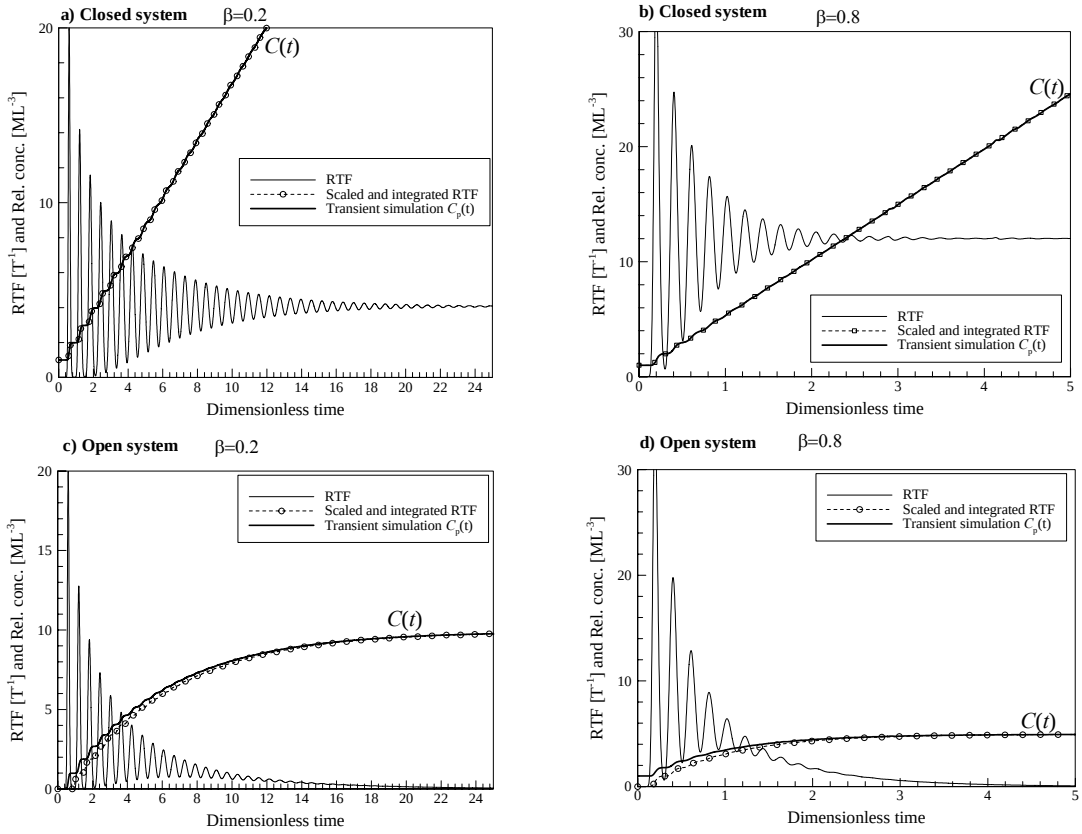

Fig. 3.7: Transient well concentration responses $C_p(t)$ (dashed lines with circles) obtained from scaling the RTFs $g_{in}^{\gamma}(t)$ (full lines) by the lateral solute mass flux I, time-integrating and normalising with the extraction rate Q_p for different spatial coordinates (β = 0.2 and 0.8) in a 1-D closed and open system. a, b: Closed systems with 100% solute recycling at spatial coordinates β = 0.2 and 0.8 respectively. c, d: Open systems with 90% solute recycling at spatial coordinates β = 0.2 and 80% solute recycling at β = 0.8 respectively, showing that the RTFs $g_{in}^{\gamma}(t)$ drop to zero and the well concentration stabilises at late times.

As illustrated in Fig. 3.7c and 3.7d, open systems attain a steady-state solute mass flux $J_p(t)$ at late times ($t \to \infty$). To determine the steady-state solute mass flux in Laplace space, $\hat{J}_p$ is multiplied by p and the limit value for p = 0 is sought (according to Box 3.1, B 3.1.5):

$$J_p(t=\infty) = \lim_{p\to 0} p\hat{J}_p \tag{3.33}$$

Combining Eq. (3.32a) and Eq. (3.33) yields:

$$J_p(t=\infty) = \frac{I}{1-\lim_{p\to 0}\hat{g}_t^{\gamma}(p)} \tag{3.34}$$

According to the definition of the Laplace transform, $\lim_{p\to 0} \hat{g}_t^{\gamma}(p)$ corresponds to the 0th moment of $g_t^{\gamma}(t)$, i.e. the capture probability $P(\boldsymbol{x})$ as defined in Eq. 3.24. Hence, Eq. (3.34) can be written as follows:

$$J_p(t=\infty) = \frac{I}{1-P(\boldsymbol{x})} \tag{3.35}$$

Applying (3.35) to closed systems, which are defined by a capture probability $P(\boldsymbol{x}) = 1$ in the entire domain, yields a solute mass flux $J_p(t=\infty) = \infty$.

Re-formulating (3.35) leads to:

$$J_p = I + P(\boldsymbol{x})J_p \tag{3.36}$$

where J_p stands for $J_p(t=\infty)$. The relationship in Eq. (3.36), valid only for recycling at steady state, shows that the solute mass flux J_p is a function of a fraction of itself, pointing out the recursive character of the process.

3.4.3 Relative steady state well solute contribution from recycling

Using the relationship in Eq. (3.36) allows us to define the relative solute recycling contribution J_{pr} to the steady state solute mass flux J_p. This can be obtained by subtracting the solute mass flux captured from the boundary (I) from the total solute mass flux J_p in (3.36) and normalising it with J_p:

$$\frac{J_p - I}{J_p} = \frac{J_{PR}}{J_p} = P(\boldsymbol{x}) \tag{3.37}$$

The steady-state fraction of recycled solutes extracted from the well corresponds to the arrival probability $P(\boldsymbol{x})$ between a recycling point $\boldsymbol{x}$ and the well.

This fraction can also be expressed differently. At steady-state solute recycling, the solute mass flux at the well J_p can be considered as a perfect mixture of fractions f_i, originating from i different sources. For the case that the flow rate at the well Q_p consists of only two components, the lateral inflowing boundary contributing with a fraction f_0 and the irrigation plot infiltration with a fraction f^* (such that $f^* + f_0 = 1$). With $Q_i = f^* Q_p$ the infiltration rate on the irrigation plot with the infiltration

concentration $C^*=(C_pQ_p)/Q_i$, and C_0 the concentration along the boundary (Fig. 3.1), the steady-state solute mass flux at the well can be expressed as follows:

$$J_p = Q_p(f^*C^* + f_0C_0) = Q_p(f^*\frac{Q_p}{Q_i}C_p + f_0C_0) = J_pf^*\frac{Q_p}{Q_i} + I \tag{3.38}$$

Reformulating Eq. (3.38) yields

$$J_p = \frac{I}{1 - f^*\frac{Q_p}{Q_i}} \tag{3.39}$$

Eq. (3.39) is equivalent to Eq. (3.35). The recycled solute mass fraction at steady-state, corresponding to the capture probability $P(\boldsymbol{x})$ between the recycling point $\boldsymbol{x}$ and the well, as shown in Eq. (3.37), can be expressed by Eq. (3.39):

$$P(\boldsymbol{x}) = f^*\frac{Q_p}{Q_i} \tag{3.40}$$

Eq. (3.40) shows that the relative solute mass fraction derived from recycling at late times, corresponding to the arrival probability $P(\boldsymbol{x})$ in Eq. 3.37, equals the flow rate fraction f^* at the well derived from the irrigation point $\boldsymbol{x}$, scaled by the concentration increase induced by evaporative losses (Q_p/Q_i). Hence, the steady-state solute mass flux at the well $J_p(t=\infty)$ can either be obtained by means of the arrival probability $P(\boldsymbol{x})$, using Eq. (3.35), or by knowing the fraction f^* at the well derived from the recycling point $\boldsymbol{x}$, using Eq. (3.39).

3.5 Conclusions

In this chapter, we have focussed on the quantification of the solute recycling process. The main objective was to identify the parameters which govern the well response and to develop an alternative way of expressing the solute mass response at the well which allows us to substitute the coupled solute source in the transport equation. In contrast to Chapter 2, where the solute recycling process was described for a perfectly mixed domain, we have focussed on the impact of the spatial variability of irrigation locations on the well salinity evolution and on the description of the well responses to solute recycling, since it is the measure which will govern the spatial salinity response to solute recycling in the entire system.

We started the mathematical analysis of the process by defining a distributed ‘recycling source’ in the 1-D advective transport equation, which was solved for homogeneous solute redistribution

over the entire domain and on a single point. We also investigated the effect of conservative solute transfer through the unsaturated zone on groundwater salinisation when solute recycling takes place. The main two components that were found to govern the well concentration evolution in closed systems were the mean travel time between the recycling point and the extraction well and the lateral solute mass flux captured by the well.

According to the considerations made in the first section, a reduction of the leaching fraction (ratio between infiltration rate and applied irrigation water) enhances groundwater salinisation, since the water deficit increases solute importation from the boundaries. In the literature, however, we find that reducing the leaching fraction enhances lime and gypsum precipitation and inhibits soil silicate dissolution and thereby reduces the saltload in the leachate that percolates to the groundwater (e.g. Tanji 1990). Hence, the validity range of the assumption of conservative transfer through the unsaturated zone requires further investigation.

The mathematical description of the solute recycling process was extended to arbitrary advective-dispersive systems by means of the transfer function theory. A recycling transfer function RTF was expressed as the sum of the n-fold self-convolutions of the travel time PDF between the recycling point and the extraction well. The RTF was then used to obtain the well response by convolution with any lateral solute mass signal captured by the well. For steady-state solute recycling, the well solute response was found to be a function of the lateral solute mass flux and the capture probability, only. The RTF describes how solutes are redistributed, while the lateral solute mass flux contributes with the solutes. Hence, a concentration increase can only be observed, if solutes from other sources exist. This fact distinguishes the solute recycling salinisation process from other salinisation processes, since it does not add any solutes to the system but leads to concentration by redistribution. The solute mass flux captured by the well from the boundaries can be applied to any solute source which may be present in the system. If for instance agrochemical additives enter the groundwater system at a constant rate, these can be accounted for by evaluating the solute mass flux captured by the wells from this salinity source, since they, too, will contribute to the recycling process and the same is true for any other source of salinity (e.g. geogenic salt, trapped seawater).

This mathematical analysis allowed us to obtain an independent expression for the solute mass extracted from irrigation wells in response to spatial variations in solute recycling. As stated in Chapter 2, simulation of solute recycling is not included as a standard option in groundwater flow and transport simulation packages. The obtained expressions in Eqs. (3.31) and (3.35) predict the solute mass evolution at a well and can therefore be used to define a distributed ‘recycling source’ in the general form of the advection-dispersion equation (ADE) for arbitrary systems, which will be discussed in the following chapter.

The main assumption we made throughout this chapter was average hydraulic steady-state conditions. Hence, before this approach can be used, the validity of this assumption for any given case has to be thoroughly assessed. As an example, in coastal settings with a highly variable exploitation history, this assumption might not be justified. Also, if density-dependent flow and transport is judged to be an important factor, this approach might not be adequate.

CHAPTER 4

SIMULATION OF SOLUTE RECYCLING IN ARBITRARY AQUIFER SYSTEMS

Partially submitted to Advances in Water Resources

Abstract

The spatial groundwater salinisation induced by solute recycling is investigated by means of different simulation procedures. Direct simulation of solute recycling is proposed for steady state hydraulic conditions, while transient hydraulic conditions are addressed with a numerical time-stepping procedure. For steady state hydraulic conditions, the expression for the solute mass flux at the well obtained from the sum of the *n*-fold convolutions of the average travel time PDF between the recycling plot and the extraction well is introduced as 'recycling source' term into the general form of the advection dispersion equation. Steady and transient state solute recycling can thereby be simulated with any standard flow and transport simulation code. Simulation of solute recycling for transient hydraulic conditions is then done numerically in a time-stepping procedure and the effect of transient hydraulic conditions on groundwater salinisation induced by solute recycling is shown on examples. Simulation options are then presented, such as an infiltration and well concentration constraint, leading to de-activation of a well when a defined limit of exploitability is reached, which is shown to have a major impact on the hydraulic conditions and in return also on solute recycling.

4.1 Introduction

In the previous chapter, we focused on the mathematical analysis of the solute recycling process, which allowed us to define the well solute extraction $J_p(t)$ in response to solute recycling for arbitrary systems. However, we did not investigate the spatial salinisation patterns which may result from solute recycling. Now, that an expression for the extracted solute mass flux $J_p(t)$ has been obtained, the behaviour of the salinisation process can be investigated on the aquifer-scale, by introducing this expression into the advection-dispersion equation (ADE).

Modelling the spatial salinity distributions arising from solute recycling is important, since the solutes introduced by irrigation do not necessarily concentrate below the irrigated surfaces, but can lead to very unexpected patterns depending on the prevailing hydraulic conditions, even in completely homogeneous aquifers. By understanding how such 'unexpected' patterns develop in response to solute recycling, distiction can be made from other salinity sources that may lead to similar patterns (e.g. upconing, geogenic salt deposits, trapped seawater etc.). An early example of a modelling approach investigating the spatial groundwater salinisation that develops in response to irrigation practices was carried out by Konikow and Bredehoeft (1974) for a stream aquifer in the Arkansas River Valley. They combined field investigations and numerical simulations to predict the long-term salinisation increase and distribution in the system. By introducing solute

recycling in their model by means of measured salinity data that had been monitored in the extraction wells, the complicated salinity distribution was impressively well simulated. A decade later, new field investigations were carried out to compare the model predictions with the real salinisation evolution (Konikow and Person 1985). They found, that the model prevision had been too pessimistic, due to calibration on an unrepresentative time-period. The field investigations suggested that the aquifer had reached steady state condition with respect to solute recycling. Hence, this example shows, that salinisation induced by solute recycling may be 'quick', reaching steady state conditions within the time-span of exploitation.

Sophocleous and Ma (1998) used numerical modelling combined with sensitivity analysis, multiple regression analysis and classification procedures to develop a decision support model to assess spatial vulnerability to groundwater salinisation in the Great Bend Prairie aquifer of Kansas. Prendergast et al. (1994) developed a theoretical basis for the evaluation of the future impact of solute recycling on well salinisation and found, that with an optimal distribution of the extracted water, the rate of groundwater degradation at the well is low. They did, however, not specify how to optimise the irrigation schemes. Al-Senafy and Abraham (2004) combined numerical simulation with field investigations to map the groundwater vulnerability towards agricultural activities and irrigation induced groundwater salinisation in southern Kuwait. None of these studies, however, were carried out in coastal areas.

In this chapter, we will present different approaches allowing simulation of solute recycling in different hydraulic settings and start by defining the 'recycling source' in the general form of the ADE, being common to all simulation approaches that will be presented.

We will first focus on solute recycling simulation for hydraulic steady state conditions, making use of the expressions developed for the extracted solute mass flux $J_p(t)$ in Chapter 3 (Eq. 3.31 and 3.35) to define the distributed 'recycling source'.

For steady state solute recycling a 'direct' simulation approach is proposed, similarly to Goode (1996), who showed that the distribution of mean groundwater age obeys the solute-transport equation with a distributed zero-order source of unit strength, corresponding to the rate of aging. We show, that a 'recycling source' in the steady-state form of the ADE can be defined to generate the effect of steady state solute recycling, being a function of the local capture probability and the solute mass flux contribution to the well from the boundaries. The predicted concentration distribution reflects the maximum concentration in response to steady state recycling and can thus be interpreted in terms of solute recycling potential of the entire domain for the given hydraulic setting.

We will then focus on transient solute recycling in hydraulic steady state conditions. The transient distributed 'recycling source' is obtained from the sum of the *n*-fold self-convolutions of the average travel time PDF $g^{\gamma}_{t}(t)$ between the irrigation plots and the extraction well and the solute mass captured by the well from the boundaries (Eq. 3.32a). We then show, that by defining an additional travel time PDF $g_o(t)$, between the irrigation plot and any point in the domain, denoted redistribution PDF, the transient concentration evolution in response to solute recycling can be obtained for any point in the domain by a pure convolution procedure of the recycling transfer function RTF $g^{\gamma}_{in}(t)$ with the redistribution PDF $g_o(t)$.

In the last section, we will present some examples of fully transient solute recycling, carried out with a numerical time-stepping procedure. Examples are shown, which were run with restrictions with respect to infiltration and extraction concentrations. The well concentration restriction leads to de-activation of wells when a threshold concentration is attained, which affects the hydraulic regime and thereby the salinisation pattern of the system. The effect on the transient groundwater salinity evolution in presence of a 'soil buffer' is also illustrated on an example.

4.2 Definition of the 'recycling source'

The main feature all the following simulation approaches have in common is the definition of the distributed solute 'recycling source' term, which can be expressed by the extracted solute mass flux and introduced into the general form of the saturated or unsaturated advection-dispersion equation (ADE). For the saturated case it reads:

$$\frac{\partial \phi C}{\partial t} = -\nabla \cdot (\mathbf{q}C - \phi \mathbf{D} \nabla C) + \frac{J_{\mathrm{p}}(t)}{\Delta} \tag{4.1}$$

where Δ [L^3] is the irrigation plot volume (surface time thickness), ϕ [-] the saturated volumetric porosity, C [ML^{-3}] the concentration, q [LT^{-1}] the specific flux vector, D [L^2T^{-1}] the dispersion tensor and $J_p(t)$ [MT^{-1}] the extracted solute mass flux. The 'recycling source' in Eq. (4.1) is only applied in the irrigation volume Δ, everywhere else in the domain it is set to zero.

Depending on the hydraulic conditions and on the purpose of the solute recycling transport simulation, simulation approaches can vary from fully steady state to completely transient conditions for flow and transport. In the following, simulation procedures will be proposed for the most common hydraulic conditions. The procedures for the steady hydraulic conditions are based on the expression of the solute mass flux developed in the previous chapter, while the fully transient conditions are treated numerically.

4.3 Direct simulation of solute recycling: steady state hydraulic conditions

Direct simulation of solute recycling implies that the distributed recycling source is defined independently of the transport simulation at the beginning of the simulation procedure. The 'recycling source' in Eq. 4.1 can be obtained with standard simulation procedures. Since solute recycling is not a standard option in commercial flow and transport packages, the proposed direct simulation procedure allows solute recycling simulation with any standard code without numerical implementation of solute recycling.

We will define the distributed 'recycling source' by means of the developed expression for the extracted solute mass flux $J_p(t)$, only valid for steady state hydraulic conditions (section 3.4.2). First, the simplest case, steady-state recycling is treated and then, in the second part, we will define the transient 'recycling source'. To obtain the general form of the 'recycling source' in Eq. (4.1), the extracted solute mass flux $J_p(t)$ in Eq. (3.31) is divided by the irrigation plot volume Δ [L^3] and can be written in the time domain in terms of the following convolution integral:

$$\frac{J_p(t)}{\Delta} = \frac{Q_p C_p(t)}{\Delta} = \frac{1}{\Delta}\int_0^t g_{in}^{\gamma}(\tau_{in}) I(t-\tau_{in}) d\tau_{in} \tag{4.2}$$

Where $I(t)$ is the solute mass flux captured by the wells from the boundaries and $g^{\gamma}_{in}(t)$ the recycling transfer function RTF, as defined in Eq. (3.28) and Eq. (3.29).

4.3.1 Steady state simulation of solute recycling

Of all the simulation procedures we will present in this chapter, the steady state solute recycling might be the least realistic, mostly because the time to attain steady state may be so long that the assumption of hydraulic steady state conditions does not hold, but also because levels of salinity may be attained which are above the limit of exploitability and would impose a change of the exploitation scheme. However, the steady state evaluation of the salinity distribution obtained in response to solute recycling is a valuable measure for the maximum salinisation of a system and reveals its salinisation potential for a given exploitation scheme (i.e. hydraulic setting). Also, this simulation approach is computationally very undemanding, several orders of magnitude smaller than transient simulations, which gives way to carry out multiple simulations, either in view of stochastic modelling or for optimisation purposes.

The extracted solute mass flux $J_p(t=\infty)$ at late times in response to solute recycling was defined in Eq. (3.35) as:

$$J_{\mathrm{p}}(t=\infty)=\frac{I}{1-P(\boldsymbol{x})} \tag{4.3}$$

Where x denotes the vector of the cartesian coordinates. The distributed 'recycling source' term in the steady-state form of the ADE is obtained by dividing the extracted solute mass flux by the irrigation plot volume Δ as shown in Eq. (4.1) and can be written as follows:

$$0=-\nabla\cdot(\mathbf{q}C-\phi\mathbf{D}\nabla C)+\frac{J_{\mathrm{p}}(t=\infty)}{\Delta} \tag{4.4}$$

In the following, $J_p(t=\infty)$ will be referred to as J_{p}. When solute recycling takes place on a zone Δ, the capture zone probability $P(x)$ as described in Eq. (4.3) is no longer related to a single point x, but to all points within Δ. Using Eq. (3.36), we can formulate the solute mass balance for the well for the case of redistribution on an irrigation surface Δ as follows:

$$J_{\mathrm{p}}=I+\frac{J_{\mathrm{p}}}{\Delta}\int_{\Delta}P d\Delta \tag{4.5}$$

The first term in Eq. (4.5) is the constant lateral solute mass flux captured by the well from the boundaries (Eq. 3.32a). The second term is the average capture zone probability ($\overline{P}(\Delta)=\frac{1}{\Delta}\int_{\Delta}P d\Delta$) multiplied by J_{p}. The 'recycling source' in Eq. (4.4) can be expressed by Eq. (4.5) and yields the steady state 'recycling source':

$$\frac{J_{\mathrm{p}}}{\Delta}=\frac{I}{\Delta(1-\frac{1}{\Delta}\int_{\Delta}P(\boldsymbol{x})d\Delta)}=\frac{I}{\Delta(1-\overline{P}(\Delta))} \tag{4.6}$$

where $\overline{P}(\Delta)$ is the average capture zone probability of the irrigation plot surface or volume (Δ). Eq. (4.6) can be seen to be equivalent to Eq. (3.35), where recycling took place on a single point only. Introducing (4.6) into (4.4) leads to the steady state form of the ADE with a distributed source accounting for solute recycling:

$$0=-\nabla\cdot(\mathbf{q}C-\phi\mathbf{D}\nabla C)+\frac{I}{\Delta(1-\overline{P}(\Delta))} \quad ; \quad \text{in/on } \Delta \tag{4.7a}$$

else,

$$0=-\nabla\cdot(\mathbf{q}C-\phi\mathbf{D}\nabla C) \tag{4.7b}$$

Eq. (4.7) with its 'recycling source' allows direct simulation of solute recycling for arbitrary systems. The only prerequisite is the average capture zone probability field $\bar{P}(\Delta)$, which has to be determined for the irrigation surface. This can be done with one single adjoint simulation (Uffink 1989, Neupauer & Wilson 1999, Cornaton 2004) and subsequent calculation of the average over the irrigation area. The adjoint or reversed flow field equation to be solved can be written as follows:

$$0 = \mathbf{q} \cdot \nabla P + \nabla \cdot \phi \mathbf{D} \nabla P \tag{4.8}$$

with the boundary conditions:

$P = 1$	on	Γ_p (at the well)	(4.9)
$P = 0$	on	Γ^+ (along the discharge areas)	
Implicit Neuman condition	on	Γ^- (inflow boundaries)	

The implicit Neuman condition evaluates the dependent variable gradient along open boundaries instead of, as classically done, assuming the concentration gradient to be zero (Cornaton et al. 2004). The 'recycling source' term in Eq. (4.7) is time-independent and is distributed on the entire irrigation surface. It generates the equivalent amount of solute mass that is being extracted from the well at steady-state and thereby guarantees solute mass conservation.

Fig. 4.1 shows two results of the same 2-D horizontal, homogeneous finite element model with an extraction well at the coordinates (200/175). The flow is directed from east to west and a constant concentration of $C_0 = 1$ is imposed along the eastern limit. Fig. 4a shows a simulation result neglecting solute recycling, whereas in Fig. 4b, Eq. (4.7) was solved for the same system, assuming that irrigation takes place on the entire domain. The regional concentration gradient can be seen to be the opposite for the two cases. In Fig. 4.1a the dilution effect of infiltration increases from the east to west, while the concentration increases from east to west in Fig. 4.1b.

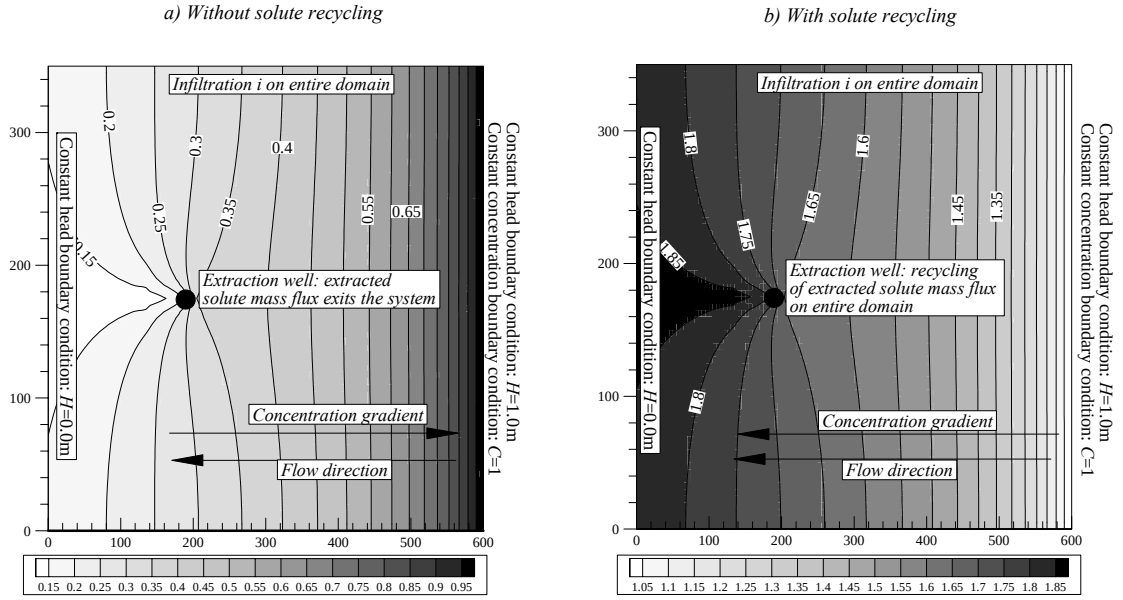

Fig. 4.1: Concentration distributions in a 2-D horizontal, homogeneous finite element model with an extraction well (corresponding to Γ_p in Eq.(4.9)) at coordinates (200/175). The flow is directed from east to west and a constant concentration of C_0=1 is imposed along the eastern limit (corresponding to Γ^- in Eq.(4.9)). (a) Concentration distribution for steady state simulation without solute recycling. (b) Concentration distribution for steady-state simulation with solute recycling, according to Eq. (4.7). All measures are in meters and note that the scales have been distorted for the purpose of lisibility.

Fig. 4.2 shows the concentration distribution obtained with a direct finite element simulation with solute recycling (grey scale) in a heterogeneous 2-D horizontal domain according to Eq. (4.7) for a slightly different hydraulic setting than shown in Fig. 4.1 (i.e. with an injection point as inflowing boundary in the east). This is compared to the result from a transient simulation with solute recycling (full lines), in which the extracted solute mass flux was evaluated in a time-stepping procedure. The CPU requirements for the transient simulation was several orders of magnitude higher than those required using Eq. (4.7). The slight differences in the simulation results may be due to the fact that a complete steady state was not attained in the transient simulation. The concentration distribution resulting from solute recycling on the entire domain is very heterogeneous, forming patch-like zones with high salinities. The down-stream areas are most affected, being the old groundwater, which has been ‘collecting’ most recycled solutes during its transit. In these areas, the fraction of irrigation return flow contained in the flow rate is the highest.

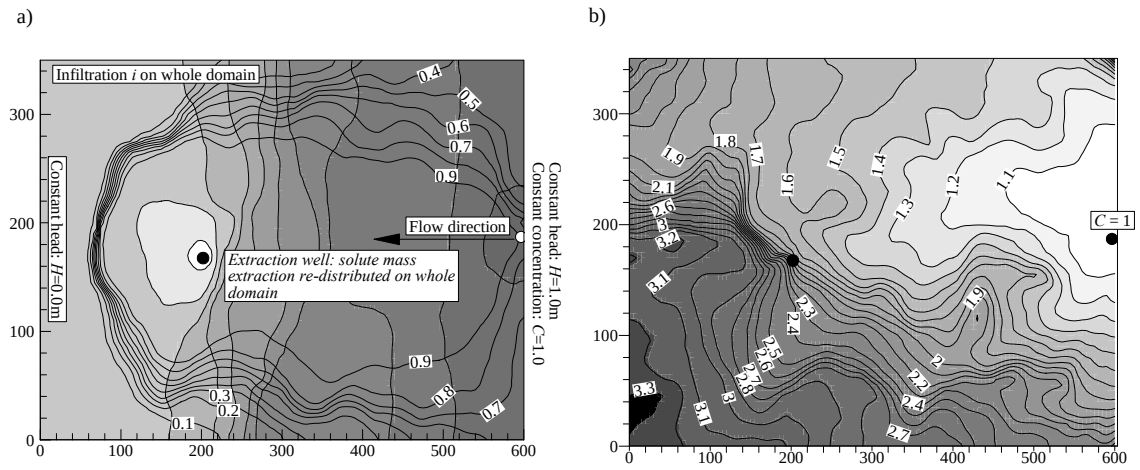

Fig. 4.2: 2-D horizontal, heterogeneous finite element model with one extraction well (coordinates 200/175); flow from east to west, inflowing boundary defined on one node (coordinates 600/200). (a) Head distribution (grey-scale) and iso-contours of capture zone probability field P(x) as full lines. (b) Comparison of concentration distribution of transient transport simulation with solute recycling (full lines) with direct steady state evaluation (grey-scale), obtained by solving Eq. (4.7). Extraction well located at coordinates (200/175), model dimensions are in meters. Recycling takes place on the entire domain.

Fig. 4.3 shows a 2-D homogeneous vertical system with solute recycling on the surface. In this case, the average capture zone probability field has to be integrated over the recycling length L. The 'recycling source' in Eq. (4.7) can then be written as follows:

$$\frac{J_p}{L} = \frac{I}{L(1-\bar{P}(L))} \quad ; \qquad \bar{P}(L) = \frac{1}{L}\int_{\Gamma_{inf}} P dl \tag{4.10}$$

where $\bar{P}(L)$ is the average capture zone probability and Γ_{inf} is the recycling surface.

Since the 'recycling source' in a 2-D vertical case is an edge, a line of 1-D finite elements (with all hydrodynamic parameters set to zero) was introduced in the model to avoid re-formulation of the problem and definition of a coupled boundary condition. Fig. 4.3 shows how solute recycling acts in the vertical dimension, creating a concentration inversion in Fig. 4.3c, but it also illustrates the impact of heterogeneous solute recycling. The maximum concentration obtained from recycling on the entire surface (Fig. 4.3b, $\bar{P}(L) = .516$) is smaller than for the two latter cases, where recycling takes place on only half the domain. Fig. 4.3c has the highest impact due to a higher average capture zone probability ($\bar{P}(L/2)_{left} = .682$ versus $\bar{P}(L/2)_{right} = .350$ in Fig. 4.3d) leading to a bigger source in Eq. (4.10) and thus to higher concentrations.

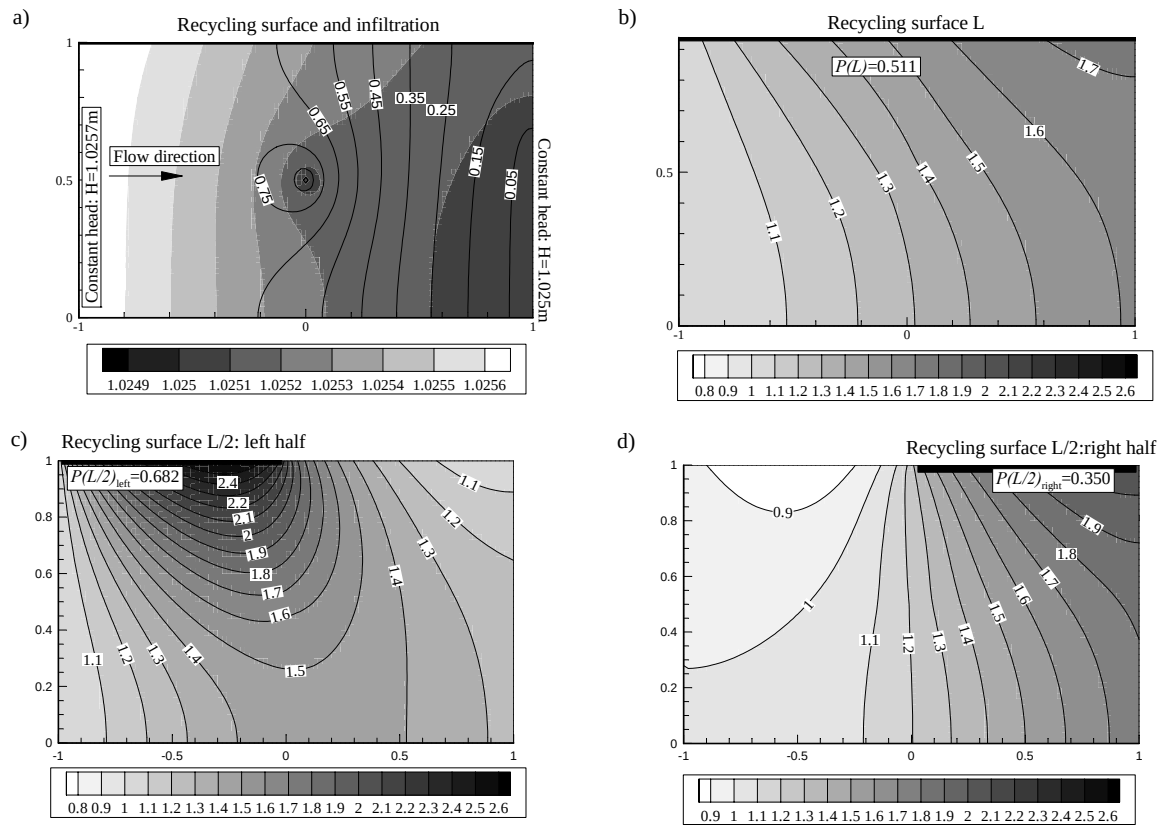

Fig. 4.3: 2-D vertical example showing (a) the boundary conditions and hydraulic head distribution (grey-scale) and the capture zone probability field P(x) (lines). (b) the concentration distribution resulting from solute recycling on the entire surface (L). (c) concentration distribution resulting from solute recycling on the left half $(L/2)_{left}$. (d) concentration distribution resulting from solute recycling on the right half of the surface $(L/2)_{right}$, while infiltration takes place homogeneously over the entire domain. Well location at coordinates (0/0.5), model dimension in meters.

A possible application of the steady state solute recycling simulation approach is to optimise irrigation plot locations. If the extraction rate remains constant and the assumption is made that changing the position of the irrigation plot will not affect the hydraulic conditions of the system, one single backward simulation is sufficient to evaluate the mean capture zone probability of any potential irrigation zone, since the capture zone probability field P(x) remains unchanged. In this case, the only parameter to be minimised in the 'recycling source' described in Eq. (4.7) is $\overline{P}(\Delta)$. This can be obtained by carrying out the spatial integrations on the capture zone probability field over the different potential irrigation zones. Fig. 4.4 shows the same model as in Fig. 4.1. The rectangular zone (bold line) indicates the area within which irrigation with the extracted water may take place. However, the extracted groundwater is only sufficient to irrigate a smaller surface (sub-zone indicated as square). This sub-zone is then moved across the possible irrigation area to find the location where irrigation will cause minimal groundwater degradation (i.e. where the mean

capture zone probability $\bar{P}(\Delta)$ is minimal). The irrigation plot location in Fig. 4.4c has the highest mean capture zone probability leading to the highest concentrations, while the sub-zone location in Fig. 4.4a has the minimal mean capture probability for this setting.

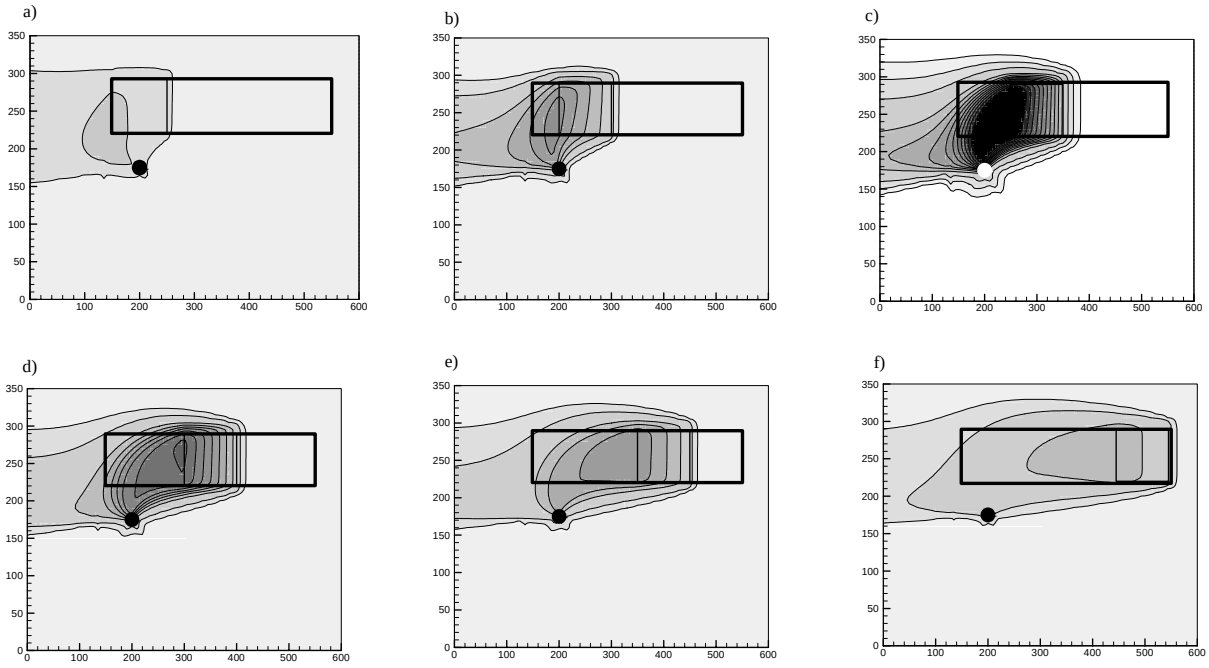

Fig. 4.4: Example of relative concentration distributions obtained from displacing an irrigation plot (square) within a possible irrigation area (thick rectangular zone). Rectangular zone (bold line): possible irrigation area. Square: irrigation plot that is moved across the irrigation area to identify the location with the minimal mean capture zone probability. (a) minimal capture probabilities and minimal concentration increase. (c) Showing the highest concentrations: irrigation plot capture probability is maximal for this case. Model dimension in meters.

4.3.1.1 Generalisation of the 'recycling source' to multiple wells and one irrigation plot

For several extraction wells irrigating the same irrigation zone, the relationship for the extracted solute mass flux J_p, established in Eq. (3.36) is used to define the recycling source in Eq. (4.6). For a case with two extraction wells and one irrigation plot, defining $J_{ptot} = J_{P1} + J_{P2}$, the 'recycling source' can be written as follows:

$$\frac{J_{p1} + J_{p2}}{\Delta} = \frac{J_{ptot}}{\Delta} = \frac{(I_1 + \bar{P}_1 J_{ptot}) + (I_2 + \bar{P}_2 J_{ptot})}{\Delta} \tag{4.11}$$

where J_{P1} and J_{P2} are the extracted solute mass fluxes from *wells* 1 and 2, respectively, with I_1 and I_2 the solute mass fluxes derived from the limits and $\overline{P}_1$ and $\overline{P}_2$ the respective average capture zone probabilities of either well. Developing Eq. (4.11), yields:

$$\frac{J_{\text{ptot}}}{\Delta} = \frac{I_1 + I_2}{\Delta(1-(\overline{P}_1 + \overline{P}_2)} \tag{4.12}$$

Generalising Eq. (4.12) to *n* extraction wells yields:

$$\frac{J_{\text{ptot}}}{\Delta} = \frac{\sum_{i=1}^{n} I_i}{\Delta(1-\sum_{i=1}^{n} \overline{P}_i)} \tag{4.13}$$

In Eq. (4.13), I_i is the lateral solute mass flux to the i^{th} well and $\overline{P}_i$ is the corresponding mean capture zone probability of well *i*.

Fig. 4.5a shows the same simulation result as in Fig. 4.2b, where irrigation takes place homogeneously over the whole domain. It is compared to a simulation carried out on the same domain with an additional extraction well (Fig. 4.5b): the two extraction wells together extract the same amount as the original single well in Fig. 4.5a. With the mean capture zone probabilities $\overline{P}_1, \overline{P}_2$, the 'recycling source' was obtained by making use of Eq. (4.13). Comparing Fig. 4.5a and Fig. 4.5b reveals that the two-well configuration (4.5b) extracting the same amount as in the single-well configuration (Fig. 4.5a) leads to a maximum relative concentration of 2.60 as compared to 3.77 in Fig. 4.5a, as a result of different hydraulic settings.

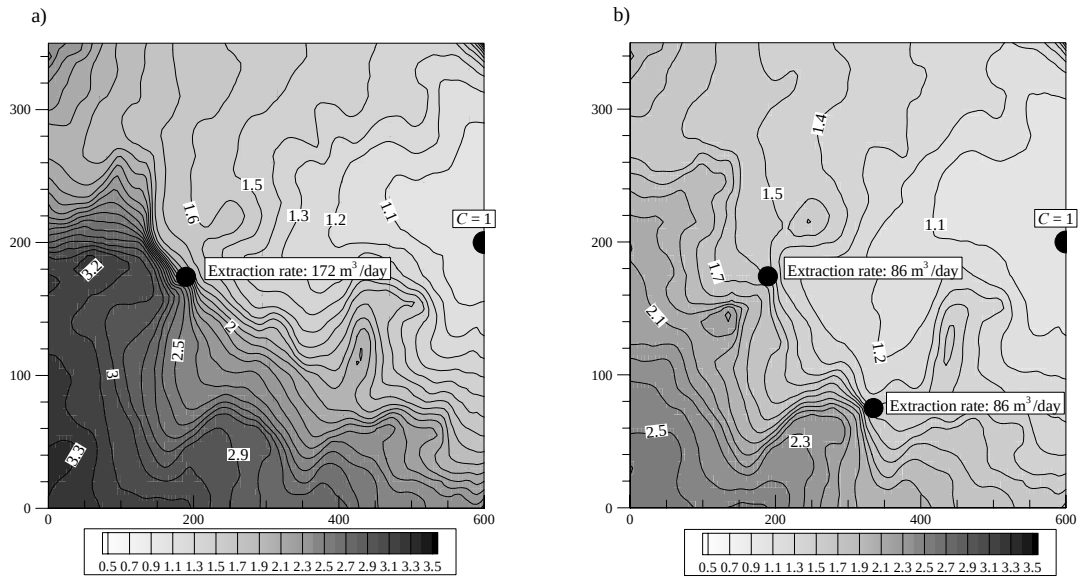

Fig. 4.5: (a) Concentration distribution as shown in Fig. 4.2b for one extraction well. (b) Concentration distribution obtained from simulation result with the same boundary conditions as in 4.5a except for an additional extraction well at coordinates (335/75): the two extraction wells together extract the same total amount as the one single well in 4.5a. Model dimensions in meters.

4.3.1.2 Generalisation of the 'recycling source' to multiple wells and multiple irrigation plots

To generalise the steady state 'recycling source' (in Eq. 4.6) to several extraction wells and irrigation plots, Eq. (3.36) has to be expanded to include the contributions to each well, captured from other irrigation plots. This leads to a system of linear equations.

We denote J_{pk} the solute mass flux distributed on the k^{th} irrigation plot which results from the solute mass extracted from i extraction wells. Eq. (4.13) has to be extended to include the solute mass contributions from the irrigation plots which are not irrigated by J_{pk}. The solute mass flux J_{pk} to be introduced onto the k^{th} irrigation plot can then be written as a sum of contributions from all irrigation plots as follows:

$$J_{pk} = \sum_{i=1}^{n_k} (I_i + \sum_{j=1}^{m} J_{pj} P_i(\Delta_j)) \tag{4.14}$$

m = number of irrigation plots
n_k = number of wells irrigating the k^{th} plot
I_i= solute mass flux captured by the i^{th} well from the boundaries
J_{pj}= solute mass flux recycled on the j^{th} irrigation plot
$P_i(\Delta_j)$= average capture probability of the i^{th} well with respect to the j^{th} irrigation plot

Developping Eq. (4.14) so that all terms of J_{pk} are on the left-hand side, allows implicit definition of the following 'recycling source' J_{pk} for the k^{th} irrigation plot:

$$\frac{J_{pk}}{\Delta} = \frac{\sum_{i=1}^{n_k}\left[I_i + \sum_{\substack{j=1 \\ j\neq k}}^{m} J_{pj}\overline{P}_i(\Delta_j)\right]}{\Delta(1-\sum_{i=1}^{n_k}\overline{P}_i(\Delta_k))} \quad ; \quad k = 1,..,m \tag{4.15a}$$

Eq. (4.15a) generates a system of m linear equations, which can be written in matrix form as follows:

$$\begin{bmatrix} 1-\sum_{i=1}^{n_1}P_i(\Delta_1) & -\sum_{i=1}^{n_1}P_i(\Delta_2) & \cdots & -\sum_{i=1}^{n_1}P_i(\Delta_m) \\ -\sum_{i=1}^{n_2}P_i(\Delta_1) & 1-\sum_{i=1}^{n_2}P_i(\Delta_2) & \cdots & -\sum_{i=1}^{n_2}P_i(\Delta_m) \\ \vdots & \vdots & \ddots & \vdots \\ -\sum_{i=1}^{n_m}P_i(\Delta_1) & -\sum_{i=1}^{n_m}P_i(\Delta_2) & \cdots & 1-\sum_{i=1}^{n_m}P_i(\Delta_m) \end{bmatrix} \begin{bmatrix} J_{p1} \\ J_{p2} \\ \vdots \\ J_{pm} \end{bmatrix} = \begin{bmatrix} \sum_{i=1}^{n_1} I_i \\ \sum_{i=1}^{n_2} I_i \\ \vdots \\ \sum_{i=1}^{n_m} I_i \end{bmatrix} \tag{4.15b}$$

With Eq. (4.15b) the m steady state 'recycling sources' J_{pk} can be defined for any configuration of extraction wells and irrigation plots.

4.3.2 Transient simulation of solute recycling

The expression for the extracted solute mass $J_p(t)$ as defined in Eqs. (3.31) and (3.32) can be used to obtain the transient 'recycling source' in Eq. (4.1) for hydraulic steady state conditions. For very complicated cases with multiple extraction wells and irrigation surfaces this may be very time-demanding. However, this approach allows transient simulation of solute recycling with any standard flow and transport simulation package.

On a simple example, we will show how the transient 'recycling source'can be obtained, for the case that the lateral solute mass contribution I is constant. However, the approach can be extended to account for a time-dependent lateral solute mass influx $I(t)$, according to Eq. (4.2).

4.3.2.1 Transient 'recycling source'

The main prerequesite in the definition of the transient 'recycling source' is the RTF $g_{in}^{\Delta}(t)$ which is obtained from the sum of the n-fold convolutions of the average travel time PDF $g_t^{\Delta}(t)$ between

the irrigation plot Δ and the extraction well. The average travel time PDF $g_t^{\Delta}(t)$ can either be obtained by a transient simulation with an initial concentration on the irrigation plot and subsequent normalisation by the injected mass and scaling by the extraction rate Q_p, or by means of a backward evaluation of the travel time distributions and integration over the irrigation plot Δ in Laplace space with subsequent inversion (e.g. Cornaton 2004). Once the PDF $g_t^{\Delta}(t)$ has been obtained, the sum of the *n*-fold convolutions can either be calculated in a discrete manner, or, remaining in Laplace space, the RTF can be obtained by the use of Eq. (3.29).

Fig. 4.6 shows a simple system for which the transient 'recycling source' was obtained by means of the travel time PDF $g_t^{\Delta}(t)$, with one inlet, one regional discharge area, one extraction well and a small irrigation plot. Fig. 4.6a shows the steady state concentration distribution without solute recycling which is used as initial concentration distribution. This implies that the solute mass flux captured by the well from the boundaries *I* remains constant. Fig. 4.6b shows the concentration distribution at steady state obtained as a late time asymptote of the constructed transient 'recycling source' which equals the concentration distribution we would obtain using the steady state approach presented in the previous section. Fig. 4.7a shows the PDF $g_t^{\Delta}(t)$ between the irrigation plot and the well and six *n*-fold self-convolutions, as well as the resulting RTF $g_{in}^{\Delta}(t)$ obtained from the sum of the discretely self-convoluted travel time PDFs $g_t^{\Delta}(t)$. These were scaled by the lateral inflowing solute mass flux *I* and integrated, yielding the transient solute mass flux $J_p(t)$ shown in Fig. 4.7b. The transient solute mass flux $J_p(t)$ obtained by means of convolution (line) compares well with the extracted solute mass flux obtained from transient simulation, using a time-stepping procedure (circles), with a minimal difference at late times

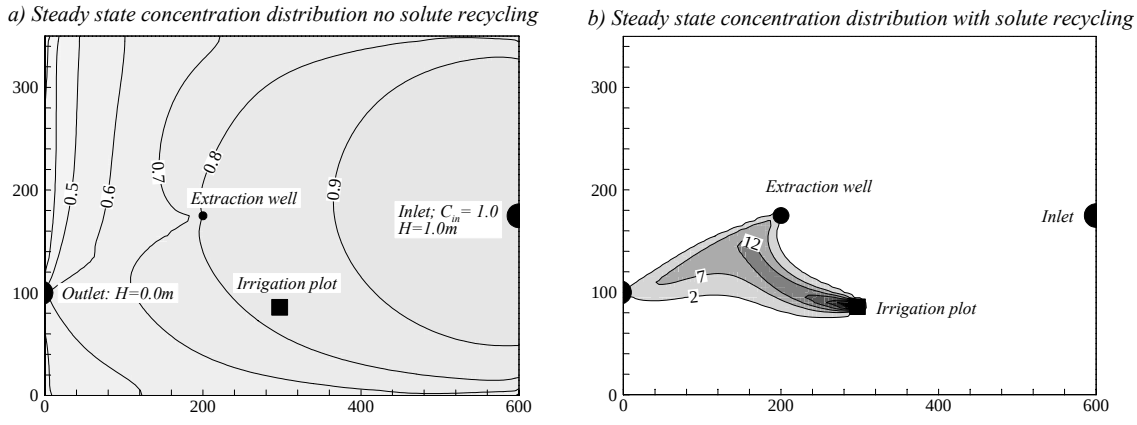

Fig. 4.6: Synthetic example for which the transient 'recycling source' was constructed, showing one inlet with a concentration C_{in}=1, a regional outlet, an extraction well and a small irrigation plot. (a) Initial concentration distribution before solute recycling takes place. (b) Steady state concentration distribution with solute recycling.

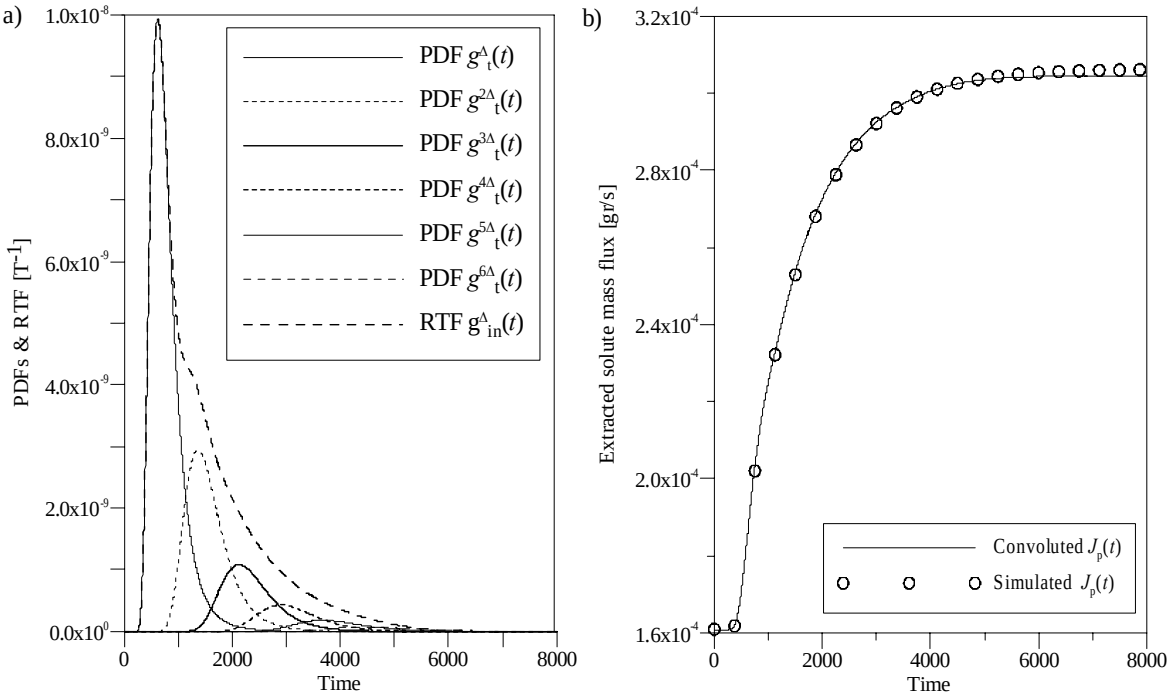

Fig. 4.7: Construction of the transient 'recycling source'. (a) RTF $g^{\Delta}_{in}(t)$ obtained by adding six self-convolutions of the mean travel time PDF $g^{\Delta}_{t}(t)$. (b) Extracted solute mass flux $J_p(t)$ as obtained from integration of the RTF $g^{\Delta}_{in}(t)$ scaled with the lateral solute mass flux I (line) versus the extracted solute mass flux as obtained from transient solute recycling simulation with time-stepping procedure (circles). Time axis in days.

4.3.2.2 Concentration evolution at any point in the domain

The recycling transfer function RTF $g^{\Delta}_{in}(t)$ (section 3.4.1) describes how solutes are redistributed in the circuit and scaled by the constant lateral solute mass flux I, it is the first time-derivative of the solute mass flux $J_p(t)$, according to Eq. (3.32b). In section 4.3.2.1 we showed how the transient well response can be 'constructed' from the mean travel time PDF $g^{\Delta}_{t}(t)$ between the irrigation plot and the extraction well. To obtain the response to solute recycling at any point in the domain, we can make use of the fact that at any point x in the domain the concentration will result from perfect linear mixing of different fractions emanating from different sources. In a system, which is at steady state with respect to the solute mass flux from the limits, any concentration change will be induced by solute recycling.

To describe the cooncentration change which is induced by solute recycling, use can be made of the RTF $g^{\Delta}_{in}(t)$, which describes how a solute mass signal is transformed by solute recycling and is proportional to the signal which is introduced on the irrigation plot. From the irrigation plot, there

is a transfer function to any point x in the system, which will be denoted redistribution PDF $g_o(t)$. The signal arriving at point x from the irrigation plot results from the RTF $g_{in}^{\Delta}(t)$ and the redistribution PDF $g_o(t)$, and is obtained by convolution of the two transfer functions. In the same way as the RTF $g_{in}^{\Delta}(t)$ is proportional to first time derivative of the solute mass flux at the extraction well, the transfer function at any point x resulting from the convolution of the RTF $g_{in}^{\Delta}(t)$ and PDF $g_o(t)$ will be proportional to the first time-derivative of the solute mass flux J_x at the point x in the system, for a constant lateral solute mass flux I.

The solute mass flux $J_x(t)$ at any point in the domain will consist of the contribution from the background or ambient solute mass flux I_{xL} and the contribution from solute recycling. Since the solute recycling contribution will result from the convolution integral of the RTF $g^{\Delta}{}_{in}(t)$ with the redistribution PDF $g_o(t)$, and convolution reduces to a simple product in Laplace space, we can formulate the resulting variation in solute mass flux as follows:

$$p\hat{J}_x = I_{xL} + I_p \hat{g}_{in}^{\Delta}(p)\hat{g}_0(p) = I_{xL} + I_p \hat{g}_{re}^{\Delta}(p) \tag{4.16}$$

where $\hat{J}_x$ is the Laplace transformed solute mass flux at a point x in the domain, consisting of the constant ambient contribution I_{xL} from the boundaries and from the constant solute mass flux captured by the well from the boundary I_p convoluted with the RTF $\hat{g}_{in}^{\Delta}$ and redistribution PDF $\hat{g}_0$. The convolution of the two transfer functions is abreviated $\hat{g}_{re}^{\Delta}$. Eq. (4.16) can be reformulated to yield the derivative of the solute mass flux at point x:

$$(p\hat{J}_x - I_{xL}) = I_p \hat{g}_{re}^{\Delta} \tag{4.17}$$

According to the Laplace transform, Eq. (4.17) shows that the transfer function $\hat{g}_{re}^{\Delta}$ scaled by $\hat{I}_p$ in the time-domain yields the temporal variation of the solute mass flux $J_x(t)$ at a point x in the domain under the condition that $J_x(t = 0)=I_{xL}$.

To obtain the concentration evolution at point x from Eq. (4.17) the solute mass flux J_x has to be scaled by the flow rate Q_x. To solve Eq. (4.17) without evaluating the flow rate, we make use of the proportionality between the solute mass flux $J_x(t)$ and $C_x(t)$. As a consequence of this proportionality, the transient evolution of $J_x(t)$, described by Eq. (4.17) will at any time be proportional to the transient evolution of $C_x(t)$. To obtain the transient concentration evolution $C_x(t)$, the transient evolution of $J_x(t)$ is scaled to fit the difference between the initial concentration $C_{ini}(x)$, and the end concentration $C_{end}(x)$. The initial concentration $C_{ini}(x)$ is obtained with a steady state simulation without solute recycling and the end concentration $C_{end}(x)$ is obtained from the

steady state simulation with solute recycling (section 4.3.1). The concentration evolution $C_x(t)$ can then be written:

$$C_x(t) = C_{\text{ini}}(\mathbf{x}) + \frac{\Delta C_{\text{rec}}(\mathbf{x})}{P_{\text{re}}(\mathbf{x})} \int_0^t g_{\text{re}}^{\Delta}(t)dt \tag{4.18}$$

Where $\Delta C_{\text{rec}}(\text{x})$ is the concentration difference between the initial concentration $C_{\text{ini}}(\text{x})$ and the steady state concentration $C_{\text{end}}(\text{x})$ with solute recycling. $P_{\text{re}}(\text{x})$ corresponds to the integral of the total transfer function $g_{\text{re}}^{\Delta}(t)$ and is used to scale the integrated transfer function to fit the initial and end concentrations $C_{\text{ini}}(\text{x})$ and $C_{\text{end}}(\text{x})$.

Fig. 4.8 shows a close-up of two concentration distributions for the same model as illustrated in Fig. 4.7. Fig 4.8a shows the concentration distribution obtained with the transient 'recycling source' defined in Fig. 4.7b for a time t = 1500 days, and Fig. 4.8b shows the distribution at steady state (like Fig. 4.6b). In both figures, observation wells are shown for which the transient concentration evolution was simulated by means of Eq. (4.18). The RTF $g_{\text{in}}^{\Delta}(t)$ and the respective redistribution PDFs $g_{\text{o}}(t)$ are shown in Fig. 4.9a, which were convoluted, scaled and integrated to obtain the transient concentration evolution $C_x(t)$, shown in Fig. 4.9b. The transient concentration evolution as derived from the convolution procedure (lines) are compared with the transient concentration evolution as obtained from a transient simulation using the time-stepping procedure and can be seen to match well (symbols).

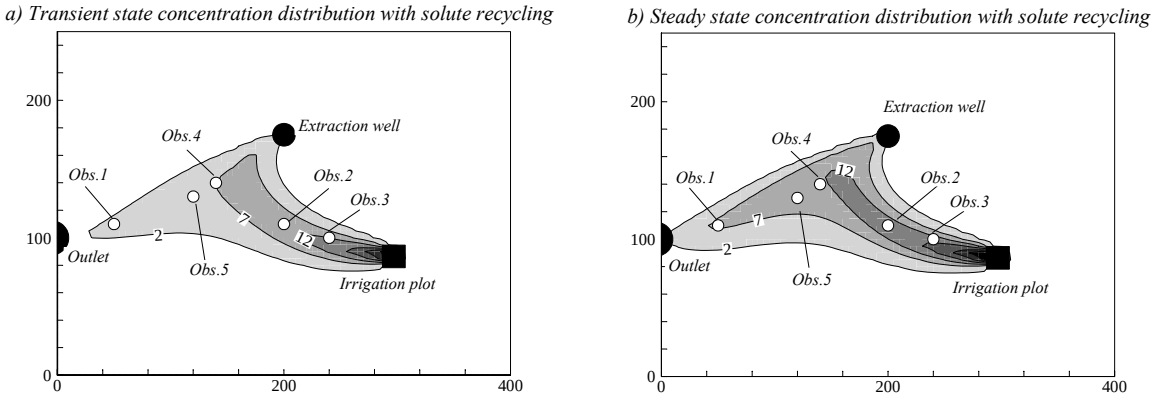

Fig. 4.8: Close-up concentration distribution in the 2-D horizontal finite element model shown in Fig. 4.6, with positions of observation points shown in Fig. 4.9. (a) Transient concentration distribution at time t = 1500 days. (b) Steady state concentration distribution with solute recycling, as shown in Fig. 4.6b.

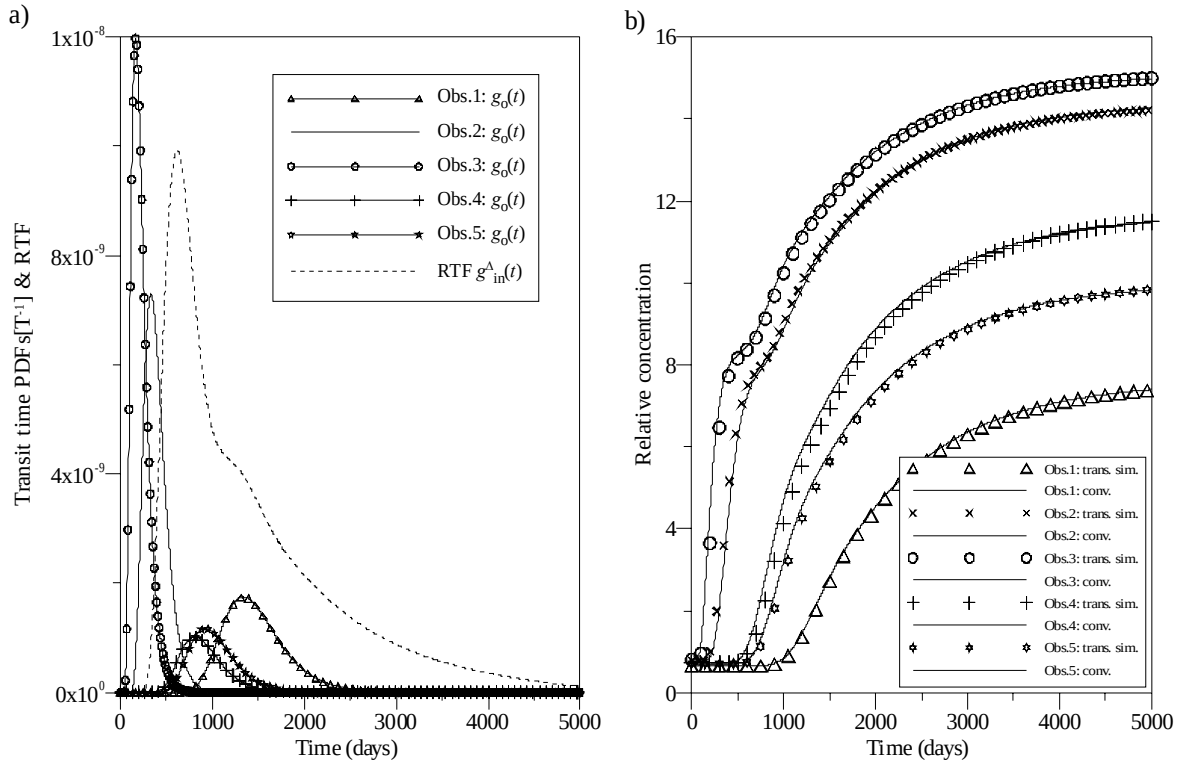

Fig. 4.9: (a) Recycling transfer function RTF, as derived from Fig. 4.7a which was convoluted with the redistribution PDFs $g_0(t)$ to solve Eq. (4.18). (b) Transient concentration evolution as obtained from the convolution procedure using Eq. (4.18) (lines), compared to the transient concentration evolution simulated with a time-stepping procedure (symbols). Time axis in days.

The described evaluation of the transient concentration response to solute recycling at any point in the domain may be extended to transient lateral solute mass flux contributions $I(t)$. If the procedure would be implemented into a tool capable of simulating the PDFs for any point in any CPU-gaining manner, it may be a promising approach for the calibration phase. The problem would then only be solved for a given number of observation points, rather than solving it for the entire domain. However, if this procedure is carried out 'manually', simulations with the transient 'recycling source' are far more convenient.

4.4 Numerical simulation of solute recycling: transient hydraulic conditions

As shown in section 4.3, solute recycling in irrigated areas may have an important impact on the groundwater salinity evolution, depending on the irrigation schemes and the general hydrogeological context. The options to simulate solute recycling as described in the previous section were all based on steady state hydraulic conditions. In many cases, this assumption might

not hold, when fully transient conditions prevail (e.g. if density dependent flow and transport is jugded to be important). In such cases, solute recycling can be simulated numerically in a time-stepping procedure.

The main prerequisite for the numerical implementation of the solute recycling process is that the distributed solute source in Eq. (4.1) can be modified according to the solute budget of the respective extraction well(s) during the simulation procedure. In certain commercial software packages solute recycling can be implemented. As an example, in FEFLOW (Diersch 2002) this can be accomplished via an interface manager (IFM module), allowing modification of boundary conditions, sources and sinks, and parameters, during the simulation procedure. A restricted access via a library of commands requires export of the target values to an external interface where they are modified and subsequently re-imported into the simulation procedure. This significantly slows down simulation. Hence, solute recycling has been implemented as a module in a finite element code developed at CHYN (Cornaton 2004). An outline of the main implementation procedure is given in Appendix 1. In this section, we will illustrate on some examples how a transient flow field may modify groundwater salinisation in response to solute recycling.

The main procedure in simple solute recycling consists of updating the distributed recycling source by means of the extracted solute mass flux $J_p(t)$. To solve Eq. (4.1), $J_p(t)$ is evaluated at each time-step. Recycling of the extracted solute mass flux onto defined irrigation surfaces is done by means of a re-distribution matrix A, assigning fractions of all irrigation wells to all the existing irrigation plots (see Appendix 1). Different options were added to the 'simple recycling procedure', such as definition of a maximum recycling concentration C^* and extraction concentration, which de-activates wells when a certain threshold value C_w is reached, and introducing a 'soil buffer' zone by means of irrigation plot averaged transfer functions.

4.4.1 'Simple solute recycling' simulation

The distributed 'recycling source' for the k irrigation plots is obtained from the extracted solute mass fluxes $J_{pi}(t)$ of the i irrigation wells by means of a redistribution matrix A and re-introduced into the system on k irrigation plots during the following time-step. Since the extracted solute mass flux is re-introduced into the system during the following time-step, a time-lag will be observed, which is completely governed by the time-step length Δt. The smaller the time-step, the more instantaneous solute recycling will appear to be. During simulation, solute recycling is interrupted if no infiltration takes place. During such 'dry' periods, the extracted solute mass flux is simply cumulated and stored, and re-introduced into the system, as soon as infiltration resumes.

Fig. 4.10 shows the concentration evolution for three spatial coordinates for transient infiltration rates in a 1-D domain (cf. Fig. 3.2). During periods when no infiltration takes place, the extracted solute mass is cumulated and re-introduced as soon as infiltration takes place again. This causes the step-like concentration increase observed in Fig. 4.10. The dashed lines indicate the concentration evolution for average steady state hydraulic conditions. The long term slopes can be seen to be slightly higher for steady state conditions, since the lateral limit is only inflowing, while during infiltration events in the transient simulation the lateral limit becomes temporally outflowing, leading to solute losses. If no solutes are lost from the system, the average transient concentration slope for this setting corresponds to the steady state concentration slope.

Fig. 4.11 shows the solute mass balances for the extracted solute mass (middle graph) and recycled solute mass (bottom graph) for the simulation shown in Fig. 4.10. No recycling takes place when infiltration is zero (Fig. 4.11 top graph) and the extracted solute mass accumulates and is recycled with the renewed onset of infiltration. This leads to very high concentration pulses, since all the solute mass that was accumulated during the dry period is re-introduced within the first time-step after the onset of infiltration.

The ‘simple solute’ recycling simulation with the time-stepping procedure is also a convenient approach for transient solute recycling simulations in hydraulic steady state conditions when the lateral solute mass flux $I(t)$ captured by the wells from the boundaries is transient. For such cases the approach described in the section 4.3.2.1, using the RTF to obtain the transient ‘recycling source’, becomes far more laboursome, especially when several limits with different salinities are involved. This is the typical case in coastal settings.

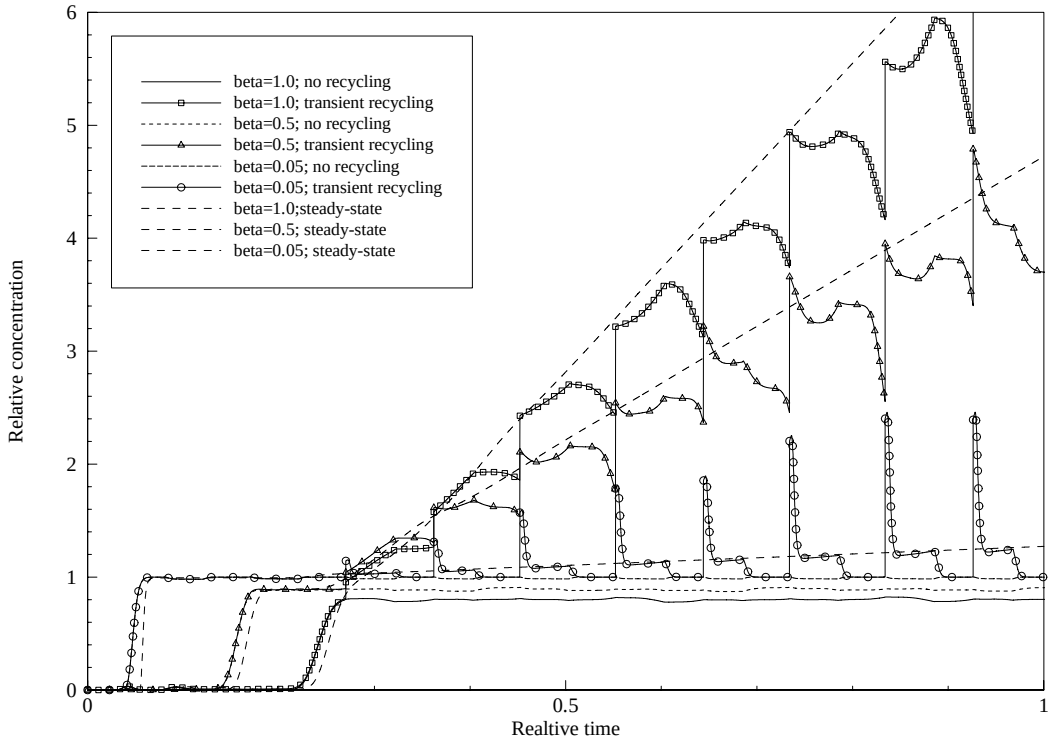

Fig. 4.10: Concentration evolution at spatial coordinates β = 0.05, 0.5 and 1 for transient hydraulic conditions with solute recycling in a 1-D closed system (full lines with symbols) and without solute recycling (lines without symbols). Thick dashed lines indicate the concentration evolution for the steady state average hydraulic condition.

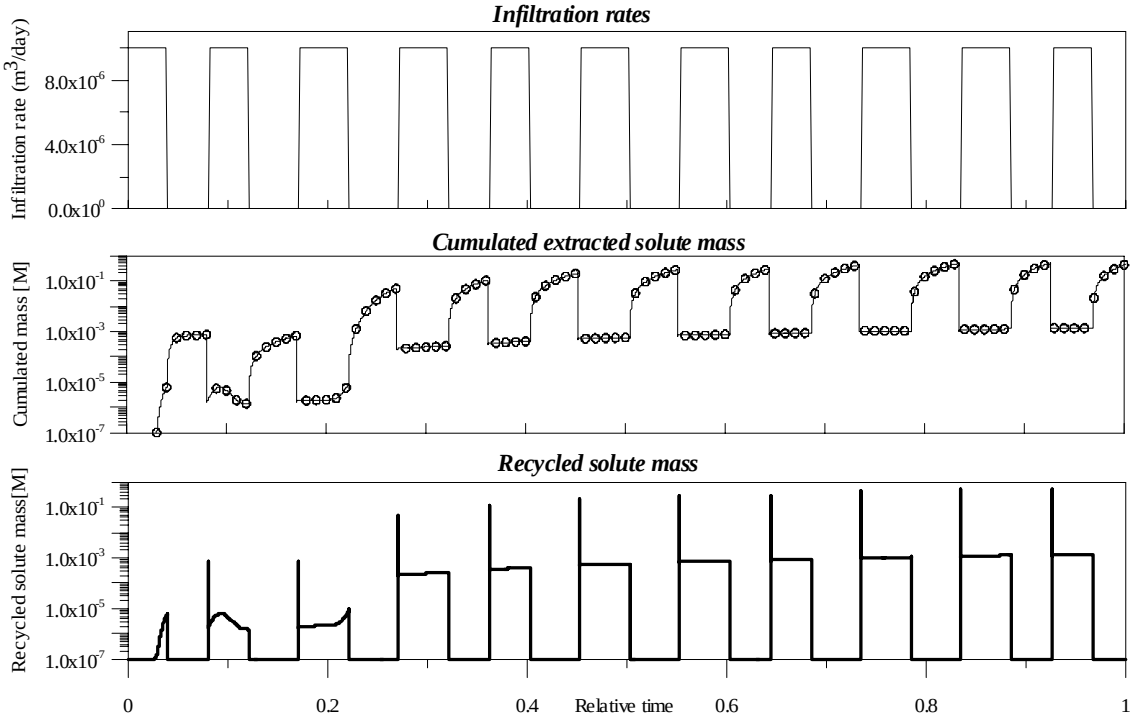

Fig. 4.11: The infiltration rate (top) indicates when recycling does not take place. Transient solute mass balance of the extracted cumulated solute mass (middle) and the recycled solute mass (bottom).

Fig. 4.12 shows a 2-D horizontal, homogeneous example of an aquifer with two lateral inflowing boundaries with different salinities, an example which may schematise a coastal aquifer. The concentration contrast of 1/30 between the two inlets is comparable to what we will encounter in coastal aquifers (seawater compared to fresh groundwater). The two wells are used to irrigate the entire zone homogeneously: *well 2* extracts twice as much as *well 1*. Fig. 4.12a shows the steady state concentration distribution for the case that no solute recycling takes place, while the result obtained from simple solute recycling is shown in Fig. 4.12b. Fig. 4.13 shows the well concentration evolutions for the two scenarios. The spatial salinity distribution obtained with solute recycling can be seen to be very different from the scenario without solute recycling (Fig. 4.12a), representing the commonly used modelling approach and so are the transient well concentration evolutions (Fig. 4.13).

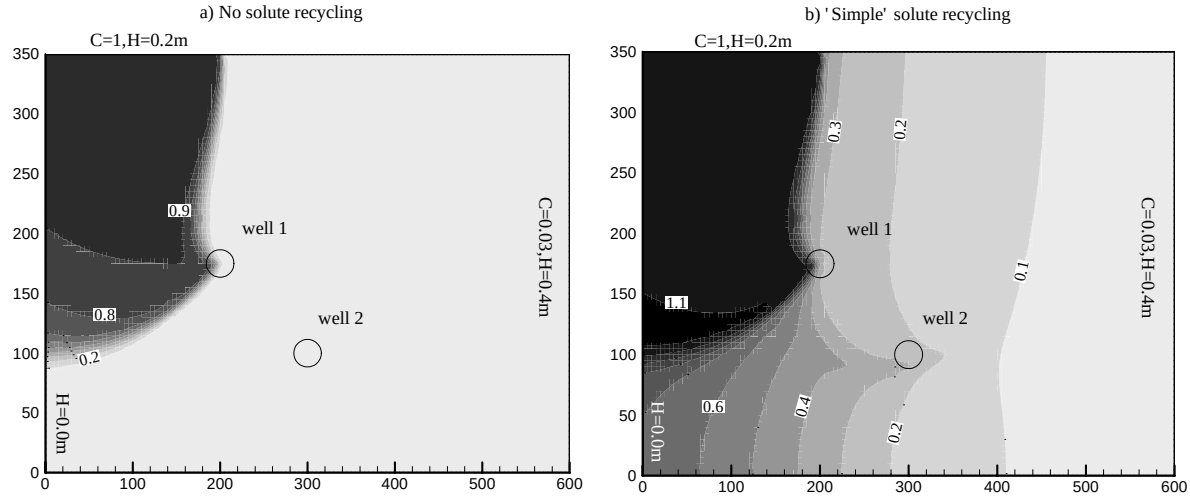

Fig. 4.12: 2-D horizontal, homogeneous finite element model with two inflow boundary with different concentrations, two extraction wells and one regional discharge area (west). (a) Steady state concentration distribution for the scenario without solute recycling. (b) Steady state concentration distribution for the scenario with solute recycling obtained from transient simulation.

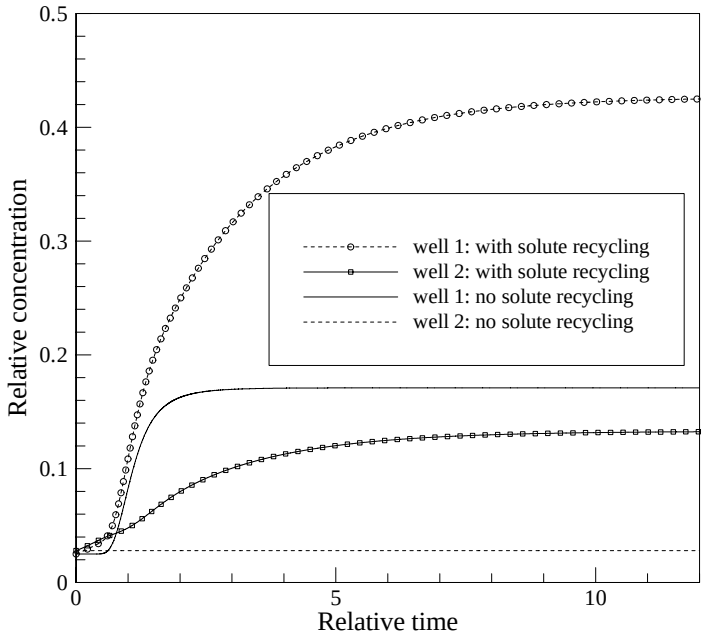

Fig. 4.13: Concentration evolutions at *well 1* and *well 2* of the simulations shown in Fig. 4.12 revealing the impact of solute recycling (symbols) with respect to the simulation scenario without recycling (lines), which is the commonly used simulation approach.

4.4.2 Solute recycling with special 'options' (concentration restrictions and accounting for the unsaturated zone)

Three additional options are presented that were implemented in the time-stepping procedure for solute recycling simulation for special cases. The two first options concern concentration restrictions. The recycling concentration and the well concentrations may be restricted, in the first case to avoid too high infiltration concentrations after dry periods and in the latter case to restrict the well extraction concentration to a threshold limit, beyond which the wells are de-activated. The third option is related to the unsaturated zone, which can be accounted for by means of irrigation plot averaged transfer functions.

4.4.2.1 Infiltration concentration restriction

As mentioned in section 4.4.1, very high infiltration concentrations may be attained, when the cumulated solute mass is recycled during the first time-step after a dry period. The concentration infiltration C^* depends very much on the time-step length Δt, the infiltration rate and the amount of solutes that have been accumulated during the dry period. High infiltration concentrations may

create numerical instabilities and mass losses. To avoid this, and to render the process more physical, a maximum recycling concentration C^*_{max} can be defined. Before solute recycling takes place, the infiltration concentration is evaluated. If it is above the defined maximum infiltration concentration, solute recycling will re-introduce as much of the cumulated solute mass as corresponds to this threshold value and the remaining cumulated solute mass is diminished by the recycled amount. This requires an external storage of solutes which does not reflect any physical processes, but introduces an external buffer between the extracted and the recycled solute mass. Fig. 4.14 shows the solute mass budget obtained from the simulation shown in Fig. 4.10 with a defined relative maximum infiltration concentration $C^*_{max}=100C_0$ (with C_0 = 1). Hence, solute recycling with C^*_{max} will take place as long as there is a surplus of solutes in the external storage, containing the solute mass cumulated during the dry period and the newly extracted solute mass.

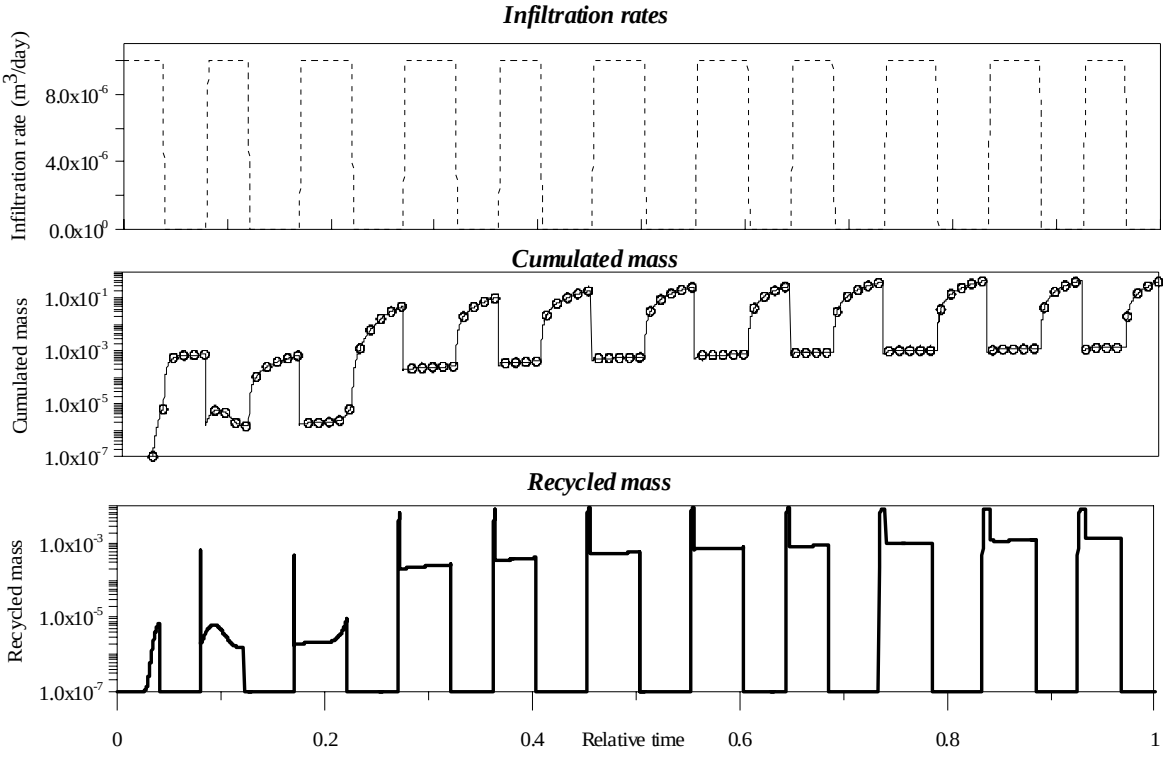

Fig. 4.14: Transient solute mass balance for the simulation shown in Fig. 4.10 with a defined maximum allowable recycling concentration of $C^*_{max}=100C_0$. Recycling of the solute mass cumulated during the dry periods takes place over several time-steps, which is not the case in Fig. 4.11.

4.4.2.2 Well extraction concentration restriction

The 2-D horizontal example shown in Fig. 4.12, representing schematically a coastal aquifer, gives rise to an additional problem, concerning well concentrations. Fig. 4.13 shows that the steady state well concentrations reach values of C_{w1} = 0.42 and C_{w2} = 0.12 respectively, relative to the concentration of the sea (C = 1). In reality, an extraction well will be de-activated, abandoned or

displaced, as soon as the concentration reaches the limit of exploitability, which depends on the salt tolerance of the irrigated crops. For the case that the wells are abandoned and not displaced, a restriction has been introduced into the solute recycling simulation procedure, which 'switches off' any extraction well exceeding a defined maximum concentration.

Fig. 4.15 shows the concentration evolution at different spatial coordinates for a 1-D domain with 480 aligned wells with a well concentration constraint of C_w=4, an initial system concentration of C_{ini}=0, and a Dirichlet-type boundary conditions of C = 1 at the relative spatial coordinate β = 0. The resulting transient concentration distribution is rather complicated. The wells in the central part of the 1-D domain are the first to attain the limit of exploitability. As they are de-activated one by one in direction towardsβ = 1, the wells closer to the inflowing boundary (β = 0) still extract and recycle on the entire domain. The extraction well located at β = 1 is de-activated at a relative time of t = 0.25. Then, the system in the area where the extraction wells have been de-activated is completely closed but the hydraulic gradient is still such that flow takes place towards this dead end (β = 1), leading to concentrations exceeding the threshold concentration. Infiltration eventually inverts the local hydraulic gradient allowing flow towards the inflowing limit β = 0. The accumulated solute mass in the distant part of the system (towards β = 1 with very high concentrations) is then being flushed towards the central part, where there are still active extraction wells. These will then reach the limit of exploitability and be 'switched off'. The last well (closest to β = 0) is de-activated at a relative time of approximately t = 1.8, leading to a regional inversion of the hydraulic gradient towards β = 1. This allows evacuation of all solutes by the now outflowing limit at β = 0.

Although the hydraulic conditions in this simple 1-D example are not very realistic, it shows that very complicated concentration evolutions and distributions can be obtained, with drastically changing hydraulic conditions. It is interesting to observe that concentrations may increase far beyond the threshold value after deactivation of a well. This indicates that salinisation by solute recycling cannot be managed locally, by deactivation of wells, but has to be done on a larger scale.

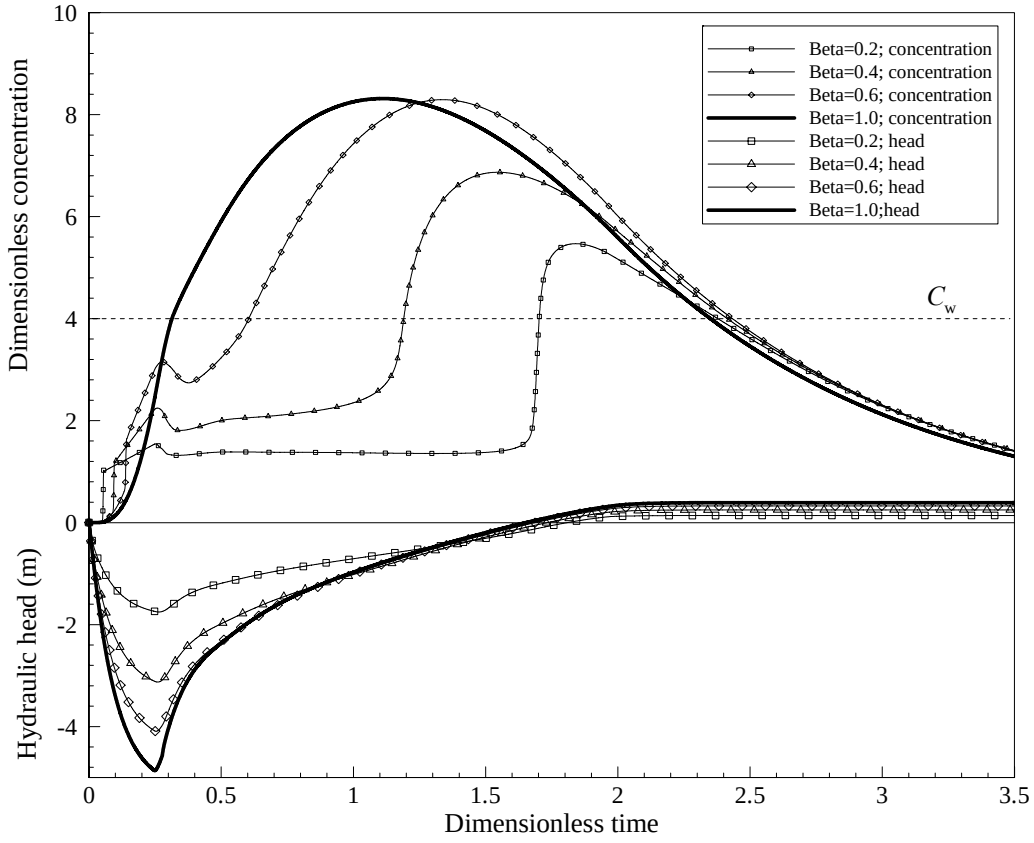

Fig. 4.15: Concentration and head evolution at four spatial coordinates (β = 0.2, 0.4, 0.6, 1.0) in a 1-D domain with well constraint, with the wells aligned along the entire system: Initial system concentration is C_{ini} = 0, lateral inflowing boundary concentration at spatial coordinate β = 0 is C_0 = 1. As soon as the well concentration of C_w = 4 is reached (dashed line), the well is 'switched off', modifying the hydraulic situation. Finally, all the wells are de-activated and the system concentration slowly decreases, since no more solute recycling takes place and the hydraulic gradient is inverted pointing in direction of the lateral boundary (β = 0) where solutes are evacuated.

Fig. 4.16 shows the model shown in Fig. 4.12b run for a relative maximum well concentration of C_w = 0.2. Deactivation of *well 1* due to salinisation by the saline boundary significantly modifies the hydraulic conditions and the salinity distribution in the domain. Fig. 4.16a shows the salinity distribution just after deactivation of *well 1*, while Fig. 4.16b shows the salinity distribution at steady state. Fig. 4.16c compares the steady state salinity distribution for simple recycling, shown in Fig. 4.12b, with the steady state distribution obtained with a well concentration constraint (Fig. 4.16b). Introducing the well restriction diminishes the overall salinity. However, in the area beyond the directly 'seawater-affected zone' the general salinisation pattern remains the same. The relative importance of salinisation by solute recycling increases for the simulation with a well concentration constraint.

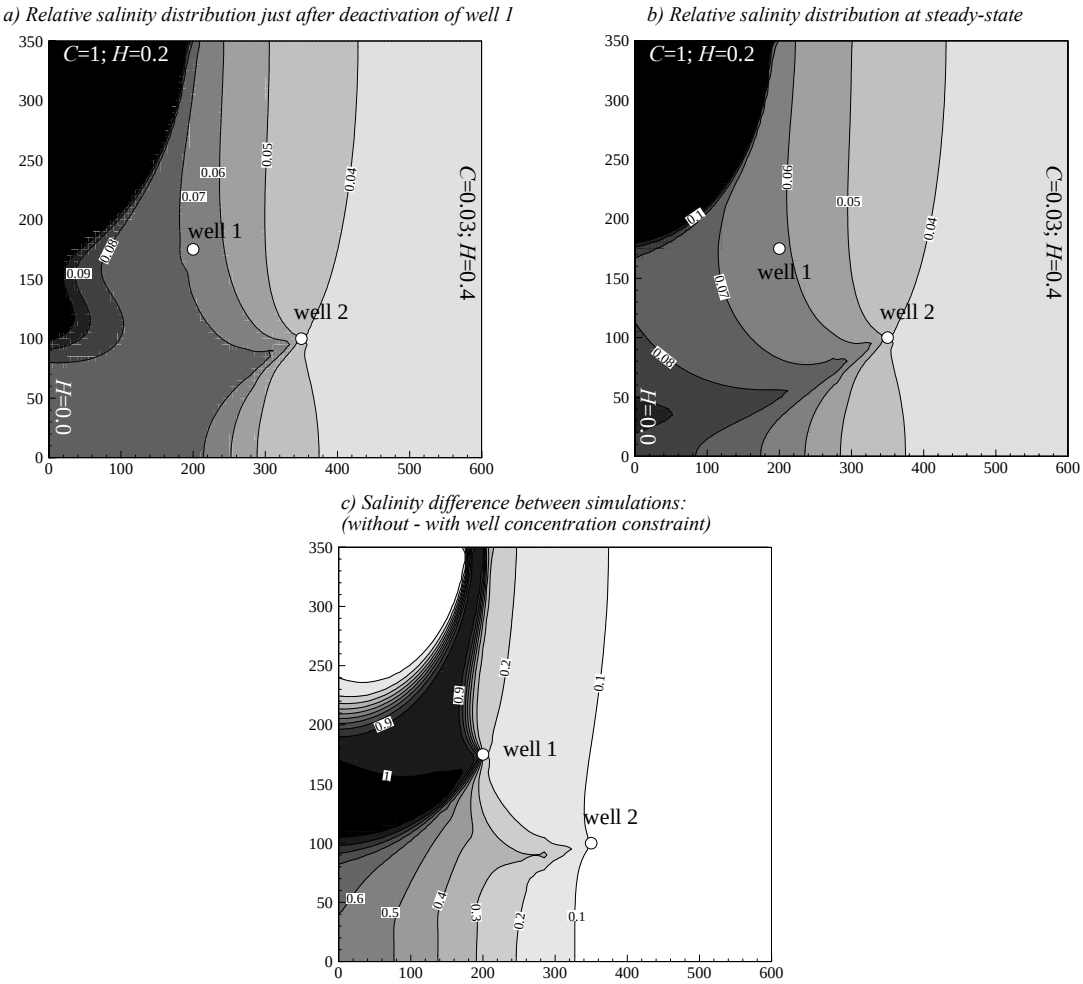

Fig. 4.16: Showing the same 2-D horizontal domain as in Fig. 4.12b. Simulation with solute recycling, deactivating the wells that attain a relative concentration of C = 0.2, leads to a different hydraulic regime and thus to a different salinity distribution. (a) Relative salinity distribution just after de-activation of *well 1*. (b) Relative salinity distribution at steady state. (c) Salinity difference between the two simulations without and with well concentration constraint (without constraint minus with constraint).

4.4.2.3 Solute recycling simulation with a 'soil buffer'(unsaturated zone transfer function)

In section 3.3.2 we discussed the effect of conservative transfer of solutes through the unsaturated zone on the well concentration evolution and concluded that the presence of a 'soil buffer' will slow down solute recycling salinisation. To simulate transient solute recycling with the 'soil buffer' effect, irrigation plot averaged transfer functions can be defined for each irrigation plot. Since simulation of saturated/unsaturated flow and transport is computationally very demanding and the aim of the 'soil buffer' in the solute recycling procedure is to create a 'resistance' to solute recycling rather than to simulate the exact transfer through the unsaturated zone, the 1-D analytical

solution of the ADE proposed in Jury and Roth (1990) is used to define irrigation-plot averaged travel time PDFs through the unsaturated zone:

$$C(t,z) = \frac{z}{2\sqrt{\pi D t^3}} \exp\left[-\frac{(z - vt)^2}{4Dt} \right] \tag{4.19}$$

However, any transfer function can be used, describing either simple models such as piston flow to more complicated ones, including processes such as adsorption and double porosity.

At the beginning of the simulation procedure, the transfer function is evaluated for each irrigation plot, making use of Eq. (4.19) solving it for a narrow pulse to obtain the corresponding PDFs. In the solute recycling routine, the extracted solute mass at any time t is convoluted with the transfer function as a step-function of length Δt. The time axis of the transfer function is always adapted so that time zero of the transfer function corresponds to the time t of the simulation. Convolution is done numerically with an analytical approximation of the convolution integral. The resulting response is added to the sum of all the previous responses, making use of the superposition theorem, which states that the response of a system to the string of impulses is just the sum of the response to the individual impulses. The 'recycling source' is then obtained from the sum of all responses evaluated at time t, corresponding to the simulation time. Hence, although the unsaturated zone is not directly simulated, the extracted solute mass is stored and filtered at each time-step.

A travel time PDF for a mobile, non-reactive chemical will not be invariant to changes in infiltration rates. Therefore, this option is only used for constant infiltration rates. Extending this approach to variable infiltration rates would imply evaluation of the 'unique drainage PDF' (Jury & Roth 1990), making the assumption that the principle of superposition is valid for varying infiltration rates (e.g. proportionality of velocity). The advantage of such an approach would be that, in addition to the solute mass, the recharge of the aquifer could be estimated.

Fig. 4.17a shows the concentration evolutions for transient solute recycling at different observation points with and without soil buffer for the 2-D homogeneous horizontal domain shown in Fig. 4.12b and Fig. 4.16. The steady state concentrations for both scenarios are identical, but the salinities rise more slowly in presence of a 'soil buffer' (full lines).

Fig. 4.17b shows the concentration difference between the salinity distribution obtained from simple recycling and with soil buffer, at a relative time of t = 20. A homogeneous transfer function was applied on the entire zone with a mean transit time of 1.5 times the mean saturated system turnover time, which means that transfer through the 'soil buffer' in this case is extremely slow with respect to the mean travel time through the aquifer. The smallest impact of the 'soil buffer'

can be seen to be close to the inflowing boundaries, indicating that dilution with water from the limits will dampen the impact of solute recycling. In the areas close to the discharge zone, the difference is most pronounced, since that is where the fraction derived from irrigation return flow is most important.

The soil buffer can be neglected if the mean travel time through the soil buffer is much smaller than the travel times in the saturated zone.

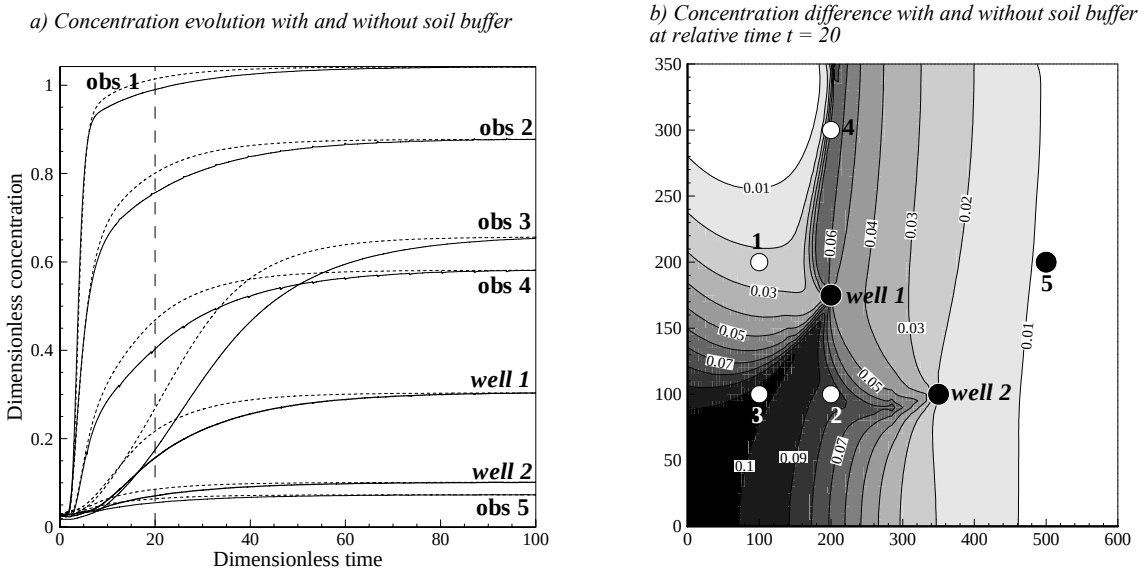

Fig. 4.17: Simulation results for the 2-D horizontal model shown in Fig. 4.12b, with a 'soil buffer'. (a) Concentration evolution at different observation points with a 'soil buffer' (full lines) and for simple recycling (dashed lines). (b) Concentration difference at relative time t = 20 between simulation with and without soil buffer.

4.5 Conclusions

Depending on the scope of a simulation and the prevailing hydraulic conditions, different methods can be used to simulate the effects of solute recycling on spatial groundwater salinisation.

For hydraulic steady state conditions, a direct simulation procedure has been proposed. The 'recycling source' term in the general form of the advection-dispersion equation is a function of the mean travel time probability density function between the irrigation plot and the extraction well and the lateral solute mass captured by the well. For steady state solute recycling the expression for the 'recycling source' is a function of the mean capture zone probability of the irrigation plot and the lateral solute mass flux captured from the wells, only. It was extended to multiple extraction wells and irrigation plots. The late time groundwater salinity distribution obtained with this expression yields the overall salinisation potential of the system, for a given

exploitation scheme. This approach is the most CPU-gaining simulation for the late-time simulation of solute recycling. A transient ‘recycling source’ was also defined with the expression for the extracted solute mass flux, based on the transfer function theory. The transfer function approach was extended to simulating transient solute recycling at any point in the system for a constant solute mass flux from the boundaries by pure convolution procedure

For transient hydraulic conditions, examples were shown, for which the solute recycling was simulated with a time-stepping procedure (Appendix 1). Recyling of solutes only takes place during infiltration events, while the extracted solute mass is cumulated during dry periods, which led to the definition of a maximum infiltration concentration. A well concentration constraint was introduced to simulate the de-activation of wells when a threshold concentration is reached that corresponds to the limit of exploitability. De-activation of wells could be seen to have a major impact on the hydraulic condition of the system and thereby also on the groundwater salinisation. Introducing the buffering effect of the soil by irrigation plot averaged transfer functions leads to the same steady state concentrations but slows down the salinisation process, as already discussed in 3.3.2. However, if the mean travel time through the soil is much smaller than the mean travel time from the irrigation plot to the extraction well, the ‘soil buffer’ may be neglected.

In the solute recycling simulations, other solute sources other than the ones coming from the inflowing limits can easily be added. This may be important for instance in areas, where considerable amounts of agricultural additives enter the system as a constant solute source. The contributions of such additional solute sources to the extracted solute mass flux I have to be evaluated, allowing these solutes to enter the recycling process as well.

CHAPTER 5

FRAMEWORK FOR SALINISATION RISK ASSESSMENT: SOLUTE RECYCLING VERSUS SEAWATER INTRUSION

Abstract

We present a framework for a salinisation risk assessment methodology in which seawater intrusion and solute recycling salinisation are evaluated separately. For this purpose, the overall salinity distribution at late times as well as the transient salinity evolution are decomposed into a seawater intrusion and solute recycling component, yielding the respective salinisation potentials, solute recycling potential (RP) and seawater intrusion potential (SIP), as well as the respective 'present state' salinity distributions. The salinisation risk index is then defined as the potential of further salinisation induced by the respective salinisation process and is obtained by comparing the 'present state' salinisations with the respective salinisation potentials. The risk index maps reveal areas which are prone to further salinity increase due to solute recycling and seawater, respectively, and are strictly related to the hydraulic setting for which the salinisation potentials were established. Comparing the solute recycling and seawater intrusion risk index distributions with the 'present state' salinity distribution allows delimitation of areas which require remediation (i.e. areas with low risk indices and high salinities) and areas which require conservation (i.e. areas with salinities close to the exploitation limit with high risk indices). The knowledge of the spatial distribution of the salinisation process which will cause further groundwater salinisation allows definition of appropriate remedial and conservation measures. Modification or optimisation of an exploitation scheme leads to modified risk index distributions. Risk index maps obtained for a modified exploitation scheme delimit areas which will suffer further salinisation from areas for which the modified exploitation scheme will have a remediating effect.

The established framework for a risk assessment methodology has to be considered as an attempt to define a measure which accounts for the dynamics of groundwater systems with the two superimposed and coupled salinisation processes, solute recycling and seawater intrusion.

5.1 Introduction

Risk assessments are becoming a standard procedure in many domains and describe the process of estimating the potential impact of a chemical, biological or physical agent on humans, plants or ecology. The basis of risk assessment is the comparison of a present state of the environment with an adverse state which may potentially occur in the future, a state which will have a negative impact on human interests. As a consequence of the different nature of the potential impacts under consideration, numerous definitions of risk exist. As an example the UNESCO defines the risk as a combination of vulnerability, potential loss with the impact of hazard (cited in Guyonnet 1998). Another defintion is given by Helm (1996), who defines risk as probability times the consequences. Although many risk definitions are similar, confusion can easily arise as to how the components leading to the estimation of the risk have to be defined (e.g. vulnerability, impact of hazard). In many areas, risk assessment methodologies are well established, which introduce precise definitions of the different components leading to the estimation of risk, as for instance in the field of contaminated sites (e.g. Ferguson et al. 1998).

Groundwater protection and management issues are also often addressed by either vulnerability or risk assessments. Vulnerability assessments identify sensitive zones of a system based on hydrogeological criteria, while groundwater risk assessments additionally consider the presence of potential contamination sources or polluting land-use activities (Gogu & Dassargues 2000). Groundwater vulnerability maps are designed to show areas of greatest potential for groundwater contamination on the basis of hydrogeologic and anthropogenic factors (Rupert 2001). The most commonly used vulnerability mapping procedures are based on empirical point rating systems, such as DRASTIC (Aller et al. 1985), that bring together key factors believed to influence the solute transport processes. Comparison of vulnerability distributions obtained from such mapping procedures with actual groundwater quality data have shown that they rarely predict the predisposition of areas to groundwater contamination (Rupert 2001). Since groundwater dynamics are not explicitly included in these mapping approaches, Gogu and Dassargues (2000) emphasize the need for process-based risk and vulnerability assessments. For instance, Stewart and Loague (2003) developed a regional-scale vulnerability assessment methodology to estimate the impact of non-point source groundwater contamination, using a generalised type transfer function. Likewise, Connell and van den Daele (2003) investigated the use of analytical solutions for unsaturated solute migration, in order to calculate contaminant transport to groundwater in view of combining it with a geographic information system (GIS) to establish vulnerability maps. In contrast to groundwater contamination, risk assessments related to irrigated agriculture aim to protect the soil from salinisation, rather than the underlying groundwater, although the impact of irrigation on groundwater quality is becoming an increasingly important issue (e.g. Tanji 1990, Ragab 2002).

The objective in this chapter is to establish a framework for a risk assessment methodology which treats seawater intrusion and solute recycling separately. It aims to identify zones in a system which are prone to further salinisation in response to either seawater intrusion or solute recycling from irrigation for a given irrigation scheme (i.e. locations of irrigated surfaces and redistribution of extracted water onto these surfaces). The framework has to be considered an attempt to point out a direction towards which a salinisation risk assessment for such settings could aim, making use of the simulation procedures developed in the previous chapters. The definition of the impact of groundwater salinisation on human interests, i.e. definition of levels of salinisation which will for instance reduce crop yields, is beyond the scope of this work.

The first step in the proposed salinisation risk assessment is the decomposition of the overall salinity potential at late times into contributions derived from seawater intrusion and solute recycling. These will be denoted seawater intrusion potential (SIP) and solute recycling potential (RP), respectively. These salinisation potentials reflect the maximum salinity that may be reached for a given exploitation and irrigation scheme. Hence, the respective salinisation potentials

indicate the salinity distribution towards which a system is heading. To evaluate what we will denote the risk index of further salinisation, the 'present state' salinisation is compared with the salinisation potential of the respective processes. The adverse state is thereby defined as the spatial potential of any further salinisation. With this comparison, the spatial salinisation risk index distribution with respect to both salinisation processes can be mapped, distinguishing areas which have a 'stable' salinity (close to steady state transport) from areas which will potentially still suffer salinity increase. Relating these risk index maps to the 'present day' salinity distributions and to given threshold values allows the identification of areas which require remediation from areas which need to be conserved or areas that do not reveal any risk at all. To obtain the seawater intrusion and solute recycling risk index maps, however, the 'present state' salinity distribution has to be obtained by simulation, since only simulation will allow decomposition of the overall salinity distribution into the two salinisation components.

Modification or optimisation of an exploitation scheme will induce a change in the salinisation potential, by modifying the hydraulic conditions. Comparing modified or optimised salinisation potentials with the 'present state' salinisation yields a risk index distribution that delimits zones for which the modified/optimised exploitation scheme will induce remediation, from zones that will suffer further salinisation. In this way, the efficiency of an optimised exploitation scheme can be evaluated and for the zones which will suffer further salinisation, the knowledge of the underlying process allows the design of appropriate remedial measures.

The proposed framework for a salinisation risk assessment methodology in coastal irrigated systems will be described step-by-step, using a synthetic 2-D horizontal model of an idealised aquifer system in a coastal irrigated area. The model is the same as that previously presented in Chapter 4 to investigate the transient effects on salinisation after de-activation of extraction wells (see Fig. 4.12, 4.16).

In the first section, we will define the seawater intrusion salinisation potential (SIP) and solute recycling salinisation potential (RP) at late times. Then, we will focus on the evaluation of the 'present state' salinisation of a transient system and identify the contributions from the respective salinisation processes. In the third section, we will establish the risk index mapping procedure, making use of the 'present state' salinity contributions and relating them to the respective salinisation potentials. In the last section, we will show how the extraction rates for fixed positions of wells can be optimised to minimise the overall salinisation potential. This optimised salinisation potential is then compared to the 'present state', yielding the optimised salinisation risk index distributions with which the impact of the modified exploitation and irrigation scheme on the spatial groundwater salinity can be evaluated.

5.2 Definition of salinisation potentials and 'present state' salinisation: solute recycling versus seawater intrusion

In coastal aquifers, which are characterised by boundaries with high contrasts in water quality, it is important to distinguish between the salinisation induced directly by the boundaries and the super-imposed effects of solute recycling. This distinction can be made by adapting the boundary conditions to account for only solute recycling or boundary salinisation. Hence, the overall salinity distribution at any time can be decomposed into a contribution derived from seawater intrusion and solute recycling, respectively.

5.2.1 Seawater intrusion potential (SIP) and solute recycling potential (RP)

In the previous chapter, the steady-state distributed 'recycling source' term in the general form of the ADE was obtained from the solute mass captured by the well from the boundary and the capture zone probability of the irrigation plot to the wells (Eq. 4.7). Solving the steady-state ADE with a 'recycling source' leads to the overall salinisation potential at late times (Section 4.3.1). Although the salinisation potential, as obtained from the steady state solute recycling approach, is believed to be applicable in most cases, the salinisation potential at late times may also be obtained from transient solute recycling simulations with a time-stepping procedure, run until steady state conditions have been attained (Section 4.4.1).

The concentration at any point in the domain results from the linear mixing of different fractions with different concentrations: from solute recycling, from lateral solute mass flux and from precipitation. The solute mass flux captured by the well from the boundaries I, in a coastal context, can be subdivided into a contribution from the sea I_s and from the fresh groundwater limit I_f. The steady-state form of the ADE with 'recycling source' as described by Eq. (4.7) can then be written as follows:

$$0 = -\nabla \cdot (\mathbf{q}C - \phi \mathbf{D} \nabla C) + \frac{I_s + I_f}{\Delta(1 - \bar{P}(\Delta))} \tag{5.1}$$

where $\mathbf{q}$ [LT^{-1}] is the specific flux vector, $\mathbf{D}$ [L^2T^{-1}] the tensor of dispersion, C [ML^{-3}] the concentration, ϕ [-] the porosity, Δ [L^3] the surface/volume of the irrigation plot and $\bar{P}(\Delta)$ [-] the average capture probability of the irrigation plot. To obtain the contribution to the overall salinisation derived from solute recycling only, Eq. (5.1) is solved for the following boundary condition:

$$C = 0 \qquad \text{on} \qquad \Gamma^- \tag{5.2}$$

where Γ^- represents all the inflowing boundaries of the system. With no solute mass flux entering the system from the boundaries, the only mass in the domain is generated by the distributed 'recycling source', yielding the spatial RP at late times.

Salinisation from solute recycling is enhanced by seawater intrusion, if the extraction wells capture solutes from the sea boundary. On the assumption that all solutes contributing to solute recycling salinisation originally entered the aquifer from one of the boundaries (i.e. neglecting agricultural additives and other salinity sources), solute recycling salinity can be defined as the contribution to the overall salinity from solutes that have been reintroduced into the system by irrigation at least once. Hence, as soon as a solute has been used for irrigation, it 'forgets' its previous attribution, e.g. seawater intrusion salinity.

To obtain the contribution to the overall salinisation from inflowing boundaries, i.e. SIP, Eq. (5.1) is solved without the 'recycling source' for the following boundary conditions:

$$C_s = 1 \qquad \text{on} \qquad \Gamma_s^- \qquad (5.3)$$

$$C_\mathrm{f} = f_\mathrm{s} \qquad \text{on} \qquad \Gamma_\mathrm{f}^-$$

where Γ_s^- is the seawater boundary, with a concentration C_s, Γ_f^- the fresh groundwater boundary with a concentration C_f. The freshwater boundary concentration is expressed as fraction f_s of the relative seawater concentration C_s = 1. To obtain the contribution to the overall salinisation derived from the seawater boundary only, the freshwater boundary in Eq. (5.3) is modified, while the seawater boundary remains unchanged:

$$C_\mathrm{s} = 1 \qquad \text{on} \qquad \Gamma_\mathrm{s}^- \qquad (5.4)$$

$$C_\mathrm{f} = 0 \qquad \text{on} \qquad \Gamma_\mathrm{f}^-$$

The RP can also be obtained by deducting the SIP from the overall salinisation potential (Eq. (5.1) with boundary conditions Eq. (5.3)).

In the following, we will reduce the subdivision of the different salinisation potentials to that derived from the inflowing boundary (SIP) and that derived from solute recycling (RP). The abbreviation SIP is used to describe the effect of all lateral boundaries and is therefore, strictly speaking, not the seawater intrusion potential. However, it is a good approximation, since the salinity along the fresh groundwater boundary is much smaller than that along the seawater boundary. Consequently, we can avoid the separate evaluation of the solute contribution derived

from the fresh groundwater and seawater boundaries, while the sum of the two salinisation fractions at any point in the system will add up to unity.

Fig. 5.1 shows a 2-D homogeneous horizontal finite element model with a fresh groundwater and a seawater boundary, two extraction wells and one regional outlet. Irrigation takes place on the entire domain. In Fig. 5.1a, the overall salinisation potential is shown, resulting from Eq. (5.1) with the boundary conditions in Eq. (5.3). Fig. 5.1b shows the SIP, resulting from Eq. (5.1) without the 'recycling source' and boundary conditions in Eq. (5.3). Fig. 5.1c shows the RP resulting from Eq. (5.1) with the boundary condition in Eq. (5.2). The RP can also be obtained by deducting the SIP from the overall salinisation potential. Fig. 5.1d shows the spatial distribution of the fraction of the RP. This is obtained by normalising the RP (Fig. 5.1c) with the overall salinisation potential (Fig. 5.1a). The spatial distribution of the solute recycling fraction f_r allows delimitation of areas dominated by 'seawater intrusion' ($f_r < 0.5$) and of areas dominated by solute recycling ($f_r > 0.5$). Since only two solute contribution components are considered, the spatial distribution of the SIP fractions f_s can be obtained by the simple relationship $f_s = 1 - f_r$. In the vicinity of the fresh groundwater boundary in the east, one can see that the SIP is dominant (Fig. 5.1d). This shows that this notion 'seawater intrusion potential' does not exactly reflect the SIP, and this becomes particularly clear when we operate with fractions.

The overall salinisation potential, shown in Fig. 5.1a, reveals the potential at any point of being salinised to the given value. Concentrations of five to ten times the concentration of the fresh groundwater boundary will usually mark the threshold limit for exploitability, depending on the salinity along the fresh groundwater boundary. In this example, the concentration iso-contour of $C = 0.2$ will indicate the limit of exploitability (with a fresh groundwater concentration of $C_f = 0.03$) . Fig. 5.1a shows that approximately half the domain will tend towards a state with salinities above the limit of exploitability, within which more than half the area is dominated by solute recycling (compare Fig. 5.1a with Fig. 5.1d).

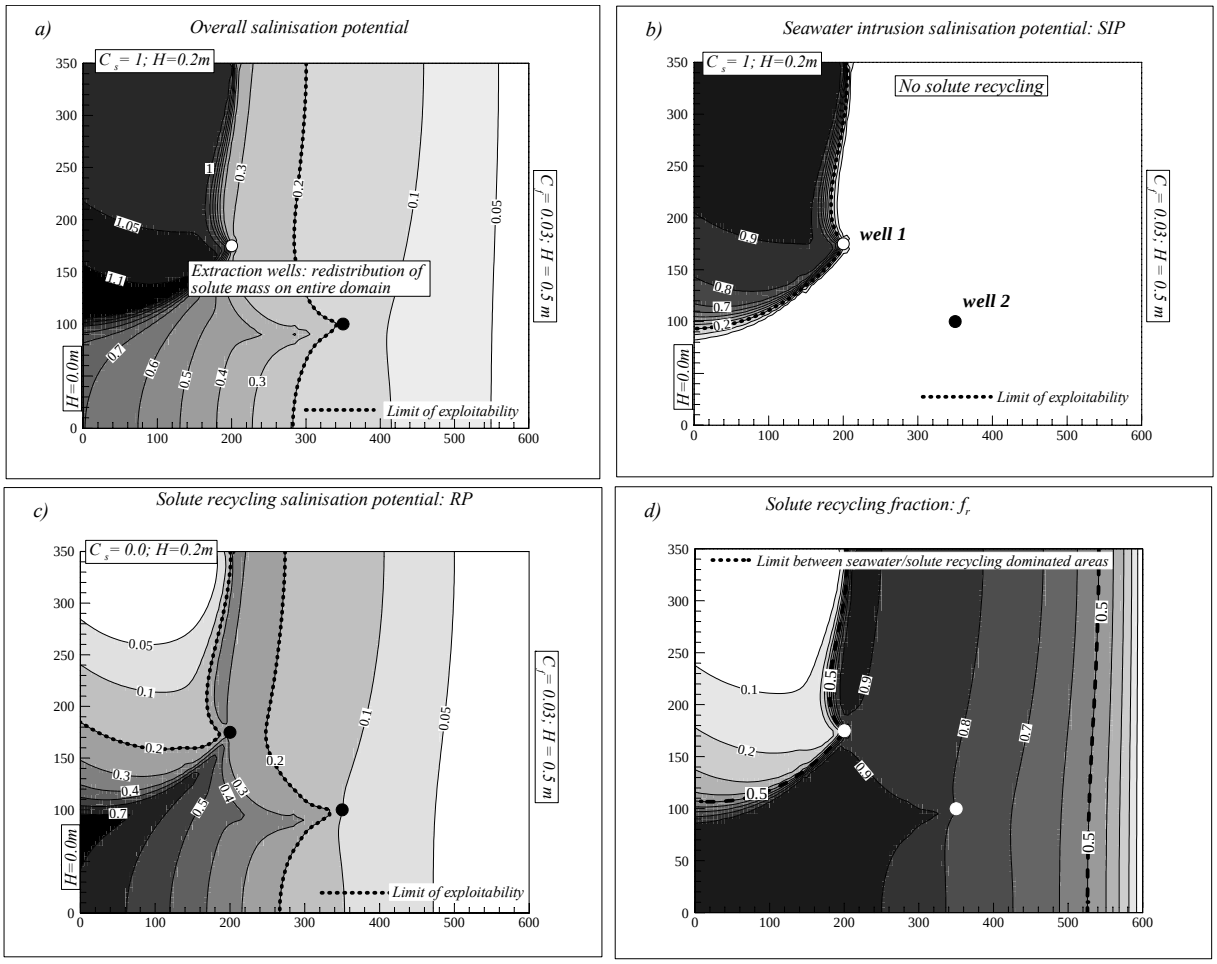

Fig. 5.1: 2-D horizontal, homogeneous finite element model with two inlets with different salinities (seawater concentration C_s=1, and fresh groundwater concentration C_f = 0.03), two wells and one outlet. The irrigation plot covers the entire surface. (a) Overall salinisation potential, (b) 'Seawater intrusion' potential (SIP), (c) Solute recycling potential (RP). Concentration iso-contour C = 0.2, defined as limit of exploitability, is indicated as a dashed line. (d) Spatial distribution of the solute recycling fraction f_r of the overall salinisation potential. The 0.5 iso-contour (thick dashed-dotted line) delimits the zones in which salinisation is dominated by solute recycling (f_r > 0.5) from those in which it is dominated by seawater intrusion (f_r < 0.5).

Fig. 5.2 shows three iso-surfaces in a 3-D domain as derived from a simulation with the boundary conditions as shown in Fig. 5.1, neglecting densety dependent flow and transport. One can see that solute recycling from irrigation leads to the most saline groundwater overlying the fresher groundwater. This is a well documented phenomenon in irrigated areas (e.g. Tanji 1990, Prendergast et al. 1994). The 2-D horizontal model operates with vertically averaged salinities and will therefore lead to another image of the salinisation potential than that encountered at the surface of the 3-D domain.

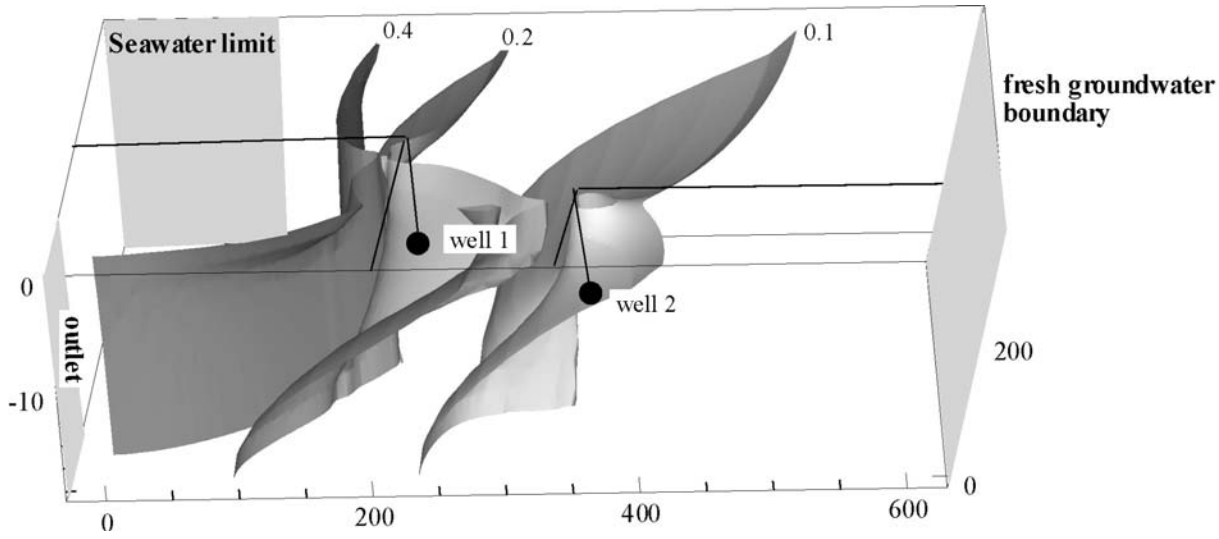

Fig. 5.2: 3-D representation of three iso-surfaces (C = 0.1, 0.2, 0.4) of the overall salinisation potential for a very similar domain to the one shown in Fig. 5.1, with the same boundary conditions. Solute recycling leads to an inversion of the salinity profile in the area where solute recycling is dominant.

If an extraction well captures solutes from the seawater boundary, solute recycling is coupled to seawater intrusion. If the steady-state well concentration is above the limit of exploitability, the salinisation potential has to be considered as a purely hypothetical extrapolation. In reality, the extraction wells would be abandoned when a certain concentration limit is attained and this would not only modify the hydraulic state of the aquifer but also the further evolution of the aquifer salinisation (*cf.* Fig. 4.16). This shows that the late time behaviour of a system, in other words the salinisation potential, does not reflect a future reality but rather the target towards which a system is directed for a given exploitation scheme. Also, it shows that it will not reflect anything approaching that which will be reached if the well concentrations at steady-state are well above the threshold limit of exploitability.

5.2.2 Transient state solute recycling versus seawater intrusion salinity evolution: simulation of the 'present state'

The salinisation distribution encountered in any aquifer is most likely to be situated somewhere within the transient salinisation evolution rather than having reached a steady state with respect to transport. With the evaluation of the salinisation potential described in the previous section, we obtained the RP and the SIP, and the spatial distribution of the fractions of the overall salinisation

potential that can be attributed to either salinisation process were evaluated. However, the transient fractions of either salinisation process may vary considerably in time. Hence, the fractions of either salinisation process contributing to the salinisation potential at steady state are not proportional to the transient state salinisation fractions and can therefore not be used to decompose a salinity distribution within the transient evolution. The overall salinisation of a 'present state' can only be decomposed into contributions from solute recycling and seawater intrusion if the 'present state' has been placed within the transient salinisation evolution of the system by simulation.

The transient salinisation evolutions of either salinisation process are obtained by decomposing the transient overall salinity evolution by adapting the boundary conditions, in the same way as shown in the previous section for the RP and the SIP (Eq. (5.2) and Eq. (5.3)). To decompose the transient salinity evolution into contributions derived from either solute recycling or seawater intrusion, the transient overall salinisation evolution has to be simulated. Then, the same simulation is run without solute recycling. Deducting the transient salinity evolution without solute recycling from the overall salinity evolution leads to the transient evolution of either salinisation process. The decomposed transient salinity evolution allows us to place the overall 'present state' salinity distribution on the time-scale and to decompose it into a 'present state' solute recycling salinity and a 'present state' seawater intrusion salinity distribution, respectively. This is the second and most delicate step in the proposed framework for a risk assessment methodology. The difficulty in real case studies arises from the considerable uncertainty related to model parameterisation, which is often based on very scarce data. The same difficulty, however, is encountered in any modelling approach.

Fig. 5.3 shows the transient concentration evolution at several observation points in the system shown in Fig. 5.1, for an initial concentration within the entire system of $C_{ini} = 0$. The overall 'present state' salinity distributions is shown in the centre, and was chosen to be at a relative time $t^* = 2$, since the salinity at *well 1* is approaching the limit of exploitability (defined as $C = 0.2$ for this hypothetical example). The graphs in Fig. 5.3 show the overall salinity evolutions (lines with circles) corresponding to the salinity evolution that requires calibration in a real case. The simulation was then run without solute recycling (fine lines) reflecting the salinity evolution induced by seawater intrusion (or rather by all boundaries). By deducting the seawater intrusion evolution curves from the overall salinity evolution we obtained the solute recycling salinity evolution (thick lines). The relative contribution of either salinisation process varies considerably in space and time. The 'present state' at the relative time $t^* = 2$ is indicated on the graphs of all the observation points. The only observation point which is clearly dominated by seawater intrusion all along the transient salinity evolution is *observation point 3*, while *observation points 1* and *2* are clearly dominated by solute recycling. *Well 1* and *observation point 5* show a late crossing-

over of the two salinisation curves: first they are clearly dominated by seawater intrusion and later by solute recycling. While *well 1* reaches the limit of exploitability when seawater intrusion is still dominant, *well 2* will never reach this threshold and is clearly dominated by solute recycling.

The iso-contour of the relative concentration C = 0.2, corresponding to the hypothetical limit of exploitability can be used as a reference line between the graphs, which have different vertical scales. The synthetic 'present state' salinity distribution shown in the centre of Fig. 5.3, which in a real case is obtained by calibration, will be used to illustrate the further steps in the salinisation risk assessment procedure.

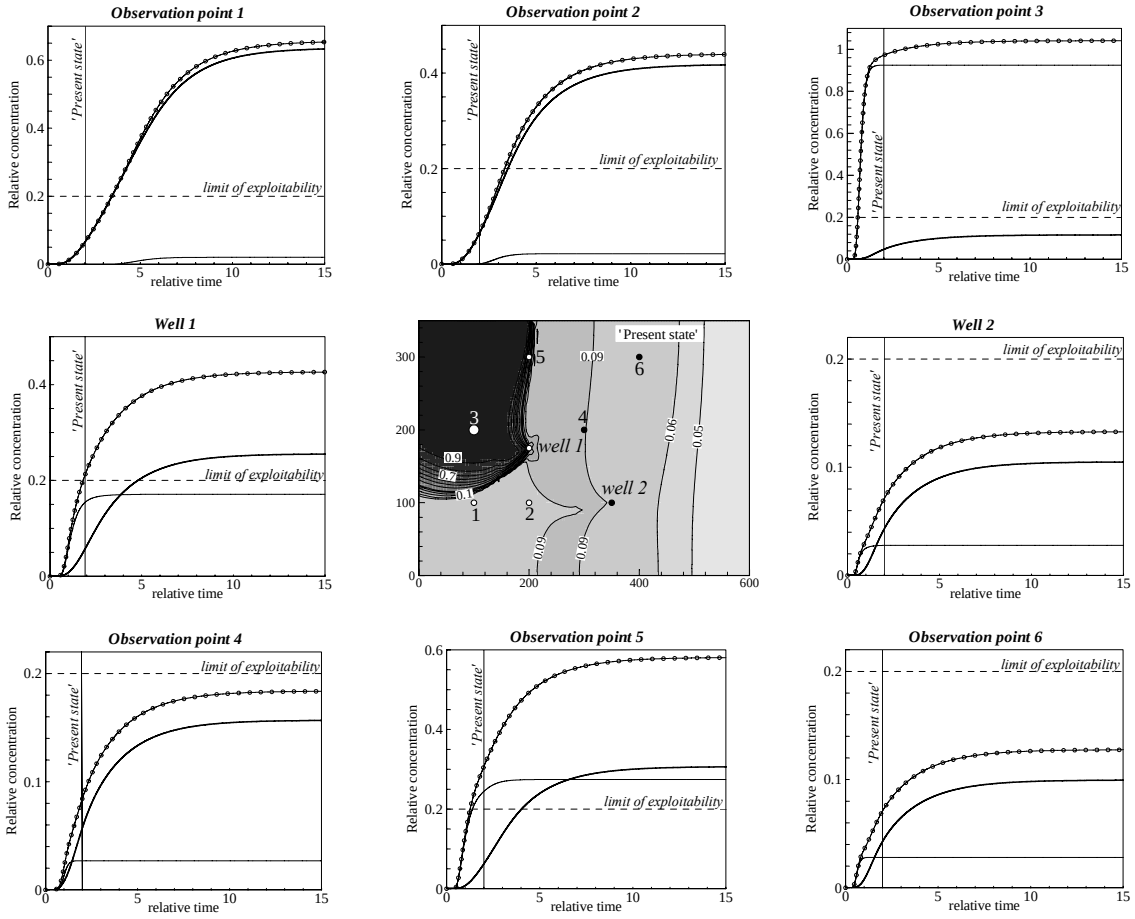

Fig. 5.3: In the central diagram, the overall 'present state' salinisation is shown (at a relative time t^*=2) on the same 2-D horizontal model shown in Fig. 5.1. The positions of six observation points and the two extraction wells are indicated. For each observation point, the transient overall salinity evolution (full lines with circles), the seawater intrusion evolution (fine lines) and the solute recycling salinisation (thick lines) are shown. The relative time t^*=2, chosen as the time corresponding to the hypothetical 'present state', is indicated on all graphs (full vertical line). The indicated relative concentration C = 0.2 corresponds to the defined limit of exploitability and is shown on all graphs as a dashed horizontal line, providing a reference for the varying scales of the different graphs.

Fig. 5.4a shows the overall 'present state' salinisation, chosen to be at the relative time t^*=2, as shown in Fig. 5.3. The iso-contour intervals in the eastern area represent multiples of the fresh groundwater salinity (C_f = 0.03), indicating slight concentration by solute recycling, while the iso-contour interval in the seawater intrusion area is 0.1. Fig. 5.4b and 5.4c show the decomposition of the overall 'present state' salinisation into the seawater intrusion and solute recycling contributions, respectively. Fig. 5.4d shows the transient evolution of the solute recycling fraction f_r(t) of all the observation points in Fig. 5.4e. The transient solute recycling fractions in Fig. 5.4d show that, a given observation point, for which the salinisation potential is dominated by solute recycling (f_r >0.5), may have been dominated by seawater intrusion (f_r <0.5) during periods of the transient evolution, and vice versa. Of all the observation points shown in Fig. 5.4d, only *observation point 3* remains within the seawater dominated region all along the transient evolution, while *observation points 1 and 2* are always dominated by solute recycling. This shows that the fractions obtained from the salinisation potential at steady state cannot be used to decompose a salinisation distribution in the transient state. Fig. 5.4e shows the solute recycling fraction distribution at 'present state'. Comparing Fig. 5.4e with Fig. 5.1d reveals that the distribution of the steady-state recycling fraction does not reflect the recycling fraction distribution during the transient phase, although the general pattern is similar.

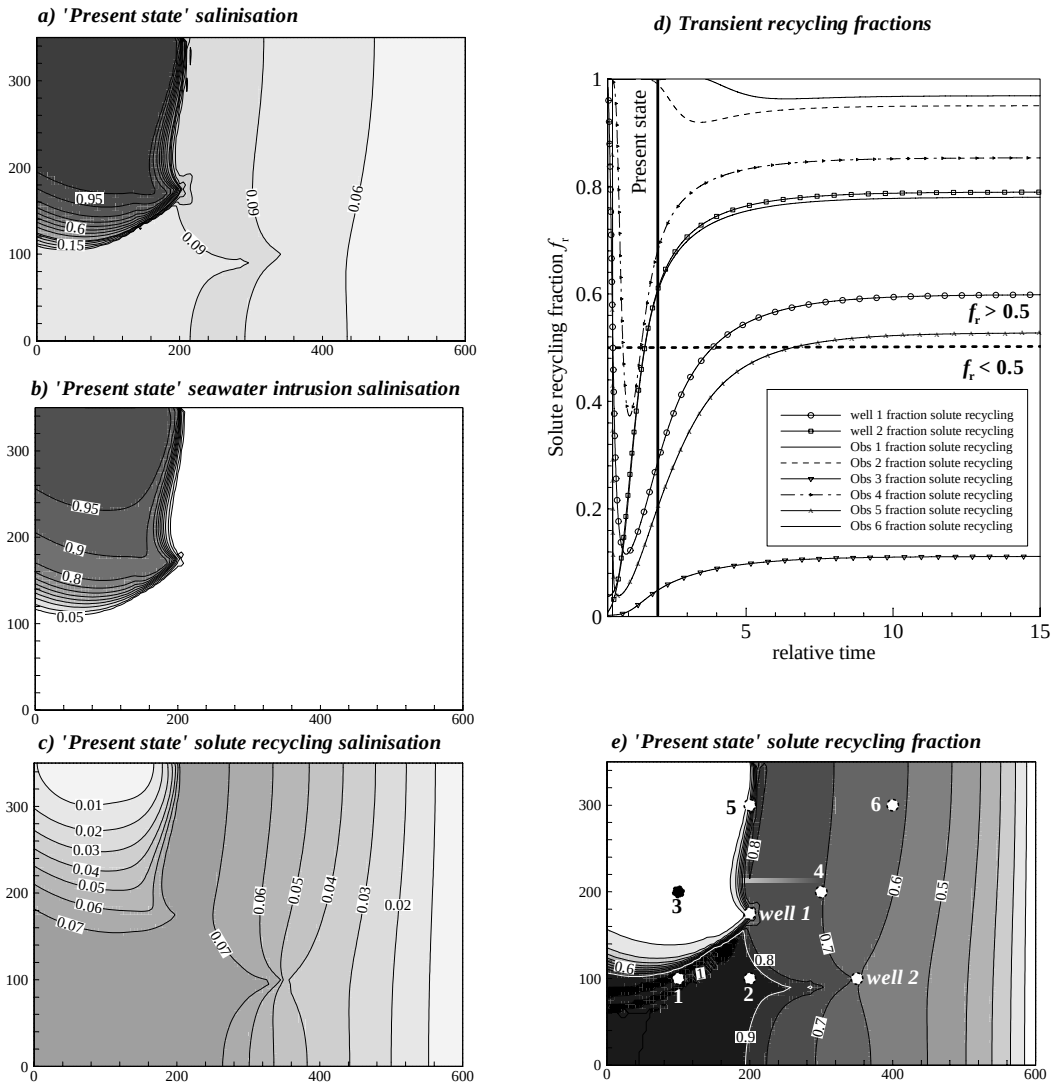

Fig. 5.4: (a) The overall 'present state' salinisation (relative time $t^* = 2$) of the model area (see Fig. 5.3), (b) 'present state' seawater intrusion salinity distribution and (c) 'present state' solute recycling salinity distribution. (d) Transient evolution of the solute recycling fraction. (e) Distribution of solute recycling fraction at 'present state' and location of the six observation points and two extraction wells for which the graphs are shown in (d).

5.3 Salinisation risk assessment based on numerical simulations

Separation of the effects of seawater intrusion and solute-recycling-induced groundwater salinisation in a risk assessment methodology has, as far as we are aware, not previously been reported in the literature. Hence, in the following, we will attempt to use the decomposed salinisation potentials SIP and RP, and the 'present state' salinisations, to define a risk index for each of the salinisation mechanisms, which indicates the spatial potential of further salinisation

due to the respective salinisation process. Wherever the two salinisation processes are present, it is critical to be able to distinguish them in order to be able to design remedial measures, since only a correctly identified process will allow the design of an efficient management scheme.

In this respect, the proposed salinisation risk assessment methodology is a first attempt to provide a tool with which the impact of exploitation schemes can be evaluated by reducing the effects of dynamic processes to static images. However, to quantify the total risk, definition of salinity thresholds which would reduce crop yields and thus have a negative impact on human interests (e.g. economy) would need to be defined. Such definitions, however, have to be based on aspects related to numerous fields (e.g. agronomy, irrigation science and economy) and is therefore far beyond the scope of this work. However, to illustrate how the risk indices can be combined with a defined threshold concentration, a 'hypothetical' concentration threshold is used to illustrate the possible delimitation of areas at high risk.

We only consider two processes, solute recycling and seawater intrusion, to illustrate the methodology. In many cases, however, it is very likely that the approach would have to be extended to include other important salinisation processes, such as agricultural additives, direct evaporation from the groundwater or the presence of geogenic salt deposits and trapped seawater, depending on special circumstances.

5.3.1 Definition of solute recycling and seawater intrusion salinisation risk indices

Risk assessment is based on comparison of a present state of the environment with a possible future adverse state of the environment, having negative impacts on human interests. Risk can be defined as the probability of the adverse state actually occurring, multiplied by the severity of the impact (Helm 1996).

Relating this general definition to the two salinisation processes we are focussing on, requires definition of an adverse state. Although we are dealing with two different salinisation processes, we will define an adverse state in both cases on the same basis: an adverse state is any further salinity increase induced by the respective salinisation process. Since all our evaluations are based on deterministic model simulations, we will not define a 'probability' of the adverse state to actually occur, but will define a risk index, being a measure of the future potential salinity increase. To obtain the risk indices, the respective 'present state' salinisations are deducted from and normalised by the overall salinisation potential. If we denote the overall, the solute recycling or seawater intrusion salinity distributions with i, the respective salinisation risk index $R_i(x)$ at any point x in the domain can be written as follows:

$$R_i(x) = \frac{SPot_i(x) - S\,\mathrm{Pr}es_i(x)}{RP(x) + SIP(x)} \tag{5.5}$$

where:

$SPot_i$ = salinisation potential of the i^{th} salinisation process, i.e. with i = solute recycling then $SPot_i=RP(x)$; i = seawater intrusion, then $SPot_i=SIP(x)$; i = (seawater intrusion+solute recycling), then $SPot_i= RP(x)+ SIP(x)$.

$SPres_i$ = 'present state' salinisation of the i^{th} salinisation process, according to $SPot_i$.

The denominator denotes the overall salinisation potential. 'Present state' salinities which are close to the respective salinisation potential will have a small risk index, whereas those which are small relative to the respective salinisation potential will have a large risk index. The overall salinisation potential is used as reference to define the risk indices, reflecting the potential further salinisation.

5.3.2 Risk index mapping procedures

Making use of the definition in Eq. 5.5 allows us to create salinisation risk index maps from the 'present state' salinity distributions and the salinisation potentials. The 'present state' can either be compared to the salinisation potential obtained with the 'present state' exploitation scheme, or, it may be compared to salinisation potentials obtained from modified or optimised exploitation schemes. In the following, we will illustrate the risk index mapping procedure on the synthetic 2-D horizontal example used throughout this chapter.

5.3.2.1 Risk index distributions for the 'present state' exploitation scheme

To obtain the salinisation risk index distributions we can make use of the 'present state' salinisations - the overall salinisation shown in Fig. 5.4a, the seawater intrusion salinisation shown in Fig. 5.4b, and the solute recycling salinisation, shown in Fig. 5.4c. The respective 'present state' salinisations at each point x in the domain are deduced from and normalised with the corresponding salinisation potentials at late times (Fig. 5.1a, b, c), according to Eq. (5.5).

Fig. 5.5 shows the risk index maps for the overall salinisation Fig. 5.5c), for the seawater intrusion (Fig. 5.5f) and solute recycling salinisations (Fig. 5.5i). In the first column, the respective 'present state' salinty distributions are shown (Fig. 5.5a, d, g), the middle column shows the respective salinisation potentials at late times (Fig. 5.5 b, e, d) and the right-hand column the respective risk index distributions(Fig. 5 c, e, i).

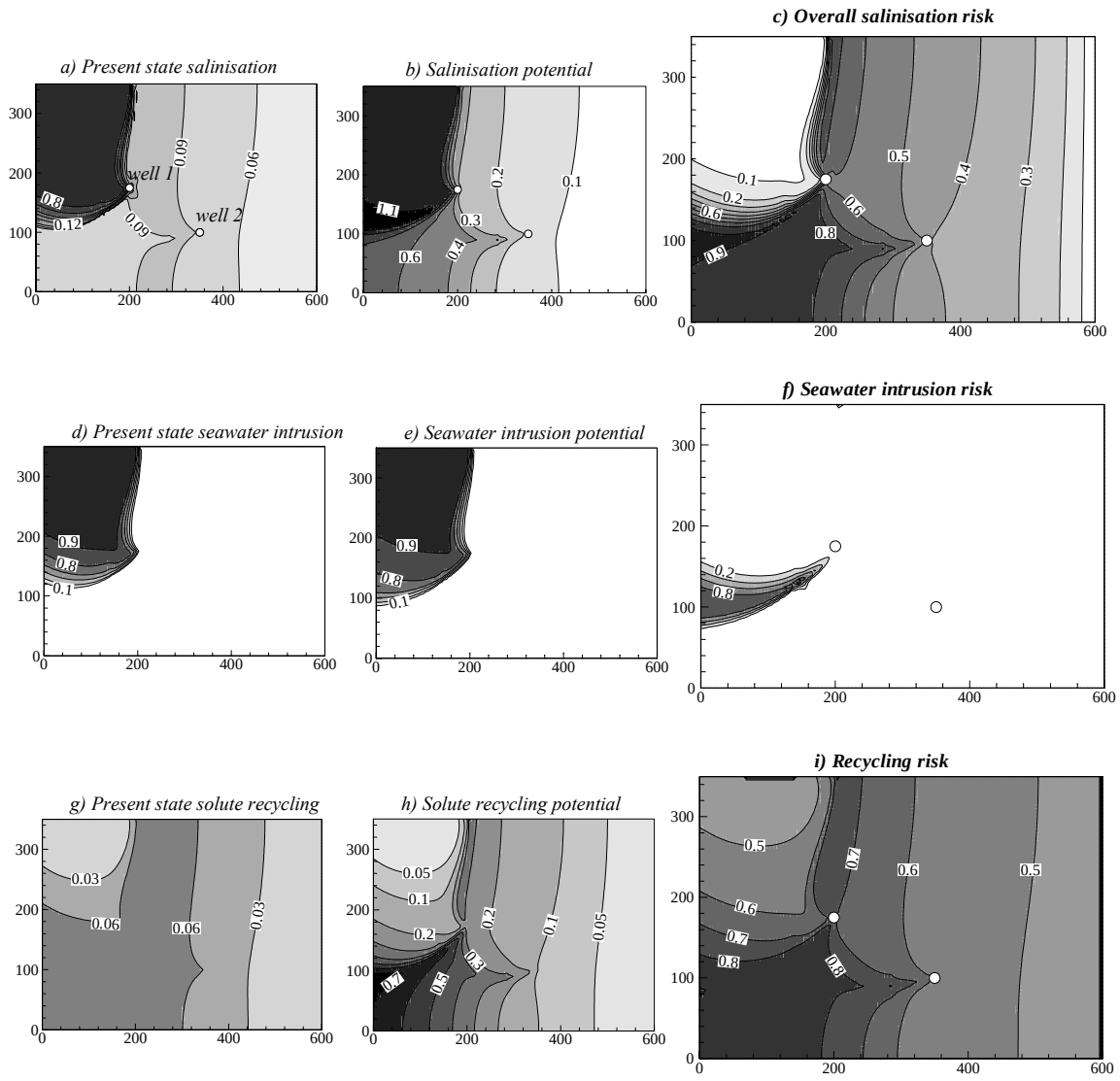

Fig. 5.5: The risk index mapping procedure illustrated with reference to the synthetic 2D aquifer used in earlier Figures. Salinisation risk index distributions: overall salinisation (a, b, c), seawater intrusion salinisation (d, e, f) and solute recycling salinisation (g, h, i) . First column shows the respective 'present state' salinity distributions, which are deduced from and normalised with the respective salinisation potentials in the second column, yielding the respective risk index distributions in the right-hand column, according to Eq. (5.5).

Fig. 5.5c shows that the lowest overall salinisation risk indices are found in the area of the seawater intrusion. The seawater intrusion risk index distribution, shown in Fig. 5.5f, was corrected for the effect of the fresh groundwater boundary and shows that seawater intrusion is approaching steady-state. In the area unaffected by seawater intrusion, solute recycling risk indices are highest (Fig. 5.5i).

In this example, the solute recycling risk indices are higher than the seawater intrusion risk indices almost everywhere in the domain, since seawater intrusion is approaching steady state (Fig. 5.5i and 5.5f). Fig. 5.5c highlights the areas which may suffer further salinisation. Comparing it with Fig. 5.5i reveals that almost the entire further salinisation will be caused by solute recycling.

As indicated in Fig. 5.3, the concentration of *well 1* at the chosen 'present state' is just about to reach the limit of exploitability. In such a case, the salinisation risk index map will be a hypothetical extrapolation which will never occur, since the exploitation scheme is bound to change. It delimits areas prone to solute recycling and seawater intrusion and their relative importance for the present exploitation and irrigation scheme, only. At a stage when a change in the exploitation scheme becomes imperative, knowledge of the relative spatial importance of the salinisation process can be a very useful information for defining the most efficient way of modifying it. The risk index distribution in such a case will, however, not be indicative of the further salinity evolution.

5.3.2.2 *Risk index distributions for modified/optimised exploitation schemes*

To evaluate the impact of a change in the exploitation scheme on the salinisation risk, we will make use of the same salinisation risk index definition (Eq. 5.5) to identify zones that will either tend towards improved water quality or suffer further deterioration in response to the modification of the hydraulic setting. Again, we will make use of the 'present state' salinisations. However, if the hydraulic setting changes, the system will be directed towards a new, modified, salinisation potential at late times. Hence, to obtain the risk distribution of the modified exploitation scheme, the 'present state' salinisations are compared to the modified salinisation potentials, which substitute the salinisation potential in Eq. (5.5). Where the salinity of the modified salinisation potential is smaller than the 'present state' salinity, negative risk index values will be obtained, which reflects the remediating effect of the modified exploitation scheme. In this way, the iso-contour of zero risk index will delimit the areas which will improve in water quality from areas which will still suffer further salinisation. Doing the procedure for the solute recycling and seawater intrusion separately will indicate where improvement or further deterioration will take place in response to either salinisation process.

To illustrate this procedure, we used the same 2-D horizontal model as in the previous sections. The solute captured from the wells was minimised, with the constraints that the well locations remain unchanged as well as the total extraction rate. The irrigation plot location in this simple case was not optimised, since it covers the entire domain. The very simple optimised exploitation scheme was done 'manually' and implied minimisation of the solute mass flux captured by the

wells from the boundaries and resulted in the de-activation of *well 1* and the increase in the extraction rate of *well 2.*

Fig. 5.6 compares the risk index maps for the present state exploitation scheme (left column), shown in Fig. 5.5, with the risk index distributions obtained from the 'modified/optimised' exploitation scheme. In the top row, the three overall salinity distributions are shown, the overall salinisation potential for the present state exploitation scheme (a), the overall 'present state' salinisation (b), and the optimised/modified salinisation potential (c). The left column shows the risk index distributions derived from the salinisation potential for the present exploitation scheme (as shown in Fig. 5.5), while the right column shows the respective modified salinisation risk index distributions.

The overall salinisation risk index maps (Fig. 5.6 d, e) show a similar pattern in the southeast. In Fig. 5.6d, all risk indices are positive, while the optimised risk index maps show that the modified exploitation scheme leads to a salinity decrease (negative values) in most of the area, apart from the southeastern area close to the regional discharge area, where the highest risk index values are encountered for the present day exploitation scheme (Fig. 5.6d).

The seawater intrusion risk index maps were corrected for the effect of the freshwater boundary. They show that, for the present state exploitation scheme, the seawater front will still advance slightly (Fig. 5.6f), while the optimised exploitation scheme will lead to negative risk indices in the whole domain (Fig. 5.5g), particularly concentrated around the de-activated *well 1*.

The solute recycling risk indices (Fig. 5.6h) and optimised solute recycling risk indices (Fig. 5.6i) show a similar pattern, but the optimised recycling risk index map reveals a vast area with negative values. It is obvious that the effect of solute recycling will diminish in most areas, since the extracted solute mass captured from the boundaries was minimised, and w*ell 2* only captures water from the freshwater boundary. However, positive values are encountered in the downstream areas, although with smaller values than in the risk index map for the present day hydraulic setting, shown in Fig. 5.6 h. The positive risk indices make up almost all the positive overall salinisation risk index values, shown in Fig. 5.6e. The slight difference is caused by the fact that the impact of the fresh groundwater boundary has been deducted from the seawater intrusion risk indices. The optimised solute recycling risk index maps show that, although the seawater intrusion is retreating, areas may still suffer salinity increase due to solute recycling. Such risk index maps can thus be useful to understand the spatial response of a system to modifications in the exploitation scheme with respect to the processes which may lead to future salinisation or remediation.

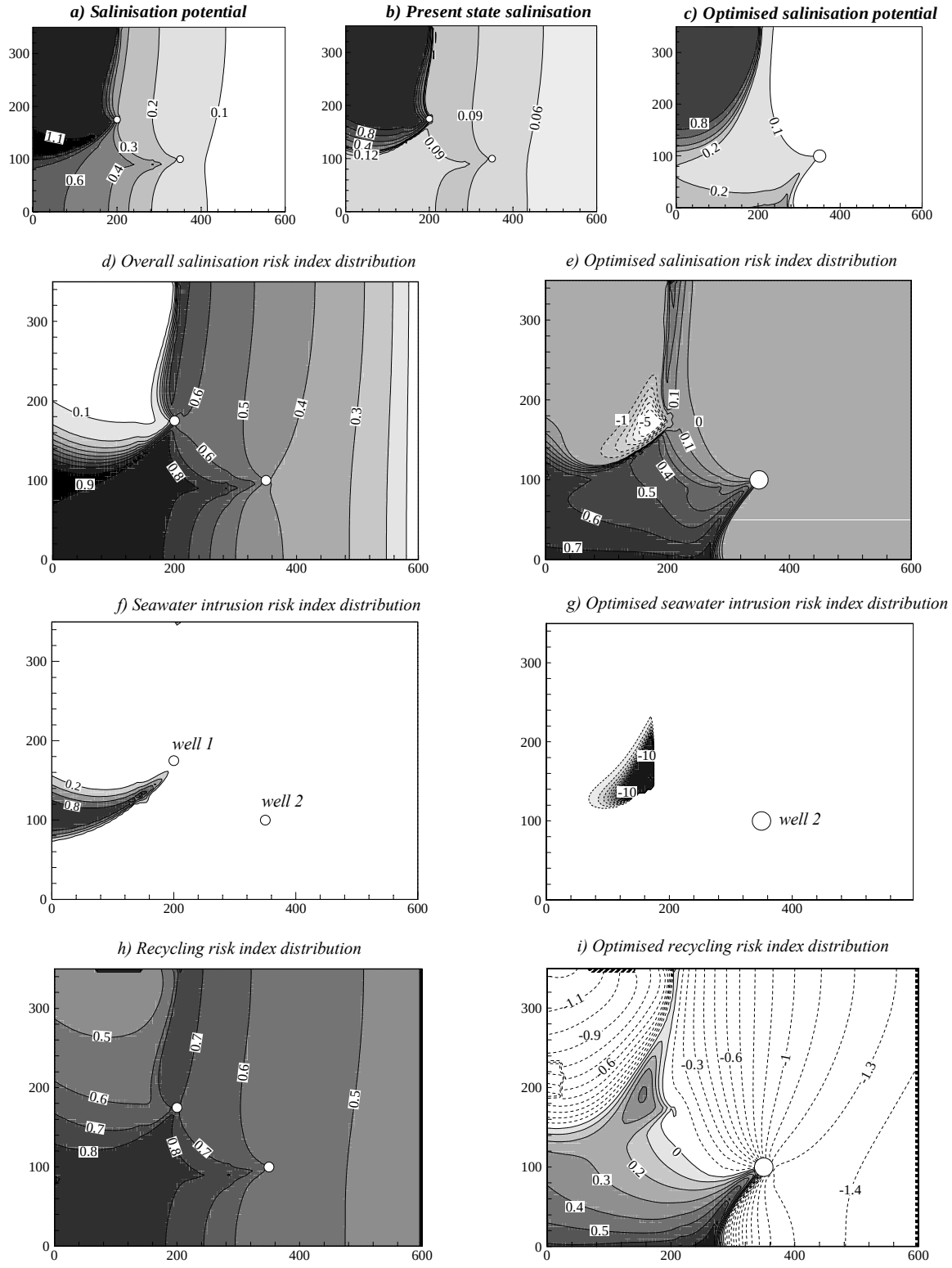

Fig. 5.6: (a) Salinisation potential for the present state exploitation scheme, (b) Overall 'present state' salinisation and (c) Salinisation potential for the 'optimised/modified' exploitation scheme, for which only *well 2* is active. The left-hand column shows risk index maps for the present state exploitation scheme and the right-hand column for the optimised exploitation scheme. (d) and (e) Overall salinisation risk index distributions. (f) and (g) Seawater intrusion risk index distributions. (h) and (i) Solute recycling risk index distributions. Negative risk indices indicate areas which will tend towards groundwater quality improvement, while positive indices indicate further salinisation.

5.4 Discussion

In this chapter, we elaborated a framework for a risk assessment methodology in irrigated coastal areas which considers two salinisation processes, seawater intrusion and solute recycling from irrigation, separately. First, the overall salinisation potential at late times was decomposed into a seawater intrusion potential (SIP) and a solute recycling potential (RP), and the fractions were used to map the relative importance of either salinisation process at late times. Then, decomposition of the transient salinity evolution was done in the same way to obtain the 'present state' solute recycling and seawater intrusion salinity distributions. Risk indices at any point were then defined as the relative potential of further salinisation induced by the respective salinisation processes. This led to risk index maps revealing the spatial distribution of the potential further seawater or solute salinisation. Then, risk index maps were established for modified or optimised exploitation schemes, which delimit the areas which will suffer further salinisation from areas where groundwater quality will improve in response to the modified exploitation scheme.

The most delicate aspect in the proposed risk assessment is that the 'present state' salinisation has to be obtained by simulation, which may be extremely difficult in real case studies. In real case studies, salinity measurements will reflect the superimposed effects of all present salinisation mechanisms, and, in coastal areas, monitoring is often denser along the seawater front, which leads to poor data sets further inland, where solute recycling may be dominant. As the risk assessment aims to separate the seawater from the solute recycling process, the measured overall salinisation has to be decomposed by simulation, which requires calibration. In any modelling approach, the calibration phase is the most challenging aspect.

Assuming that a satisfactory 'present state' can be simulated for a real case, the decomposition of the 'present state' salinity distribution may give a feedback with respect to the measured salinities, which will always reflect the overall salinity of a system. This would allow quantification of the spatial contributions of either salinisation process, which cannot be inferred from the salinity data alone, but may be cross-validated with other hydrochemical fingerprints. Making use of a quantitative approach as an interactive tool to interpret field data is reasonable, particularly in settings where identification of superimposed salinisation processes will always be ambiguous.

In the proposed salinisation risk assessment, time has not been directly included, e.g. the time to reach a certain salinity. However, this aspect could possibly be added, by, for instance, evaluating the average recycling time in an area, according to Eq. (3.30). In this way, the impact of solute recycling could be estimated by comparing the average recycling time with the irrigation period.

With respect to solute recycling, the risk index, defined as the potential of a future positive salinity change occuring at a point due to solute recycling, will be fairly homogeneous over time. For

locations with high risk indices, the future salinity slope will in general be steeper than for locations with small risk indices. With respect to seawater intrusion on the other hand, the risk index definition is far more delicate, since future salinity increase may be very heterogeneous, i.e. a point that will suffer from seawater intrusion at steady-state might not be affected until 'just before' steady-state, while other locations might suffer this salinity increase much earlier and salinity increase may take place over a very short time-period. Hence, salinity increase is not constant over time and hence the potential of attaining a the steady state salinity may not be adequate. Hence, it is not an easy task to establish a risk assessment for seawater intrusion and solute recycling based on the same criteria. Although the defined risk index definition seems more adequate for solute recycling than for seawater intrusion, solute recycling is dependent on the solute mass captured from the limits, and thus from seawater and the freshwater boundary. Hence, if the lateral solute mass flux is highly variable over time, salinisation induced by solute recycling will also be highly variable.

The proposed framework for a risk assessment methodology has to be considered as an attempt to define a measure which accounts for the groundwater dynamics of a system with two superimposed salinisation processes, and an attempt to investigate the stability of the system with respect to the different salinisation processes. It is, however, not related to any fixed values (e.g. limit of exploitability) nor to any time frame, factors which would have to be included in the risk assessment to quantify the actual salinisation risk. The risk index definition alone will not allow estimation of the risk, as can be seen on the example, where a point which is completely seawater intruded shows a risk index of zero, although the water quality is far beyond the limit of exploitability. For that reason, it would be important to define threshold concentrations indicative of an economical impact and relate these to the risk index maps.

Risk index maps for optimised or modified exploitation schemes can be useful in the delimitation of zones for which groundwater will improve from zones where it will suffer further degradation. In this way, sensitive areas can be identified and the proposed risk assessment could be used as a dynamic tool for the design of appropriate remedial measures. However, it is important to repeat that only a framework has been proposed, pointing out a possible direction to explore and define in far more detail the threat of the different salinisation processes.

CHAPTER 6

AKROTIRI AQUIFER (SOUTHERN CYPRUS): IDENTIFICATION OF SALINISATION PROCESSES AND APPLICATION OF THE SALINISATION RISK ASSESSMENT PROCEDURE

Abstract

In the Akrotiri aquifer in Southern Cyprus, field investigations were carried out to confirm the existence of solute recycling salinisation and to determine the spatial distribution of different salinisation processes. On the basis of this data analysis, a 3-D finite element model, reflecting the main features of the aquifer, was used to illustrate and test the salinisation risk assessment procedure developed in the previous chapter. The results indicate that the central area of the aquifer is a zone endangered with respect to salinisation from solute recycling, whereas the western area is endangered with respect to seawater intrusion. This correlates well with the spatial distribution of the dominant salinity sources as derived from the field investigations. However, essential data for the solute recycling simulations, i.e. the distribution pattern of the extracted groudwater from the irrigation wells onto the irrigated surfaces, was not available, rendering the results of the simulations 'hypothetical'. At this stage, therefore, the results cannot be used to define any action plans, since the necessary monitoring data related to solute recycling salinisation was lacking. Data related to solute recycling is rarely monitored in coastal aquifers, but is essential for the calibration and cross-validation of the proposed salinisation risk assessment procedure. However, key-factors identified in the theoretical description of the solute recycling process can be used in the field for a preliminary and inexpensive qualitative identification and evaluation of endangered areas, indicating where the installation of monitoring networks would be adviseable in order to obtain the data necessary for a quantitative salinisation risk assessment.

6.1 Introduction

In the previous chapter, we established a framework for a quantitative salinisation risk assessment methodology and illustrated it on a synthetic example. Although the proposed salinisation risk assessment is process-based, in contrast to risk and vulnerability approaches based on the empirical evaluation of key-factors (e.g. Aller et al. 1985), the results will entirely depend on the model used for the purpose. To estimate the reliability of the elaborated model, the different salinisation processes and their spatial distribution have to be identified and monitored in the field.

In coastal aquifers, a large number of monitoring strategies have been developed to follow the evolution of seawater intrusion (e.g. Custodio 1997), whereas monitoring networks focussing on solute recycling or other salinisation processes in coastal settings are rarely reported in literature.

This fact leads to a considerable discrepancy in the availability of data sets necessary for modelling seawater intrusion in comparison to the other processes.

The aim of this chapter is to illustrate the salinisation risk assessment procedure on a real case study, the Akrotiri aquifer in Southern Cyprus. The presented results are 'hypothetical', since the discrepancy in the available data noted above also applies to this case. The information on irrigation schemes which would provide the basic data for simulating solute recycling is scarce and the distribution patterns were not retrieved for this study. However, the 'hypothetical' results lead to an elucidation of the data requirements for the proposed quantitative salinisation risk assessment procedure. Also, based on the understanding we have gained from the theoretical description of the solute recycling process, practical recommendations can be made for field hydrogeologists to enable them to approximately localise the areas in which the salinisation risk is high, either from seawater intrusion or solute recycling, using the classical tools. In this way, preliminary and inexpensive estimations of the salinisation risk can be made, which can be used, for instance, to implement the monitoring networks necessary to obtain data for the quantitative salinisation risk assessment in the most sensitive areas.

Within the framework of this thesis field investigations were carried out in the Akrotiri aquifer with the specific aim of identifying the superposition of different salinisation processes and their spatial distribution. Meilhac (2003) carried out a large-scale hydrogeochemical investigation to identify the different salinisation processes in the Akrotiri aquifer for her Master thesis and a second Master thesis was conducted by Yeo (2003) making use of geoelectrical methods to map the seawater encroachment on the large scale. On the small scale, he carried out high-resolution electrical resistivity tomography (ERT) to map the soil salinity at two sites within the citrus plantations, where monitoring wells had been installed.

The Akrotiri aquifer has been monitored for several decades and several hydrogeological studies have been carried out covering a time-span of thirty years (Constantinou 1970, Kitching 1975, Jackovides, 1982, Milnes 2000, Meilhac 2003, Yeo 2003). Hence, the aquifer is well known and the amount of available data is believed to be well above the average.

To establish and illustrate the salinisation risk assessment procedure proposed in the previous chapter, use was made of a previously constructed 3-D finite element model, reflecting the average hydraulic conditions of the past twenty years (Milnes 2000). Due to the lack of data in the central area of the aquifer, calibration of the transport parameters was not carried out. Hence, the model is used as 'synthetic reality', similar to the treatment of the Kiti aquifer, presented in Chapter 2. Nevertheless, the simulated risk index distributions are compared with the spatial distribution of the dominant salinisation processes, as derived from the large-scale hydrogeochemical

investigation (Meilhac 2003). This leads to a discussion of the essential data which would have been required for a successful elaboration of a numerical model taking into account solute recycling. With the available data set for the Akrotiri aquifer, a qualitative estimation of the relative impact of solute recycling and seawater intrusion is presented, which, in a general way, illustrates how classical hydrogeological data can be interpreted to account for the solute recycling process.

6.2 General description of the Akrotiri Aquifer

The porous Akrotiri aquifer is located on a peninsula in Southern Cyprus, just west of Limassol, covering an area of approx. 40 km^2 (Fig. 6.1), and is built up of delta deposits underlain by Miocene carbonates. In the east and the west, the aquifer is delimited by the sea, and to the south, by a salt lake which forms a regional discharge area with an average water table of -2.5 masl. In the north, the alluvial aquifer pinches out against shallowly south-dipping Miocene carbonates. Several of the carbonate units act as aquifers, with a well-developed secondary porosity, and these convey groundwater towards the Akrotiri area from a catchment of approx. 100 km^2 (Jackovides 1982). The climate is typically semi-arid, with an average annual rainfall of 450 mm and an average pan evaporation of 1300 mm. In the central area of the aquifer, large citrus plantations cover an area of approx. 13km^2 (Fig. 6.1).

The hydraulic setting of the Akrotiri aquifer changed drastically in 1987, when the Kouris river, which had been a main recharge component of the aquifer, was retained behind the largest dam on Cyprus, the Kouris dam (Fig. 6.1). After the dam construction, exploitation of the Akrotiri aquifer continued at the same rate as before, with an average of 18 million m^3/year until the early 90's, when seawater intrusion became alarming and the aquifer was declared a conservation area by the authorities. Later, exploitation was first reduced to an average of 12 million m^3/year, and has been further diminished to 7 million m^3/year in the past five years.

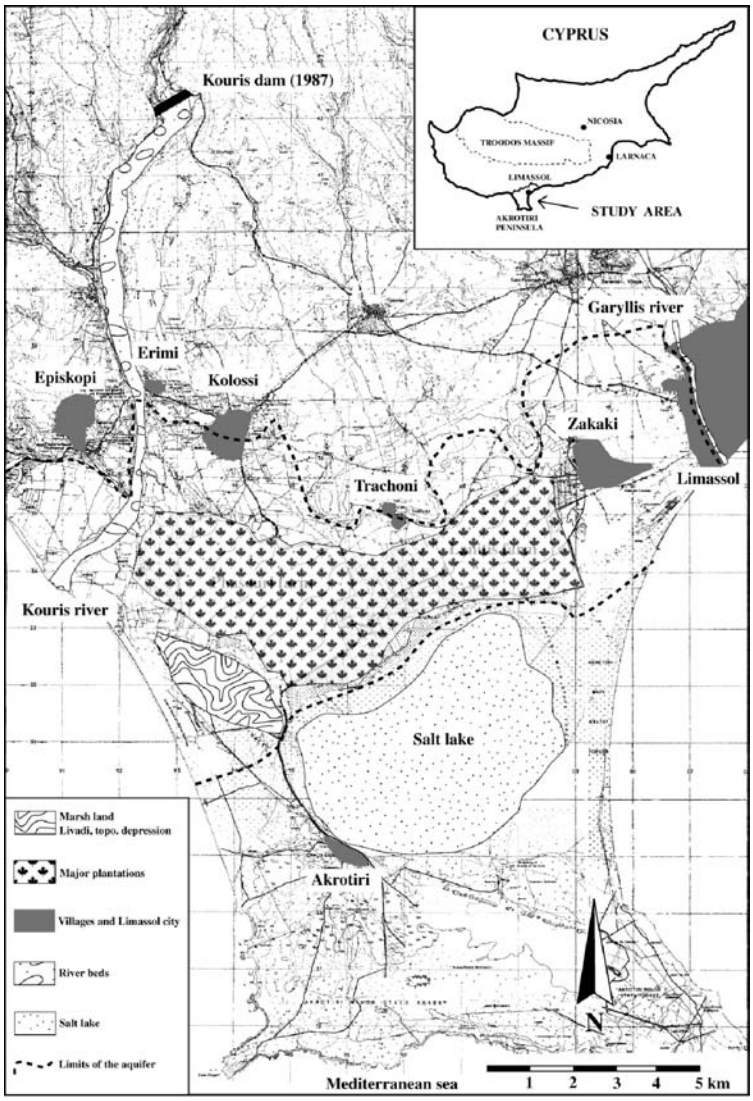

Fig. 6.1: Main physiographic features of the Akrotiri aquifer, showing the aquifer boundary and the extend of the citrus plantations. In the west, the aquifer is crossed by the Kouris River bed, with the Kouris dam in the north, and it is bounded to the south by the salt lake.

6.2.1 Assessment of groundwater salinity and irrigation practices

In the Akrotiri aquifer, a landward advance of the seawater intrusion front has been observed since the late 1980s, particularly in the western area. Ahead of this front, a rather broad zone with intermediate salinities reaches into the area of the citrus plantations (Fig. 6.2). In the east, the irrigated area north of the salt lake is strongly affected by salinisation. In contrast, the salinity distribution in the aquifer prior to the construction of the Kouris dam in 1984 (Fig. 6.3) reveals that seawater intrusion was not present in the west at that time (Hydrological Year Book, WDD, 1984). The year 2000 salinity map (Fig. 6.2) shows that high salinities are found in the vicinity of the salt lake, in the same area that was already the most affected in 1984 (Fig. 6.3). The pattern of

the intermediate salinities in the central irrigated area is far less pronounced than what was observed in the Kiti aquifer, presented in Chapter 2 (see Fig. 2.5).

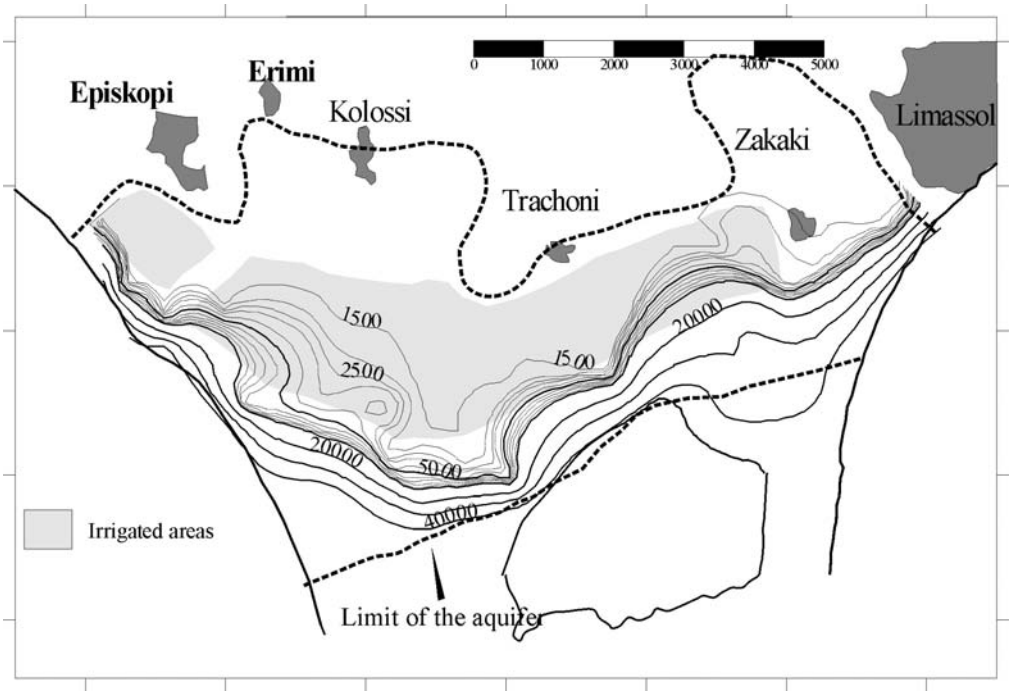

Fig. 6.2: Salinity distribution in superficial groundwater measured in year 2000 (in μS/cm). Iso-contour interval below 5000μS/cm is 500μS/cm. The grey area indicates all irrigated surfaces. Intermediate salinities (< 5000μS/cm) reach far into the irrigated areas.

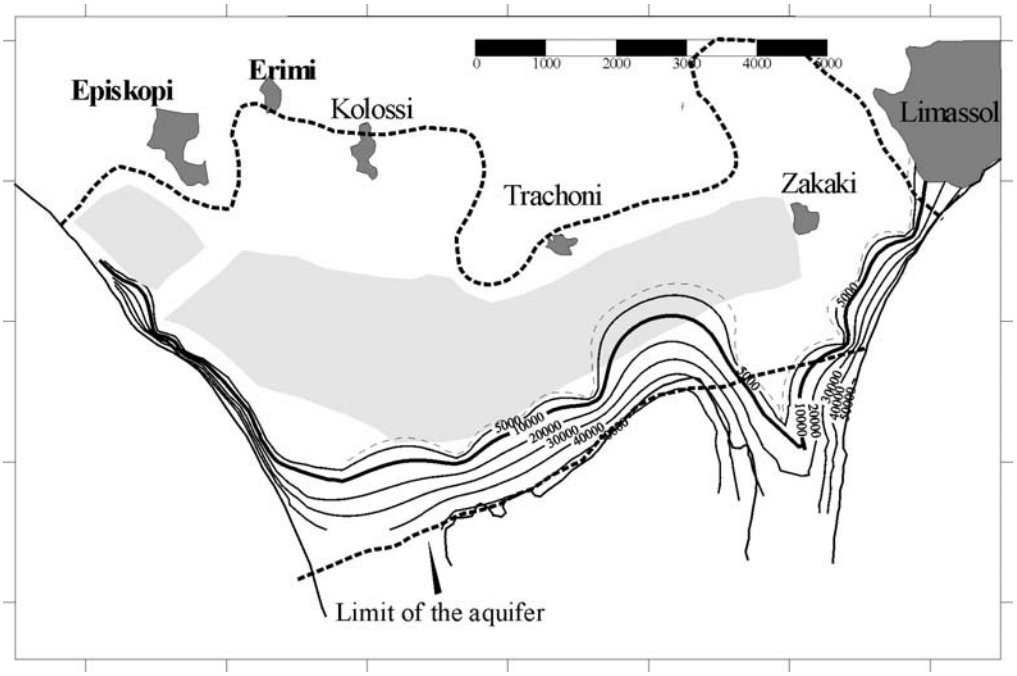

Fig. 6.3: Salinity distribution in superficial groundwater measured in year1984 (in μS/cm), prior to the construction of the Kouris dam (Hydrological Year Book 1984, WDD). Lowest iso-contour (stippled line) equals 2500 μS/cm. The grey area indicates all irrigated surfaces.

The groundwater salinity measured in the field is the most widespread monitoring method in coastal settings and reflects the overall salinisation, i.e. the total salinity resulting from different processes (Custodio 1997). Hence, the measurement of salinity in itself does not allow the identification of different salinisation processes, and yet the different processes require remedial measures which can be very different, or even opposed (see Fig. 1.1). In the Akrotiri aquifer, salinities in the superficial groundwater have been measured sporadically for several decades. For the past 7 years, vertical salinitiy logs have been carried out on a three-monthly basis in boreholes close to the sea. In the area of the citrus plantations, monitoring of salinities is done by the farm owners and is not accessible to the authorities, whereas the water table measurements from this zone are delivered on a monthly basis.

Above the Akrotiri aquifer, the citrus plantations have been irrigated with water salinities between 0.5-2.5 gr/l for the past 50 years. Irrigation practices have changed significantly during this period, from the original furrow irrigation up to the 1970's, to sprinkler irrigation today. With an average irrigation requirement of 8000 m^3/ha/year for citrus cultures and a roughly estimated deep percolation of 2000-4000 m^3/ha/year (from irrigation return flow and precipitation), the solutes in the deep percolation are expected to be concentrated by a factor of 2-4. In the literature, however, seasonal concentration factors of up to 7 are reported, depending on the ratio between the applied irrigation rate and the deep percolation rate to the groundwater (Aragüés et al 1985). Extrapolating these values over the whole irrigation period (approx. 50 years) leads to an accumulated salt load from solute return flow that would be almost sufficient to salinise a water volume corresponding to the porous aquifer volume below the irrigation surface to the salinity of seawater. Since we are dealing with a dynamic system, such an estimation is in itself meaningless, but it indicates that salinisation by solute recycling from irrigation might be of importance in the Akrotiri aquifer, since migration of solutes out of the system is believed to be slow.

6.2.2 Conceptual model

The Akrotiri porous aquifer is built up of three intersecting and overlapping delta lobes, which has resulted in a high degree of heterogeneity. In the east, there is one delta lobe from the Garyllis River and in the west there are two overlapping delta lobes from the Kouris River. The thickness of the porous aquifer is highly variable, with a maximum thickness in the west of approximately 100 m and a minimum thickness in the central area of approximately 30 m (Fig. 6.4).

The bedrock topography was constructed from 100 borehole logs (Fig. 6.4) and represents a paleo-erosional surface, which developed during the Late-Miocene desiccation of the Mediterranean

(Hsü et al. 1973). In most of the area, Pliocene marls overlie the carbonates, but they are discontinuous. The analysis of the bedrock lithologies revealed a lateral stratigraphic gap of several million years, which strongly suggests the presence of a major fault zone with an estimated vertical displacement of several hundred meters (Milnes 2000). The presence of such a large-scale structure in the Akrotiri area is plausible from a tectonic point of view, since an active subduction zone is located just south of the Akrotiri peninsula (Robertson et al. 1990). Meilhac (2003) found that oxygen isotopic values were significantly depleted along the inferred fault trace, suggesting recharge of the porous aquifer from the lower carbonate units with water circulating in a regional-scale flow system. Also, radon concentrations followed the inferred fault zone trace. Piezometric data indicate higher hydraulic heads in the carbonate aquifer than in the above porous aquifer, suggesting recharge of the porous aquifer from below, along the fault zone, as schematically illustrated in Fig. 6.4.

The conceptual model of the area, shown in Fig. 6.4, is characterised by three main recharge components: 1) from infiltration of precipitation and irrigation return flow on the aquifer, 2) from the lower carbonate aquifer along the large-scale fault zone that connects the bedrock aquifer with the porous aquifer, and 3) from seawater intrusion. Discharge takes place to the salt lake, to the sea, and to extraction wells. Fig. 6.5 shows the average water table in the porous aquifer between 1987-2003, together with the nitrate concentrations measured by Meilhac (2003). The salt lake to the south can be seen to act as regional discharge area. A prominent hydraulic depression can be seen in the central irrigated area, particularly towards the west (zone of plantations can be seen as chequered pattern). The highest nitrate concentrations measured in 2003 can be seen to in the central irrigated area, where the aquifer thickness is smallest.

Recharge by infiltration from precipitation and irrigation return flow has been estimated to be approximately 7 mio. m^3/year and artificial recharge contributes to the recharge with approx. 4 million m^3/year (Fig. 6.5). Subsurface recharge from the northern carbonate hills has been estimated to be approximately 12 million m^3/year. Losses due to evaporation in the area of the salt lake and by direct evapotranspiration from the groundwater by vast Eucalyptus forests were estimated to be approximately 2-3 million m^3/year (Jackovides 1982) and the average extraction from wells between 1987-2003 was 13 million m^3/year. The water balance indicates that the system does not suffer an overall freshwater deficit.

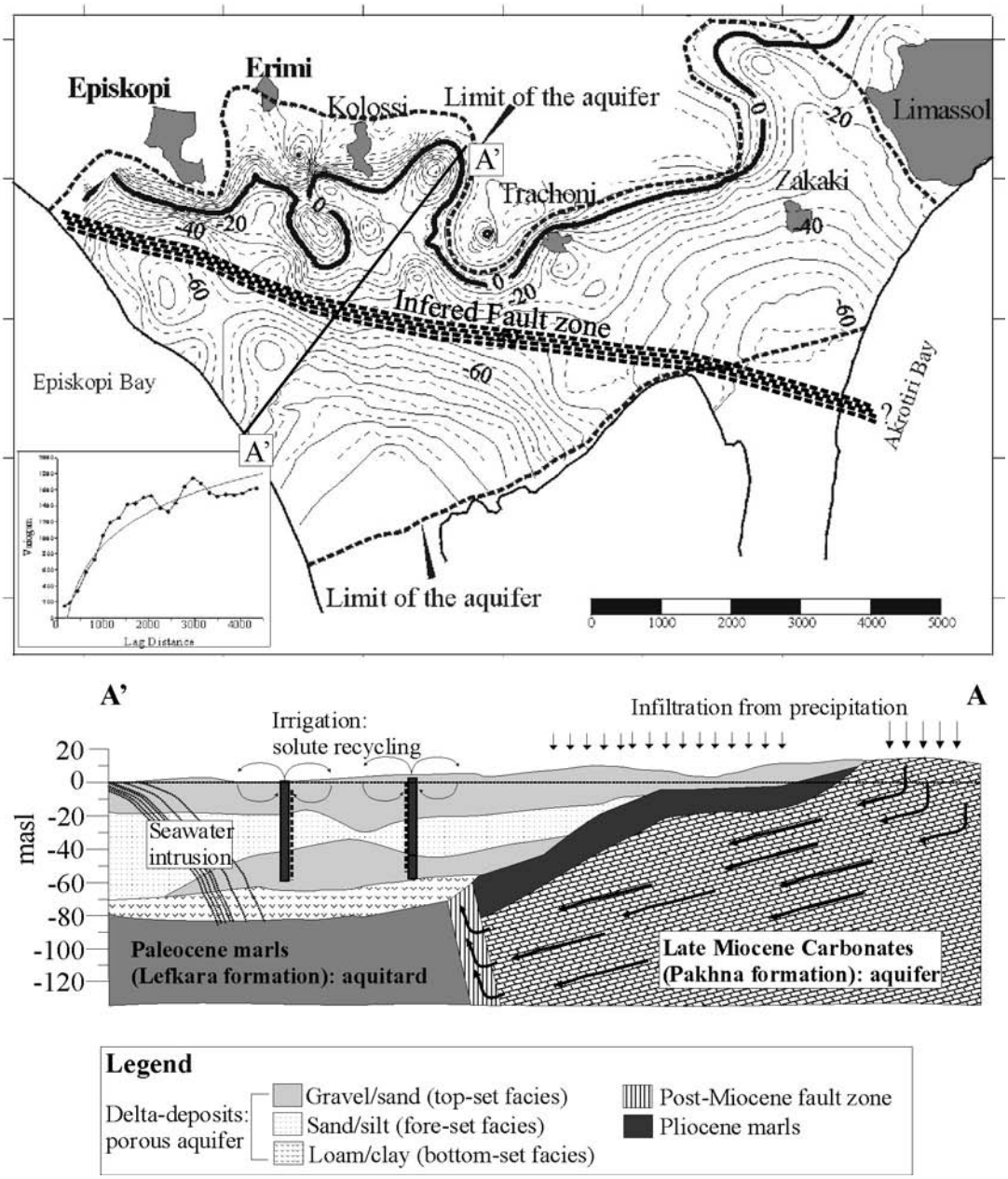

Fig. 6.4: Bedrock topography and conceptual model of the Akrotiri aquifer as derived from borelog information and general hydrogeological investigations. The inferred large-scale fault zone is indicated, recharging the porous aquifer from below.

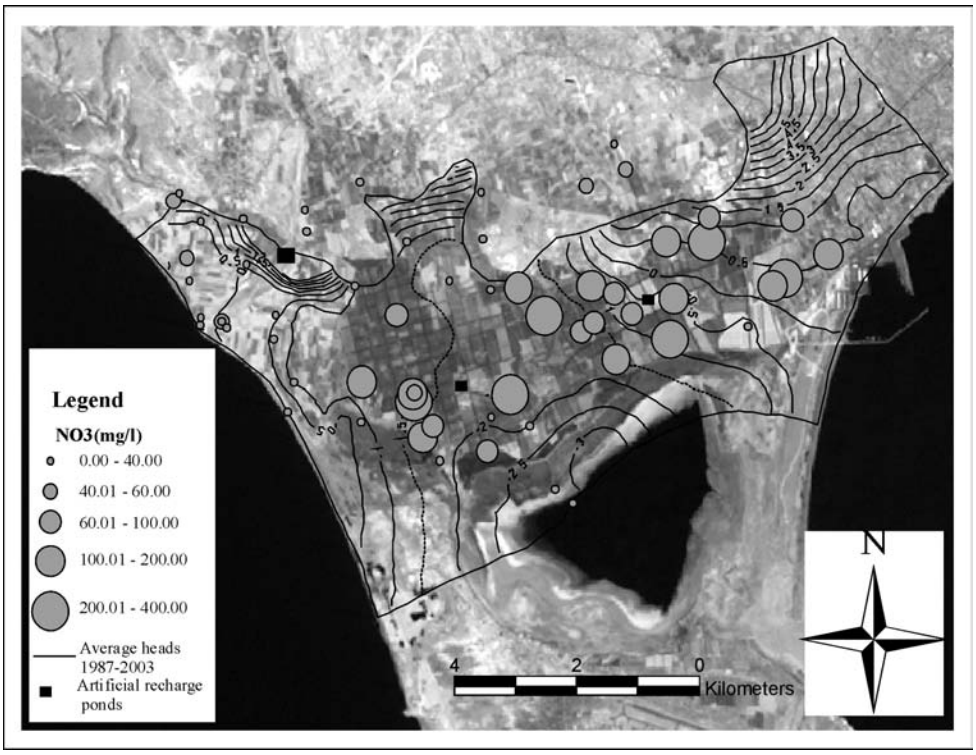

Fig. 6.5: Average water table between 1987-2003, together with the nitrate concentrations measured in 2003 (Meilhac 2003). Artificial recharge pond locations are indicated and their size is approximately proportional to recharge. Intensively irrigated citrus plantations can be seen as a chequered pattern in the central area.

6.2.3 Spatial distribution of dominant salinisation processes

Vengosh and Rosenthal (1994) and Custodio (1997) list several possible salinity sources which are not directly related to seawater intrusion but which are often superimposed in coastal areas. Such sources include pollution from anthropogenic activity, such as solute return flow from irrigation (Vengosh & Rosenthal 1994) and pollution from sea-spray, dissolution of evaporitic deposits or contamination by fossil seawater or ancient saline groundwater (Sukhija et al. 1996, Vengosh et al. 1999).

A hydrochemical investigation was carried out in the Akrotiri aquifer with the aim of identifying different salinisation processes (Meilhac 2003). The study included the analysis of major ions, trace elements, stable isotopes (oxygen, hydrogen and sulphur) and radioisotopes (uranium and radon). Fig. 6.6 shows the spatial distribution of the three main salinisation processes identified in the course of that work. Salinisation by seawater intrusion was clearly identified in the western part of the aquifer, whereas the salinity in the southern part, close to the salt lake, is dominated by evaporative processes, related to the presence of the salt lake and direct evaporation from the shallow groundwater. In contrast, the hydrochemical signatures of the groundwater in the entire

central area indicated that agricultural impact (i.e. solute return flow and recycling from irrigation and agrochemical additives) are dominant. More detailed information on the parameters Meilhac (2003) used to distinguish between the different processes is given in Appendix 2.

As part of the field investigation program, two monitoring wells were installed in areas where irrigation salinity was suspected to be completely or partially responsible for the local salinisation of the aquifer. The monitoring positions were chosen in two different hydrogeological environments, the Phasouri site being closer to the sea and the Lanitis site being located further inland, north of the salt lake (Fig. 6.6). High-resolution electrical resistivity tomography (ERT) profiles were run at the beginning of the monitoring period, to map the soil salinity around the monitoring holes (Yeo 2003). These results were compared with the vertical soil salinity profiles measured on extracted saturated soil paste from soil samples retrieved during the drilling of the monitoring wells. The first monitoring site, the Phasouri site, revealed high soil salinities and relatively homogeneous subsurface conditions, based on geophysical resistivity profiles, while the surroundings of the second site, the Lanitis site, was characterised by a high degree of heterogeneity (see Appendix 3).

Groundwater salinity, temperature and water table as well as irrigation water salinity were measured during 9 months in the two monitoring wells, between July 2003 and April 2004. A prominent groundwater salinity response was observed at the Phasouri site and was interpreted as being directly related to a seasonally varying leaching fraction and thus to irrigation. The combined effect of irrigation rates and plant water uptake is believed to have caused concentration of solutes in the root zone in the early irrigation season and subsequent flushing at the end of the irrigation season, prior to the onset of rainfall. None of the data suggested that the prominent seasonal variations recorded in the shallow groundwater were related to the dynamics of the seawater/freshwater front. A detailed field test description of the two monitoring sites, results and numerical experiments are presented in Appendix 3.

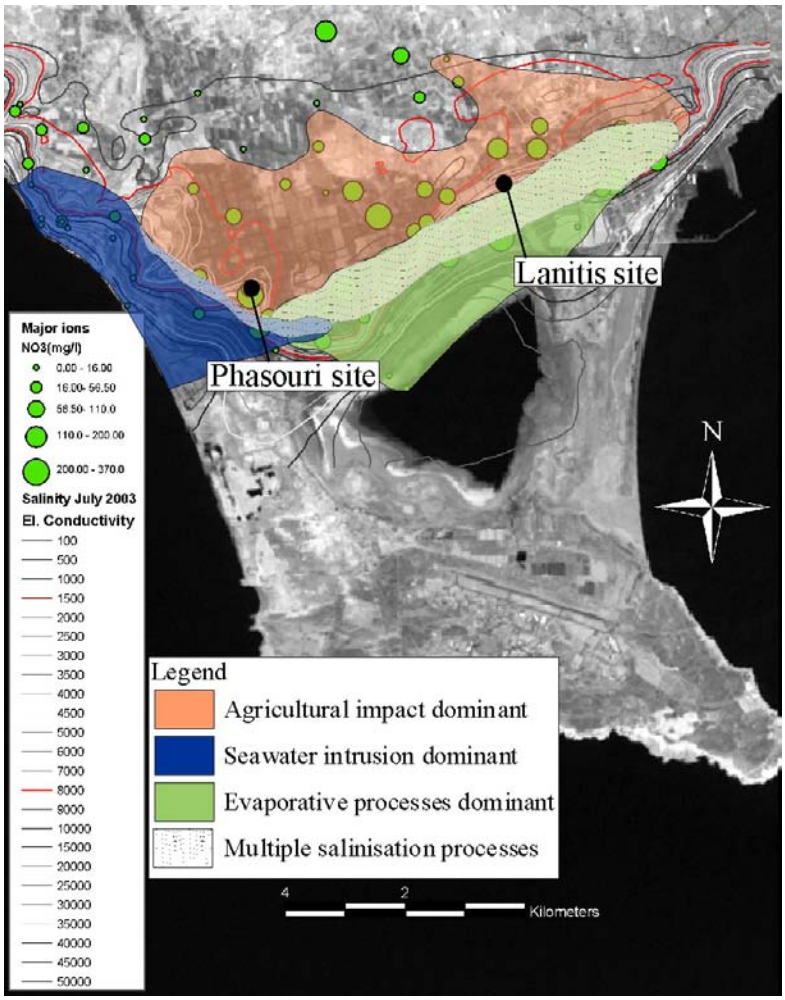

Fig. 6.6: Schematic map of spatial distribution of dominant salinisation sources (modified after Meilhac 2003). The stippled zone indicates the areas where different salinisation processes are superimposed (seawater intrusion, agricultural salinisation and evaporative processes). Monitoring sites are indicated with black circles.

6.3 3-D finite element model description

The hydrogeological information from the Akrotiri aquifer was used to elaborated a 3-D finite element model within the framework of the Master thesis by Milnes (2000). The new data collected in the 2003-2004 field campaigns did not cause the main features of the aquifer model to be modified. In the following, therefore, the same model will be used to illustrate the salinisation risk assessment methodology, established in Chapter 5. All simulations were run with a 3-D finite element code developed at CHYN (Cornaton 2004), which was extended to allow solute recycling in a time stepping procedure (see Appendix 1). In contrast to the 2-D implementation, which has been thoroughly tested, the verification stage of the 3-D implementation is at present not yet

finalised. Nevertheless, the 3-D version was used to run transient simulations to obtain the 'present state', with which the salinisation risk assessment procedure can be illustrated.

Another problem is that the density dependency which was implemented in the code has not yet been tested or benchmarked, and because of this the simulations were run without density-dependency. With all these weaknesses in mind, the model was calibrated on the basis of the average hydraulic condition between 1987-2003. However, historical salinity data were also lacking and the distribution patterns of the irrigation wells were unknown. These deficiencies did not allow the calibration of the transport parameters and no sensitivity analyses could be carried out. For all these reasons, the simulation results have to be considered 'hypothetical'. With this model, however, the methodology can be illustrated using a complicated natural system, and the results clearly reveal which data are essential for a quantitative salinisation risk assessment. Nevertheless, the obtained risk index distributions can be compared qualitatively with the large-scale spatial distribution of the dominant salinisation processes, identified by means of hydrochemical fingerprints (Fig. 6.6).

6.3.1 Model delimitation and internal geometry

The inland limit of the finite element model was defined by the presence of a saturated thickness of the porous aquifer. On each side, the model was extended offshore using a bathymetric map for the seafloor geometry and was cut at a depth of -50 masl. In the south, the model limit was drawn along the northern boundary of the salt lake (Figs. 6.7 and 6.8).

The internal model geometry was based on approx. 200 borehole logs, using a sedimentary facies concept derived from models of multiple delta-fan depositional environments (Reading 1986, Visher 1990). The lithofacies encountered in the borelogs were assigned to one of the three classic delta facies, which are characterised by different hydraulic properties: (a) the bottom-set facies consisting of fine-grained deposits, overlain by (b) the fore-set facies, consisting of medium-grained deposits and finally (c) the top-set facies with the coarsest-grained deposits (gravels). From the borelog record, the respective facies deposits were then lumped together, which led to a total facies thickness distribution. The three units that were constructed in this way reflect the absolute thicknesses of the respective facies but not any heterogeneity arising from intercalations and no statistical analysis was carried out on the borehole data.

The Pliocene marl deposits, the Miocene carbonate unit and the fault zone were incorporated in the model to accommodate the recharge that had been estimated to transit through the carbonate unit from the northern foothills, recharging the porous aquifer from below (Fig. 6.4). Introducing the fault zone with its large-scale draining effect ameliorated the hydraulic calibration.

Fig. 6.7 shows the subdivision of the 3-D model into the six identified hydrostratigraphic units, which were subsequently used to calibrate the model, each of them with an equivalent hydraulic conductivity.

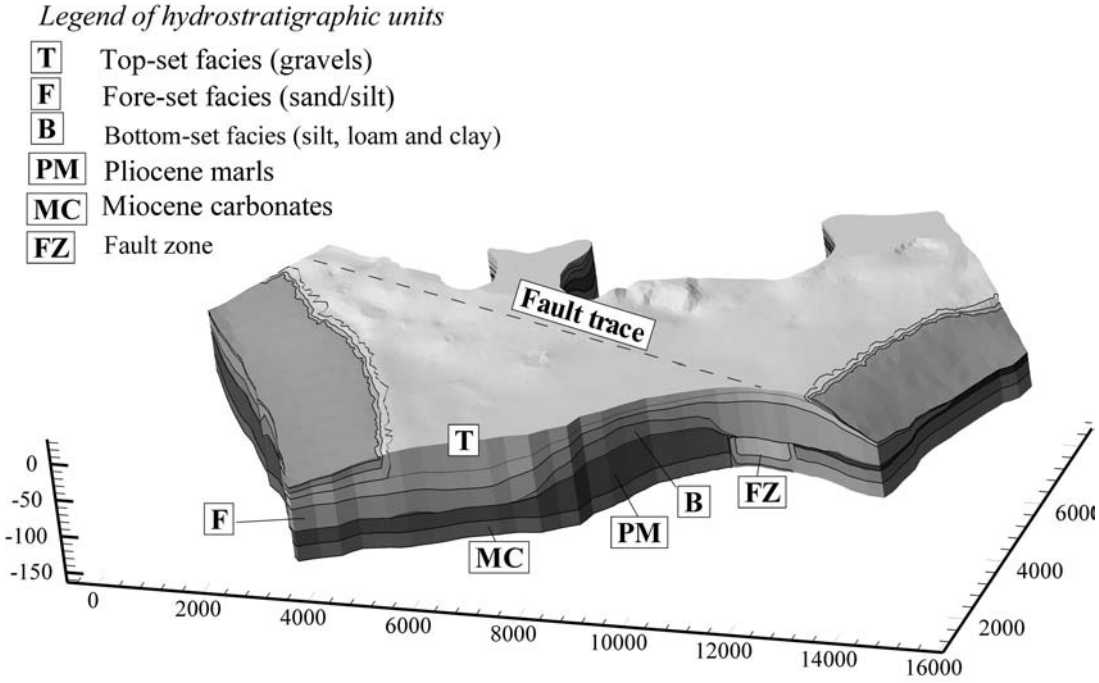

Fig. 6.7: 3-D view of the Akrotiri aquifer model showing the subdivision into six hydrostratigraphic units. The trace of the large-scale fault zone cutting through the Miocene carbonates and Pliocene marls is indicated on the surface. Vertical exaggeration 1:15.

6.3.2 Boundary conditions, model parameters and hydraulic steady state calibration

6.3.2.1 Hydraulic boundary conditions

Dirichlet-type boundary conditions were imposed on the seafloor. Since the simulation was done with freshwater heads, depth-dependent hydraulic heads were assigned on the seafloor, using a density-contrast of 0.025, leading to $H = 0.025^{*}$elevation (below sea level) (Fig. 6.8).

On the surface of the model, outflowing fluxes were imposed on the marshland and along the salt lake boundary to account for the strong evaporation in this area (cf. Fig. 6.1). Inflowing fluxes were imposed along the northern boundary in the carbonate layer and were calculated to correspond to 70% of the average net infiltration on the northern foothills, which drain towards the Akrotiri aquifer.

Well-type boundary conditions were used for the extraction wells. To simplify the solute recycling simulation, the major irrigation wells were retained and the extractions from minor irrigation wells were added to the nearest major irrigation well. Since no information on the distribution pattern of the water from the irrigation wells onto the irrigation surfaces was available, this simplification adds itself to the numerous other assumptions.

Recharge from infiltration was introduced into the model as a fluid source. Average annual infiltration from precipitation in the un-irrigated areas was calculated using the Thorntwaite & Mather (1955) method, applied with an average soil retention of 50 mm. In the irrigated areas, the average fluid flux derived from a 1-D vertical finite element simulation presented in Appendix 3 was used.

6.3.2.2 Transport boundary conditions

Dirichlet-type boundary conditions were imposed on the seafloor with a relative concentration of $C = 1$. Along the northern inflowing boundary (in carbonates), a relative concentration of $C = 0.03$ was used, corresponding roughly to the ratio of total dissolved solids in fresh groundwater relative to seawater.

No transport boundary condition was imposed along the salt lake, which is not appropriate if simulation of the overall degree of salinisation is to be undertaken, since the evaporative processes leading to salt precipitation and very high concentrations around the salt lake are not simulated. Since no reactive transport is simulated with the code, introducing the salt lake as evaporative boundary with a fluid sink leads to infinitely high concentrations when running the steady state simulations, since no solute sink (mineral precipitation) exists. This is a problem which needs to be adressed, but for the present simulations, where focus is placed on the impact of solute recycling, a more adequate treatment of this boundary was not pursued.

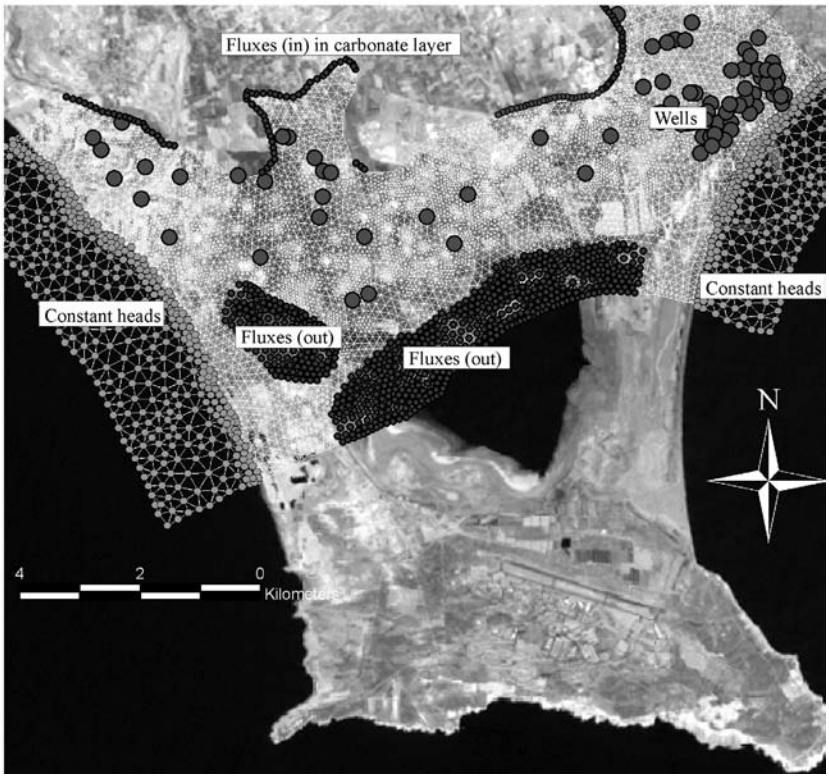

Fig. 6.8: 2-D finite element mesh and projected boundary conditions.

6.3.2.3 Hydraulic parameter distribution

The hydraulic conductivities obtained from original calibration of the model (Milnes 2000) for the three hydrostratigraphic units of the porous aquifer were used at the beginning of the calibration procedure. For the underlying Pliocene marls, a mean thickness of 10 m and a hydraulic conductivity of K_{xyz}=1E-7m/d was assumed, while the lower carbonate unit and the fault zone were then calibrated. The calibrated hydraulic conductivity distribution retained for the further simulations in this Chapter are summarised in Table 6.1.

Hydrostratigraphic unit	**Hydraulic conductivity (m/d)**
Gravels (top-set facies)	4.0 E-4
Sands & silt (fore-set facies)	1.0 E-4
Marls & clays (bottom-set facies)	5.0 E-6
Pliocene marls	1.0 E-7
Miocene carbonates	1) 1.0 E-4 2) 1.0 E-5
Fault zone	5.0 E-4

Table 6.1: Calibrated hydraulic conductivities of the six hydrostratigraphic units. Two values are given for the Miocene carbonates: 1) for the area north of the fault zone and 2) for the area south of the fault zone.

6.3.2.4 Transport parameter distribution

Homogeneous transport parameters were used and no sensitivity analysis was carried out. For the longitudinal dispersivity, an average value of α_L = 130 m was used, roughly corresponding to the element size and a transversal dispersivity of α_T =10 m. A homogeneous porosity of 0.3 was adopted. Particularly for the carbonate unit, this value seems exaggerated. However, the carbonate unit has to be considered as an 'extended' boundary condition, rather than as an unit within which we are interested to simulate transport processes.

6.3.2.5 Hydraulic steady state calibration

Hydraulic calibration was carried out on the basis of the average hydraulic condition between 1987 and 2003. This period was chosen because 1987 brought a prominent change in the hydraulic setting, with the construction of the Kouris dam. Fig. 6.9 shows the simulated hydraulic head distribution in the gravel unit as compared to the average water table between 1987-2003. 120 observation points were used, for which monthly values were available.

Calibration of the hydraulic conductivities was carried out by trial and error, and in the last stage, the infiltration rates in the irrigated and un-irrigated areas were optimised using the Pest-algorithm (Doherty, Watermark Computing) included as a module in FEFLOW (Diersch 2002). During the optimisation procedure, the infiltration values were constrained to remain within the 10% limit of the originally assigned values.

The calibrated hydraulic condition reflects the main features of the average hydraulic situation, being the prominent depression induced by the salt lake, forming the regional discharge area. In the western area, a depression could not be reproduced by the model (square indicated in Fig. 6.9).

Fig. 6.9: Simulated hydraulic head distribution within the gravel unit (thick lines) and measured average water table between 1987-2003 (fine lines). In the western area (square), a prominent depression could not be reproduced during calibration.

6.4 Simulation of salinisation potential: decomposition into recycling potential (RP) and seawater intrusion potential (SIP)

Using the 3-D aquifer model with the above bondary conditions, simulation of the salinisation potential was carried out according to the procedures explained in Chapter 5 (Section 5.2.1). Since the presented model is only an approximate representation of the Akrotiri aquifer, and since no information is available on the redistribution of extracted water on fields, we further simplified the problem by defining the entire irrigated area as one single irrigation plot. According to Chapter 4, the spatial variation of the irrigation plots relative to the extraction wells may significantly influence the salinisation pattern (cf. Fig. 4.4). However, reducing the entire irrigated area to one single irrigation plot may be justified by the fact that many extraction wells at Akrotiri are connected to a vast irrigation network, within which mixing of the extracted water will take place. However, we do not know whether several independent networks exist and how they are interconnected with the extraction wells. The ‘recycling source’, as described by Eq. (4.13), was then obtained by evaluating the average capture probability of each well with respect to the irrigation plot and the lateral solute mass flux captured by the wells from the boundaries. Fig. 6.10

shows the overall salinisation potential obtained from the steady state simulation using this 'recycling source'. It shows a significant advance of the seafront in the west, as well as high salinities in the central irrigated zone.

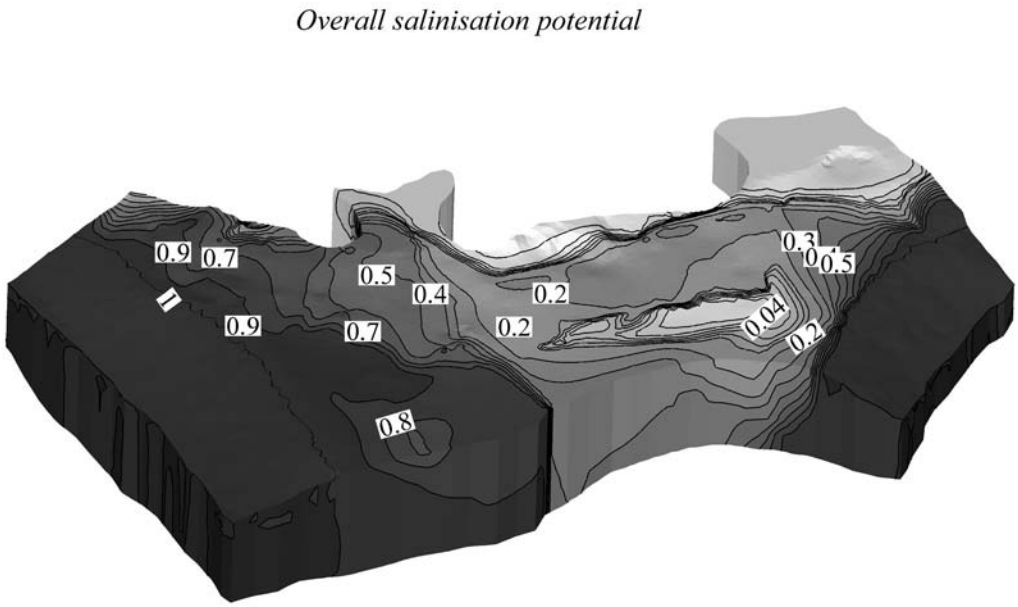

Fig. 6.10: Relative concentration distribution representing the overall salinisation potential for the average exploitation scheme between 1987-2003 with reference seawater concentration C= 1.

The overall salinisation potential was then decomposed into the RP and SIP, according to Section 5.2.1. Fig. 6.11 shows the solute recycling potential RP and Fig. 6.12 the seawater intrusion potential SIP. The RP reveals salinities up to 0.2 times the seawater salinity in the central area, where irrigation takes place. The SIP, on the other hand, shows no salinity in the central area but prominent seawater intrusion in the western area, resulting from the pronounced hydraulic depression in the west.

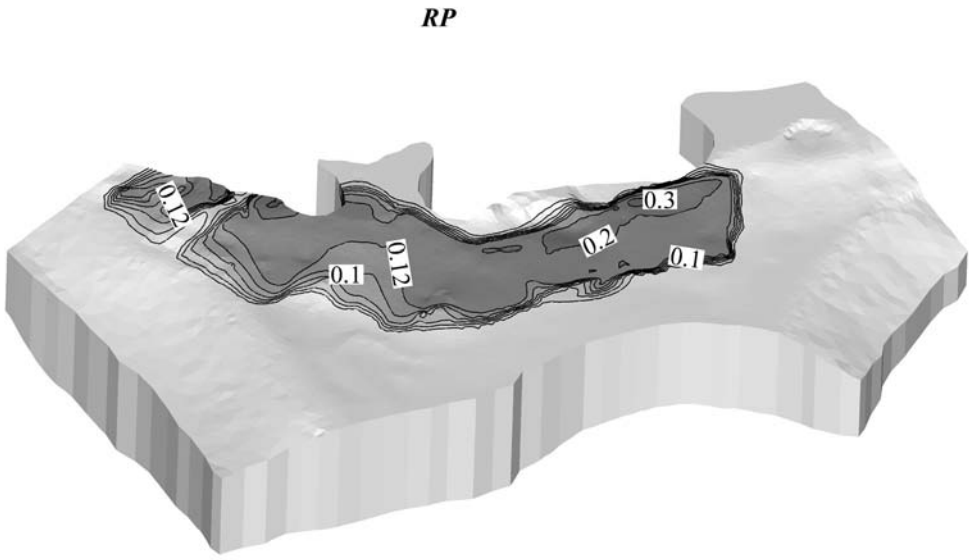

Fig. 6.11: Solute recycling potential RP for the average hydraulic setting 1987-2003. The irrigated area is well delineated.

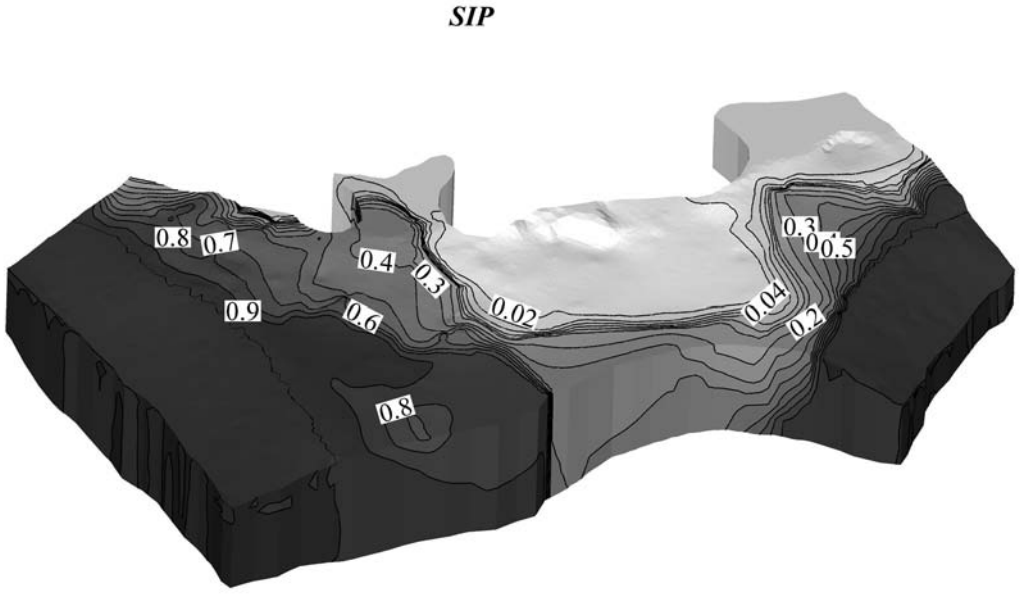

Fig. 6.12: Seawater intrusion potential SIP for the average hydraulic setting 1987-2003.

6.5 Transient simulation with solute recycling: 'Present state'

A transient state simulation with solute recycling was carried out with the time-stepping procedure over twenty years, distributing the cumulated extracted solute mass flux of all irrigation wells homogeneously over the entire irrigation zone (Appendix 1). To obtain an initial distribution of the advancing seafront, a transient simulation was first carried out over 40 years with only half the extraction rate. No information on the extraction rates is available for the time-period prior to 1987. However, we know that aquifer recharge before 1987 was very much governed by the presence of the Kouris River in the western part of the aquifer, inhibiting the formation of a pronounced inland hydraulic depression (cf. Fig. 6.3). Reducing the extraction rates by 50% led to a seaward-directed hydraulic gradient in this zone.

Irrigation has been ongoing in the Akrotiri aquifer since the late 1940's, but the initial concentration distribution we used did not have any initial solute recycling salinisation nor any initial loading from agricultural additives. Fig. 6.13 shows the overall salinity distribution after twenty years of transient transport simulation with solute recycling. The salinity distribution in the central area is entirely caused by solute recycling. The seawater/freshwater front is fairly advanced in the western area.

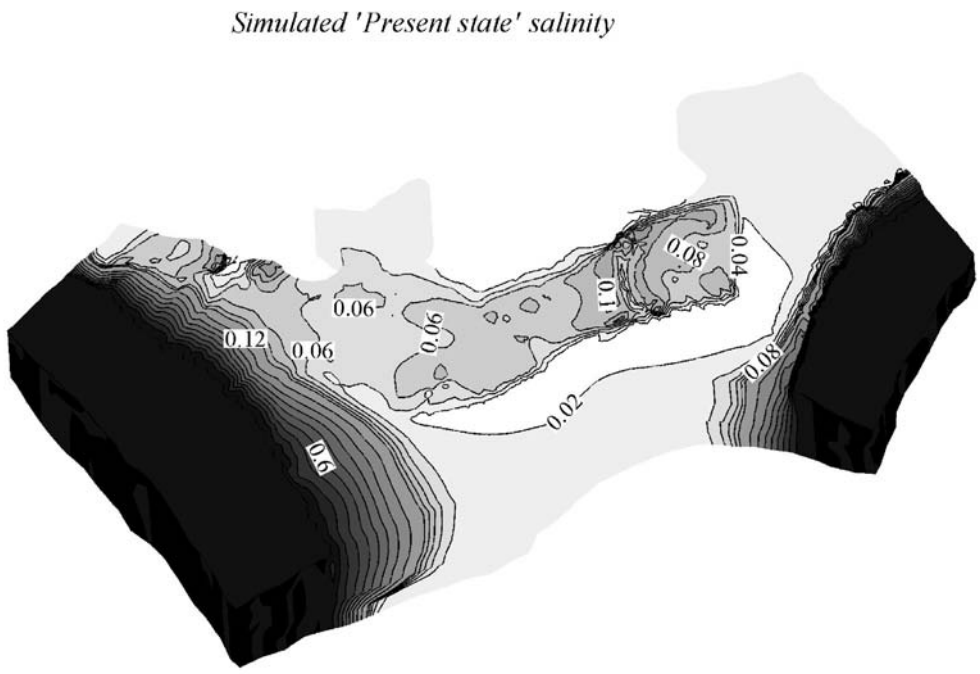

Fig. 6.13: Overall salinity distribution of the 'present state', revealing the formation of high relative salinities in the central irrigated area.

The same transient simulation was carried out without solute recycling, yielding the 'present state' seawater intrusion salinity distribution (see Chapter 5, Section 5.2.2). Fig. 6.14 shows the 'present state' seawater intrusion salinity distribution at Akrotiri, clearly showing the completely unaffected central area. The advancing of the seawater/freshwater front in the western area is similar to the salinity distribution measured in 2000 (cf. Fig. 6.2). Apart from the neglect of density-dependent flow and transport, this simulation corresponds to the 'classical seawater intrusion simulation approach', which does not account for solute recycling.

The solute recycling 'present state' salinity distribution, shown in Fig. 6.15, was obtained by subtracting the 'present state' seawater intrusion salinity distribution (Fig. 6.14) from the overall 'present state' salinity distribution (Fig. 6.13). The salinity distribution that develops in response to solute recycling forms a heterogeneous pattern with the highest salinities located in the central area, where the highly permeable top-set facies deposits (gravels) are almost absent (cf. Fig. 6.7). This is also the area in which the nitrate concentrations are highest (cf. Fig. 6.4).

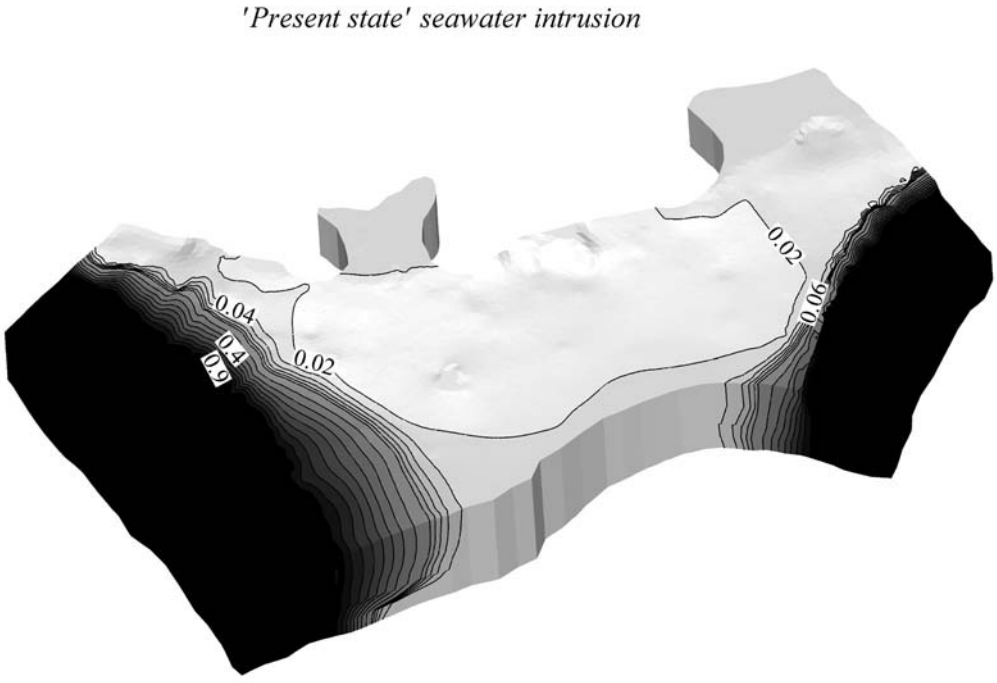

Fig. 6.14: 'Present state' seawater intrusion salinity distribution, revealing a completely unaffected central area.

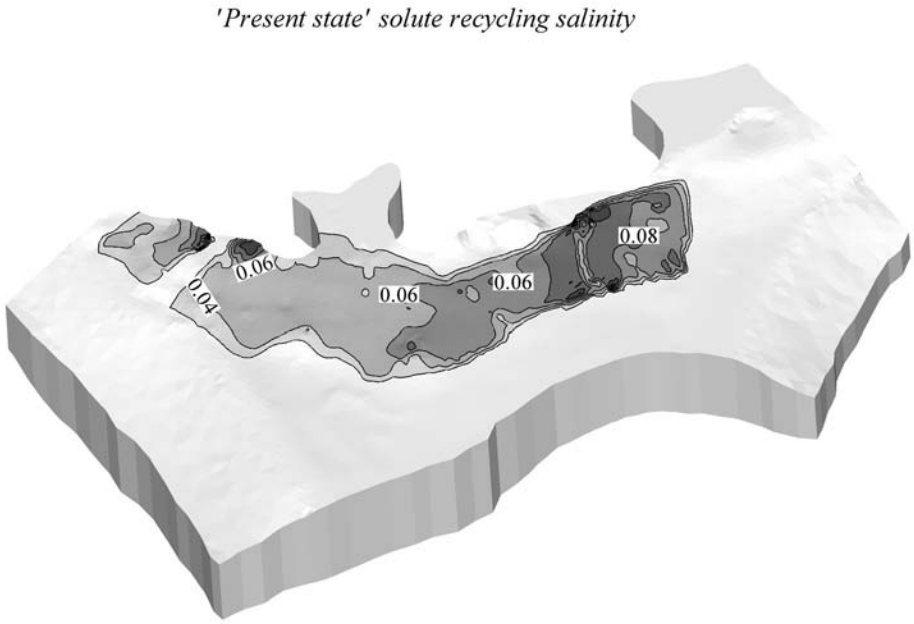

Fig. 6.15: 'Present state' solute recycling salinity distribution, outlining the irrigated area with the highest salinities forming in the central Lanitis area, where highly permeable deposits (gravels) are almost absent (Fig. 6.7).

6.6 Salinisation risk index mapping

To obtain the overall salinisation, the seawater intrusion salinisation, and the solute recycling salinisation risk index distributions with respect to the average exploitation scheme between 1987-2003, use was made of the respective salinisation potential maps (Figs. 6.10-6.12) and 'present state' salinity distribution maps (Figs. 6.13-15). According to the salinisation risk index defined in Eq. (5.5), the difference between the respective 'present state' and salinisation potential is normalised by the overall salinisation potential to obtain the respective salinisation risk indices. To evaluate the salinisation risk, the salinisation risk indices are superimposed onto the 'present state' salinities.

Fig. 6.16 shows the overall salinisation risk index distribution for the average exploitation scheme (i.e. average hydraulic setting) between 1987-2003. A very prominent strip of high risk index values can be seen ahead of the 'present state' advancing seawater/freshwater front. In the area of the salt lake, the risk indices should be disregarded, since that boundary condition is not adequately treated in the model. In the central irrigated area, salinisation risk index values as high as 0.8 are found. Low risk index zones can be seen along the shorelines, indicating that seawater intrusion has already reached an advanced stage, approaching its steady state.

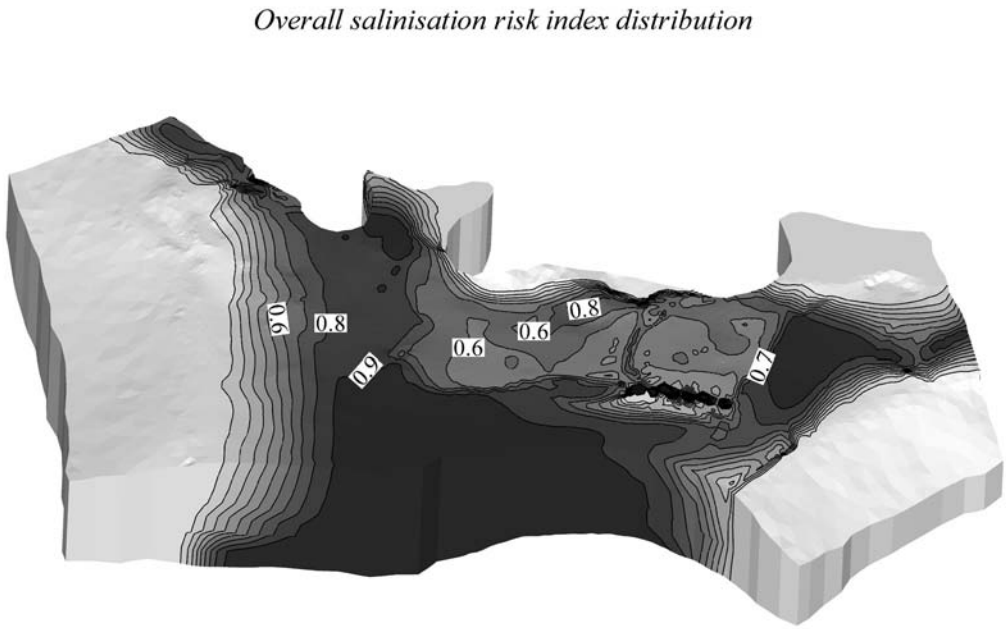

Fig. 6.16: Overall salinisation risk index distribution for the average exploitation scheme between 1987-2003.

Treating the salinisation processes separately, we obtain individual risk index distribution maps, Fig. 6.17 for seawater intrusion and Fig. 6.18 for solute recycling.

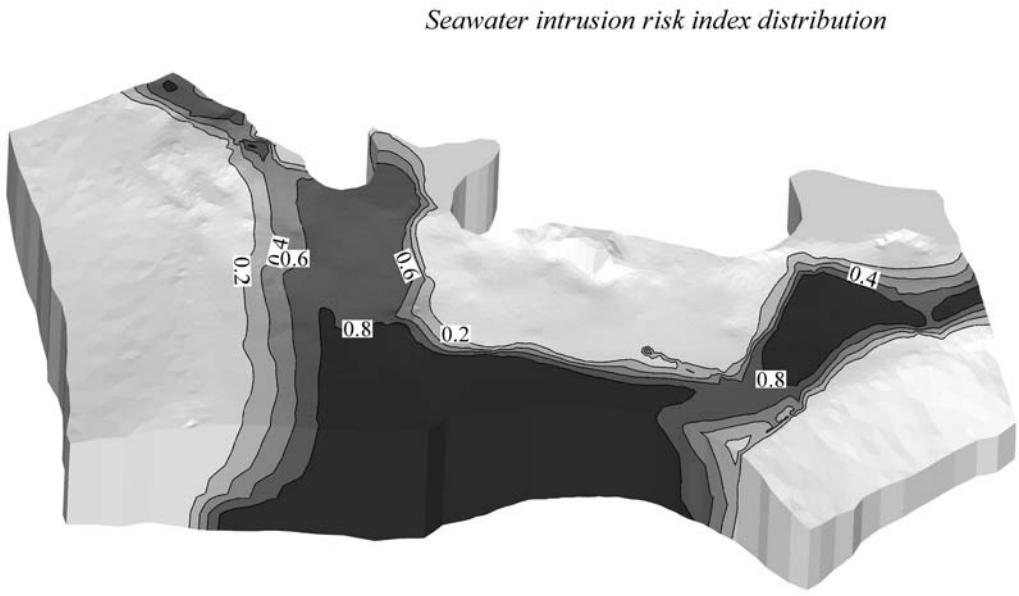

Fig. 6.17: Seawater intrusion risk index distribution, being most pronounced ahead of the 'present state' advancing seawater front.

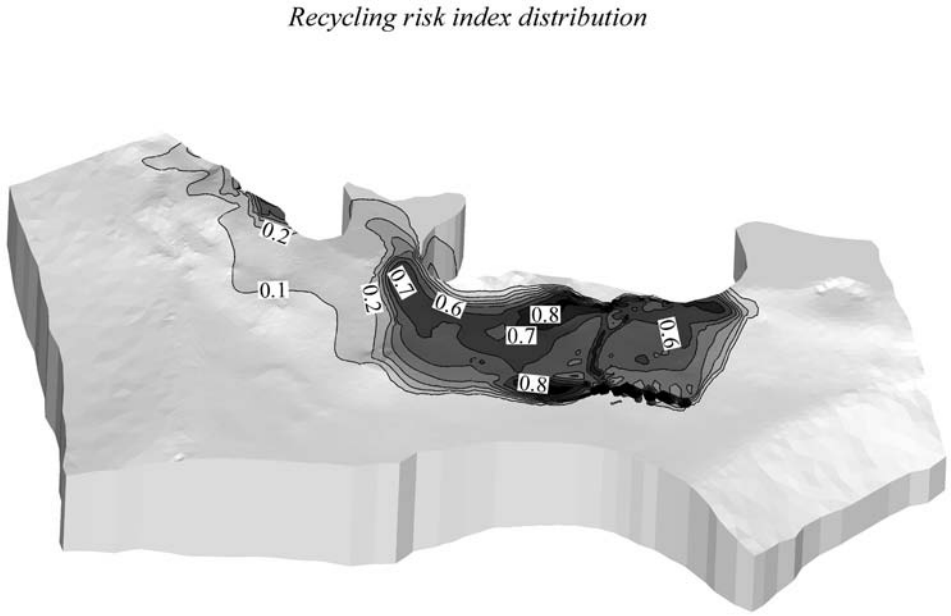

Fig. 6.18: Solute recycling risk index distribution, being most pronounced in the area of the Lanitis farm, where the highly permeable gravel unit is almost absent.

The seawater intrusion risk indices (Fig. 6.17) can be seen to be very low along the coastline and in the central area. Along the coastline, as indicated above, the seawater intrusion risk indices are low because water quality degradation has already reached a maximum, whereas in the central area, they are low because groundwater degradation will never be affected by seawater intrusion. Fig. 6.18 shows that the entire central area is prone to solute recycling, reaching risk index values up to 0.8.

By superimposing the salinisation risk indices onto the 'present state' salinisation, high-risk areas can be delimited. Fig. 6.19 and Fig. 6.20 show the areas identified as high-risk zones, obtained by combining the salinisation risk indices with the 'present state' salinity distributions. In this example, we were interested in identifying areas with concentrations higher than the threshold concentration C = 0.06, corresponding to twice the salinity of the fresh groundwater having a respective salinisation risk index of 0.5 or more. These values are chosen arbitrarily, but if threshold values were known, for instance for crop tolerance or yield reduction, these values could be chosen as threshold values against which the risk indices could be compared. The black areas indicate the respective zones with a salinisation risk index higher than 0.5, and the white dashed lines show the 'present state' threshold concentration iso-contours of C = 0.06. We then extracted the areas with concentrations above to the threshold concentration and salinisation risk indices higher than 0.5.

Fig. 6.21 shows the projection of these areas onto the map with the spatial distribution of the dominant salinisation processes as derived from the hydrochemical investigation (Meilhac 2003). The central area shows the highest risk for solute recycling, whereas the area ahead of the seawater intrusion in the west has the highes seawater intrusion risk. The high solute recycling risk coincides well with the area where the nitrate concentrations are highest (cf. Fig. 6.5). However, in this example, the simplifications we made to obtain the risk index distributions as well as the 'present state' salinity distribution were numerous, so that a comparison with the field data cannot be more than just indicative. According to this risk assessment, the monitoring site Phasouri (cf Fig. 6.6) is running risk of eventually being dominated by seawater intrusion, with salinities exceeding the defined threshold concentration, although during the transient salinisation stage, solute recycling will be dominant until the seawater/freshwater front eventually arrives. For the Lanitis site (cf. Fig. 6.6), however, the risk related to seawater intrusion is negligible, whereas the solute recycling risk is, and will continue to be, high.

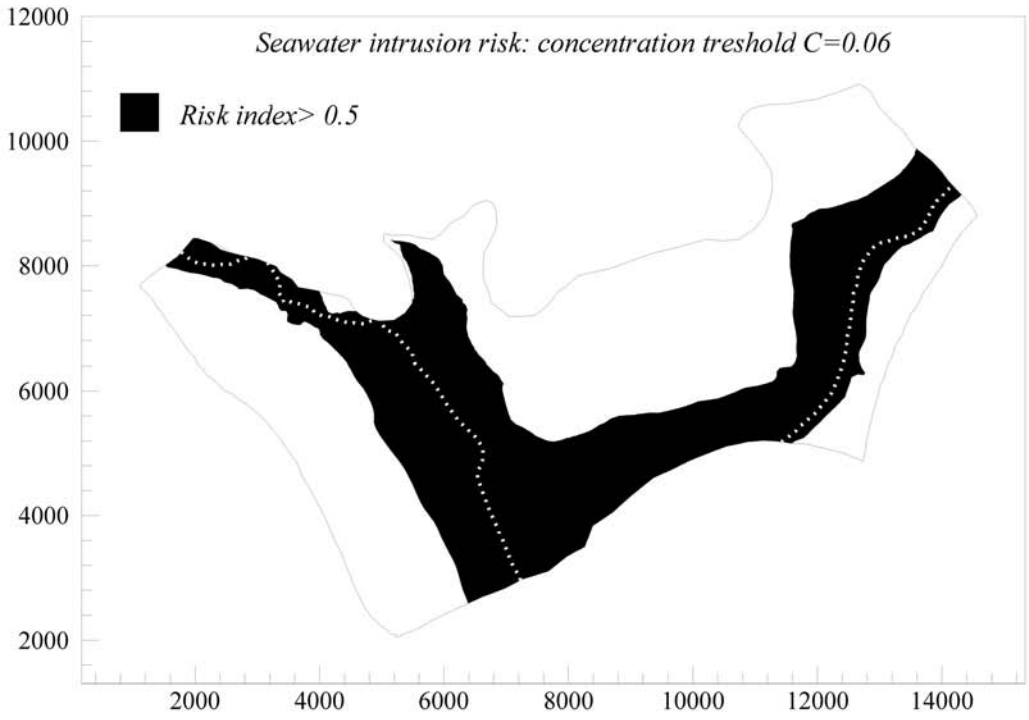

Fig. 6.19: Delimitation of high-risk areas with respect to seawater intrusion in superficial groundwater, Akrotiri aquifer: black area corresponds to a seawater intrusion risk index > 0.5. White dashed line: 'present state' seawater intrusion salinity iso-contour $C = 0.06$.

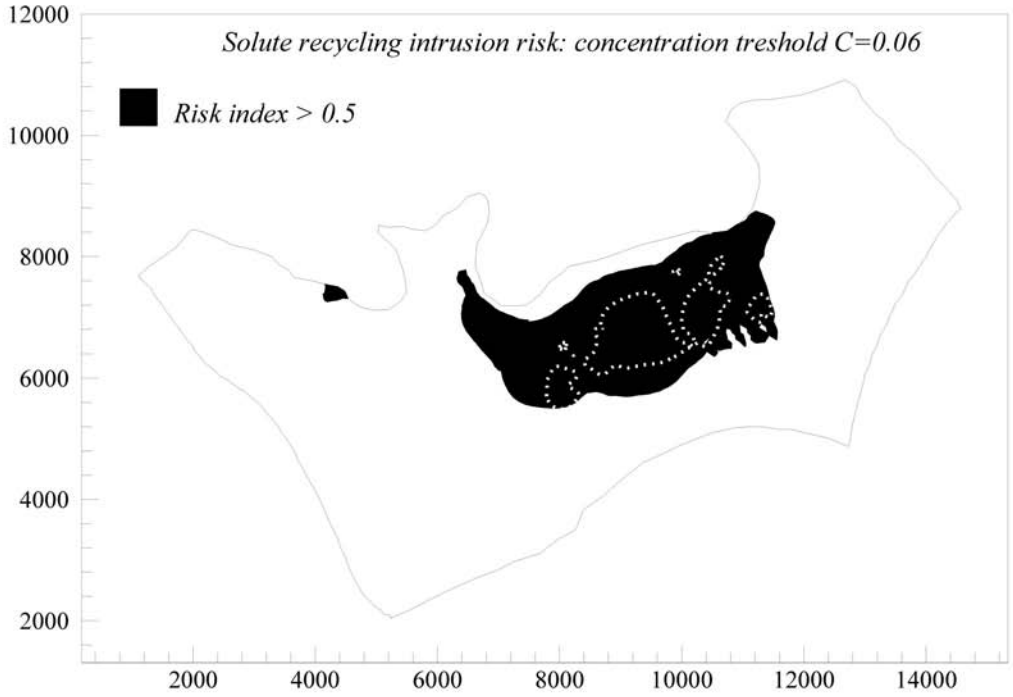

Fig. 6.20: Delimitation of high-risk areas with respect to solute recycling in superficial groundwater, Akrotiri aquifer: black area corresponds to a seawater intrusion risk index > 0.5. White dashed line: 'present state' seawater intrusion salinity iso-contour $C = 0.06$.

If the uncertainty of the simulation results could be estimated for this example, the presented risk assessment shown on the example of the Akrotiri aquifer could be a means to identify the areas prone to either salinisation process. The map shown in Fig. 6.21 would then be useful, as a first step, to identify areas where monitoring should be intensified.

If the model calibration is judged to be satisfactory, then a map as the one shown in Fig. 6.21 could be used to determine potential remedial or preventive measures. In the presented example, this could, for instance, imply that in the central area the effects of solute recycling should be minimised by applying the freshest possible irrigation water, i.e. applying water from the dams instead of mixing it with extracted groundwater. Another implication would be that in the Phasouri area measures should be taken to minimise the prominent hydraulic depression.

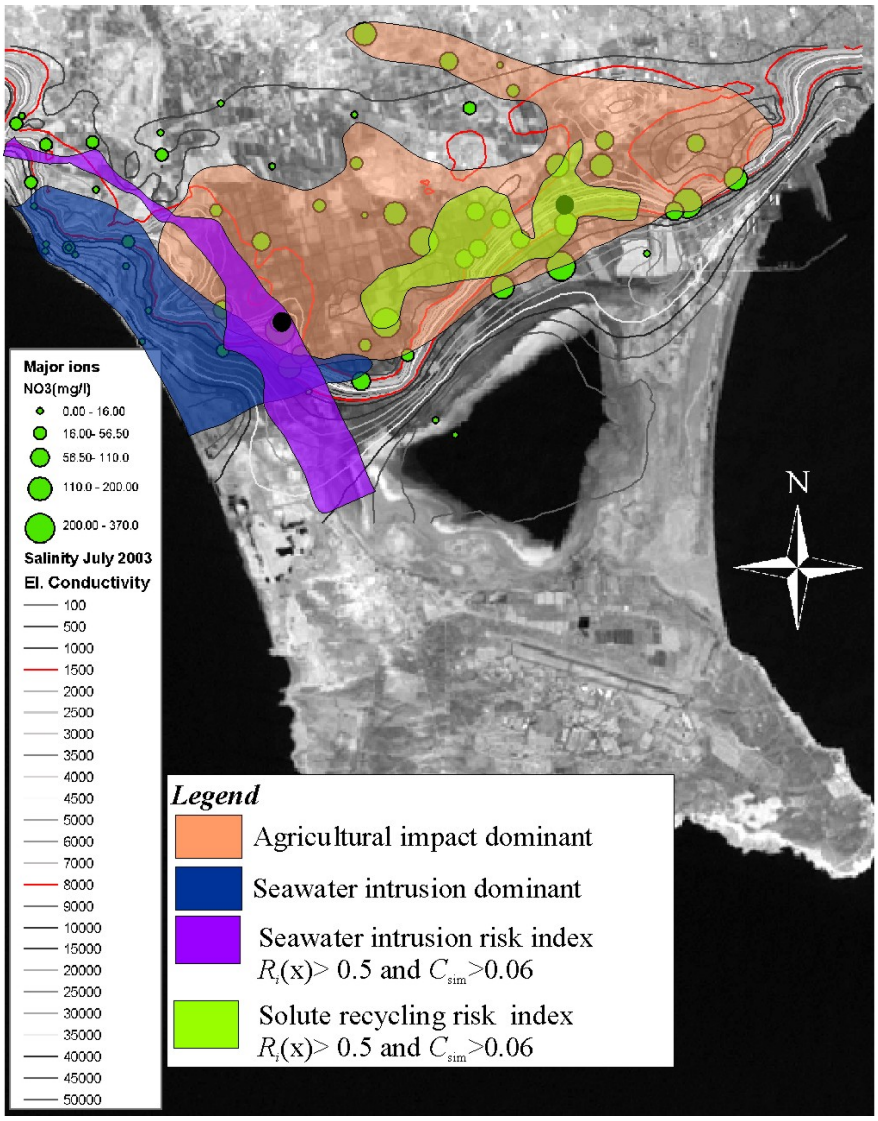

Fig. 6.21: Distribution of hydrochemical fingerprints indicating areas dominated by agricultural activity and seawater intrusion as well as nitrate concentration (green dots) and electrical conductivity distribution. Seawater intrusion risk index >0.5 and relative simulated 'present state' concentrations C_{sim}> 0.06 indicated in violet and solute recycling risk index >0.5 and relative simulated 'present state' concentrations C_{sim} > 0.06 indicated in green.

6.7 Data requirements

As already mentioned earlier, considerable discrepancy between data available to estimate the uncertainty related to the seawater intrusion as opposed to solute recycling arises from the fact that the monitoring of salinisation in coastal aquifers mostly concentrates on the problem of seawater intrusion (e.g. Custodio 1997). Hence, it is important to identify the essential information required

to increase the applicability of the presented quantitative approach, in which solute recycling simulation is an integral part.

Assuming a 'perfect' model, the most essential information for solute recycling simulations is the **distribution pattern** of the extraction wells onto irrigation surfaces. In Chapter 4, Section 4.3.1, we illustrated the importance of the spatial position of irrigation plots with respect to the extraction wells. The hypothetical example of irrigation plot location optimisation, shown in Fig. 4.4, illustrates the importance of the irrigation plot location relative to the extraction well. The outcome of the salinisation risk assessment for different distribution patterns may be entirely different. This also applies to the present example, where the simulations were run assuming homogeneous redistribution on the entire irrigated surface. Although we were specifically investigating the impact of solute recycling in the Akrotiri aquifer, we were not conscious of the importance of this information at the time, and we failed to retrieve the data during the field investigations. However, in the Akrotiri aquifer, this information is sure to exist.

A second important parameter for solute recycling simulations is the solute mass input from agriculture. Since areas far from the sea, such as the central area of the Akrotiri aquifer, only capture water from infiltration and fresh groundwater, the agricultural input may significantly enhance the solute recycling process. Neglecting this input can lead to an underestimation of the potential impact.

For all seawater and solute recycling simulations, reliable piezometric data is a fundamental data requirement. The head distribution will govern seawater intrusion as well as the capture probability fields of the irrigations wells, which will influence the solute recycling process. In many coastal areas, piezometric levels are monitored but equally often the problem of exact levelling will diminish the data reliability. Therefore, exact surveying is indispensable: hydraulic gradients are often small and the mean sea level will have great influence on the dynamics in the system. When wells have not been surveyed for a long time-period, during which exploitation has led to significant decrease in water levels, land subsidence is a common phenomenon, and this may significanty falsify the elevations of the previously surveyed wells (e.g. Chi & Reilinger 1984, Larson et a. 2001, Stiros 2001)**.**

Table 6.2 gives an overview of the data requirements for a numerical model in general and the data requirements specific to seawater intrusion and solute recycling respectively, based on the experience gained from the present work.

<table>
<tr><td colspan="2">General data requirements for a numerical flow and transport models of coastal aquifers</td></tr>
<tr><td colspan="2">Aquifer geometry and parameter distributions (hydraulic and transport)</td></tr>
<tr><td colspan="2">Boundary conditions (identification of all components contributing to the water balance)</td></tr>
<tr><td colspan="2">Piezometric and salinitiy evolutions</td></tr>
<tr><td>Data requirements specific or essential to seawater intrusion</td><td>Data requirements specific or essential for solute recycling</td></tr>
<tr><td>Exploitation history (component in boundary conditions)</td><td>Exploitation history with distribution patterns onto irrigated surfaces</td></tr>
<tr><td>Piezometric evolution</td><td>Solute input other than from seawater intrusion (agricultural additives)</td></tr>
<tr><td rowspan="2">Salinity monitoring in space and time along the seawater freshwater interface</td><td>Long term monitoring of salinity evolution in irrigated areas and chemical analysis</td></tr>
<tr><td>Irrigation requirements/effective infiltration rates (soil properties)</td></tr>
</table>

Table 6.2: Summary of the data requirements for the elaboration of a numerical model with specific requirements for seawater intrusion and solute recycling models. In bold are the data requirements for solute recycling which are the most essential.

Nevertheless, it will be equally important to obtain data related to the different salinisation processes to cross-validate and calibrate a model. We will therefore attempt, in the next section, to combine the understanding we have gained from the theoretical description of the solute recycling process with the classical hydrogeological data to roughly estimate which areas are prone to solute recycling. This would be a means of developing appropriate monitoring programmes, which would then yield the necessary data for a quantitative approach.

6.8 Estimation of the spatial impact of solute recycling based on a field hydrogeological approach

For many problems that hydrogeologists are asked to solve, there will not be sufficient resources to establish a numerical model with which to address a specific question. Therefore, simple field approaches are required to estimate the potential impact of different processes by means of key-

factors related to a given process. This is the main principle of most empirical groundwater vulnerability mapping procedures, such as DRASTIC (Aller et al. 1985).

With respect to solute recycling, the main key-factors identified in the theoretical development of the process which will govern the well solute mass response to solute recycling, described in Chapters 3 and 4, are the following:

- The average capture probability field of the irrigation wells (according to Eq. 3.35)
- The solute mass flux captured by the well from the limits (according to Eq. 3.35)
- The average recycling time, which is a measure for the speed of the solute recycling process (according to Eq. 3.30)

Combining information from 'classical' hydrogeological data, such as piezometric levels, salinity distributions, aquifer thickness, extraction rates and other aquifer parameters to obtain indications on the spatial importance of these key-factors can be a starting point for a qualitative estimation of areas prone to solute recycling salinisation. A step-by-step design of monitoring networks can then be envisaged, eventually the yielding data required for a quantitative approach.

***Estimation of the average capture probability field of the irrigation wells*:**

Areas where this key-factor will be important are detected by:

- Identifying areas with pronounced piezometric depressions below irrigated zones.
- Identifying regional flow field direction and combine it with the distribution of irrigation wells to detect vulnerable down-stream areas.

***Estimation of the solute mass flux captured by the well from the limit*:**

Areas where this key-factor will be important are detected by:

- Identifying areas with major extraction rates and combining them with the salinity data (e.g also distance to sea)

Estimation of the average recycling time, indicating 'speed' of solute recycling salinisation:

Areas where this key-factor will be important are detected by:

- Aquifer thickness, extraction rates and parameters to estimate sub-drainage basin turnover time.

- Nitrate concentrations to estimate relative fraction in extraction rate derived from infiltration on irrigated surfaces.

Fig. 6.23 shows a compilation of the above-described hydrogeological information for the Akrotiri aquifer, which indicates localised areas, where solute recycling is believed to be important and where implementation of monitoring would be advisable.

With respect to seawater intrusion (shown as the blue square in Fig. 6.23), the piezometric depression connected to the sea in a highly permeable zone can be delimited. In reality this is the area which is carefully surveyed with respect to seawater intrusion, with a dozen slotted piezometers through the entire aquifer, allowing vertical salinity logging and detection of the seawater freshwater interface.

With respect to solute recycling, two areas can be delimited, where solute recycling may be an important salinisation source, based on the above described criteria. The two areas were, however, delimited for slightly different reasons.

Zone 1: The yellow area (zone 1) indicated in Fig. 6.23 was delimited due to the presence of the pronounced inland piezometric depression, which will give rise to high mean capture probabilities. The aquifer thickness reaches from 30 meters to almost 100 meters in the south, which suggests long recycling times and important dilution of the recycled solutes. The high extraction rates in that area (approx. 50% of the total aquifer extraction) and the presence of relatively high salinities in the western area, leading to an important solute mass flux captured from the boundaries, make this zone potentially prone to solute recycling.

Zone 2: The yellow area (zone 2) indicated in Fig. 6.23 was delimited for slightly different reasons than zone No. 1. In the central irrigated area, the shallow aquifer thickness (< 30m) and high nitrate concentrations (> 200mg/l) indicate that an important fraction of the extracted water is derived from the irrigated surfaces, which will diminish the recycling time. Also, the relatively high salinities in that area indicate that the captured solute mass flux may be considerable. These factors make this area potentially prone to solute recycling. This area corresponds roughly to the area which was evaluated as a high-risk area with the salinisation risk assessmen (Fig. 6.21).

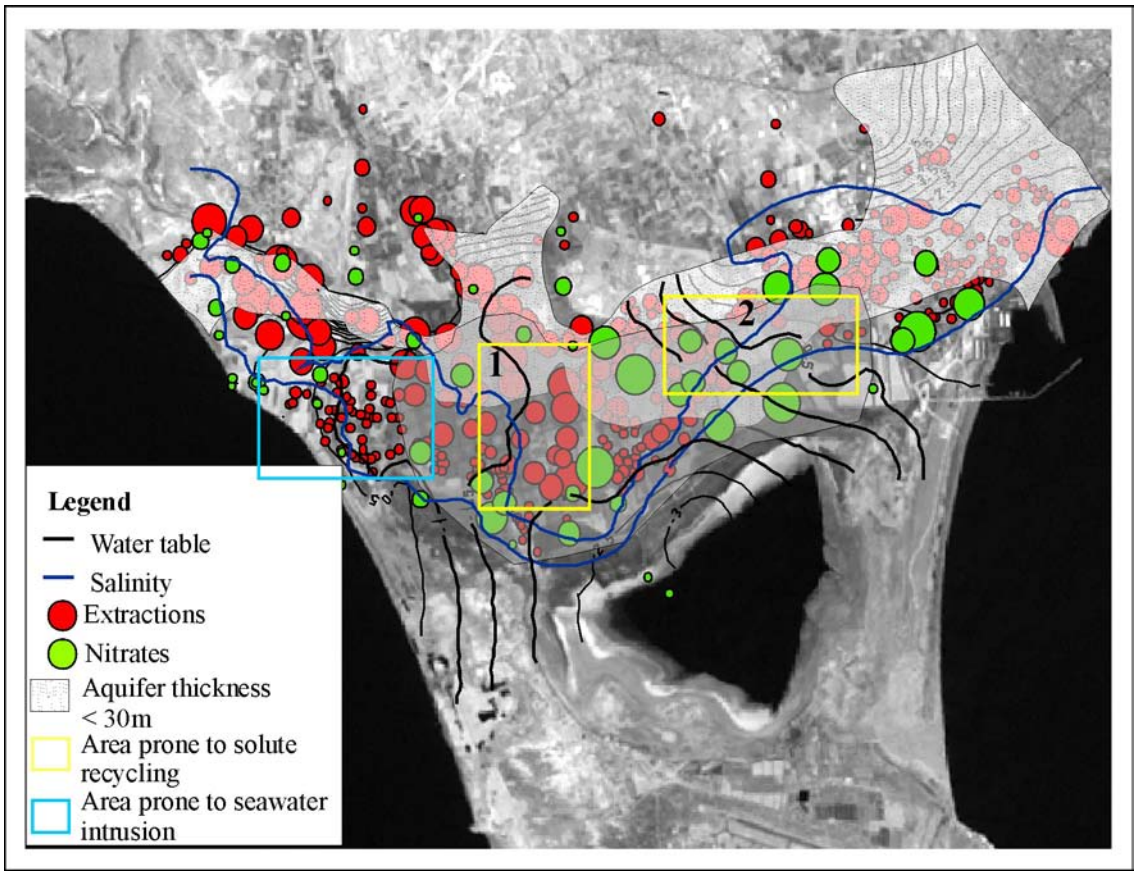

Fig. 6.23: Superposition of 'classical hydrogeological data': average water table (black), two salinity contours (2500 μS/cm and 5000 μS/cm), extractions (red circles, size proportional to extraction rate), nitrate concentrations (green circles, size proportional to concentration). Light grey area indicates where aquifer thickness is smaller than 30 m. Zone prone to seawater intrusion (blue square) and areas potentially prone to solute recycling (yellow squares), delimited on the basis of the key-factors governing the salinisation processes (for explanation, see text) .

Possible monitoring options related to solute recycling should be implemented on a larger scale than seawater intrusion monitoring. Since solute recycling and agricultural inputs are closely related, monitoring of nitrates in a large number of extraction wells should be carried out on a regular basis. Small-scale monitoring, similar to the monitoring wells implemented during the field campaign (see Appendices 3), could yield very useful information on the solute recycling process, but multiple monitoring sites would be required for reasons of representativity.

6.9 Specific recommendations for the Akrotiri aquifer

On the basis of the field investigations carried out in the Akrotiri aquifer, three specific recommendations can be made.

1) The first recommendation is purely technical. Piezometric data is the basis for all hydrogeological investigations. A long-established and extensive monitoring network exists in the Akrotiri aquifer, where water levels are measured on a monthly basis. It is highly recommendable to have the entire network re-surveyed. The investment in man-hours to collect this important data is considerable. However, the fact that the boreholes were surveyed at the time of drilling (between the 1960s and today), that the hydraulic situation has drastically changed in the past 20 years, which may have induced settlement, and that in many wells it is no longer clear where the benchmark is located, suggest that the investment in a new survey of all monitoring wells would enormously increase the value of this most essential data set.

2) The second recommendation is related to the artificial recharge pond located in the Kouris River bed (see Fig. 6.5, the western-most artificial recharge pond). According to the piezometric data available, and the investigations carried out in the course of this work, it seems that the effectiveness of the artificial recharge pond located in the bed of the Kouris River is questionable. The most pronounced piezometric depression and the citrus plantations are located approximately 2 kilometers to the east of this pond. A considerable amount of water is infiltrated there (approximately 2 million m^3/year), and it is believed that most of this water directly flushes down towards the sea in the extremely coarse-grained gravel and boulder material within the river bed, without being of any benefit to the main plantations and the main piezometric depression. To investigate the efficiency of this artificial infiltration ponds, tracer tests could be very useful to evaluate if the recharged water is flushed directly towards the sea, in which case the efficiency of the infiltration pond along the M1 (infiltration pond that has not been used very much), located just north of the Phasouri plantations, should be tested. If the model could be improved, the effects of such a displacement of the artificial recharge pond could be investigated.

3) The third recommendation is more of a suggestion: since a significant amount of work has been conducted in this aquifer on the possible effects of the different salinisation processes, it would be interesting to retrieve the required information on the distribution patterns of the irrigation wells and re-run simulations. Since a model already exists, a monitoring network for the different salinisation processes, based on numerical simulations, could be defined. Implementation of such a combined ‘seawater intrusion-solute recycling and direct evaporation’ monitoring network in the Akrotiri aquifer could act as a pilot project, contributing data that could be very useful for the

increasing the efficiency of the management of the aquifer, but also that would assist in deepening our knowledge of the interplay of these processes in a real aquifer setting.

6.10 Summary and conclusions

Field investigations carried out in the Akrotiri aquifer revealed presence of three major salinisation processes, seawater intrusion, salinisation related to agricultural activity and evaporative processes related to the salt lake, which could be spatially distinguished (Meilhac 2003). Assessing the salinisation risk by means of a 3-D finite element model revealed that the central irrigated area was at high risk with respect to solute recycling. This area corresponds to where a hydrochemical investigation (Meilhac 2003) inferred agricultural activity to be the dominant process.

According to the risk assessment, the high-risk seawater intrusion zone is located in the west, which is also in correspondance with field data. However, with respect to solute recycling, the model results had to be considered as 'hypothetical', since essential data had not been retrieved, particularly the distribution patterns from irrigation wells onto irrigation surfaces. Also, the elaboration of the proposed salinisation risk assessment requires data related to both (all) salinisation processes for calibration and cross-validation purposes. Data related to the temporal evolution of solute recycling salinisation is rarely monitored in coastal areas which diminishes the applicability of the quantitative approach at this stage.

To obtain data related to the solute recycling process, which can then be used in a quantitative approach, we suggest that the spatial impact of this process first needs to be assessed qualitatively. For this purpose, three key-factors have been identified, based on the theoretical description of the solute recycling process: 1) Estimation of the mean capture probability fields by means of piezometric data, 2) estimation of the solute mass flux captured by the wells from the limits and 3) estimation of the agricultural input from the salinity data and from indications relative to the recycling time obtained from aquifer thickness and nitrate concentrations. Based on the principles set out in this thesis, this highly simplified field approach allows the solute recycling process to be integrated into any standard field approach, a process which has so far not found its way into everyday coastal hydrogeology.

CHAPTER 7

CONCLUSIONS AND PERSPECTIVES

7.1 Summary

The main objective of this thesis was to investigate quantitatively groundwater salinisation induced by solute recycling from irrigation, and to elucidate its implications for overall groundwater salinisation in coastal settings. Since the modelling approaches proposed in the literature to simulate seawater-intruded areas rarely account for the coupled and superimposed effects of solute recycling and seawater intrusion, simulation procedures were developed which allowed separate evaluation of the salinisation induced by seawater intrusion and by solute recycling.

In the first instance, the problem of solute recycling was illustrated using an example from Cyprus, the Kiti aquifer, where field investigations suggested that a prominent tongue-like salinity anomaly reaching far into the agriculturally exploitated area was not only related to seawater intrusion, but also to solute recycling (Chapter 2). This observation, combined with the fact that 'classical' seawater intrusion models do not comply with the solute mass budget of a system, if the extracted water is used for irrigation, instigated the investigation of the problem on a more general basis. A transient solute mass budget was established for a perfectly mixed system, and the impact of solute recycling on the spatial salinity distribution was then illustrated using a coupled finite element model, reflecting the main features of the Kiti aquifer. Two simulation scenarios were run, one with seawater intrusion alone (without solute recycling), and one with both seawater intrusion and solute recycling. The results showed that introducing solute recycling into the numerical model not only respects the overall solute mass balance but can also have an important impact on the salinity distribution, leading to a significant spreading of the mixing zone, similar to that observed in the field. Overall, the example showed that neglecting solute recycling in areas where extracted groundwater is highly mineralised (e.g. in seawater intruded settings) may lead to a significant error in a predictive solute mass balance.

A theoretical analysis was then carried to identify and describe the solute recycling process mathematically (Chapter 3). An analytical solution of the 1-D advective transport equation was developed, by defining a distributed 'recycling source', corresponding to the solute mass flux extracted from the wells. The well response to spatial variations in solute recycling led to the

identification of two parameters with which the late time concentration slope at the well could be described: the travel time between the recycling point and the extraction well, and the lateral solute mass flux captured by the well from the boundaries. The mathematical description of the process was then extended to arbitrary advective-dispersive systems by means of the transfer function theory, leading to a formulation for the transient extracted solute mass flux in hydraulic steady state conditions. A recycling transfer function (RTF) $g_{in}(\gamma,t)$ was expressed as the sum of the n-fold self-convolutions of the travel time probability density function between the recycling point and the extraction well, describing the transformation of a signal captured by the well in response to solute recycling. Convolution of the RTF with the solute mass captured from the boundaries yielded the exact transient well response to solute recycling in arbitrary advective-dispersive systems. In this way, the well solute mass response could be predicted, reducing the problem of solute recycling to a standard flow and transport problem, with a distributed 'recycling source' term in the general form of the advection-dispersion equation.

To investigate the effect of solute recycling on the spatial groundwater salinisation, different simulation procedures were developed for the most common hydraulic conditions (Chapter 4). For hydraulic steady state conditions, introducing the 'recycling source' term into the general form of the advection-dispersion equation allowed simulation of the spatial groundwater salinity evolution in response to solute recycling for arbitrary aquifer systems. At late times, the 'recycling source' was found to be a function of the capture zone probability and the lateral solute mass flux, only. This yielded the salinisation potential or maximum salinity distribution which may be reached for the given hydraulic setting in response to solute recycling. Hence, for hydraulic steady state conditions, steady state or transient solute recycling can be simulated with any standard flow and transport simulation code. A numerical procedure was adopted to investigate transient solute recycling for transient hydraulic conditions and showed that strongly varying hydraulic conditions will in turn also change the impact of solute recycling on the spatial groundwater salinisation.

Placing the developed solute recycling simulation procedures in a coastal context led to a framework for a process-based salinisation risk assessment methodology, in which seawater intrusion and solute recycling salinisation are evaluated separately (Chapter 5). For this purpose, the overall salinity distribution at late times, as well as the transient salinity evolution, were decomposed into a seawater intrusion and solute recycling component. This yielded the respective salinisation potentials, the solute recycling potential (RP) and the seawater intrusion potential (SIP), as well as the respective 'present state' salinity distributions. A salinisation risk index was then defined as the potential of further salinisation induced by the respective salinisation process, obtained by comparing the 'present state' salinisations with the respective salinisation potentials. The risk index maps, being strictly related to the hydraulic setting for which they were established,

reveal areas prone to further salinity increase due to solute recycling and seawater, respectively. Comparing the solute recycling and seawater intrusion risk index distributions with the 'present state' salinity distribution allows, for instance, the delimitation of areas requiring remediation (i.e. areas with low risk index values and high salinities) and areas requiring conservation (i.e. areas with salinities close to the exploitation limit with high risk index values). Modification or optimisation of an exploitation scheme leads to modified risk index distributions, indicating those areas which will suffer further salinisation and those for which the modified exploitation scheme will have a remediating effect. This framework for a risk assessment methodology is a first attempt to define a measure for the salinisation hazard induced by the two superimposed and coupled salinisation processes, solute recycling and seawater intrusion, which accounts for the dynamics of groundwater systems.

In the last chapter (Chapter 6), the results of field investigations carried out to confirm the existence of solute recycling salinisation and to determine the spatial distribution of different salinisation processes in the Akrotiri aquifer in Southern Cyprus are presented. On the basis of this data analysis, a 3-D finite element model, reflecting the main features of the aquifer, was used to illustrate and test the salinisation risk assessment procedure developed in Chapter 5. The results obtained from the simulations indicated that the central area of the aquifer is an endangered zone with respect to solute recycling, whereas the western area is endangered with respect to seawater intrusion. This correlates well with the spatial distribution of the dominant salinity sources, as derived from the field investigations. However, essential data for the solute recycling simulations, i.e. the distribution pattern of the extracted groundwater from the irrigation wells onto the irrigated surfaces, was not available, rendering the results of the simulations 'hypothetical'. At this stage, the results cannot be used to define any action plans, also because the necessary monitoring data related to solute recycling salinisation is lacking. Data related to solute recycling is rarely monitored in coastal aquifers, but is essential for the calibration and cross-validation of the proposed salinisation risk assessment procedure. However, qualitative estimation of key-factors, such as the capture probability field, the solute mass flux captured by the wells from the limits, and the mean recycling time, can be used in the field as a preliminary and inexpensive approach to identify salinisation-endangered areas, indicating where the installation of monitoring networks would be advisable in order to obtain the data necessary for a quantitative salinisation risk assessment.

7.2 Limitations and perspectives

Perhaps the most striking aspect about solute recycling is its almost parasitic character. It entirely depends on other salinity sources to cause any damage or to 'proliferate'. Compared to all other

salinisation processes encountered in coastal aquifers (e.g. seawater intrusion, geogenic salt, agricultural additives etc.), it is the only one that does not add any solutes to the system. However, by redistributing the solutes that have been added to the system from other salinity sources, it can lead, as we have shown, to seemingly incomprehensible salinity patterns, without any evidence of a salinity source, in a similar way that invisible parasites can cause extensive damage without any conspicuous evidence. This characteristic makes solute recycling very difficult to track down in the field, since solutes of any origin, extracted by irrigation wells and redistributed over the irrigated area, may suffer recycling, leaving some of their 'original' fingerprints behind as they mix with solutes of other origins. The fact that solute recycling does not actually produce any solutes but only redistributes them may be a reason why this process has not obtained the attention it deserves in coastal settings.

In this thesis, solute recycling was identified and described by means of a quantitative approach. Since a considerable amount of assumptions were made in the course of the mathematical development, particularly with respect to processes taking place in the unsaturated zone, future investigations would urgently require an interdisciplinary approach, involving soil scientists, agronomists, irrigation scientists and hydrogeologists. In coastal aquifers, solute recycling acts in all the domains represented by these different disciplines in a seemingly unthreatening way. Hence, the contribution in this thesis to the understanding of the solute recycling process is limited to the aspects related to the dynamics of the saturated zone and would therefore require a coordinated investigation in the different domains in order to gain a more fundamental understanding of the process as a whole. Using an interdisciplinary approach, methods could hopefully be developed to identify solute recycling with field investigations in a more straight-foreward way.

Another aspect which would require close collaboration between the different disciplines is related to the proposed framework for a salinisation risk assessment methodology. Again, the presented approach focussed only on aspects concerning the saturated zone and cannot be conceptually developed any further without the involvement of experts who can evaluate and define the total risk, which has to involve the interplay between crop tolerance, yields and potential economic damage.

Numerous assumptions within the quantitative approach need to be more closely assessed, as for instance, the effects occuring when density-dependent flow and transport plays an important role. This aspect has to be evaluated not only for seawater intrusion but perhaps also for solute recycling, since instable density stratification can develop when the concentration below the irrigated surfaces becomes very high. In the presence of density-dependent flow and transport, the validity of the assumptions forming the basis of transfer function theory (principle of linear

superposition), and thus of the formulation of the ‘recycling source’, would have to be assessed. It would then be important to evaluate its impact on the ‘salinisation potentials’ and on the salinisation risk assessment methodology. A further extension of the proposed framework for a salinisation risk assessment methodology would be to combine the approach with optimisation procedures, which could yield estimates of the uncertainty, and thus the reliability, of the obtained results.

In the presented quantitative description of the solute recycling process, we observed that infinitely high concentrations will be reached in closed systems (e.g. in areas with a capture probability of $P(\mathbf{x}) = 1$), since the process of salt precipitation or reactive transport was not included. However, these processes cannot be left aside, and in future would need to be addressed within the framework of the description and simulation of the solute recycling process.

Field investigations focussing on the identification of the solute recycling process and the installation of appropriate monitoring networks, in parallel to further investigations in the area of the quantitative treatment of the problem, would be essential for the validation and evaluation of the applicability of the developed approaches to real case studies. For this purpose, however, it would be important that this elusive salinisation process should gain more attention within the hydrogeological circles which actively investigate the salinisation of coastal aquifers.

REFERENCES

Al-Senafy M, Abraham J. Vulnerability of groundwater resources from agricultural activities in southern Kuwait. Agricultural Water Management 2004; 64: 1-15.

Aller L, Bennet T, Lehr JH, Petty RJ. DRASTIC: a standarised system for evaluating groundwater pollution potential using hydrologic settings. US EPA Report 600/2-87/035, Robert S. Kerr Environmental Research Laboratory, Ada, OK, 1987.

Andreasen DC, Fleck WB. Use of Bromide/chloride ratios to differentiate potential sources of chloride in a shallow, unconfined aquifer affected by brackish-water intrusion. Hydrogeology Journal 1997; 5 (2):17-26.

Aragüés R, Tanji K K, Quilez D, Alberto F, Faci J, Machin J, Arrué J L. Calibration and verification of an irrigation return flow hydrosalinity model. Irrigation Science 1985; 6: 85-94.

Badon-Ghijben W. Nota in verband met de voorgenomen putboring nabij Amsterdam. Tijdschr. k. inst. ing., the Hague, 1888: 8-22.

Bear J, Cheng AH-D, Sorek S, Ouazar D, Herrera I (Eds.). Seawater intrusion in coastal aquifers-concepts, methods and practices. Kluwer Academic Publishers, 1999.

Beke GJ, Entz T, Graham DP. Long-term quality of shallow groundwater at irrigated sites. Journal of irrigation and drainage engineering-ASCE 1993; 119 (1): 116-128.

Beltrán JM. Irrigation with saline water: benefits and environmental impact. Agricultural Water Management 1999; 40: 283-294.

Bouwer H. Effect of irrigated agriculture on groundwater. Journal of irrigation and drainage engineering-ASCE 1987; 113 (1): 4-15.

Cardona A, Carillo-Rivera J J, Huizar-Alvarez R, Graniel-Castro E. Salinization in coastal aquifers of arid zones: an example from Santo Domingo, Baja California Sur, Mexico. Environmental Geology 2004; 45: 350-366.

Cheng AHD, Halhal D, Naji A, Ouazar D. Pumping optimisation in saltwater-intruded coastal aquifers. Water Resources Research 2000; 36(8): 2155-2165.

Chi SC, Reilinger RE. Geodetic evidence for subsidence due to groundwater withdrawal in many parts of the United States of America. Journal of Hydrology 1984; 67(1-4): 155-182.

Cirpka OA, Kitanidis PK. Travel-time based model of bioremediation using circulation wells. Groud Water 2001; 39(3): 422-432.

Close ME. Effects of irrigation on water-quality of a shallow unconfined aquifer. Water Resources Bulletin 1987; 23(5): 793-802.

Connell LD, van den Daele G. A quantitative approach to aquifer vulnerability mapping. Journal of Hydrology 2003; 276: 71-88.

Constantinou C. Hydrogeology of the Akrotiri Peninsula, Cyprus. Geological Survey Department, Nicosia, 1970.

Cornaton F. Deterministic models of groundwater age, life expectancy and transit time distributions in advective-dispersive systems. PhD thesis, University of Neuchâtel (Switzerland) 2004.

Cornaton F, Perrochet P, Diersch HJ. A finite element formulation of the outlet gradient boundary condition for convective–diffusive transport problems. International Journal for Numerical Methods in Engineering 2004; 61: 2716–2732.

Crump K.S. Numerical Inversion of Laplace Transforms Using Fourier Series Approximation. J. Ass. Comp. Mech. 1976; 23(1): 89–96.

Custodio E, Bruggemann GA. Groundwater Problems in Coastal Aquifers. UNESCO 1987. ISBN 92-3-102415-9.

Custodio E. Studying, monitoring and cotrolling seawater intrusion in coastal areas. In: Guidelines for Study, Monitoring and Control, FAO Water Reports 1997; 11(1): 7-23.

Diersch HJ. FEFLOW Reference Manual 4.9. WASY Institute for Water Resources Planning and Systems Research LTD, Berlin 1998.

Diersch HJ. FEFLOW Reference Manua 5.1. WASY Institute for Water Resources Planning and Systems Research LTD, Berlin 2002.

El Achheb A, Mania J, Mudry J. Processus de salinisation des eaux souterraines dans le basin Sahel-Doukkala (Maroc occidental). First International Conference on Saltwater Intrusion and Coastal aquifers- Monitoring, Modeling and Management, Essaouira, Morocco, 2001.

Eliades G, Metochis C, Papadopolous S. ΤΕΧΝΟΟΙΚΟΝΟΜΙΚΙ ΑΝΑΛΨΣΗ ΤΟΝ ΑΡΔΕΨΣΕΟΝ ΣΤΗΝ ΚΨΠΡΟ. Technical Bulletin, Agricultural research institute, Nicosia, 1995.

Essaid HI. A multilayered sharp interface model of coupled freshwater and saltwater flow in coastal systems: model development and application. Water Resources Research 1990; 26(7): 1431-1454.

Fedrigoni L, Krimissa M, Zouari K, Maliki A, Zuppi GM. Origine de la minéralisation et comportement hydrogéochinique d'une nappe phréatique soumise à des contraintes naturelles et anthropiques sévères : exemple de la nappe de Djerbeniana (Tunisie). C.R. Acad. Sci. Paris, Sciences de la Terre et des Planètes 2001; 332 : 665-671.

Ferguson C, Darmendrail D, Freier K, Jensen BK, Kasamas H, Urzelaï A, Vegter J (Eds.). Risk assessment for contaminated sites in Europe. Scientific Basis, LQM Press, Nottingham, 1998.

Frind EO. Seawater intrusion in continuous coastal aquifer-aquitard systems. Advances in Water Resources 1982; 5: 89-97.

Freeze RA, Cherry JA. Groundwater. Prentice Hall, 1979.

Gambolati G, Putti M, Paniconi C. Three-dimensional model of coupled flow and miscible salt transport. In: Seawater intrusion in coastal aquifers- concepts, methods and practices. Bear J, Cheng AHD, Sorek S, Ouazar D, Herrera I, (Eds.), Kluwer Academic Publishers 1999.

Gascoyne M. Geochemistry of actinides and their daughters. In: Uranium series Disequilibrium, Ivanovich M, Harmon RS (Eds.), 2nd Edition, Oxford Science Publications 1992.

Gogu RC, Dassargues A. Current trends and future challenges in groundwater vulnerability assessment using overly and index methods. Environmental Geology 2000; 39(6): 549-559.

Goode DJ. Direct simulation of groundwater age. Water Resources Research 1996; 32(2): 289-296.

Gordon E, Shamir U, Bensabat J. Optimal management of a regional aquifer under salinization conditions. Water Resources Research 2000; 36(11): 3193-3203.

Guyonnet D. Approche mathématique de l'impact des sites contaminés sur les eaux souterraines dans un contexte d'analyse de risque. Thèse de doctorat, Ecole Polytéchnique Fédérale de Lausanne, 1998.

Helm P. Integrated Risk Management for Natural and Technological Disasters. Tephra 1996; 15(1): 4-13.

Henry HR. Salt intrusion into fresh-water aquifers. Journal of Geophysical Research 1959; 64(11): 1911-1919.

Herzberg B. Die Wasserversorgung einiger Nordseebaeder, J. Gasbeleucht. Wasserversorg. 1901; 44: 815-819, 842-844.

Hsiouss J, Mudry J, Mania J, Bouchaou L, Chauve P. Utilisation de rapport Br/Cl pour déterminer l'origine de la salinité des eaux souterraines : exemple de la plaine de Souss (Maroc). C.R. Acad. Sci. Paris, Sciences de la Terre et des Planètes 1999 ; 328 : 381-386.

Höltin B. Hydrogeologie: Einführung in die allgemeine und angewandte Hydrogeolgogie. 5. Auflage, Ferdinand Enke Verlag, Stuttgard 1996.

Hsü KJ, Ryan WBF, Cita MB. Late Miocene desiccation of the Mediterranean, Nature 1973; 20(242): 240-244.

Huyakorn PS, Andersen PF, Mercer JW, White HO Jr. Saltwater intrusion in aquifers: development and testing of a three-dimensional finite element model. Water Resources Research 1987; 23(2): 293-312.

Jackovides J. Southern Conveyor Project. Feasibility study, Groundwater Resources, Vol.3, Cyprus Water Development Department, Nicosia 1982.

Johannsen K, Kinzelbach W, Oswald S, Wittum G. The saltpool benchmark problem - numerical simulation of saltwater upconing in a porous medium. Advances in Water Resources 2002; 25(3); 335-348.

Jury WA. Solute travel-time estimates for tile-drained fields: I, Theory. Soil Sci. Soc. Am. J. 1975; 39:1020-1024.

Jury WA. Solute travel-time estimates for tile-drained fields: II, Application to experimental studies. Soil Sci. Soc. Am. J. 1975; 39:1024-1028.

Jury WA. Simulation of solute transport using a transfer function model. Water Resources Research 1982; 18(2): 363-368.

Jury WA, Sposito G, White RE. A transfer function model of solute transport through soil, 1: fundamental concepts. Water Resources Research 1986; 22(2): 243-247.

Jury WA, Roth K. Transfer functions and solute movement through soil: theory and applications. Birkhäuser Bosten, Cambridge, Mass, 1990.

Kass A, Gevrieli I, Yechieli Y, Vengosh A, Starinsky A. The impact of freshwater and wastewater irrigation on the chemistry of shallow groundwater: a case study from the Israeli Coastal Aquifer. Journal of Hydrology 2005; 300: 314-331.

Kelleners TJ, Kamra SK, Jhorar RK. Prediction of long term drainage water salinity of pipe drains. Journal of Hydrology 2000; 231: 249-263.

Kim Y, Lee KS, Koh DC, Lee DH, Lee SG, Park WB, Koh GW, Woo NC. Hydrogeochemical and isotopic evidence of groundwater salinisation in a coastal aquifer: a case study in Jeju volcanic island, Korea. Journal of Hydrology 2003; 270: 282-294.

Kitching R. A mathematical model of the Akrotiri Plio-Pleistocene gravel aquifer, Cyprus. IGS, RN 75/2, London, 1975.

Kolodny Y, Katz A, Starinsky A, Moise T, Simon E. Chemical tracing of salinity sources in Lake Kinneret (Sea of Galilee), Israel. Limnology and Oceanography 1999; 44 (4): 1035-1044.

Konikow LF, Bredehoeft JD. Modeling flow and chemical quality changes in an irrigated stream-aquifer system. Water Resources Research 1974; 10(3): 546-561.

Konikow LF, Person M. Assessment of long-term salinity changes in an irrigated stream-aquifer system. Water Resources Research 1985; 21(11): 1611-1624.

Larabi A, De Smedt F, Tanarhte M. Modelling saltwater intrusion by the finite element method. Hydrochemistry 1997. Proceedings of the Rabat Symposium, April 1997. IAHS Publ. Nr. 244: 83-95.

Larson KJ, Besagaoglu H, Marino MA. Prediction of optimal safe groundwater yield and land subsidence in the Los Bano-Kettleman City area, California, using calibrated numerical simulation. Journal of Hydrology 2001; 242(1-2): 79-102.

Lozano E, Coleto C, Manzano M, Custodio E. Saline waters in the coastal area of the national park of Donana (SW of Spain) in absence of saline water intrusion. Proceedings SWIM 17, Delft 2002: 238-249.

Meilhac C. Hydrogeological and geochemical investigation of the Akrotiri aquifer, Cyprus. Master thesis, Formation postgrade en hydrologie et hydrogéologie, Specialisation hydrogéologie, Université de Neuchâtel, 2003.

Mercado A. The use of hydrogeochemical patterns in carbonate sand and sandstone aquifers to identify intrusion and flushing of saline water. Ground Water 1985; 23 (5): 635-645.

Milnes E. Hydrogeological investigation of the Akrotiri porous aquifer, Southern Cyprus: seawater intrusion modelling. Master thesis, Formation postgrade en hydrologie et hydrogéologie, Specialisation hydrogéologie, Université de Neuchâtel, 2000.

Milnes E, Renard P. The problem of salt recycling and seawater intrusion in coastal irrigated plains: an example from the Kiti aquifer (Southern Cyprus). Journal of Hydrology 2004; 288: 327-343.

Neupauer RM, Wilson JL. Adjoint method for obtaining backward-in-time location and travel time probabilities of a conservative groundwater contaminant. Water Resources Research 1999; 35(11): 3389-3398.

Oster JD. Leaching for salinity control. In: Soil salinity under irrigation, Eds. Shainberg I. And Shalhevet J., Springer Verlag, Berlin, New York, Tokio 1984; 190-197.

Oster JD. The use of models in salinity assessment: steady-state rootzone salt balance. In: Agricultural Salinity Assessment and Management. Tanji KK (Ed.), ASCE (American Society of Civil Engineers) Manuals and Reports on Engineering Practice 1990; 71.

Oster JD. Irrigation with poor quality water. Agricultural Water Management 1994; 25(3): 271-297.

Oude Essink GHP. Salt water intrusion in a three-dimensional groundwater system in the Netherlands: a numerical study. Transport in Porous Media 2001; 43: 137-158.

Paniconi C, Khalifi I, Lecca G, Giacomelli A, Tarhouni J. Modeling and analysis of seawater intrusion in the coastal aquifer of Eastern Cap-Bon, Tunisia. Transport in Porous Media 2001; 43: 3-28.

Pearce MW, Schumann EH. The impact of irrigation return flow on aspects of the water quality of the Upper Gamtoos Estuary, South Africa. Water SA 2001; 27(3); 367-372.

Ploethner D, Avramadis C, Charalambidis A, Geyh MA, Schmidt G, Wagner W, Zomenis S. Hydrochemistry and quality problems of groundwater in the Kiti area. Project Report Hydrochemistry, Technical Cooperation Cyprus-German Geological and pedological project (Nr. 81.222.4). Bundestanstalt für Geowissenschaften und Rohstoffe, Hannover 1986.

Prendergast JB, Rose CW, Hogarth WL. Sustainability of conjunctive water use for salinity control in irrigated areas: theory and application to the Shepparton region, Australia. Irrigation Science 1993; 14: 177-187.

Post VEA. Fresh and saline groundwater interaction in coastal aquifers: is technology ready for the problems ahead? Hydrogeology Journal 2005; 13(1): 120-123.

Ragab R. A holistic integrated approach for irrigation, crop and field management : the SALTMED model. Environmental Modelling & Software 2002; 17: 345-361.

Reading HG. Sedimentary Environments and Facies. Blackwell Scientific Publications 1986, ISBN 0-632-01223-4.

Reynolds WD, Elrick DE. Ponded infiltration from a single ring: 1. Analysis of steady flow. Soil. Sci. Soc. Am. J. 1990; 54: 1233-1241.

Richter BC, Kreidtler CW. Geochemical techniques for identifying sources of groundwater salinisation. Smoley, Boca Raton 1993: 258.

Rhoades JD, Chanduvi F, Lesch S. Soil salinity assessment : methods and interpretation of electrical conductivity measurements. FAO irrigation and Drainage Report 57, 1999.

Robertson AHF. Tectonic evolution of Cyprus. In: Ophiolites. Malpas J, Moores A, Panayiotou A, Xenophontos C (Eds.). Oceanic Crustal Analogues, Cyprus Geological Survey Department, Nicosia, 1990: 235-250.

Ruppert MG. Calibration of the DRASTIC ground water vulnerability mapping method. Ground Water 2001; 39(4): 625-630.

Schmidt G, Ploethner D, Avraamadis C, Wagner W, Zomenis S. Groundwater Model Investigation on the Kiti Aquifer. Technical Cooperation Cyprus-German Geological and Pedological Project, Bundestanstalt für Geowissenschaften und Rohstoffe, Hannover 1988.

Sherif M, Hamza K. Mitigation of seawater intrusion by pumping brackish water. Transport in porous media 2001; 43: 29-44.

Shainberg I, Shalhevet J. (Eds.) Soil salinity under irrigation: processes and management. Ecological studies 51. Springer Verlag 1984.

Sites W, Kraft GJ. Groundwater quality beneath irrigated vegetable fields in a north-central US sand plain. Journal of Environmental Quality 2000; 29(5): 1509-1517.

Sophocleous M, Ma T. A decision model to assess vulnerability to salt water intrusion in the Great Bend Prairie aquifer of Kansas. Ground Water 1998; 36(3): 476-483.

Strigter TY, Van Ooijen SPJ, Post VEA, Appelo CAJ, Carvahlo Dill AMM. A hydrogeological and hydrochemical explanation of the groundwater composition under irrigated land in a Medriterranean environment, Algarve, Portugal. Journal of Hydrology 1998, 208: 262-279.

Steward IT, Loague K. A type transfer function approach for regional-scale pesticide leaching assessments. Journal of Environmental Quality 1999; 28: 378-387.

Stiros SC. Subsidence of the Thessaloniki (northern Greece) coastal plain, 1960-1999. Engineering Geology 2001; 61(4): 243-256.

Sukhija BS, Varma VN, Nagabhushanam P, Reddy DV. Differentiation of paleomarine and modern seawater intruded salinities in coastal groundwaters (of Karaikal and Tanjavur, India) based on inorganic chemistry, organic biomarker fingerprints and radiocarbon dating. Journal of Hydrology 1996; 174: 173-201.

Tanji KK. A conceptual hydrosalinity model for predicting salt load in irrigation flows. In: Managing saline water for irrigation, Proc. Int. Conf. on Managing saline water for irrigation 1977.

Tanji KK. (Ed.) Agricultural salinity assessment and management. ASCE Manuals and Reports on Engineering Practice No. 71, American Society of Civil Engineers, New York. 1990.

Uffink GJM. Application of the Kolmogorov's backward equation in random walk simulation of groundwater contaminant transport. In: Contaminant Transport in Groundwater. Kobus HE and Kinzelbach W (Eds.), Balkema, Rotterdam, 1989: 283-289.

Van Genuchten MTh, Dalton FN. Models for simulating salt movement in aggregated soils. Geoderma 1980; 38: 165-183.

Van Schilfgaarde J. Drainage design for salinity control. In: Soil salinity under irrigation. Shainberg I and Shalhevet J (Eds.), Springer Verlag 1984: 190-197.

Vengosh A, Starinsky A, Kolodny Y, Chivas AR, Raab M. Boron isotope variations during fractional evaporation of seawater: new constraints on the marine vs. non marine debate, Geology 1992; 20: 799-802.

Vengosh A, Benzvi A. Formation of a salt plume in the coastal-plain aquifer of Israel- The Beer-Toviyya Region. Journal of Hydrology 1994; 160(1-4): 21-52.

Vengosh A, Rosenthal E. Saline groundwater in Israel: its bearing on the water crisis in the country. Journal of Hydrology 1994; 156: 389-430.

Vengosh A, Pankratov I. Chloride/bromide and chloride/fluoride ratios of domestic sewage effluents and associated contaminated groundwater. Ground Water 1998; 36 (5): 815-824.

Vengosh A, Spivack A, Artzi Y, Avner A. Geochemical and boron, strontium and oxygen isotopic constraints on the origin of the salinity in groundwater from the Mediterranean coast of Israel. Water Resources Research 1999; 35 (6):1877-1894.

Vengosh A, Gill J, Davisson ML, Hudson GB. A multi-isotope (B, Sr, O, H and C) and age-dating (H-3, He-3 and C-14) study of groundwater from salinas Valley, California: Hydrochemistry, dynamics and contamination processes. Water Resources Research 2002; 38 (1): 1008.

Visher G. Exploration stratigraphy, PennWell Publishing Company 1990; ISBN 0-87814-342-4.

Voss CI. USGS SUTRA Code-History, practical use, and application in Hawaii. In: Seawater intrusion in coastal aquifers- concepts, methods and practices. Bear J, Cheng AHD, Sorek S, Ouazar D, Herrera I (Eds.), Kluwer academic publishers 1999.

Xue Y, Chunhong X, Wu J, Liu P, Wang J, Jiang Q. A three-dimansional miscible transport model for seawater intrusion in China. Water Resources Research 1995; 31(4): 903-912.

Yeo D. Utilisation de la géophysique de surface pour la localisation des biseaux salés. Master thesis, Formation postgrade en hydrologie et hydrogéologie, Specialisation hydrogéologie, Université de Neuchâtel, 2003.

APPENDIX 1

MAIN FEATURES OF THE IMPLEMENTATION OF SOLUTE REYCLING INTO A NUMERICAL CODE.

Since solute recycling is not included as a standard option in flow and transport simulation codes, this process recycling was added as a module to a finite element code FEMFT3 developed at CHYN within the framework of an earlier thesis (Cornaton 2004). In this way, solute recycling could be simulated for any hydraulic conditions in a CPU gaining way, since the required operations are directly done within the source code, avoiding modification of boundary conditions manually or via an external library (e.g. interface manager in FEFLOW, Diersch 2002).

The main principle of the numerical procedure to simulate solute recycling is the updating of the 'recycling source' term in Eq. (4.1) at each time-step. This is done by cumulating the extracted solute mass at each irrigation well at the end of each time-step and redistributing it by means of a redistribution matrix onto the assigned irrigation surfaces during the following time-step. The fractions that are distributed from each irrigation well to each irrigation plot have to be known.

Cumulation of extracted solute mass flux

The main procedure in the numerical solute recycling simulation consists in updating the cumulated extracted solute mass vector $M_p(t)$ [M] with dimension j (number of extraction wells) between the time (t-Δt) and t. The cumulated mass $M_{pj}(t)$ [M] extracted between (t-Δt) and t from the j^{th} extraction well is approximated as follows:

$$M_{pj}(t) = \frac{Q_{pj}(t)(C_{pj}(t) + C_{pj}(t - \Delta t))\Delta t}{2} \qquad \text{(A 1.1)}$$

Where Q_{pj} and C_{pj} are the respective extraction rates and concentrations at the well j. At the beginning of the simulation procedure, no solute has been cumulated, so that $M_{pj}(0) = 0$.

Solute recycling in transient hydraulic conditions presupposes that the 'recycling source' is affected by transient infiltration rates on the irrigation surfaces. During periods when no

infiltration i_k takes place on the *k*-th irrigation plot ($i_k(t) = 0$), no recycling will take place. Therefore, the cumulated solute mass vector $M_{pj}(t)$ will add the cumulated extracted solute mass to the mass that has not yet been recycled. To know whether recycling will take place or not, the infiltration rate is evaluated at the begining of the each time-step.

In absence of infiltration, the 'recycling source' $J_p(t)$ = 0, and therefore the cumulated mass extracted during the previous time-step is not re-introduced but added to the cumulated solute mass that is extracted during the time step with no infiltration:

$$M_{pj}(t) = \left[\frac{Q_{pj}(t)(C_{pj}(t) - C_{pj}(t - \Delta t))\Delta t}{2} \right] + M_{pj}(t - \Delta t) \qquad \text{(A.1.2)}$$

Where $M_{pj}(t\text{-}\Delta t)$ contains the cumulated extracted solute mass stored during the previous time-step.

Updating of distributed 'recycling source'

A matrix A is defined which distributes defined fractions of the cumulated extracted solute mass from the *j* irrigation wells to the *k* irrigation plots. Then, the solute source $J_p(t)$ in Eq. (4.1) for the *k* irrigation plots is obtained by multiplying $M_p(t)$ with the re-distribution matrix A (*j*, *k*) as follows:

$$\mathbf{J_p}(t) = \mathbf{A}\mathbf{M}_p(t) \qquad \text{(A 1.3)}$$

To define the re-distribution matrix A, the fractions n_{jk} of extracted solute mass of each extraction well *j* attributed to the *k* irrigation plots have to be defined. For the case that all the extracted solute mass from well *j* is recycled, $\sum_k n_{jk} = 1$. To obtain the re-distribution matrix A, all the fractions n_{jk} have to be divided by the appropriate irrigation plot surfaces S_k and the time-step length Δt. The irrigation plot surfaces S_k are evaluated in a pre-processing step. The components of the Matrix A ($j \times k$) are then:

$$A_{jk} = \frac{n_{jk}}{\Delta t S_k} \qquad \text{(A 1.4)}$$

with which the solute source $J_p(t)$ vector in Eq. (A 1.3) is updated at each time-step.

For the case that the irrigation plot surfaces S_i and the time-step length Δt remain constant in time, the re-distribution matrix A needs to be evaluated only once, in a pre-processing stage.

APPENDIX 2

IDENTIFICATION OF DIFFERENT SALINISATION SOURCES IN THE AKROTIRI AQUIFER BY GEOCHEMICAL INVESTIGATIONS

The main parameters which were used by Meilhac (2003) to identify different salinisation sources and their spatial distribution (see Fig. 6.6) in the Akrotiri aquifer are summarised. Although geochemical fingerprints of different salinisation sources are well documented in the literature, Meilhac (op. cit) found that identification of the origin of the salinisation was often ambiguous.

Additional stable and radio isotopic data was interpreted and is presented. The results indicated that combination of such isotopic data with salinity data may be a promising tool to identify solute recycling.

Geochemical fingerprints indicating seawater intrusion

The only major ions found to be conservative are chloride and bromide and hence they are the most commonly used indicators of mixing fractions between the seawater and freshwater end members. The molar Br/Cl ratio has a typical and distinct value of 0.0015 for seawater (Mercado 1985; Andreasen & Fleck 1997; Hsiouss et al. 1999; Vengosh et al. 1999; Vengosh et al. 2002). Meilhac (2003) used the the Br/Cl molar ratios combined with the ionic ratios Mg/Cl, Ca/Cl and Na/Cl to identify samples for which the slopes were smaller than one, indicating pure seawater-freshwater mixing (Custodio 1987, Richter & Kreidtler 1993). The oxygen stable isotope signatures of these samples which were identified to be affected by seawater intrusion also indicated mixing between the freshwater end-member and seawater. With these data, Meilhac (2003) determined mixing fractions. The samples for which the analysis suggested pure mixing between seawater and fresh groundwater were located in the eastern part of the aquifer (Fig. 6.6).

Geochemical fingerprints indicating agricultural activity and solute return flow from irrigation

Using conservative tracers (Cl, Br and $\delta^{18}O$) and nitrates (used as a tracer of agricultural activity), Fedrigoni et al. (2001) found that recharge flushes high contents of nitrates and other dissolved

solides into the groundwater, thus adding an anthropogenic salinity source to the salinisation due to seawater intrusion. In the Akrotiri aquifer, nitrate concentrations ranging from 50-370 mg/l are found in the area of the citrus plantations (Fig. 6.5), indicating the transfer of solutes through the unsaturated zone (Meilhac 2003). In the area between the seawater affected zone in the east and the central plain, samples were identified with high nitrate concentrations, but the Br/Cl ratio and the major ion ratios indicating seawater-freshwater mixing. In this area, salinisation induced by seawater intrusion is clearly overprinted by an agricultural component.

Dissolution of evaporitic rocks and anthropogenic impacts have characteristic Br/Cl ratios (Vengosh & Pankratov 1998), making this ratio a valuable parameter for the identification of different salinity sources. The Br/Cl ratios, as well as the oxygen and sulphur isotopic compositions of the samples retrieved from the irrigated central area of the aquifer (with high nitrate concentrations), correlated well with a significant enrichment in minor and trace elements, indicating an anthropogenic contribution and thus solute return flow. The chemical composition of these samples is significantly displaced from the seawater/freshwater mixing line for all conservative tracers and the sample locations are located in the central area of the aquifer with intensive citrus cultures (Fig. 6.6).

Geochemical fingerprints indicating evaporative processes

Evaporation is a process leading to fractionation of the the analysed stable isotopes (^{18}O, ^{2}H) but also to a relative fractionation of major ion ratios (in particular Br and Cl ions), and thus to a change with respect to the typical ratios characterising the seawater composition (Vengosh et al. 1992, Lozano et al. 2002). In the cultivated central area of the aquifer, Br/Cl ratios were found to be generally low, indicating evaporation. δO^{18}-enrichment correlates with salinity increase in the area just north of the salt lake, and a regional trend of depletion from west to east can be detected. This led to the delimitation of the area characterised by salinisation induced by evaporitic processes (Fig. 6.6). Note that the example of the dying orange trees, shown in Fig. 1.1 is located juts south of the Lanitis monitoring well (Fig. 6.6) in the area where evaporative processes are found to dominate the groundwater chemical signatures.

The highest evaporation in the Akrotiri aquifer is encountered in the area of the salt lake (Fig. 6.1), where salinities are several times that of seawater, leading to salt precipitation. The samples taken in the immediate area of the salt lake have a clear Na-Cl facies, and are enriched in Na, Cl, Mg, K and SO_4 and depleted in HCO_3 (Fig. 6.6). Meilhac (2003) found that most trace elements were abundant and that uranium concentrations were abnormally depleted. She suggests that this may be

due to high organic activity (the smell of HS_2 comes from several boreholes), leading to a reducing environment and thus to uranium adsorption.

In the agriculturally exploited area to the north of the salt lake, samples were found indicating evaporation (δO^{18} depletion) and low Br/Cl ratios. In this area, the water table is very shallow enhancing direct evapotranspiration from the groundwater.

Groundwater fluctuations caused by diurnal evaporative processes

Before installing the monitoing equipment in the monitoring wells, air temperature and water table fluctuations were measured over a period of several days in July 2003 in a well located in the Eucalyptus forest to the north of the salt lake (Fig. A2.1). The results suggest that evapotranspiration takes place directly from the groundwater, leading to the observed diurnal water table fluctuations. This is a process which will contribute to salinisation, since even salt-tolerant plants, such as Eucalyptus trees, will leave most solutes behind, thus salinising the soil and the groundwater.

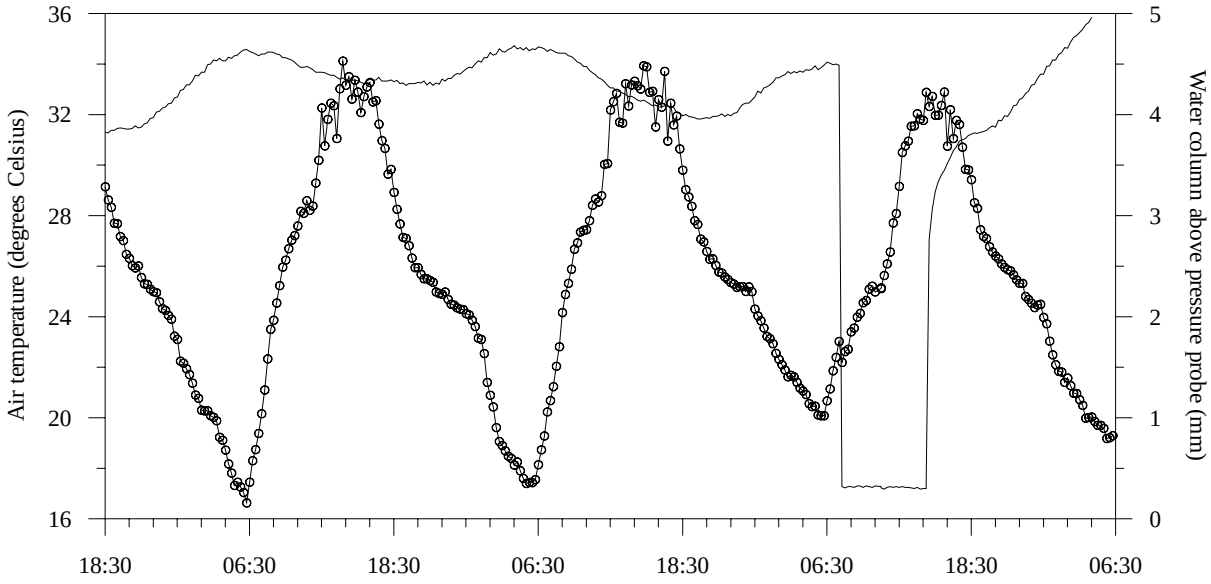

Fig. A 2.1: Results from continuous relative water table (line) and air temperature (circles) measurements in a borehole located to the north of the salt lake, in a Eucalyptus forest, measured between 11th and 14th July 2003. At the beginning of the third day, a pumping event can be seen.

Uranium and stable isotopes combined with salinity data: potential indicators of solute recycling?

Since solute return flow from irrigation in semi-arid and arid regions is linked to an important evaporative component, parameters sensitive to this process are useful. However, the definition of hydrochemical fingerprints which allow a distinction to be made between direct evaporation from the groundwater and evaporation having taken place during irrigation and subsequent percolation to the groundwater is not straight- foreward.

A second sampling campaign was carried out in April 2004 to investigate the potential use of uranium as tracer of solute return flow from irrigation. Combining the results of this investigation with the ones obtained by Meilhac during the 2003 field campaign revealed a correlation between high uranium concentrations and increasing salinities in the agriculturally exploited area. The use of $^{234+238}U$ in coastal contexts to distinguish between salinisation due to seawater intrusion and solute return flow from irrigation has not previously been reported. These preliminary results show that it might be a promising fingerprint, since uranium enrichment by evaporative concentration will deviate significantly from the seawater-freshwater mixing line. Uranium has a conservative behaviour, unless very reducing conditions prevail (Gascoyne 1992). If other external uranium sources, leading to enrichment, can be excluded, the increase in uranium concentration and salinity observed in many of the groundwater samples located in the agriculturally exploited area can be explained by concentration of fresh groundwater (Fig. A2.2a). Such concentration can either take place by direct evaporation, by evaporation of applied irrigation water or by long-term concentration due to solute recycling. High uranium concentrations were found in the groundwater samples at both monitoring sites (F1, F2, Mon675, Mon778 in Fig. A2.2). Their uranium enrichment to values beyond the seawater concentration indicates that their salinity is not related to seawater intrusion. In Fig. A2.2, the samples that are located in an intermediate position (between the pure concentration-line and the seawater-freshwater line) correspond to samples in which both seawater intrusion and solute return flow/recycling impact were identified.

A similar feature can be observed for the oxygen isotopes compared to the uranium concentration. δO^{18}-enriched samples having high uranium concentrations suggest concentration by evaporation, which can be attributed to solute return flow and recycling (Fig. A2.2b). This suggests that the uranium signature is potentially a good tracer for irrigation return flow and even for solute recycling, but a more detailed and extensive investigation is required for confirmation.

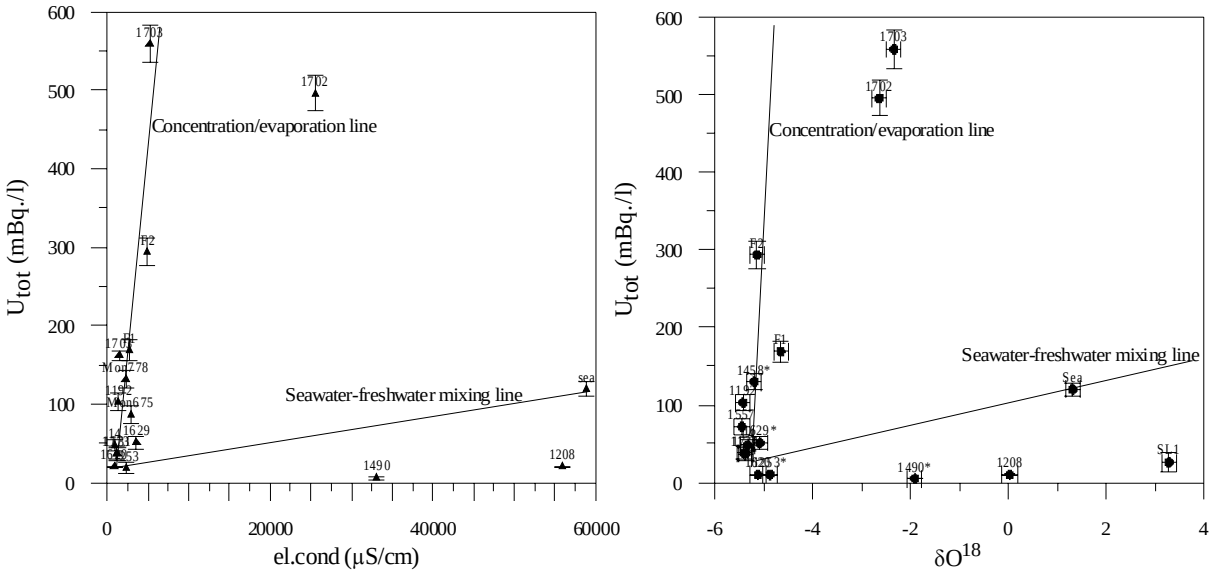

Fig. A 2.2: Electrical conductivity (left) and oxygen isotopic composition (right) versus uranium concentration, showing the seawater-freshwater mixing line and the concentration/evaporation line. Samples retrieved from within the citrus plantations are aligned along the concentration/evaporation line, indicating that their salinity is not related to seawater intrusion. $U_{tot} = {}^{234+238}U$.

APPENDIX 3

SMALL-SCALE FIELD EXPERIMENTS IN CITRUS PLANTATIONS

The aim of two monitoring sites was the identification of solute concentration of the applied irrigation water and solute transfer to the groundwater, since irrigation-induced solute concentration in the unsaturated zone and solute transfer to the groundwater has never been studied in the Akrotiri aquifer before. Therefore, these experiments were conducted to determine whether and to what degree variations in the groundwater salinity result from solute return flow from irrigation rather than from seawater intrusion.

The locations of two monitoring sites were chosen on the basis of existing borehole logs and logistical criteria and are shown in Fig. 6.6. The sites were located at different distances to the sea, and to show different local geological subsurface conditions. The monitoring location called the Phasouri site lies near to the seawater intruded area and is characterised by gravelly-sandy deltaic deposits. The other monitoring well, called the Lanitis site, is located further inland, close to the salt lake (Fig. 6.1). In this area, most existing borehole logs revealed sandy-silty deltaic deposits with clay intercalations.

The drilling of the monitoring boreholes was done by hammer drilling, and mixed soil samples were retrieved from each 0.5 m interval. These were used to determine vertical soil salinity and major ion analysis profiles on extractions from saturated soil paste (Rhoades et al. 1999). The drilling diameter was 4 inches and the borehole was subsequently equipped with a 2 inch diameter fully slotted PVC tube covered with geotextile. The top of the hole was cemented and covered, leaving a small opening for the permanently installed instrumentation (Fig. A 3.1). A second soil salinity profile was done at the end of the monitoring period. The soil samples were retrieved with a hand auger, which inhibited penetration below 2.6 m at the Phasouri site and 1.3 m at the Lanitis site.

At each site, two perpendicular high-resolution electrical resistivity tomography (ERT) profiles were carried out with *Campus Tigre* equipment, with electrode spacings 1-1.5 m. This geoelectrical survey was carried out within the framework of a second Master thesis, which was aimed at using this method to map aquifer and soil salinity distributions in the Akrotiri aquifer (Yeo 2003).

The monitoring sites were equipped to continuously measure the temporal groundwater salinity, the water table, and the temperature evolution from the irrigation peak to the end of the rainy season (July 2003-April 2004).

At the Phasouri site, a second conductivity probe was installed in the irrigation tube and at the Lanitis site a miniature Schlumberger array was installed at a depth of 20 cm below the surface to measure the relative soil salinity.

In setting up the monitoring sites the main hypothesis was that solute transfer to the groundwater would be mainly in a vertical direction. As we will see, this hypothesis did not seem to apply to the Lanitis site.

Fig. A 3.1: Monitoring well Phasouri, showing the cemented borehole head (left), and the instrument box (right) with the data logger and power supply in a waterproof box, attached to the closest orange tree.

A 3.1 Field site 1: Phasouri site

The Phasouri site was chosen for its vicinity to the sea and to the area interpreted as dominated by seawater intrusion. It is located within the largest citrus plantation in the Akrotiri area, surrounded to all sides by at least 1 km of cultivated land. At the site itself, an intermediate groundwater salinity was measured (approx. 5.5 mS/cm).

A 3.1.1 Borehole log and salinity profiles

The borelog at the Phasouri site (Fig. A 3.2) shows a topsoil consisting of 1m of silty clay-rich earth, followed by 2 m of Havara (white silt with little clay). During drilling, this layer was found to be humid, while the underlying 2.5 m of clayey silt were drier. At a depth of 5.5 m, sandy well-rounded gravel was encountered. During much of the season, the groundwater table coincided with

this lithological change, although towards the end of the measuring period it had risen to a depth of 4.5 m.

The soil salinity profiles measured at the beginning and at the end of the monitoring period were used to evaluate the degree of flushing of the unsaturated zone. The first, complete, soil profile, representing the soil salinity profile at the beginning of the monitoring period, shows salinities of up to 14 mS/cm at a depth of 1.5 –2 m, and the salinities stay high (10-12 mS/cm) all the way down to the level of the groundwater table (Fig. A 3.2). The groundwater salinity at the beginning of the monitoring season was 5.5 mS/cm, i.e. significantly lower than the overlying soil salinity. This salinity distribution indicates solute accumulation below the tree root zone. The nitrate profile shows a slightly different pattern, with its peak of 1.5 gr/l displaced downward by one soil sample. These are extraordinarily high values, indicating overfertilisation of the field. At the end of the monitoring period, a second soil salinity and nitrate concentration profile was obtained from soil samples gathered with a hand auger down to a depth of 2.6 m. The obtained values were far smaller, with a peak of 5 mS/cm at a depth of 2.0 m and nitrate concentrations of 0.4 gr/l. At the time of the second soil salinity profile, irrigation had taken place for almost three months, after an exceptionally dry February and March. Hence, it probably does not reflect the maximum 'flushed' state at the end of the rainy season, but rather the increasing soil salinisation stage of the following irrigation season (2004). Nevertheless, qualitatively, a prominent decrease in soil salinity was observed between the two profiles, indicating solute transfer to the groundwater during the monitoring period.

Comparison of the groundwater chemical composition in July 2003 and April 2004 shows a dilution of approximately a factor 2 for most components (Fig. A 3.2). A relative chloride depletion and nitrate enrichment can also be observed. Chloride depletion can be explained by mixing with freshly infiltrated groundwater, poor in chloride, while the nitrate enrichment can be due to the late winter application of fertilizers on the fields.

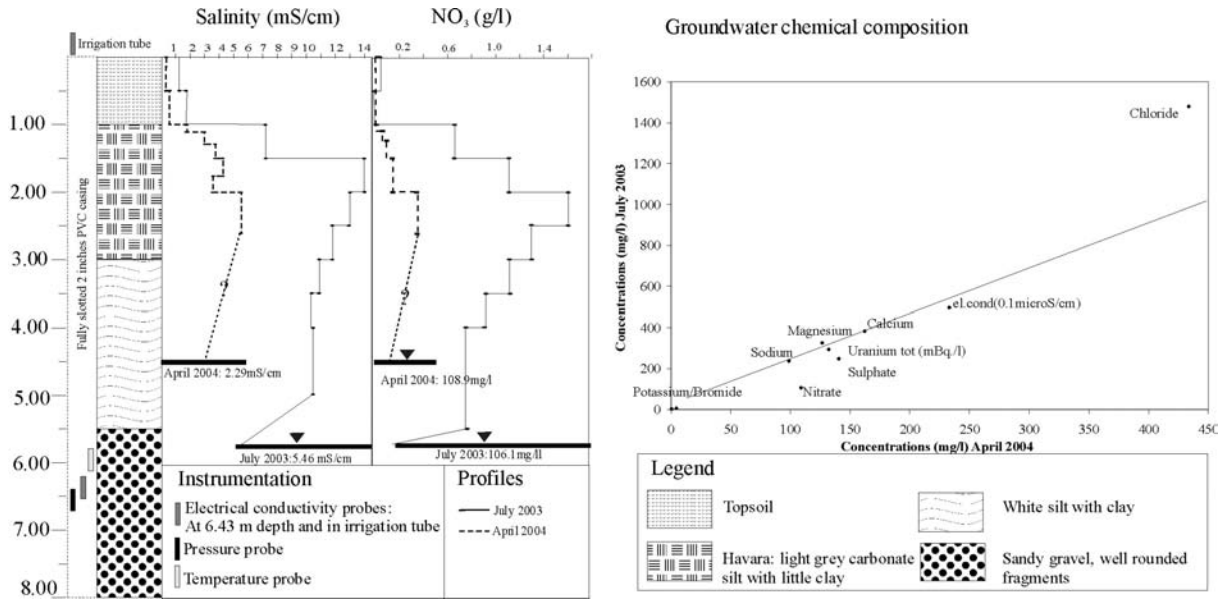

Fig. A 3.2: Selected data from the Phasouri monitoring borehole. Left: Borehole log, salinity profiles (mS/cm), and nitrate profiles (g/l) for the extracted saturated soil pastes taken in July 2003 and April 2004. Right: Groundwater chemical composition of major ions (mg/l) and uranium (mBq./l) in July 2003 and April 2004.

A 3.1.2 Electrical resistivity tomography imaging (ERT)

Two perpendicular electrical resistivity tomography (ERT) profiles were measured, positioned so that the monitoring well lay close to the intersection (Yeo 2003). The electrode spacing was one meter in order to obtain a high resolution of the unsaturated zone and to map out the lateral extent of soil salinisation, since soil resistivity is closely linked to the electrolyte content of the soil matrix. Fig. A 3.3 shows the profiles obtained, expressed in terms of bulk electrical conductivities (inverse of resistivity). It reveals a highly conductive layer (values above 2000 μS/cm) at a depth of 1.5 – 3 m. This corresponds to the depth where high salinity values were measured in the extraction of the saturated soil paste samples (Fig. A 3.2). That the maximum measured soil salinity was 14 mS/cm as compared to 2.0 mS/cm in the ERT profiles shows that the bulk electrical conductivity is reduced due to the resistance of the soil matrix, which at that depth consists of carbonate sand and silt.

The two ERT profiles reveal a relative lateral homogeneity apart from a minor dome-like structure in the NW-SE section, which shows that the soil salinity profile measured in the borelog can be considered representative for this zone, and that solute transport is likely to have a strong vertical component.

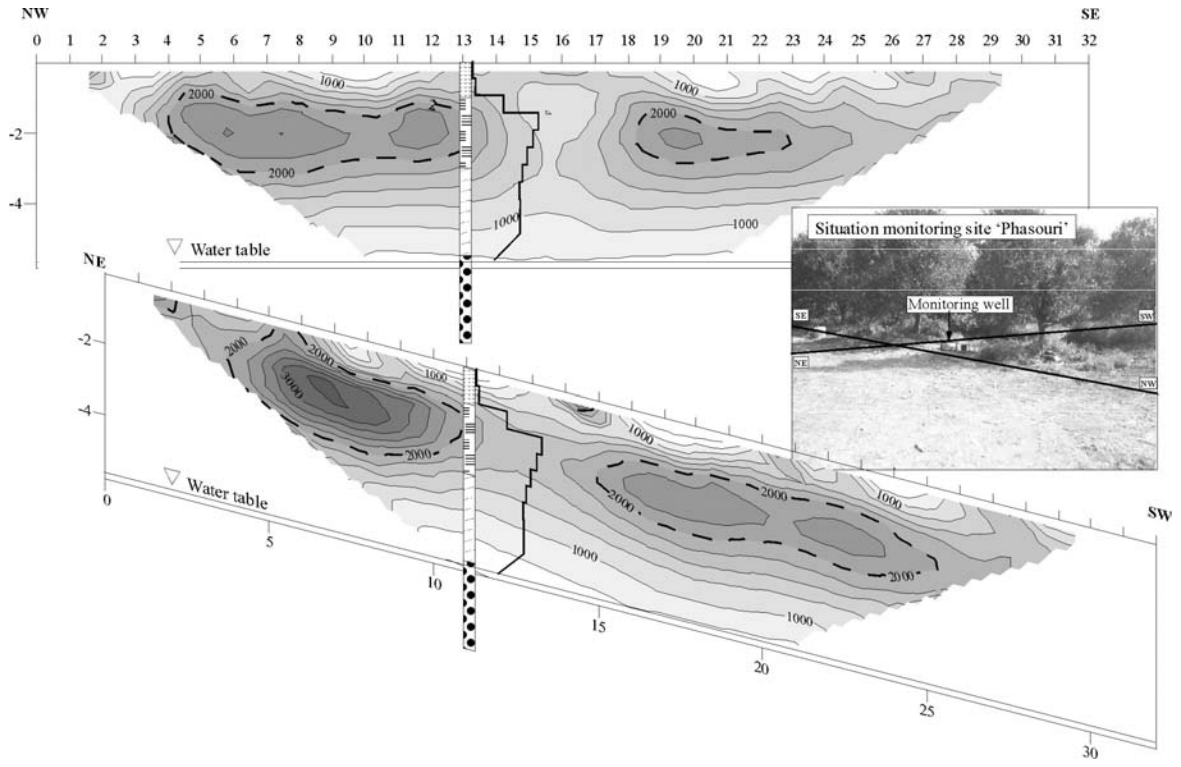

Fig. A 3.3: Two perpendicular electrical resistivity profiles intersecting at the monitoring borehole Phasouri (modified after Yeo 2003). The profiles show the bulk electrical conductivity distribution (in μS/cm) of the unsaturated zone and the projected position and lithology of the borehole. The lateral extent of the high salinity zone below the root zone is clearly seen. The soil salinity profile (Fig. A 3.2) is shown schematically along the borehole axis. Electrical conductivity iso-contour intervals are 250 μS/cm and length units are in meters.

A 3.1.3 Monitoring results

In the monitoring well, continuous measurement of water table, groundwater temperature and electrical conductivity (both of the goundwater and irrigation water) were carried out at 30 minute intervals. A measurement gap of five weeks, between 15th Dec 2003- 21st Jan 2004, was caused by power supply failure. The probes were calibrated at the beginning and at the end of the monitoring period and at the re-installation after the power failure. The electrical conductivity and temperature probes showed no drift, whereas the pressure probe drifted significantly.

The electrical conductivity curve has two prominent features (Fig. A.3.4). The salinity peak at 7 mS/cm in August 2003, and the following a plateau at salinities of approximately 6 mS/cm up to the end of October 2003, is the first characteristic feature. Even more prominent, however, is the second feature - the sharp salinity decline within a period of one month at the end of November 2003. This rapid salinity decrease took place prior to the onset of the rainy season. A rainfall event

took place before the decline started, while a second one occurred during the sharp salinity decrease, but both were very minor. Hence, we believe that this feature is not related to recharge and dilution by rainfall infiltration, which would be seen in a change in water table but rather to a leaching fraction which increases towards the end of the irrigation season, flushing the accumulated solutes to the groundwater. The pressure probe showed a drift, its absolute values were not used, but it did indicate that there was no significant change during the salinity decline in November 2003. The water table measurements did not indicate any significant change until January 2004, with the onset of heavy rainfall. The temperature of the shallow groundwater continued to rise during the decrease of the salinity and only started to drop in late winter, indicating percolation of rainwater to the groundwater. Following the intensive winter rains, a small and wide electrical conductivity peak could be observed in February 2004, probably indicating the complete flushing of the soil with water in abundance. At this stage, the water table rose by approximately 1.5 m.

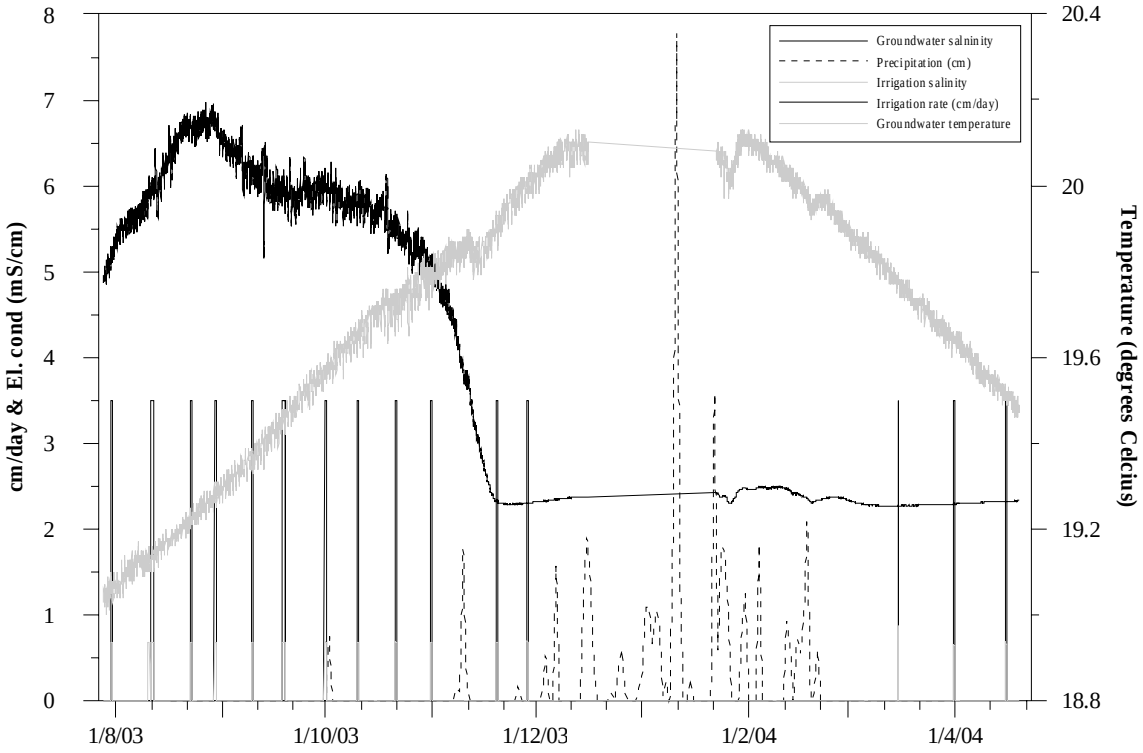

Fig. A 3.4: Monitoring data from the 'Phasouri site'; black: groundwater electrical conductivity (mS/cm), grey: temperature (degrees Celsius), black/light grey: irrigation rate (cm/day) and irrigation water electrical conductivity (mS/cm), stippled lines: precipitation (cm/day).

A 3.2 Field site 2: Lanitis site

The Lanitis monitoring site is located just north of the salt lake (Fig. 6.6) in the middle of a large citrus plantation. A combination of a technical failure and short-circuiting of surface waters with the groundwater made it difficult to come up with any straight-foreward interpretations of the monitoring data. Some of the results we obtained were unexpected and required explanation, which was found in the effect of local heterogeneities, inhibiting vertical flow and transport through the unsaturated zone. Vertical movement, however, was the main prerequisite of the monitoring setup.

A 3.2.1 Borehole log and soil salinity profile

The borehole log shows that a 1 m thick soil cover is underlain by a 1.5 m thick sandy-gravelly layer (Fig. A 3.5). A 3 m thick clay layer underlies the sandy gravel and goes over into a clay-rich silty layer at its base. At a depth of 5 m, the deposits were humid, but the groundwater was only encountered at a depth of 7.2 m and was found to be confined, rising up to 4 m depth. The soil salinity profile reveals an accumulation of solutes just below the static water table, between 4 and 4.5 m depth. A second soil salinity profile after the monitoring period could only be done to a depth of 1.3 m, since deeper penetration with the hand auger was impossible. Amongst the anions, sulphate was found to be dominant.

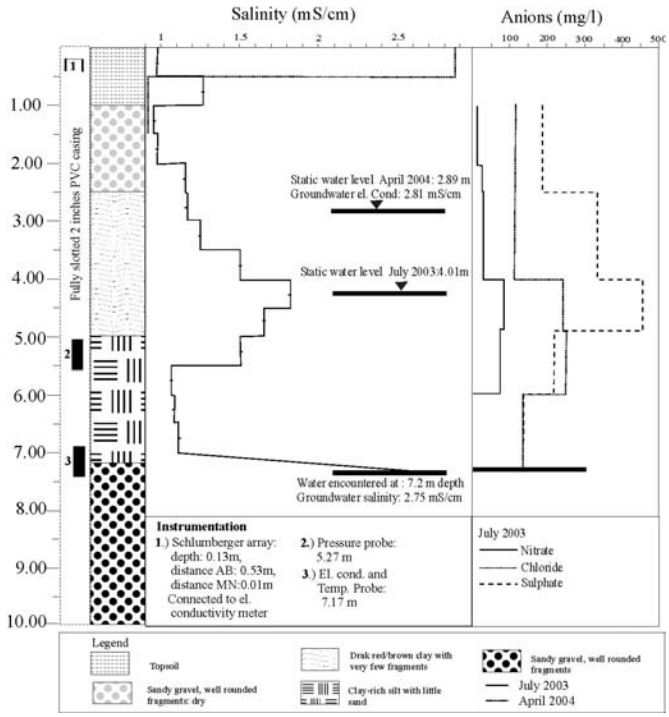

Fig. A 3.5: Borehole log and vertical salinity profile of the Lanitis monitoring well, and major anion profiles, showing accumulation just below the static water table.

A 3.2.2 Electrical resistivity tomography imaging (ERT)

The electrical resitivity profiles carried out at the 'Lanitis' site are shown in Fig. A 3.6, where the results are presented as bulk electrical conductivities. Two perpendicular high-resolution profiles with an investigation depth of 6-9 m reveal the sandy gravel layer encountered in the lower root zone at a depth of 1-2.5 m. The WE profile (Profile 1 in Fig. A 3.6) with a 1.5 m electrode spacing shows a high salinity zone in the west. The low-salinity zone, corresponding to the sandy gravel layer detected in the monitoring well at a depth of 1-2.5 m can be seen to pinch out in the central part of the section. The lateral extent of this sandy gravel layer (high resistivity zone) is small, approx. ten meters. This inclined permeable layer might act as a subsurface natural drain or as capillary barrier, and inhibiting vertical flow and transport, inhibiting vertical solute transport through the unsaturated zone to the groundwater. The same high resistivity layer (high permeability) below the root zone can also be detected on the NS profile (Profile 2 in Fig. A 3.6). The good correlation between the borehole log and the resistivity profiles shows the usefulness of the ERT method also for the detection of small-scale heterogeneities. A long resistivity profile (Profile 3 in Fig. A 3.6), with an electrode spacing of 5 m and an investigation depth of 20 m, shows that not only the unsaturated zone but also the aquifer is characterised by a high degree of heterogeneity, with frequent lateral changes from low to high resistivity.

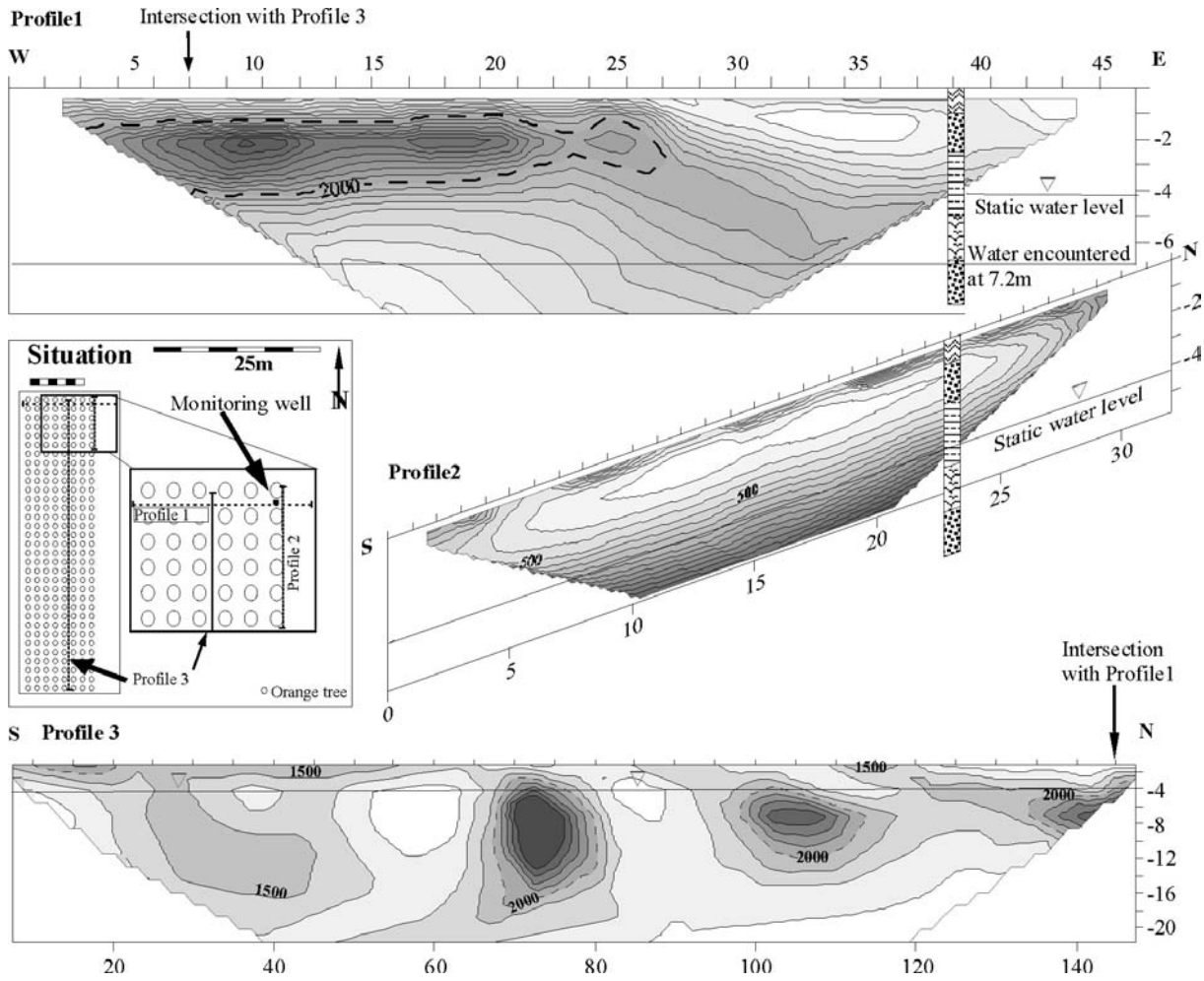

Fig. A 3.6: ERT profiles showing bulk electrical conductivities (μS/cm). 200 μS/cm iso-contour on Profiles 1 and 2 and 500 μS/cm isocontours on Profile 3. Profiles 1 and 2 are perpendicular, intersecting at the monitoring well, with electrode spacings of 1.5 m and 1 m, respectively. Profile 3 is paralell to Profile 2 with electrode spacing of 5m.

A 3.2.3 Monitoring results

Water table depth, shallow groundwater salinity and temperature were measured at 30 minute intervals until January 2004, when the data logger failed. The water table can be seen to decrease up to the end of October 2003, with short-term fluctuations (Fig. A 3.7). To monitor the relative soil salinity, a miniature Schlumberger array was installed and connected to an electrical conductivity meter. This gave a relative measure only, since calibration could not be done. It reveals the irrigation cycles, which can be seen to be very regular, every ten days. The irrigation onset is characterised by a very sharp relative soil salinity increase, followed by a slow decline, corresponding to the drying cycle. During the monitoring period, one can see that the relative soil salinity decreases steadily. This could be due to a decreasing water requirement of the plants,

leading to flushing of the soil with an ever increasing surplus of irrigation water. However, another explanation could be a technical one, e.g. formation of oxides on the surface of the copper electrodes installed in the soil, which would reduce their conductance and thus lead to lower measured conductivities.

The groundwater electrical conductivity can be seen to slightly decrease during the first three monitoring months. At the end of October 2003, there was an event, lasting a few days, which can be clearly seen in Fig. A 3.7 in all the measured parameters and which is not linked to any technical failure or instability (stable voltage and current). The relative soil salinity shows a double peak, followed shortly after by a significant water table rise and drop in electrical conductivity in the shallow groundwater. A possible interpretation is that irrigation had such an immediate impact on all the measured parameters, due to a very strong, large-scale and repeated irrigation event lasting over several days. A more likely explanation is, however, that it is a local artefact, caused by a repeated local irrigation event. If the sandy gravel layer in the root zone receives water in abundance, percolation down along the borehole can occur, thus short-circuiting the clay-layer, locally reducing the groundwater salinity and temperature, and causing a rise in the water table.

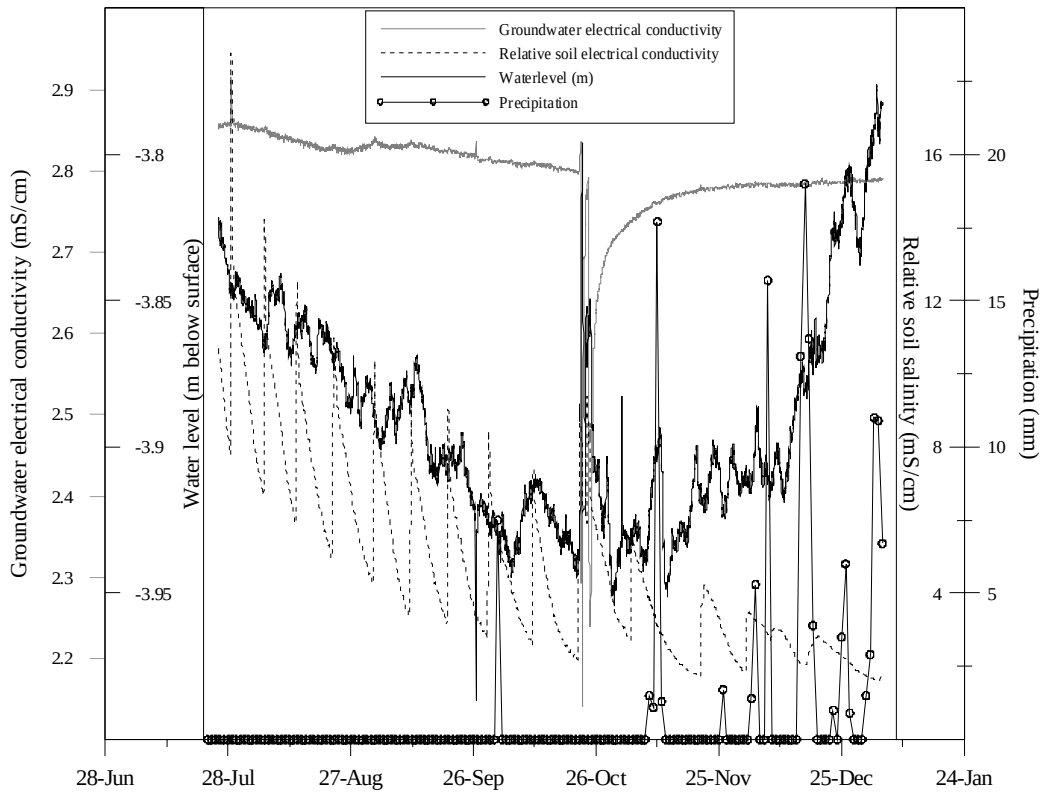

Fig. A3.7: Monitoring data from the 'Lanitis site', showing water table, groundwater salinity, relative soil salinity and precipitation data.

A 3.3 Conceptual models

In this section we will try to synthesize the measured monitoring data tin order to build up conceptual models of the two sites, since they showed such different results.

A 3.3.1 Conceptual model of the Phasouri site

To understand the two prominent features observed in the monitoring data of the Phasouri site, it is important to analysie the seasonal variations of the water balance components. For this purpose, rainfall and evaporation data were retrieved from the nearby meteorological station, located one kilometre from the investigation site. Information on the irrigation schedules were obtained from the farm owners. Studies of plant water uptake and water requirements carried out in Cyprus estimate that citrus water requirement equals 60% of the Pan A evaporation (Eliades et al. 1995). A moving average was made of the evaporation data and was used to estimate the daily water requirement (Fig. A3.8), with a data gap of 3 weeks in the month of May-June 2003. Irrigation took place every seven to ten days, depending on the season, and the rate varied between 1800 l/tree/month (early irrigation season: April-May) to 3600 l/tree/month (August). These irrigation rates were transformed into daily average irrigation rates to enable comparison with the theoretical daily water requirement of the trees, based on the Pan A evaporation data. Fig. A3.8 shows the water requirement and the irrigation rates for the entire irrigation season 2003, including the period prior to monitoring, as well as the groundwater electrical conductivity measured in the Phasouri site.

The ratio of irrigation rate to deep percolation is known as the leaching fraction (LF). Deep percolation can be estimated by the difference between the irrigation rate and the plant water uptake, if direct evaporation is neglected. Fig. A3.8 reveals under-irrigation during the early irrigation season (May 2003), with the water requirement of the trees being greater than the irrigation rate. During this period, salt accumulates and concentrates in and below the root zone and the leaching fraction is close to zero. From June 2003 onwards, irrigation rates can be seen to be greater than the water requirement of the trees and steadily increase until late August 2003, while the plant water uptake is on its decline from June 2003 onwards. This leads to a temporally increasing leaching fraction, with a maximum in mid August 2003, when over-irrigation is at its maximum. The time between the maximum under-irrigation and the concentration peak observed in the groundwater indicates a time-delay of approximately 2 months. A similar time-delay can be seen between the maximum over-irrigation in August 2003 and the sharp groundwater salinity decline in November 2003.

This observation led to the hypothesis that the salinity peak observed in the groundwater is the groundwater response to the solute accumulation during the early irrigation period, while the sharp concentration decline in November 2003 resulted from flushing of the soil by excess irrigation water in the late irrigation period.

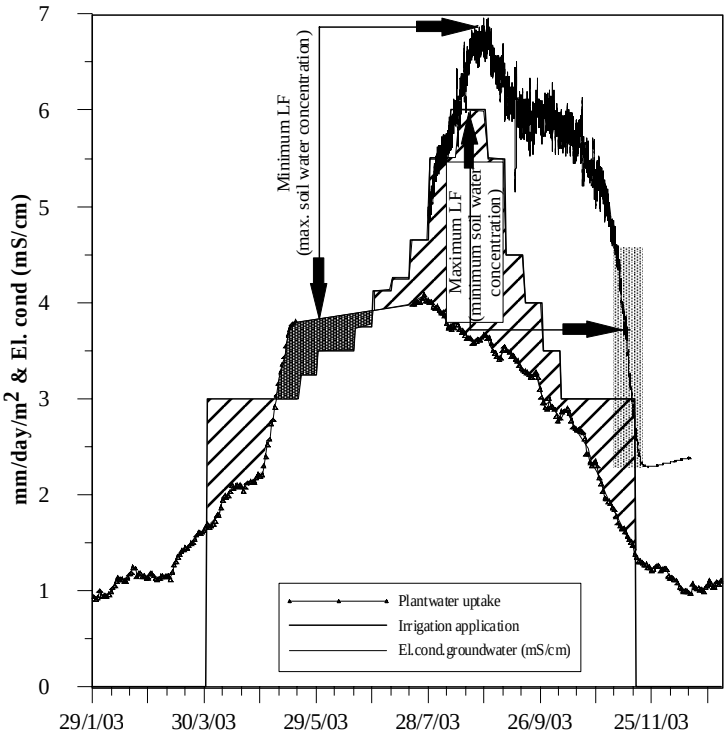

Fig. A3.8: Plant water uptake versus irrigation rates compared to the salinity curve measured in the Phasouri monitoring well. The minimum leaching fraction (LF) is believed to correlate with the salinity peak observed in the groundwater, while the maximum LF is attributed to the salinity decrease in November 2003.

A 3.3.2 Conceptual model of the Lanitis site

The features observed at the Lanitis site indicate a very different behaviour to the Phasouri site, in that solute return flow could not be identified. The question therefore arises, whether this process is absent in this zone. This seems unlikely, since a similar irrigation scheme was used on the crops with the same water requirement, leading to a similar overall solute mass flux at both sites. Hence, either the electrical conductivity probe was located too far below the static water level in a the confined dynamic aquifer where solutes will be readily diluted, or lateral transport takes place along the inclined sandy gravel layer below the root zone, acting as natural drain or capillary barrier (Fig. A3.9). This could explain the measured signals interpreted as short-circuit of irrigation water with the groundwater through the borehole (Fig. A3.7). The geometry of the high

permeability zone, as obtained from the ERT profiles, suggests a very simplified conceptual model of the Laintis site, with lateral movement creating a perched water table above the impermeable clays during and after irrigation events (Fig. A3.9). Solutes do not easily accumulate in sandy-gravelly soils, since fluid movement is faster than plant water uptake.

These explanations are in no contradiction with the interpretation of the groundwater salinity response observed at the Phasouri site, but indicate that local heterogeneities can strongly influence local solute return flow from irrigation. On the small-scale, vertical movement is very sensitive to local geological conditions, but considering the extent of the plantations with respect to the thickness of the unsaturated zone, vertical movement can be a reasonable assumption on the large-scale (scale of the whole irrigated surface).

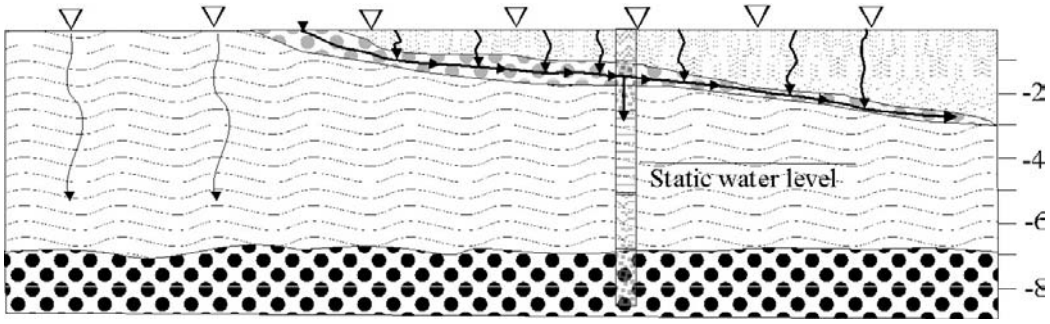

Fig. A3.9: Conceptual model for solute transport at the Lanitis site that could explain the monitoring data as well as the short-circuiting of fresh irrigation water with the groundwater, based on the geometry obtained from the ERT WE profile (Fig. A 3.6).

A 3.4 Numerical experiments

Based on the conceptual models established in the previous section, we carried out some numerical experiments to test the established hypotheses. Beginning with the Phasouri site, the main hypothesis to be tested is, whether the groundwater salinity response may be linked to the combined effect of seasonally varying irrigation rates and plantwater uptake. In the case of the Lanitis site, the same irrigation scheme and plantwater uptake is then used to test the impact of local heterogeneities on the groundwater salinity response.

A 3.4.1 1-D numerical column experiment: Phasouri site

A 1-D numerical finite element column experiment was carried out to test the hypothesis, that both the salinity peak and sharp salinity decline observed in the Phasouri monitoring well are linked to the temporal variation of the leaching fraction. The advantage of using a 1-D column to investigate the effect of the particular boundary conditions, resulting from the combined effect of irrigation rates and plant water uptake, is that the process can be studied under controlled conditions. From the ERT profiles, we deduced that the subsurface structure in the surroundings of the Phasouri site was mainly planar, justifying the use of a 1-D approach. The main features we wanted to simulate were the salinity peak and the sharp decline prior to the onset of precipitation for a homogeneous medium. The simulation period was chosen from one evapotranspiration minimum to the next, thus from December 2002 to December 2003. The column length was chosen to be 6.5 m, to avoid interference with the lower boundary condition, and observation points were placed according to the position of the instrumentation.

The unsaturated flow through the finite element column was simulated with the computer package FEFLOW (Diersch 2002), solving Richard's equation. The model was discretised into 130 elements, each of them 0.05m wide. Transport of solutes was considered to be conservative, e.g no chemical reactions such as dissolution, precipitation, sorption or plant solute uptake.

The salinity evolution observed in the observation well was simulated using the range of hydraulic conductivities deduced from two single ring infiltration tests carried out at a distance of 5-10 m from the monitoring well. The infiltration tests were carried out according to the method described by Reynold and Elrick (1990). The saturated hydraulic conductivities deduced for these tests were 1×10^{-5} m/s and 7×10^{-5} m/s for injected water volumes of 170 litres and 430 litres respecively. The α - parameter (Gardner, 1958), corresponding to the inverse of the air entry pressure, was also deduced from these tests, but is described as being far less reliable: the obtained values were α = 0.4 [1/m] and α = 19.7 [1/m], respectively. The van Genuchten model was used for the dependency between the saturation and hydraulic conductivity in the simulations, and the corresponding parameters A and n used in the simulations ranged between A = 1 – 4 [1/m], n = 2 – 5 [-], while the porosity was varied between 0.15 and 0.3. The longitudinal dispersivity was varied between 0.05 - 0.1 m.

The flow boundary condition (Neuman-type) assigned to the top of the column consisted of the irrigation rates plus the precipitation rates (Fig. A3.10). The corresponding transport boundary condition was a Dirichlet-type condition at the top boundary: for the time when there was only precipitation, the concentration was set to C_{in} = 0, and for the period when there was only irrigation it became C_{in}=1, with an intermediate value in the time period when there was both irrigation and

precipitation. To simulate the plant water uptake, a fluid sink was assigned to a zone of one meter thickness at a depth of 0.5 meters below the soil surface. This was adjusted for the time-period when irrigation rates were below the plant water requirement to values slightly below to the irrigation rates. The transient fluid sink corresponded to the plant water uptake as shown in Fig. A3.8. Introducing a fluid sink allows simulation of evapotranspiration, only extracting the fluid and thereby concentrating the solutes in the root zone during the periods when the leaching fraction is small.

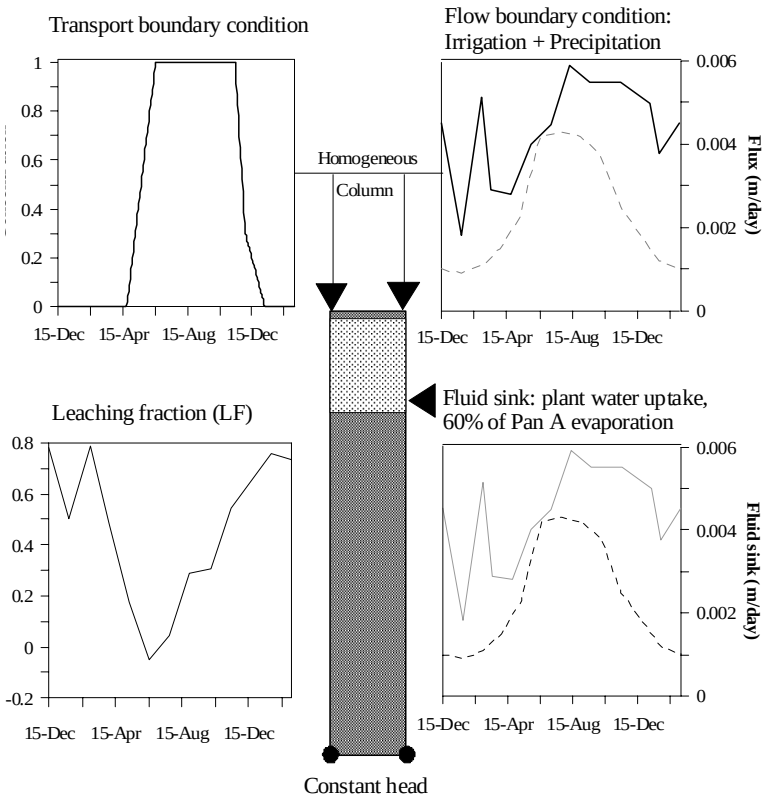

Fig. A3.10: Schematic illustration of the 1D column, showing all boundary conditions. The flow boundary condition at the top boundary (Neuman-type) corresponds to the sum of precipitation and irrigation (full line, top right), with a corresponding Dirchlet-type transport boundary condition (C_{in} = 1 during irrigation, C_{in} = 0 during precipitation, top left), fluid sink in root zone corresponding to 60 % of Pan A evaporation (stippled line, bottom right). Dirichlet-type flow boundary condition at the bottom, corresponding to mean water table. Bottom left: temporal variation of leaching fraction LF (infiltration-plant uptake/infiltration).

The model results were compared more or less directly to the measured groundwater electrical conductivities, since the irrigation water electrical conductivity was approximately 1 mS/cm and the assigned relative irrigation concentration in the model C_{in}=1. The background salinity corresponding to the electrical conductivity attained during winter of 2 mS/cm in the groundwater was subtracted from the monitoring data to allow comparison. Fig. A3.11a shows a whole range of

simulation results, revealing the main features; particularly the salinity maximum in August 2003 followed by a very sharp salinity decline in November 2003, prior to the onset of precipitation. There is no point in calibrating the model to the measured values any better. Firstly, borehole measurements could have been affected by interaction with the groundwater, but in the simulations no interaction with the graoundwater takes place. Secondly, what we simulated is purely the effect of concentration of irrigation water, neglecting any agricultural additives, although the measured nitrate profile in Fig. A 3.2 showed, that a considerable fraction of the soil salinity consists of nitrates. Fig. A3.11b shows the comparison between the measured soil salinity profile (in mS/cm) and the simulated soil salinity profile of 'simulation 59' (best fit) at the beginning of the monitoring period. We can see, that the salinity accumulation just below the root zone is well reflected in the simulation. The solutes in the lower section of the soil column, however, are almost completely absent, as opposed to the measured profile. These profiles cannot be easily compared, since the soil salinity was measured on extracted saturated soil paste, and the simulated salinity refers to the concentration corresponding to the simulated soil water content. Scaling the simulated relative concentration by the simulated water content to obtain a 'simulated extraction of saturated soil paste' reveals that the simulated salinity is approximately an order of magnitude inferior to the measured salinities.

For all these reasons, showing that the 1-D column cannot be calibrated, it is useless to determine a best-fit of hydrodynamic parameters. The results show, however, that the observed salinity distribution can be explained by this mechanism. The simulation results supported the hypothesis that solute return flow from irrigation was a dominant process around the Phasouri borehole during the monitoring period, rather than seawater intrusion. None of the measured data indicated seawater advance or retreat during the monitoring period, although the variations in salinity were significant. To really quantify the impact of solute return flow on groundwater salinisation, the chosen approach is insufficient, since the groundwater dynamics will very much govern the salinisation process.

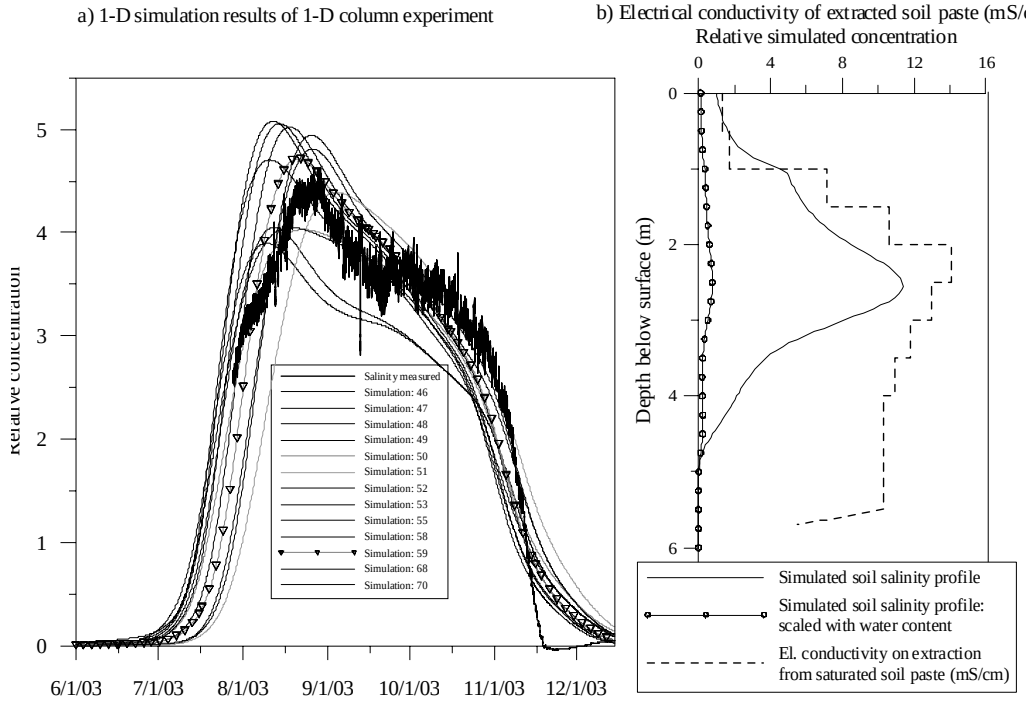

Fig. A3.11: Range of numerical simulation results of the 1-D column experiment, showing the main feature the salinity curve (left). Measured and simulated soil salinity profiles at the beginning of the monitoring period (right).

A 3.4.2 2-D vertical numerical experiment: Lanitis site

As suggested in the conceptual model of the Lanitis site, solute movement is not believed to be dominatnly vertical in that section, and this explains why the retrieved data did not show any significant response. The question we attempted to answer with a highly schematised 2-D vertical finite element model is how the high contrasts in subsurface conditions would react to exactly the same boundary conditions as defined for the Phasouri site. The irrigation scheme and the plantwater uptake being identical in the two cases implies that the net applied solute mass flux is similar too. With this second numerical experiment we wanted to test, how the gravel layer below the root zone may act as subsurface drain above the impermeable clays.

In Fig. A3.12, the 2-D vertical model is schematised, showing the saturated hydraulic conductivities (in m/s) and boundary conditions. The boundary conditions are identical to the ones used in the Phasouri siumlations. At the downstream side of the gravel layer, an constrained head boundary condition was imposed, allowing outflow out of the section if saturation is attained, but no inflow. For the van Genuchten parameters, the top soil and the clay layer were assumed to be more capillary than the gravel layers. The following parameters were assigned: A = 4 [1/m] and n =2 for the topsoil and clay layer and A= 1 [1/m] and n = 5 for the gravel layers. The width of the

model is 15 m and its height is 7 m, discretised into 7800 quadrilateral finite elements. No sensitivity analysis was carried out for this experiment, but observation points were placed along the vertical section, corresponding to the monitoring well and along the gravel layer from the monitoring well in the dip direction of the layer.

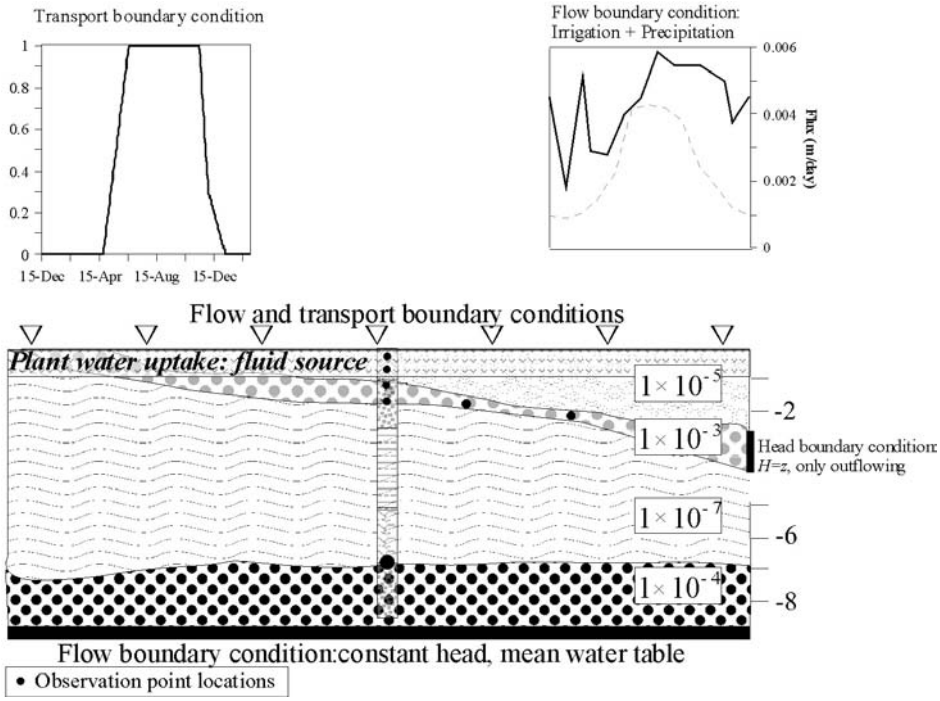

Fig. A3.12: Schematic illustration of the 2-D vertical model of the Lanitis site, showing boundary conditions (identical to the Phasouri simulation), saturated hydraulic conductivity distribution and observation point locations.

Fig. A3.13 shows the concentration evolution at the different observation points. Fig. A3.13a shows five observation points in the vertical section below the 'theoretical' monitoring position, where the hydraulic parameter distribution corresponds to the borelog. One can see that the concentration in the topsoil is inferior to the concentration in the gravel layer, which is characterised by a very low water content during the peak of plantwater uptake. At the bottom of the gravel layer, the humidity is very high and therefore the simulated concentrations very low. The observation point located at the depth where the electrical conductivity probe was located (7 m depth) shows no variations at all, which means that the solutes have not been transferred through the vertical section. Fig. A3.13b shows three observation points located within the gravel layer. The first observation point corresponds to the observation point in the vertical section of the monitoring well, followed by two other obsevation points located at 5 m and 8 m in the dip direction of the gravel layer (Fig. A3.12). The concentration signal can be seen to be transmitted laterally and the amplitude decreases, reflecting an increase in moisture content and lateral transport within this layer. The general form of the concentration evolution in the gravel layer

corresponds very much to the groundwater salinity response measured at the Phasouri site, where transfer of solutes is believed to be mostly vertical.

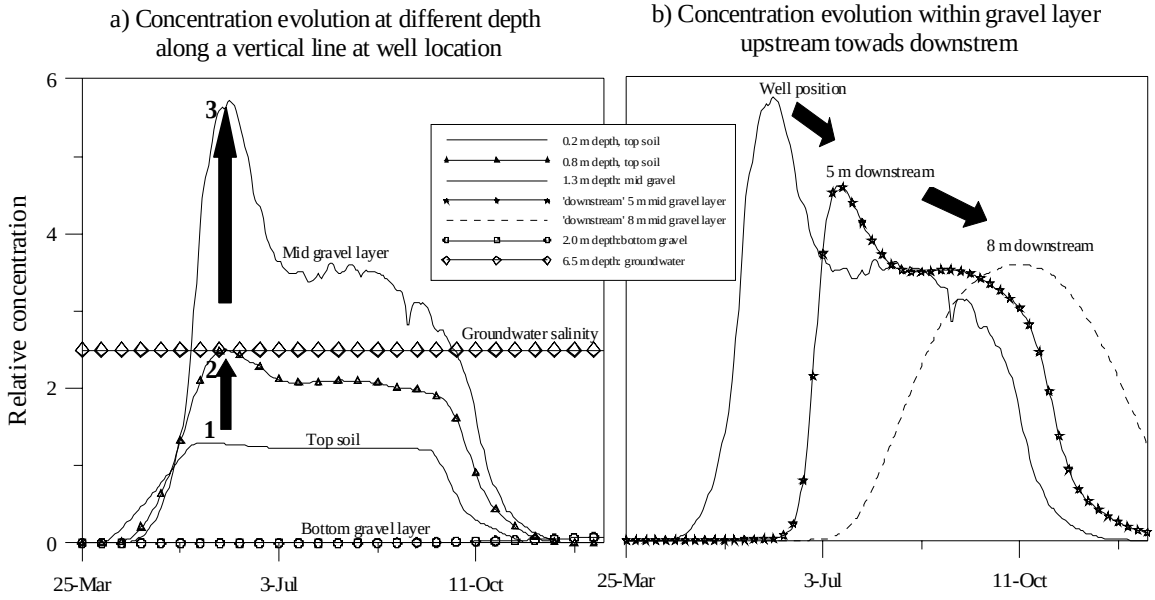

Fig. A3.13: Concentration curves at different observation points. (a) concentration responses within the vertical section at the 'monitoring well' position. (b) concentration evolution within the gravel layer in three observation wells: well position and two observation points at 5 m and 8 m in dip direction of the gravel layer (cf. Fig. A3.12).

Fig. A3.14 shows results from the 2-D vertical simulations. Fig. A3.14a shows the saturation at a simulation time of 200 days, corresponding to the peak irrigation season and approximately to the beginning of the monitoring period. The gravel layer can be seen to be almost completely dry, acting as a capillary barrier to the moisture coming from the top soil. The moisture increases towards the downstream area of the gravel layer. Fig. A3.14b illustrates the velocity distribution for the same simulation time and shows that the high velocities are concentrated at the bottom of the gravel layer. Fig. A3.14c and A3.14d show the mass distributions at two different simulations times, at 200 and 300 days, respectively. The clay layer can be seen to inhibit vertical movement, and the gravel layer conveys the solutes laterally. At 300 days (Fig. A3.14d), at the end of the irrigation season, corresponding to the time when the sharp salinity decline was observed and simulated in the Phasouri site, the mass is drastically dimished, while the moisture content has increase significantly.

The results from the synthetic Lanitis site indicate, that although the we did not measure any significant change in the groundwater salinity evolution, the same solute mass flux may have been introduced into the system, for that particular configuration. The transferred solutes will thus,

sooner or later, be transferred to the groundwater. Whether they lead to rapid variations in the groundwater salinity or slow changes will, however, very much depend on the groundwater dynamics.

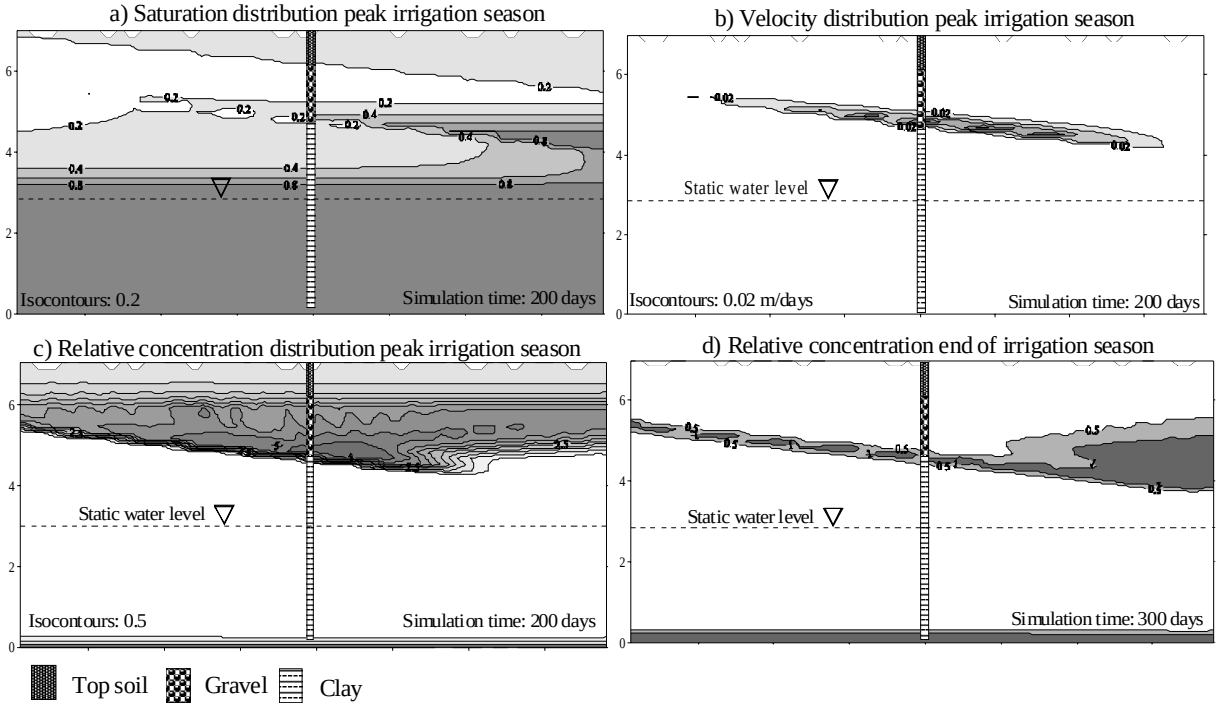

Fig. A3.14: Results from the 2-D vertical finite element simulations of the synthetic Lanitis section. (a) saturation at a simulation time of 200 days, (b) velocity distribution (m/s) with iso-contours of 0.1 m/s, (c) mass distribution at a simulation time of 200 days (peak irrigation season), (d) mass distribution at a simulation time of 300 days (end of irrigation season).

These simulations showed, that although the monitoring data of the two sites were very different, they are not in any contradiction with the process of solute return flow. Local heterogeneities may considerably influence vertical transfer of solutes to the groundwater. Considering the size of the citrus plantations, being approx. 10 km^2, solute return flow may very well be considered as mainly vertical.

For the numerical experiments we assumed conservative transport of solutes. However, transfer of solutes through the unsaturated zone is highly complex, implying a multitude of processes, such as sorption, ion exchange, dissolution, precipitation and plant uptake. Additionally, the unknown amount of agrochemical additives render solute mass estimations even more complicated. Also, the soil hydraulic properties change as function of soil water salinity, cation exchange processes, dissolution and precipitation of salts as well as with drying and wetting cycles. Plant water uptake will also vary as function of the soil water salinity, which in turn will have an impact on deep

percolation, dissolution and precipitation. Microbial activity in the soil will influence the CO_2 partial pressure and will thereby control the pH and redox potential, which again influence dissolution and precipitation as well as sorption processes (e.g. Tanji 1990). Hence, a combination of the effect of heterogeneity and processes taking place in the unsaturated zone as the above-mentioned might be a explanation for the very different results obtained at the two monitoring sites.